frontiers | Research Topics

MRI in veterinary neurology

Edited by
Adriano Wang-Leandro

Published in
Frontiers in Veterinary Science

ISSN 1664-8714
ISBN 978-2-8325-5681-8
DOI 10.3389/978-2-8325-5681-8

About Frontiers

Frontiers is more than just an open access publisher of scholarly articles: it is a pioneering approach to the world of academia, radically improving the way scholarly research is managed. The grand vision of Frontiers is a world where all people have an equal opportunity to seek, share and generate knowledge. Frontiers provides immediate and permanent online open access to all its publications, but this alone is not enough to realize our grand goals.

Frontiers journal series

The Frontiers journal series is a multi-tier and interdisciplinary set of open-access, online journals, promising a paradigm shift from the current review, selection and dissemination processes in academic publishing. All Frontiers journals are driven by researchers for researchers; therefore, they constitute a service to the scholarly community. At the same time, the *Frontiers journal series* operates on a revolutionary invention, the tiered publishing system, initially addressing specific communities of scholars, and gradually climbing up to broader public understanding, thus serving the interests of the lay society, too.

Dedication to quality

Each Frontiers article is a landmark of the highest quality, thanks to genuinely collaborative interactions between authors and review editors, who include some of the world's best academicians. Research must be certified by peers before entering a stream of knowledge that may eventually reach the public - and shape society; therefore, Frontiers only applies the most rigorous and unbiased reviews. Frontiers revolutionizes research publishing by freely delivering the most outstanding research, evaluated with no bias from both the academic and social point of view. By applying the most advanced information technologies, Frontiers is catapulting scholarly publishing into a new generation.

What are Frontiers Research Topics?

Frontiers Research Topics are very popular trademarks of the *Frontiers journals series*: they are collections of at least ten articles, all centered on a particular subject. With their unique mix of varied contributions from Original Research to Review Articles, Frontiers Research Topics unify the most influential researchers, the latest key findings and historical advances in a hot research area.

Find out more on how to host your own Frontiers Research Topic or contribute to one as an author by contacting the Frontiers editorial office: frontiersin.org/about/contact

MRI in veterinary neurology

Topic editor
Adriano Wang-Leandro — University of Veterinary Medicine Hannover, Germany

Citation
Wang-Leandro, A., ed. (2024). *MRI in veterinary neurology*.
Lausanne: Frontiers Media SA. doi: 10.3389/978-2-8325-5681-8

Table of contents

05 Case report: Recovery and sequential imaging of a patient with osmotic demyelination syndrome
Stephanie Harris, Adrien Dupanloup, Pen-Ting Liao and Tom Jukier

12 Case report: Sacral agenesis in two boxer dogs: clinical presentation, diagnostic investigations, and outcome
Diletta Dell'Apa, Martina Fumeo, Antonella Volta, Marco Bernardini, Francesca Fidanzio, Valentina Buffagni, Matthias Christen, Vidhya Jagannathan, Tosso Leeb and Ezio Bianchi

19 Measurement of brainstem diameter in small-breed dogs using magnetic resonance imaging
Jihyun Kim, Danbee Kwon, Sung-Soo Kim, Kichang Lee and Hakyoung Yoon

29 Single-slab 3D double inversion recovery for magnetic resonance brain imaging in clinically healthy dogs
Miseong Je, Sunho Yang, Dongjae Lee, Jihye Choi and Junghee Yoon

37 Significance of intramedullary T2* signal voids in the magnetic resonance imaging of paraplegic deep pain-negative dogs following intervertebral disc extrusion at short-term follow-up
Robert Clark, Amy Ferreira and Sebastien Behr

45 Comparison of standard T2-weighted turbo spin echo and volumetric interpolated breath-hold examination magnetic resonance imaging sequences in the assessment of articular process dysplasia in Pug dogs with thoracolumbar myelopathy
Emma Gilbert, Jeremy Rose, Lorna Arrol and Colin J. Driver

51 Case report: Traumatic hemorrhagic cervical myelopathy in a dog
Koen M. Santifort, Ines Carrera and Simon Platt

57 Regional ADC values of the morphologically normal canine brain
Lea Carisch, Blanca Lindt, Henning Richter and Francesca Del Chicca

68 Prevalence, MRI findings, and clinical features of lumbosacral intervertebral disc protrusion in French Bulldogs diagnosed with acute thoracic or lumbar intervertebral disc extrusion
Claudia La Rosa, Simona Morabito, Andrea Carloni, Tommaso Davini, Carlotta Remelli, Swan Specchi and Marco Bernardini

76 Are postnatal traumatic events an underestimated cause of porencephalic lesions in dogs and cats?
Tommaso Davini, Chiara Mattei, Claudia La Rosa, Carlotta Remelli, Swan Specchi, Elena Lionello, Elena Dell'Era and Marco Bernardini

84 Diffusion tensor-based analysis of white matter in dogs with idiopathic epilepsy
Katrin M. Beckmann, Adriano Wang-Leandro, Frank Steffen, Henning Richter, Matthias Dennler, Rima Bektas, Ines Carrera and Sven Haller

95 Magnetic resonance imaging subtraction vs. pre- and post-contrast 3D gradient recalled echo fat suppressed imaging for evaluation of the canine and feline brain
Heather Simon, Silke Hecht, Constance Fazio and Xiaocun Sun

103 Modic changes in the lumbar vertebral column of chondrodystrophic and non-chondrodystrophic dogs with intervertebral disc disease
Dyah Agustini, Mary K. Heimann, Megan Co, Benjamin A. Walter, Devina Purmessur and Sarah A. Moore

114 Case report: Focal heterotopic ossification in paravertebral muscles as a cause of neurogenic lameness in a dog
Ivo Hajek, Marco Rosati, Kaspar Matiasek, Michal Babinsky, Abby Caine and Viktor Palus

frontiers | Frontiers in Veterinary Science

TYPE Case Report
PUBLISHED 28 April 2023
DOI 10.3389/fvets.2023.1146091

OPEN ACCESS

EDITED BY
Adriano Wang-Leandro,
University of Veterinary Medicine
Hannover, Germany

REVIEWED BY
Rodrigo Gutierrez-Quintana,
University of Glasgow, United Kingdom
Marco Rosati,
AstraZeneca, United Kingdom

*CORRESPONDENCE
Tom Jukier
✉ tzj0034@auburn.edu

RECEIVED 16 January 2023
ACCEPTED 05 April 2023
PUBLISHED 28 April 2023

CITATION
Harris S, Dupanloup A, Liao P-T and Jukier T (2023) Case report: Recovery and sequential imaging of a patient with osmotic demyelination syndrome.
Front. Vet. Sci. 10:1146091.
doi: 10.3389/fvets.2023.1146091

Case report: Recovery and sequential imaging of a patient with osmotic demyelination syndrome

Stephanie Harris[1], Adrien Dupanloup[2], Pen-Ting Liao[1] and Tom Jukier[1]*

[1]Department of Clinical Sciences, Auburn University College of Veterinary Medicine, Auburn, AL, United States, [2]Veterinary Medical Teaching Hospital, School of Veterinary Medicine, University of California, Davis, Davis, CA, United States

A 4-year-old neutered-male Australian Shepherd was presented to an emergency and referral hospital for an acute onset of neurologic signs and abnormal mentation. Seven days prior, the patient had been diagnosed with hypoadrenocorticism and was treated accordingly at another hospital. Based on recent clinical history, the neurologic signs were consistent with thalamic and brainstem deficits and suspected to be caused by osmotic demyelination syndrome secondary to rapid correction of hyponatremia. A brain MRI confirmed lesions consistent with osmotic demyelination syndrome. The patient's clinical signs initially worsened, and he required intensive nursing care with multimodal sedation, close monitoring of electrolytes and tailored fluid therapy. The patient recovered and was discharged on day seven of hospitalization. Four and a half months later, re-evaluation of the patient showed complete resolution of the neurological deficits with a now unremarkable neurological exam, and follow-up MRI revealed still present, yet improved bilateral thalamic lesions. This is the first known veterinary case report of sequential brain imaging of a dog that has recovered from osmotic demyelination syndrome. In humans, patients can have evidence of near to full clinical recovery, yet imaging findings may still be abnormal several months after recovery. This report details similar imaging findings in a canine with improved clinical signs, despite persistent lesions on brain MRI. Prognosis of canines with osmotic demyelination syndrome may be better than previously perceived, despite the severity of clinical signs and brain lesions apparent on MRI.

KEYWORDS

pontine myelinolysis, extrapontine demyelination, osmotic demyelinating syndrome, magnetic resonance imaging, dog, veterinary

1. Introduction

Osmotic demyelination syndrome (ODS), formerly referred to as "pontine and extrapontine myelinolysis," is a condition first described in four individuals with alcoholism and malnourishment by Adams et al. (1). This condition was later associated with rapid correction of chronic hyponatremia and with this, a wide spectrum of symptoms have been described, including severe movement disorders, mental status changes, and acute death (2, 3). Histopathologically, degeneration of oligodendrocytes and myelin is evident, with the types of lesions varying from mild edema noted in myelin and intracellularly, to more severe lesions characterized by myelinolysis, degeneration of oligodendrocytes, and degeneration

of axons and neuronal cell bodies, with the latter occurring at the center of the lesion (1, 4). There are infrequent reports in veterinary medicine describing ODS, both with and without recovery, with few documenting MRI lesions at time of diagnosis and post-mortem (5, 6). In human medicine, the prognosis was initially described to be grave. However, with the advent of advanced imaging, appropriate nursing care, sedation and regular monitoring of sodium levels, the prognosis may be more favorable with good recovery in more than half of cases (7).

2. Case description

A 4-year-old male castrated Australian Shepherd weighing 10.7 kg was presented to the emergency service of a veterinary teaching hospital for a rapidly worsening tetraparesis with deterioration of mental status of a 2-day duration. Seven days prior to presentation, the patient was treated at another veterinary hospital for gastrointestinal signs, where he was hospitalized and diagnosed with hypoadrenocorticism based on ACTH stimulation testing (pre- and post- cortisol levels were <0.2 ug/dL). After 3 days of hospitalization, the patient clinically improved and was discharged with his first mineralocorticoid injection[1] and 0.25 mg/kg/day of prednisone.[2] No additional information was available at that time, other than the patient's sodium to potassium ratio had been low. Two days after discharge, the owner noted that the patient was becoming weak in his pelvic limbs, which seemed to worsen over the following day. Pelvic muscle fasciculations also developed and were most notable when attempting to eat or drink. At that point, the patient was referred to the authors' institution for further workup of progressive neurologic signs.

On presentation, the patient's general physical examination was within normal limits. On neurological examination, the patient vocalized intermittently, and his mentation was described as disoriented. A left head turn was present. He was non-ambulatory but could stand with support. The thoracic limbs showed increased extension, and a severe proprioceptive ataxia was noted when assisted to walk. Postural reactions (knuckling and hopping) were absent in the thoracic limbs and decreased in the pelvic limbs. Limb reflexes tested were normal. Cranial nerve assessment revealed absent menace response bilaterally, present but decreased palpebral reflex, decreased sensation of the face and pinnae, and symmetrically mild atrophy of muscles of mastication. Given these neurological findings, neurolocalization was considered to likely be multifocal, with involvement of the brainstem and thalamus. Due to these findings and patient history, the leading differential was ODS, with other differentials that were considered less likely being an inflammatory or infectious process.

The patient was admitted for further diagnostics, supportive care, and monitoring. A minimal database was obtained. The chemistry profile revealed abnormalities of a sodium of 154 mmol/L (142–151), a potassium of 6 mmol/L (3.6–4.9), chloride of 123 mmol/L (105–117), calcium of 2.25 mmol/L (2.4–2.99), along with an albumin of 0.3897 mmol/L (0.451–0.647) and a total protein at 5.24 g/dL (5.50–7.70). The urinalysis and CBC results were within the institution's normal reference intervals. The patient was placed on an isotonic balanced crystalloid[3] at 32 ml/h and was administered dexamethasone SP[4] IV at 0.05 mg/kg/day. Over the following 24 h, the patient's neurological status continued to progress where he became more agitated and vocal, and his tetraparesis worsened so that he could no longer stand without support. Due to severe agitation, he was administered butorphanol[5] at 0.3 mg/kg IV, which did not change his clinical signs. He was then administered 0.5 mg/kg midazolam[6] IV, which temporarily alleviated his signs. However, his agitation worsened again rapidly with severe continual vocalization that manifested as paroxysmal events, which motivated initiation of levetiracetam[7] at 30 mg/kg IV q8h, for which an equivocal response was noted.

The following day, medical records from the patient's recent hospitalization were obtained, and it was noted that 9 days prior, the patient's initial serum sodium level was reported to be 106 mg/dL (144–160 mg/dL). During that hospitalization, the patient had received a 250 mL bolus of 0.9% NaCl[8], followed by 60 ml/h over the following 3 days (a total of 2,590 mL). There was no record of sodium levels being checked until time of referral; therefore, it is unknown how quickly the sodium level had risen.

On day three of hospitalization, the patient's clinical signs continued to progress where his mentation and agitation worsened, and he developed difficulty with prehension of food. For sedation, he was placed on both CRI's of dexmedetomidine[9] (1–5 mcg/kg/h) and midazolam (see text footnote 6; 0.1–0.5 mg/kg/h), which successfully limited his agitation to times of stimulation. The patient's electrolytes were monitored at minimum every 24 h, and his sodium had slightly increased from 154 to 155 mmol/L (142–151 mmol/L). The patient's potassium was noted to be decreasing from 4.2 mmol/L on presentation to 3.7 mmol/L (3.6–4.9 mmol/L). Therefore, spironolactone[10] (12.5 mg PO q24h) was added as a potassium-sparing diuretic in attempt to prevent further increase in the sodium level. The isotonic balanced crystalloid (see text footnote 3) was also discontinued and a hypotonic solution[11] was initiated at maintenance rate. Due to the patient's increased sedation and recumbency, a urinary catheter was placed to aid with nursing care and to allow monitoring of urine output.

On day four of hospitalization due to continued progression of clinical signs, the patient was anesthetized for MRI and CSF analysis. MRI showed a bilaterally symmetric T2W/T2-FLAIR hyperintense/T1 hypointense non-contrast enhancing lesion within the thalamus and to a lesser extent the caudal aspect of the caudate nuclei, rostral cerebral peduncles, and claustrum (see Figure 1). DWI showed hyperintense signal in the corresponding lesions on B0 images, and mildly hypointense signal on the B1000 (Figure 3). The ADC map showed hyperintense

1 Desoxycorticosterone Pivalate, Elanco Animal Health, Greenfield, IN.

2 Prednisone, West-ward Pharmaceutical Corp, Eatontown, NJ.

3 Normosol R®, Hospira, Lake Forest, IL.

4 Dexamethasone SP, Phoenix pharmaceutical, Burlingame, CA.

5 Butorphanol titrate, Zoetis, Parsippany, NJ.

6 Midazolam, Fresenius Kabi, Bensenville, IL.

7 Levetiracetam, Hospira, Lake Forest, IL.

8 NaCl 0.9%, Dechra, Overland Park, KS.

9 Dexmedetomidine hydrochloride, Dechra, Overland Park, KS.

10 Spironolactone, Accord healthcare, Durham, NC.

11 NaCl 0.45%, Dechra, Overland Park, KS.

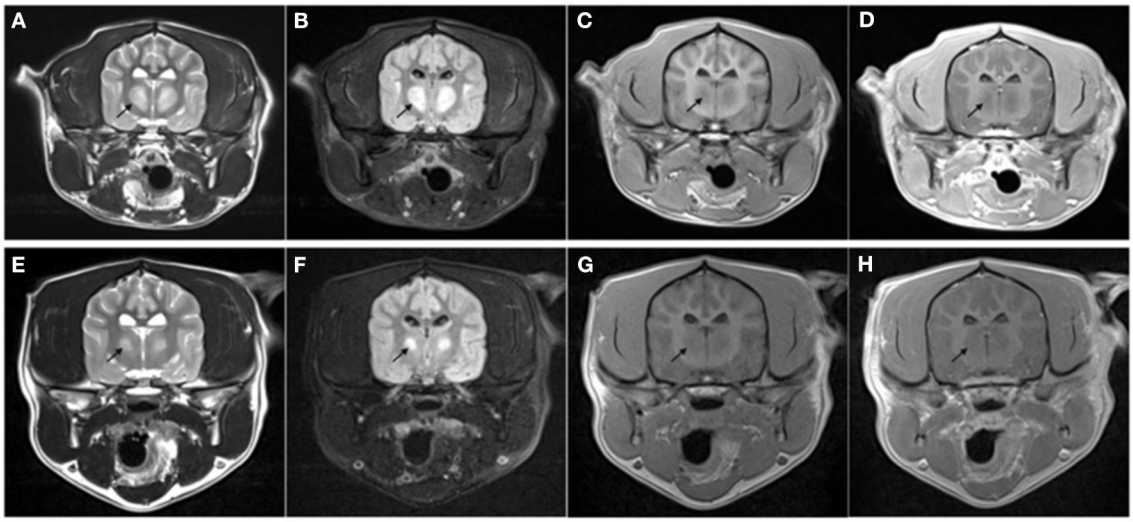

FIGURE 1
Transverse MRI images performed on day 4 of hospitalization **(A–D)** and at recheck 130 days later **(E–H)**. The images are at the level of the thalamus. T2-weighted **(A, E)**, T2 FLAIR **(B, F)**, T1-weighted pre- **(C, G)**, and post- **(D, H)** administration of intravenous gadolinium. Note the bilateral symmetric T2W and T2-FLAIR hyperintense [arrow in **(A, E)**], T1 hypointense non-contrast enhancing lesions present within the thalamus. The lesion was markedly reduced in size at follow-up MRI with the same MRI characteristics.

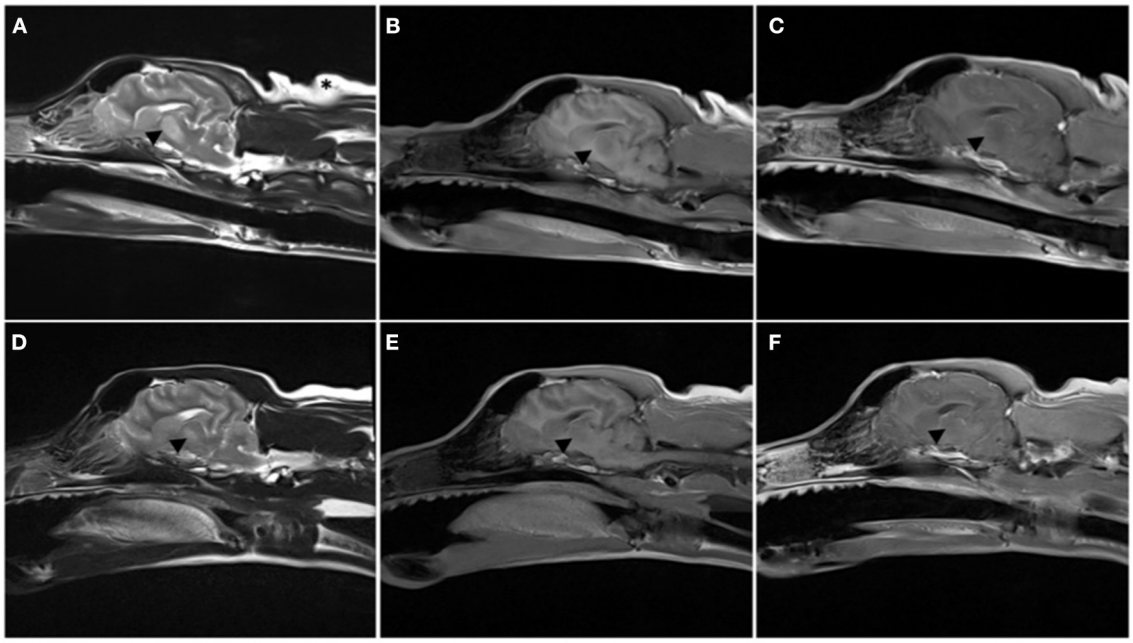

FIGURE 2
Parasagittal MRI images performed on day 4 of hospitalization **(A–C)** and at recheck 130 days later **(D–F)**. T2-weighted **(A, D)**, T1-weighted pre- **(B, E)**, and post- **(C, F)** administration of intravenous gadolinium. Note the T2W hyperintense lesion extending from the thalamus to the midbrain [arrowhead in **(A)**], T1 hypointense non contrast enhancing lesion is mostly present within the thalamus. The lesion was markedly reduced in size at follow-up MRI, only present in the thalamus, and with the same MRI characteristics.

signal in the same areas. These findings suggest lack of fluid restriction in the affected areas and would support vasogenic edema over cytotoxic edema. Given the patient's history MRI findings, progression, myelinolysis was considered the primary differential however, inflammatory/infectious process was also considered. Clinical pathologic review of CSF was cytologically unremarkable. Given the signalment at time of development of clinical signs, other demyelinating conditions were considered to be much less likely.

The findings were discussed with the owner and based on historical reports in both human and veterinary literature, a fair to guarded prognosis was given (2, 8, 9). The owner elected to continue supportive care and monitoring over the following

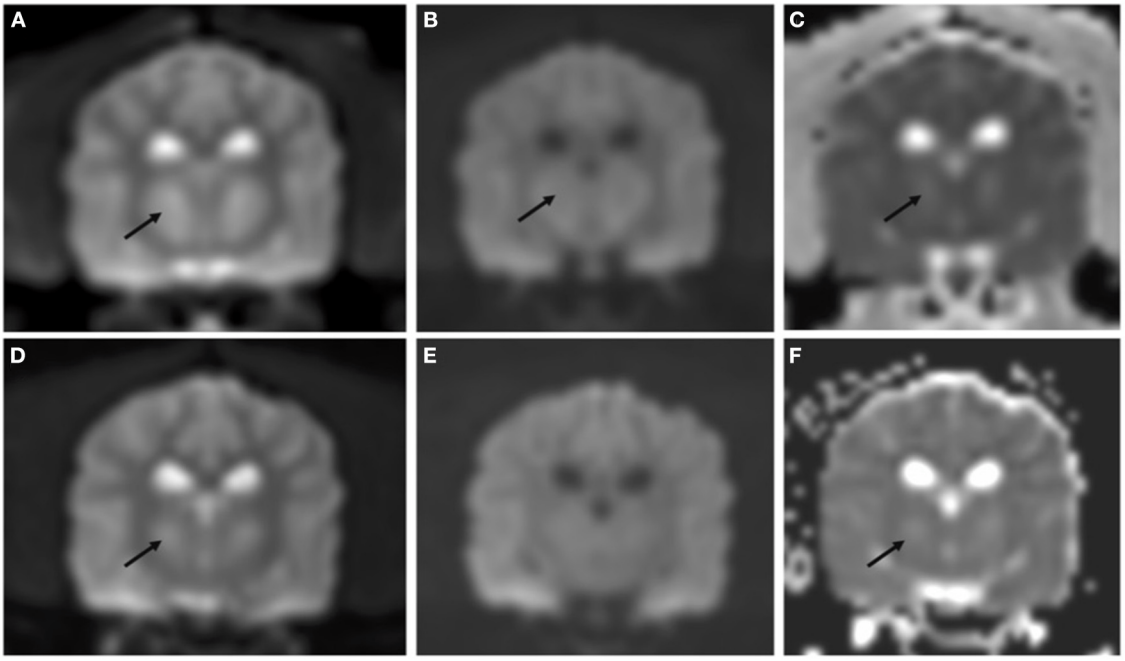

FIGURE 3
Transverse DWI and ADC map performed on day 4 of hospitalization **(A–C)** and at recheck 130 days later **(D–F)**. Bilateral symmetric hyperintensity on DWI B0 images **(A, D)** and ADC map **(C, F)** is most consistent with T2 shine through. DWI B1000 showed mild hypointensity [arrow in **(B)**] not present at the follow up MRI **(E)**, these findings were most consistent with non-restrictivity.

days. A nasogastric tube was administered to facilitate enteral nutrition. The patient's midazolam (see text footnote 6) and dexmedetomidine (see text footnote 9) infusions were continued. For additional sedation, a ketamine[12] CRI (0.1–0.5 mg/kg/h) was started, and a metoclopramide[13] CRI (5 mg/kg/day) was initiated for promotility effects to decrease risk of aspiration pneumonia. Liquid enteral nutrition[14] was initiated through his nasogastric tube.

On day five of hospitalization, the patient seemed more aware of his surroundings and appeared visual as witnessed by tracking movements. He was calmer and less hyperreactive. Physical therapy was initiated with range of motion and standing exercises. He continued to show marked improvement throughout the day and began to stand and ambulate independently. That evening he started to eat on his own. His urinary catheter, nasogastric tube and IV catheter were all removed. Metoclopramide (see text footnote 13) was discontinued, and the intravenous medications dexamethasone SP (see text footnote 4), ketamine (see text footnote 12), and dexmedetomidine (see text footnote 4) were discontinued and transitioned to oral prednisone (see text footnote 2; 0.5 mg/kg/day), amantadine[15] (0.4 mg/kg/day), and trazodone[16] (3–5 mg/kg/day), respectively.

The next day, the patient continued to improve. He was more ambulatory with improving ataxia and he exhibited less agitation. He was discharged on day seven with oral prednisone (see text footnote 2), amantadine (see text footnote 15), and trazodone (see text footnote 16). A recheck exam 1 week later revealed a normal neurological examination.

2.1. Follow up

The patient represented for follow-up imaging four and a half months later. The owner reported that clinically the patient was doing well and had resumed normal activity. A neurologic exam performed by the same clinicians revealed normal neurologic assessment. A brain MRI was repeated, showing improved bilaterally symmetric T2/T2 FLAIR hyperintense/T1 hypo- to isointense non-contrast enhancing lesion of the thalamus, that appeared moderately reduced in size and intensity, and no longer affected the midbrain, which was consistent with resolving myelinolysis. The lesions within the caudate nuclei, rostral cerebral peduncles, and claustrum were less evident (see Figures 1–3).

3. Discussion

ODS has been reported in human and canine patients following rapid correction of chronic hyponatremia and is associated with transient or permanent neurologic sequelae (1, 5, 6, 10). Dogs at risk of developing ODS include those that undergo rapid correction of chronic hyponatremia secondary to conditions such as intestinal parasitism, hypoadrenal crisis, chronic effusions, or liver dysfunction (5, 11–13).

12 Ketamine Hydrochloride, Dechra, Overland Park, KS.
13 Metoclopramide, Hospira, Lake Forest, IL.
14 Jevity, Abbott, Abbott Park, IL.
15 Amantadine, Actavis, Parsippany-Troy Hills, NJ.
16 Trazodone, Teva, Parsippany, NJ.

The influences of hyponatremia and associated treatments to the brain has been thoroughly reviewed (14). With hyponatremia, the brain takes adaptive measures to ensure the brain cell volume is tightly regulated. Initially, one protective physiologic measure is the shifting of fluid from parenchyma to CSF. The increase in intracranial pressure is postulated to cause hydrostatic water movement from brain tissue into CSF, where it will then be shifted into systemic circulation (15, 16). Additionally, inorganic osmolytes, such as electrolytes, followed by organic osmolytes will be expelled from the brain cells in the minutes to hours and hours to days after the development of hyponatremia, respectively. This reverses and prevents further intracellular movement of water and consequential cerebral edema. When sodium levels rise in a patient with chronic hyponatremia, the opposite processes take place. The brain cells take back the electrolytes and synthesize intracellular proteins and receptors to reuptake the previously secreted organic osmolytes. This process can take up to a week to return to the baseline, and if hyponatremia is corrected too quickly, then these compensatory responses are overwhelmed, and water is allowed to move outside of brain cells, causing shrinkage and apoptosis (15, 16). Furthermore, it was proposed that cytokine release from local inflammation may cause an increase in permeability of the blood brain barrier, allowing additional myelinolytic toxins to enter the privileged CNS, causing damage to the myelin (17). Recent studies suggest an early and central role of astrocyte injury and subsequent blood brain barrier damage. With the development of inflammation, axons may further degenerate, leading to neuronal degeneration (12, 18).

Formerly known as central pontine myelinolysis, this condition was originally thought to solely affect the pons. However, in humans, other locations have demonstrated lesions such as thalamus, cerebellum, lateral geniculate nuclei, and the external and extreme capsules (19). This is consistent with the lesion characteristic and distribution that has thus far been reported in the dog as well (5, 6). Other differentials that could be considered for bilaterally symmetric lesions would include enzyme deficiencies such as the gangliosidoses, toxicities (e.g., bromethalin toxicosis), or nutritional deficiencies (e.g., thiamine deficiency) (20, 21). However, the signalment, history, and lesion distribution differs than that in this condition. For example, dogs affected with gangliosidosis often show signs at a much younger age (22, 23). Thiamine deficiency may also show bilaterally symmetric lesions, however, MRI lesions have been demonstrated in the caudate nuclei, red nuclei, and caudal colliculi (24–26).

Treatment of ODS primarily consists of supportive care and much of the literature focuses on prevention through careful monitoring of sodium levels and slow correction of sodium over several hours to days. However, it is worth noting that experimental animal models showed it is the sodium level changes over 24 h more important than the hourly changes (27, 28). Some novel adjunctive therapies have been reported to help in the treatment of ODS, such as the use of therapeutic plasmapheresis or IVIG, indicating a potential immunological component to the disease process (2, 10, 18). The intravenous administration of myoinositol, a sugar alcohol, suggests improved survival in animal studies, and the use of thiamine supplementation and corticosteroids has also been documented in the treatment of ODS (18, 29). Other pharmacologic interventions described in people include the use of dopamine agonists to aid in the parkinsonian-like symptoms (30). One suggested therapy for treatment in the acute phase of ODS is the use of desmopressin and D5W[17] to rapidly relower sodium, suggesting that ODS is reversible for a short period of time, despite neurologic signs already occurring (10, 18, 31).

Importantly, in humans with ODS, MRI findings did not prognosticate outcome (2). Laureno et al. performed an experimental study where ODS was induced in dogs, and sequential daily brain MRI were performed up until 6 days. Some dogs showed changes on MRI prior to clinical signs of myelinolysis while other dogs showed clinical signs before changes were detected on imaging (6). These findings are consistent with the unpredictable timeline of clinical signs and imaging abnormalities in humans (2, 6, 10). DWI and ADC map were not supportive of restrictive lesions, unlike what has been reported in some cases of myelinolysis in people (32, 33). This may be due to different timelines in MRI studies; while MRI is typically performed immediately after the onset of clinical signs in people, the MRI study was performed 4 days after the onset of clinical signs in the dog of the present report. It is also possible that the lack of restrictivity may support vasogenic oedema over cytotoxic oedema.

The patient described in this study had a similar progression of clinical signs and was successfully discharged 9 days after the start of neurologic signs, comparably to other case reports in dogs (5, 11). In the described case, adequate pharmacologic support was an essential component of successful management. Midazolam (see text footnote 6), dexmedetomidine (see text footnote 9), and ketamine (see text footnote 12) were all used to facilitate appropriate nursing care, provide nutritional support, and perform blood sampling for monitoring of electrolytes. Midazolam (see text footnote 6) was chosen due to suspected seizure activity and the positive response from the patient. A low dose dexmedetomidine (see text footnote 9) CRI was chosen for its potential muscle relaxation, and ketamine (see text footnote 12) was used for its potential neuroprotective effects of preventing excitotoxic injury.

Lastly, dopamine agonists are chosen in people for its treatment of parkinsonian symptoms such as tremors and bradykinesia. Amantadine (see text footnote 15) is a dopamine agonist and weak antagonist of NMDA-type glutamate receptors. Because of these reports, the patient was started on amantadine (see text footnote 15) at an oral dose of 0.4 mg/kg daily once ketamine (see text footnote 12) infusion was discontinued and oral medications were tolerated. It is suggested that with the use of ketamine (see text footnote 12) and amantadine (see text footnote 15), optimizing dopamine concentration in the synaptic cleft and thus transmission to the post synaptic membrane may be recommended in other suspected or confirmed ODS cases that display tremors (34).

4. Concluding remarks

This case report describes the successful management and MRI of a patient with confirmed ODS. Brain MRI was performed at time of diagnosis and at time of follow-up, four and a half months after hospital discharge. This is the first known veterinary case report describing follow-up imaging of a canine after full neurologic recovery of ODS. In humans, patients can have evidence of near to full clinical recovery, yet imaging findings may still be abnormal

17 D5W, Dextrose with water, Baxter, Deerfield, IL.

(7, 35). Another human case report describes full clinical and radiographic recovery 5 months after therapy (10). In this case, the patient had full clinical recovery with evidence of persistent, yet improved myelinolysis. Dogs affected by myelinolysis show very severe clinical signs that may discourage treatment by fear of negative prognosis. However, this report provides evidence that prompt recognition of this pathology by MRI evaluation and intensive management with adequate pharmacologic and nursing support may allow successful improvement of neurological deficits and return to a normal life.

Data availability statement

The original contributions presented in the study are included in the article/supplementary material, further inquiries can be directed to the corresponding author.

Ethics statement

Written informed consent was obtained from the participant/patient(s) for the publication of this case report.

Author contributions

SH and AD wrote the first draft of the manuscript. All authors contributed to conception, design of the manuscript, manuscript revision, read, and approved the submitted version.

Conflict of interest

The authors declare that the research was conducted in the absence of any commercial or financial relationships that could be construed as a potential conflict of interest.

Publisher's note

References

1. Adams RD, Victor M, Mancall EL. Central pontine myelinolysis: A hitherto undescribed disease occurring in alcoholic and malnourished patients. *Archiv Neurol Psychiatry.* (1959) 81:154–72. doi: 10.1001/archneurpsyc.1959.02340140020004

2. Bose P. Central pontine myelinolysis and the osmotic demyelination syndromes: An open and shut case? *Acta Neurol Belg.* (2021) 2021:1–10. doi: 10.1007/s13760-021-01634-0

3. Norenberg MD, Leslie KO, Robertson AS. Association between rise in serum sodium and central pontine myelinolysis. *Ann Neurol.* (1982) 11:128–35. doi: 10.1002/ana.410110204

4. Nicaise C, Marneffe C, Bouchat J, Gilloteaux J. Osmotic demyelination: From an oligodendrocyte to an astrocyte perspective. *Int J Mol Sci.* (2019) 20:1124. doi: 10.3390/ijms20051124

5. Churcher R, Watson A, Eaton A. Suspected myelinolysis following rapid correction of hyponatremia in a dog. *J Am Anim Hosp Assoc.* (1999) 35:493–7. doi: 10.5326/15473317-35-6-493

6. Laureno R, Lamotte G, Mark AS. Sequential MRI in pontine and extrapontine myelinolysis following rapid correction of hyponatremia. *BMC Res Notes.* (2018) 11:707. doi: 10.1186/s13104-018-3816-5

7. Singh TD, Fugate JE, Rabinstein AA. Central pontine and extrapontine myelinolysis: A systematic review. *Eur J Neurol.* (2014) 21:1443–50. doi: 10.1111/ene.12571

8. Sterns RH, Cappuccio JD, Silver SM, Cohen EP. Neurologic sequelae after treatment of severe hyponatremia: A multicenter perspective. *J Am Soc Nephrol.* (1994) 4:1522–30. doi: 10.1681/ASN.V481522

9. Eze C, Agha YH, Duran B. Favorable outcomes following the use of triple therapy in a patient with osmotic demyelination syndrome. *Kans J Med.* (2020) (13):191–3. doi: 10.17161/kjm.v13i.13875

10. Wijayabandara M, Appuhamy S, Weerathunga P, Chang T. Effective treatment of osmotic demyelination syndrome with plasmapheresis: A case report and review of the literature. *J Medical Case Rep.* (2021) 15:6. doi: 10.1186/s13256-020-02573-9

11. O'Brien DP, Kroll RA, Johnson GC, Covert SJ, Nelson MJ. Myelinolysis after correction of hyponatremia in two dogs. *J Vet Intern Med.* (1994) 8:40–8. doi: 10.1111/j.1939-1676.1994.tb03194.x

12. Burton AG, Hopper K. Hyponatremia in dogs and cats. *J Vet Emerg Crit Car.* (2019) 29:461–71. doi: 10.1111/vec.12881

13. MacMillan KL. Complications following treatment of canine hypoadrenocorticism. *Can Vet J.* (2003) 44:490–2.

14. Kengne FG, Decaux G. Hyponatremia and the brain. *Kidney Int Rep.* (2018) 3:24–35. doi: 10.1016/j.ekir.2017.08.015

15. Hochwald GM, Wald A, Malhan C. The sink action of cerebrospinal fluid volume flow. Effect on brain water content. *Arch Neurol.* (1976) 33:339–44. doi: 10.1001/archneur.1976.00500050025005

16. Melton JE, Nattie EE. Brain and CSF water and ions during dilutional and isosmotic hyponatremia in the rat. *Am J Physiol.* (1983) 244:R724–32. doi: 10.1152/ajpregu.1983.244.5.R724

17. Kengne FG, Nicaise C, Soupart A, Boom A, Schietteatte J, Pochet R, et al. Astrocytes are an early target in osmotic demyelination syndrome. *J Am Soc Nephrol.* (2011) 22:1834–45. doi: 10.1681/ASN.2010111127

18. Nelson NR, Tompkins MG, Bastin MLT. Plasma exchange as treatment for osmotic demyelination syndrome: Case report and review of current literature. *Transfus Apher Sci.* (2019) 58:102663. doi: 10.1016/j.transci.2019.10.005

19. Lambeck J, Hieber M, DreBing A, Niesen WD. Central pontine myelinosis and osmotic demyelination syndrome. *Deutsches Ärzteblatt Int.* (2019) 116:600–6. doi: 10.3238/arztebl.2019.0600

20. Murthy VD, McLarty E, Woolard KD, Parker RL, Kortz G, King JN, et al. Case report: MRI, clinical, and pathological correlates of bromethalin toxicosis in three dogs. *Front Vet Sci.* (2022) 9:879007. doi: 10.3389/fvets.2022.879007

21. Kent M, Glass EN, Boozer L, Song RB, Hankin EJ, Barber RM, et al. Correlation of MRI with the neuropathologic changes in two cats with bromethalin intoxication. *J Am Anim Hosp Assoc.* (2019) 55:e55302. doi: 10.5326/JAAHA-MS-6724

22. Hasegawa D, Tamura S, Nakamoto Y, Matsuki N, Takahashi K, Fujita M, et al. Magnetic resonance findings of the corpus callosum in canine and feline lysosomal storage diseases. *PLoS ONE.* (2013) 8:e83455. doi: 10.1371/journal.pone.0083455

23. Hasegawa D, Yamato O, Nakamoto Y, Ozawa T, Yabuki A, Itamoto K, et al. Serial MRI features of canine GM1 gangliosidosis: A possible imaging biomarker for diagnosis and progression of the disease. *Sci World J.* (2012) 2012:250197. doi: 10.1100/2012/250197

24. Singh M, Thompdon M, Sullivan N, Child G. Thiamine deficiency in dogs due to the feeding of sulphite preserved meat. *Aust Vet J.* (2005) 83:412–7. doi: 10.1111/j.1751-0813.2005.tb13078.x

25. Garosi LS, Dennis R, Platt SR, Corletto F, de Lahunta A, Jakobs C. Thiamine deficiency in a dog: Clinical, clinicopathologic, and magnetic resonance imaging findings. *J Vet Intern Med.* (2003) 17:719–23. doi: 10.1111/j.1939-1676.2003.tb02507.x

26. Song J, Jung D. Thiamine deficiency in a dog associated with exclusive consumption of boiled sweet potato (Ipomoea batatas): Serial changes in clinical findings, magnetic resonance imaging findings and blood lactate and thiamine concentrations. *Vet Medicine Sci*. (2021) 7:69–76. doi: 10.1002/vms3.352

27. Soupart A, Penninckx R, Stenuit A, Perier O, Decaux G. Treatment of chronic hyponatremia in rats by intravenous saline: Comparison of rate versus magnitude of correction. *Kidney Int*. (1992) 41:1662–7. doi: 10.1038/ki.1992.239

28. Soupart A, Penninckx R, Crenier L, Stenuit A, Perier O, Decaux G. Prevention of brain demyelination in rats after excessive correction of chronic hyponatremia by serum sodium lowering. *Kidney Int*. (1994) 45:193–200. doi: 10.1038/ki.1994.23

29. Silver SM, Schroeder BM, Sterns RH, Rojiani AM. Myoinositol administration improves survival and reduces myelinolysis after rapid correction of chronic hyponatremia in rats. *J Neuropathol Exp Neurol*. (2006) 65:37–44. doi: 10.1097/01.jnen.0000195938.02292.39

30. Maraganore DM, Folger WN, Swanson JW, Ahiskog JE. Movement disorders as sequelae of central pontine myelinolysis: Report of three cases. *Mov Disord*. (1992) 7:142–8. doi: 10.1002/mds.870070208

31. Rondon-Berrios H. Therapeutic relowering of plasma sodium after overly rapid correction of hyponatremia: What is the evidence? *Clin J Am Soc Nephro*. (2019) 15:4880419. doi: 10.2215/CJN.04880419

32. Chu K, Kang DW, Ko SB, Kim M. Diffusion-weighted MR findings of central pontine and extrapontine myelinolysis. *Acta Neurol Scand*. (2001) 104:385–8. doi: 10.1034/j.1600-0404.2001.00096.x

33. Förster A, Nölte I, Wenz H, Al-Zghloul M, Kerl HU, Brockmann C, et al. Value of diffusion-weighted imaging in central pontine and extrapontine myelinolysis. *Neuroradiology*. (2013) 55:49–56. doi: 10.1007/s00234-012-1083-z

34. Dagur G, Khan SA. Current concepts in pontine myelinolysis: Review of literature. *Transl Biomed*. (2016) 6:38. doi: 10.21767/2172-0479.100038

35. Graff-Radford J, Fugate JE, Kaufmann TJ, Mandrekar JN, Rabinstein AA. Clinical and radiologic correlations of central pontine myelinolysis syndrome. *Mayo Clin Proc*. (2011) 86:1063–7. doi: 10.4065/mcp.2011.0239

frontiers | Frontiers in Veterinary Science

TYPE Case Report
PUBLISHED 25 May 2023
DOI 10.3389/fvets.2023.1201484

OPEN ACCESS

EDITED BY
Adriano Wang-Leandro,
University of Veterinary Medicine Hannover, Germany

REVIEWED BY
Sam Long,
Veterinary Referral Hospital, Australia
Aris Pourlis,
University of Thessaly, Greece

*CORRESPONDENCE
Diletta Dell'Apa
✉ diletta.dellapa@unipr.it

RECEIVED 06 April 2023
ACCEPTED 09 May 2023
PUBLISHED 25 May 2023

CITATION
Dell'Apa D, Fumeo M, Volta A, Bernardini M, Fidanzio F, Buffagni V, Christen M, Jagannathan V, Leeb T and Bianchi E (2023) Case report: Sacral agenesis in two boxer dogs: clinical presentation, diagnostic investigations, and outcome. *Front. Vet. Sci.* 10:1201484. doi: 10.3389/fvets.2023.1201484

Case report: Sacral agenesis in two boxer dogs: clinical presentation, diagnostic investigations, and outcome

Diletta Dell'Apa[1]*, Martina Fumeo[1], Antonella Volta[1], Marco Bernardini[2,3], Francesca Fidanzio[1], Valentina Buffagni[1], Matthias Christen[4], Vidhya Jagannathan[4], Tosso Leeb[4] and Ezio Bianchi[1]

[1]Department of Veterinary Science, University of Parma, Parma, Italy, [2]Neurodiagnostic Unit, Anicura Portoni Rossi Veterinary Hospital, Bologna, Italy, [3]Department of Animal Medicine, Production and Health, Clinical Section, University of Padua, Legnaro, Italy, [4]Vetsuisse Faculty, Institute of Genetics, University of Bern, Bern, Switzerland

Two boxer dogs from the same litter were presented at 3 months of age for urinary and fecal incontinence. Both dogs had an abnormal tail consisting of a small stump, an atonic anal sphincter, and absent perineal reflex and sensation. Neurological evaluation was indicative of a lesion of the cauda equina or sacral spinal cord. Radiology and CT scan of the spine displayed similar findings in the two dogs that were indicative of sacral agenesis. Indeed, they had 6 lumbar vertebrae followed by a lumbosacral transitional vertebra, lacking a complete spinous process, and a hypoplastic vertebra carrying 2 hypoplastic sacral transverse processes as the only remnant of the sacral bone. Caudal vertebrae were absent in one of the dogs. On MRI, one dog had a dural sac occupying the entire spinal canal and ending in a subfascial fat structure. In the other dog, the dural sac finished in an extracanalar, subfascial, well-defined cystic structure, communicating with the subarachnoid space, and consistent with a meningocele. Sacral agenesis—that is the partial or complete absence of the sacral bones—is a neural tube defect occasionally reported in humans with spina bifida occulta. Sacral agenesis has been described in human and veterinary medicine in association with conditions such as caudal regression syndrome, perosomus elumbis, and Currarino syndrome. These neural tube defects are caused by genetic and/or environmental factors. Despite thorough genetic investigation, no candidate variants in genes with known functional impact on bone development or sacral development could be found in the affected dogs. To the best of the authors' knowledge, this is the first report describing similar sacral agenesis in two related boxer dogs.

KEYWORDS

sacral agenesis, sacro-caudal dysgenesis, Currarino syndrome, spina bifida, congenital spine malformation, caudal regression syndrome

1. Introduction

Neural tube defects (NTD) are the most common human birth defects. In both humans and animals, these malformations can be caused by genetic or environmental factors. Genetic factors account for approximately 70% of human cases (1). Other non-genetic factors involved in the abnormal closure of the neural tube include drugs (e.g., valproic acid) (2),

environmental teratogens (industrial waste and pesticides) (3), and maternal factors like obesity, folic acid deficiency, diabetes mellitus, and hyperthermia during the first trimester of pregnancy (1, 4).

NTDs are usually divided into open and closed defects. The open defects are characterized by external protrusion and/or exposure of neural tissue, while in closed defects the neural tissue is covered by other tissue (4).

Spina bifida (SB) is an NTD caused by incomplete caudal neurulation (4). It results in the failure of fusion of one or more vertebral arches with or without protrusion of the meninges and the spinal cord. This malformation, with hemivertebrae and transitional vertebrae, frequently occurs in dogs with screw tails. Vertebral malformations do not necessarily produce neurological signs and are often seen in radiographs as incidental findings (5).

In humans, sacro-caudal dysgenesis and sacral agenesis (SA) are rarely described NTDs. These terms are used to identify a spectrum of malformations of the sacrum and caudal vertebrae of varying severity. In particular, the term SA identifies the partial or complete absence of the sacral bones. In these syndromes, the most frequent neurological signs are urinary and fecal incontinence, sometimes accompanied by hind limb paresis or paralysis (5).

In small animals, similar malformations have previously been reported in Manx cats and occasionally in dogs (6, 7). In Manx cats, sacro-caudal dysgenesis is well known and can also be associated with myelodysplasia, meningocele, meningomyelocele, tethered spinal cord, hydromyelia, and/or syringomyelia (8, 9). An autosomal dominant inheritance with incomplete penetrance has been demonstrated for this feline disease (7). The tailless phenotype and increased risk for sacro-caudal dysgenesis in Manx and other tailless cats is caused by variants in the *TBXT* gene encoding the T-box transcription factor T (10). Tailless or short-tailed phenotypes in several dog breeds are also caused by dominant alleles of the *TBXT* gene (11, 12).

Perosomus elumbis (PE) is a complex syndrome that has been commonly described in farm animals and more rarely in puppies. It is characterized by partial or complete agenesis of the lumbar, sacral, and coccygeal vertebra, and sometimes by other malformations involving the limbs, such as arthrogryposis (13, 14).

In this case report we describe the clinical signs, imaging, and electrodiagnostic findings and outcome of SA in two related boxer dogs. The results of genetic investigation are also reported.

2. Case description

Two 3-month-old intact female boxer dogs from the same litter were presented to the Veterinary Teaching Hospital (VTH) of the University of Parma for the presence of urinary and fecal incontinence since birth. The other four littermates and the parents did not present similar clinical signs.

On presentation, physical examination was unremarkable except for the tail, which appeared as a small stump in both dogs. Neurological examination revealed the presence in both dogs of an atonic anal sphincter and the absence of perineal reflex and nociception. No signs of paraparesis or sciatic nerve involvement were present. Hyperestesia of the lumbosacral spine was not detected. A cauda equina or sacral spinal cord lesion was suspected based on neurological examination. Differential diagnoses included, in particular, anomalous diseases such as SB associated with meningocele or meningomyelocele, sacral dysgenesis/agenesis, and other spine malformations.

A radiographic study of the lumbosacral spine was made in the two puppies in both lateral and ventro-dorsal views. Both patients showed six typically shaped lumbar vertebrae, followed by a lumbosacral transitional vertebra lacking the spinous process and a hypoplastic vertebra carrying two hypoplastic sacral transverse processes as the only remnant of the sacral bone. These findings were considered compatible with SA. Caudal vertebrae were absent in dog 1 (Figure 1A), while in dog 2 several coccygeal vertebrae not articulating with the rest of the spine were present (Figure 2A).

Ultrasound examination of the dorsal sacral region was carried out using a microconvex probe (6–10 MHz). In both patients, the spinal cord was visible, partially protruded caudally, due to the incomplete fusion of the dorsal lamina (Figure 3B). In dog 2, a well-defined anechoic oval 2 x 0.8 cm structure consistent with a meningocele was observed (Figure 4A).

At 4 months of age, complete blood count and blood chemistry values were unremarkable. In view of eventual surgical planning, an MRI (1.5 T, Vantage Elan, Canon Medical Systems Europe B.V., Zoetermeer, The Netherlands) of the lumbosacral spine was performed under general anesthesia with the dogs in dorsal recumbency. The imaging protocol included sagittal and transverse fast spin echo (FSE) T2-weighted (T2W) images [repetition time (ms) (TR)/echo time (ms) (TE), 3886–6353/108]; sagittal and transverse FSE T1-weighted (T1W) images (TR/TE, 480-745/14-15); transverse short tau inversion recovery (STIR) (TR/TE, 7139/48); 3D T1W fat suppressed gradient echo (GE) images (TR/TE, 32.2/5.5). No contrast medium was used. Besides the osteoarticular abnormalities in the radiographs, in dog 1, a dural sac occupying the entire spinal canal and ending abruptly in a subfascial, somewhat organized fat structure was observed (Figures 3A–C). In dog 2, the dural sac occupied the entire spinal canal and ended in a well-defined extracanalar, subfascial cystic structure, caudal to the spine and likely communicating with the subarachnoid space, and probably consisting of a meningocele, thus confirming ultrasound findings (Figure 4B). Surgical treatment of the meningocele was proposed but was declined by the owner. The dogs were discharged without medication, with the indication to monitor urination and defecation.

In the following months, urinary and fecal incontinence persisted without any other major symptoms. On the occasion of ovariohysterectomy, at 18 months of age, a computed tomography (CT) scan was performed as a follow-up. CT examination confirmed and better defined the skeletal malformations previously detected. In particular, both dogs presented L7 sacralization and partial sacral agenesis, consisting of the presence of a vestigial S1, and presenting a severely incomplete body that was not dorsally fused and had no spinous process, likely compatible with a SB (Figures 1B, 2B). The dural sac protruded caudally and dorsally in the subfascial fat, slightly in dog 1, while in dog 2 it formed a 1.3-cm oval hypoattenuating pouch compatible with meningocele. Needle electromyography (EMG) performed following CT scan revealed the presence of spontaneous pathological activity in the perineal muscles of both dogs, represented mainly by complex repetitive discharges.

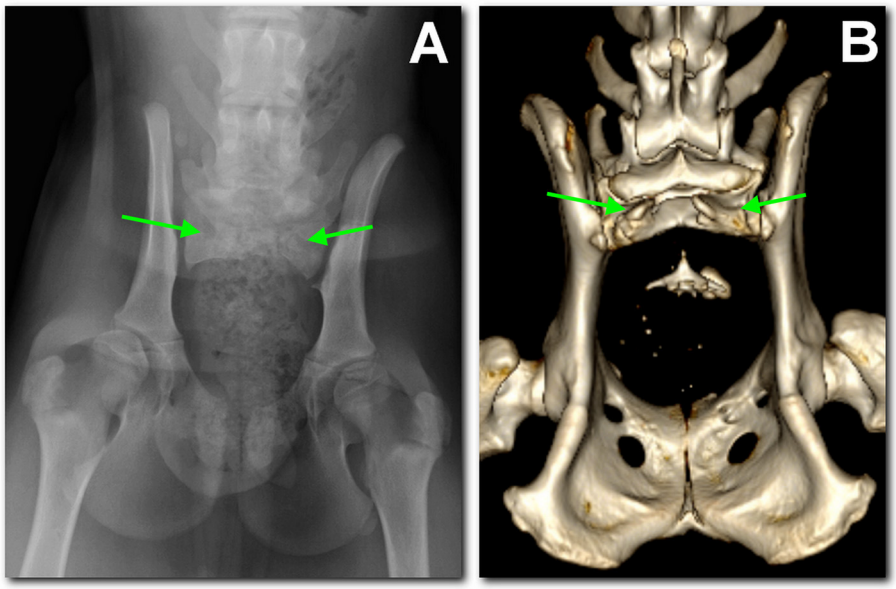

FIGURE 1
Dog 1, radiographic study with a ventro-dorsal projection of the pelvis performed at 3 months of age **(A)** in comparison to the tomographic 3D volume rendering reconstruction of the pelvis at 18 months of age **(B)**. There is sacralization of L7. Only S1 is present and hypoplastic; the dorsal part of the arch is not fused and has no spinal process (between arrows). Caudally, there is a single coccygeal vertebra not articulating with the sacrum.

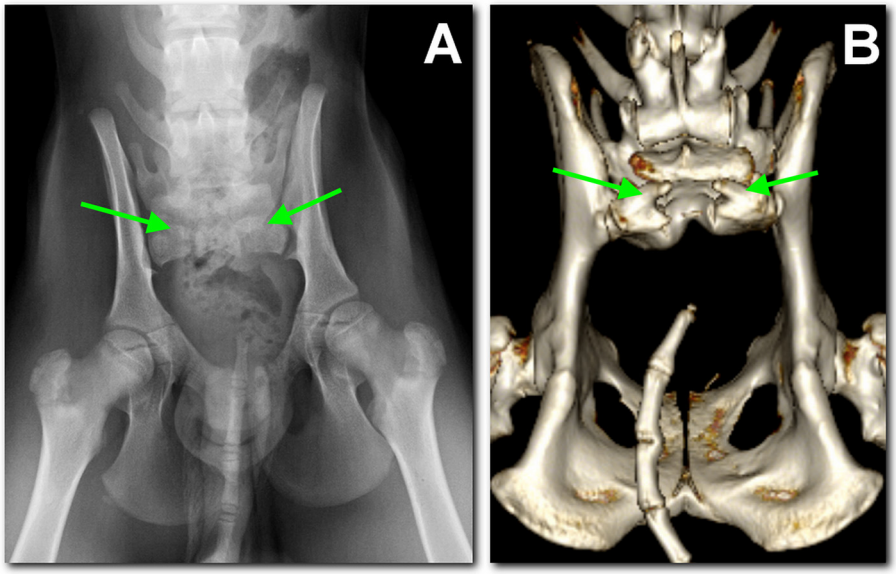

FIGURE 2
Dog 2, radiographic study with a ventro-dorsal projection of the pelvis performed at 3 months of age **(A)** in comparison to the tomographic 3D volume rendering reconstruction of the pelvis at 18 months of age **(B)**. Similar findings as in dog 1 are noted: L7 sacralization, S1 with spina bifida (between arrows), and sacral agenesis. Caudally, several coccygeal vertebrae are present, not articulating with S1.

To identify a potential causative genetic variant, whole genome 2 x 150 bp paired-end-sequencing at 20x coverage of one of the affected dogs was performed. The sequence data were deposited under study accession PRJEB16012 and sample accession SAMEA110415686 in the European Nucleotide Archive. The whole genome sequence data were compared to 924 control genomes (Supplementary Table 1), and variants particular to the boxer with sacral agenesis were identified as described (15). All identified private homozygous and private heterozygous variants are listed in Supplementary Table 2. None of these variants represented a strong plausible candidate for the sacral agenesis.

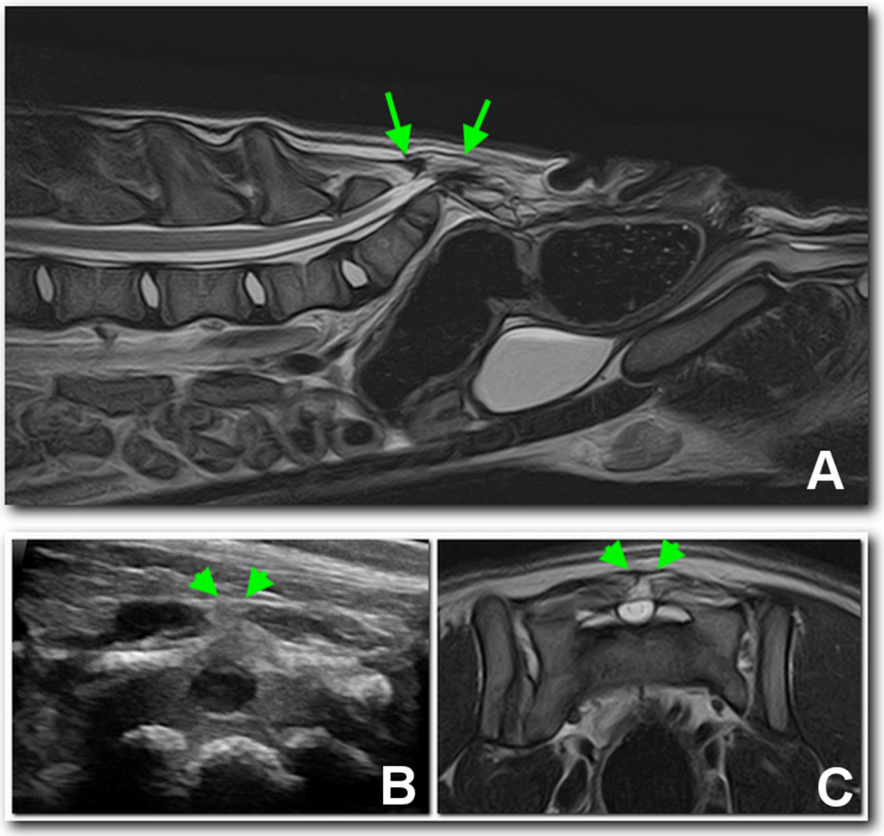

FIGURE 3
Sagittal **(A)** and transverse **(C)** T2 MRI images of the lumbosacral region of dog 1, compared with an ultrasonographic transverse scan **(B)** of the dorsal sacral aspect. A dural sac occupying the entire spinal canal protruding dorsally (arrows) and ending in a subfascial fat structure may be noted between the arrowheads.

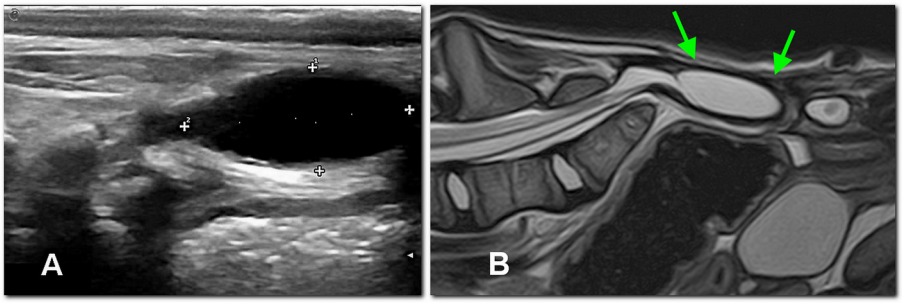

FIGURE 4
In dog 2, an extracanalar, well-defined subfascial cystic structure caudal to the spine, likely consisting of meningocele, is displayed between calipers by the ultrasonographic sagittal study **(A)** at 3 months of age and later confirmed by MRI [sagittal T2 image, **(B)**] at 4 months of age (arrows).

3. Discussion

In this case report we describe an NTD in two boxer dogs from the same litter. To precisely define the spinal anomaly present, the dogs underwent a complete diagnostic work-up that included various imaging modalities. In particular, radiology, ultrasonography, CT, and MRI performed at different stages of the dogs' growth were indicative of the presence of sacral agenesis (SA) associated with meningocele. Further, the incomplete S1 bone, which was not dorsally fused and had no spinous process, was compatible with an SB.

NTDs have a multifactorial etiology, with contributions from genetic, environmental and nutritional factors synergistically affecting normal embryonic development (3, 16).

During neurulation, the ectoderm grows in a longitudinal axis on the notochord and thickens to become a neural plate. Then, a neural groove appears as the edges of the neural plates become raised on each side of a midline depression, and, following the fusion of the edges in a bidirectional way, the neural tube is formed. In dogs, the closure starts in the cervical region and then progresses rostrally to form the future brain, and caudally to form the spinal cord. During this process, the ectoderm separates from the neural tube and fuses dorsally to create the overlying skin (17).

SB is an NTD reported in both humans and animals that results from the incomplete fusion of the dorsal lamina with or without protrusion of meninges (meningocele) or meninges and spinal cord (meningomyelocele). SB can also be classified as closed (occulta) or opened (manifesta/aperta) if there is communication between the neural tissue and the external environment. SA is occasionally reported in humans with SB occulta (5, 18–21).

SA with associated meningocele was initially identified in our patients at 3 months of age with radiographs and ultrasound of the lumbosacral spine. In human medicine, ultrasonography is also commonly used as a first-line screening test for spinal cord abnormalities in infants (9, 22). This rare malformation has previously occasionally been reported in dogs and in Manx cats (6, 7).

A more detailed characterization of SA and SB of the two subjects was possible in the following months with advanced imaging techniques (CT and MRI). Abnormalities similar to those detected in the two dogs have been reported in some rare syndromes described in humans and animals: Caudal regression syndrome (CRS), perosomus elumbis (PE), and Currarino syndrome (CS).

CRS is reported in humans, characterized by different degrees of anomaly of the caudal spinal cord and spine. In CRS there is the partial or total absence of the thoracic, lumbar, sacral, or coccygeal vertebrae associated with visceral organ malformations, but there is also imperforate anus and severe limb deformities. Diagnostic follow-up of suspicion can be made during pregnancy, detecting anomalies in the limbs and vertebral column with prenatal ultrasound. A prevalence of this congenital malformation has been identified in children of diabetic mothers, but other risk factor include cocaine and alcohol consumption. In children, walking disabilities are most commonly detected because of limb deformities (23–25).

SA is considered a part of CRS and can be classified into four types. In type I, there is partial or total unilateral agenesis localized to the sacrum; type II is characterized by partial bilaterally symmetrical agenesis with a firm articulation between the ilia and a normal or hypoplastic first sacral vertebra; in type III there is total sacral agenesis and a variable lumbar vertebra articulating with the ilia; and in type IV the sacrum is absent, while the caudal end plate of the lumbar vertebra is fused with the ilia. These anomalies are associated with a high prevalence of fecal incontinence and urinary symptoms (26, 27). Our patients display similarities with Type II SA.

SA is also a feature of CS, another syndrome reported in human medicine. Two forms of CS have been described: the classic form in which there is partial sacral agenesis, presacral mass (meningocele, lipoma, enteric cyst, teratoma, or a combination of these), and anorectal malformation, and the incomplete form in which only one or two of these malformations are present (28, 29). *HLBX9* gene variants have been reported in some CS patients (30–32). In the two boxer dogs included in the present study, anorectal malformation was absent, but presacral mass and SA were detected without other anomalies affecting the hind limbs.

PE is a rare complex congenital malformation that has been described in animals. It has been reported in only one dog, and one cat, and occasionally in cattle, buffalos, sheep, foals, pigs, rhesus macaques (*Macaca mulatta*), and it has been experimentally induced in mice (13, 33–43). As with CRS, animals with PE display agenesis of the caudal spinal cord and spine. Other signs associated with this syndrome are arthrogryposis and hypoplastic hind limbs, urogenital and intestinal tract defects, craniofacial malformation, synophthalmia, and brachygnatia. If the affected animal survives the first hours of life it usually displays severe difficulty in standing, due to the anomalies affecting the hind limbs and vertebra column. Euthanasia is usually performed, in light of the severity of this condition (34–36, 40).

In children, these congenital malformations require a multidisciplinary approach depending on the identified severity of anomalies. The diagnostic approach to fecal and urinary incontinence in patients with sacral anomalies is complex and involves various tests such as contrast colonography, colonic transit time, anorectal manometry, urodynamics, and EMG (44–46).

Unfortunately, tests for colonic function and urodynamic studies were not performed in these dogs. EMG in both dogs showed the presence of complex repetitive discharges of the perineal muscles as a possible consequence of chronic denervation. The absence of spontaneous pathologic activity at EMG of the muscles of the hind limbs further ruled out the presence of sciatic nerve involvement.

Early surgical treatment of meningocele/meningomyelocele associated with SB has been reported to improve neurological signs in some cases (18). Surgical treatment was declined by the owner, who considered the quality of life of the dogs to be good.

In the long-term follow-up (∼3 years from the first examination), the two boxer dogs remained clinically stable and developed no major complications as a result of their urinary and fecal incontinence.

The occurrence of sacral dysgenesis in more than one puppy from a litter with healthy parents and an uneventful pregnancy suggested a genetic disorder with autosomal recessive inheritance. Alternatively, a *de novo* mutation event in the germline of one of the two parents might have generated a dominant allele causing the SA. Despite extensive genetic investigation, no candidate variants in genes with known functional impact on bone development or sacral development were found. One cautionary note is that short read whole genome sequencing does not have 100% sensitivity in detecting all genetic variants. In particular, large structural variants involving more than ∼30 nucleotides are easily missed with the approach. Furthermore, gaps in the genome reference assembly or errors in the gene annotation of the dog genome might also explain why we were not able to identify a candidate for causative variant. The presence of environmental factors (toxic, nutritional, metabolic) as a possible cause of the malformation cannot be excluded.

Moreover, the concomitant presence of both genetic and non-genetic factors acting synergistically is also a possibility in the two boxer siblings. Indeed, in human medicine, the most reliable pathogenetic model for NTDs (*multifactorial threshold model*) considers either genetic and environmental factors on their own insufficient to affect neural tube closure. The concomitant presence of genetic and non-genetic factors is usually deemed necessary to induce NTDs (4).

To the best of the authors' knowledge, this is the first report of a similar SA in two related boxer dogs. Further studies including subjects with similar NTDs from this and other breeds should be performed in order to improve understanding of the role of genetic and non-genetic factors in these defects of neural tube closure.

Data availability statement

The datasets presented in this study can be found in online repositories. The names of the repository/repositories and accession number(s) can be found below: https://www.ncbi.nlm.nih.gov/biosample; SAMEA110415686.

Ethics statement

Ethical review and approval were not required for the animal study because the case report is a description of a clinical case. Written informed consent was obtained from the owners for the participation of their animals in this study.

Author contributions

DD, EB, MF, AV, and FF contributed to management of the case. MF and AV were in charge of the CT scan, and MB of the MRI. MC, VJ, and TL performed the genetic testing. DD, VB, MF, MC, MB, AV, TL, and EB participated in the review and editing of the manuscript. All authors contributed to the article and approved the submitted version.

Conflict of interest

The authors declare that the research was conducted in the absence of any commercial or financial relationships that could be construed as a potential conflict of interest.

Publisher's note

Supplementary material

The Supplementary Material for this article can be found online at: https://www.frontiersin.org/articles/10.3389/fvets.2023.1201484/full#supplementary-material

References

1. Finnell RH, Caiaffa CD, Kim SE, Lei Y, Steele J, Cao X, et al. Gene environment interactions in the etiology of neural tube defects. *Front Genet.* (2021) 12:659612. doi: 10.3389/fgene.2021.659612

2. Wlodarczyk BJ, Palacios AM, George TM, Finnell RH. Antiepileptic drugs and pregnancy outcomes. *Am J Med Genet A.* (2012) 158A:2071–90. doi: 10.1002/ajmg.a.35438

3. Copp AJ, Greene ND. Genetics and development of neural tube defects. *J Pathol.* (2010) 220:217–30. doi: 10.1002/path.2643

4. Avagliano L, Massa V, George TM, Qureshy S, Bulfamante GP, Finnell RH. Overview on neural tube defects: from development to physical characteristics. *Birth Defects Res.* (2019) 111:1455–67. doi: 10.1002/bdr2.1380

5. Westworth DR, Sturges BK. Congenital spinal malformations in small animals. *Vet Clin North Am Small Anim Pract.* (2010) 40:951–81. doi: 10.1016/j.cvsm.2010.05.009

6. Choi SY, Lee I, Cho NY, Shin BH, Lee KJ, Choi HJ, et al. Imaging diagnosis of sacrocaudal dysgenesis in a shih-tzu dog. *J Vet Clin.* (2016) 33:389–91. doi: 10.17555/jvc.2016.12.33.6.389

7. Deforest ME, Basrur PK. Malformations and the Manx syndrome in cats. *Can Vet J.* (1979) 20:304–14.

8. Leipold HW, Huston K, Blauch B, Guffy MM. Congenital defects on the caudal vertebral column and spinal cord in Manx cats. *J Am Vet Med Assoc.* (1974) 164:520–3.

9. Plummer SB, Bunch SE, Khoo LH, Spaulding KA, Kornegay JN. Tethered spinal cord and an intradural lipoma associated with a meningocele in a Manx-type cat. *J Am Vet Med Assoc.* (1993) 203:1159–61.

10. Buckingham KJ, McMillin MJ, Brassil MM, Shively KM, Magnaye KM, Cortes A, et al. Multiple mutant T alleles cause haploinsufficiency of Brachyury and short tails in Manx cats. *Mamm Genome.* (2013) 24:400–8. doi: 10.1007/s00335-013-9471-1

11. Haworth K, Putt W, Cattanach B, Breen M, Binns M, Lingaas P, et al. Canine homolog of the T-box transcription factor T; failure of the protein to bind to its DNA target leads to a short-tail phenotype. *Mamm Genome.* (2001) 12:212–8. doi: 10.1007/s003350010253

12. Hytönen MK, Grall A, Hédan B, Dréano S, Seguin SJ, Delattre D, et al. Ancestral T-box mutation is present in many, but not all, short-tailed dog breeds. *J Hered.* (2009) 100:236–40. doi: 10.1093/jhered/esn085

13. Amaral CB, Romão MA, Ferreira AM. Perosomus elumbis in a puppy. *J Comp Pathol.* (2012) 147:495–8. doi: 10.1016/j.jcpa.2012.03.003

14. Son JM, Yong HY, Lee DS, Choi HJ, Jeong SM, Lee YW, et al. A case of perosomus elumbis in a Holstein calf. *J Vet Med Sc.* (2008) 70:521–3. doi: 10.1292/jvms.70.521

15. Jagannathan V, Drögemüller C, Leeb T, Dog Biomedical Variant Database Consortium (DBVDC). A comprehensive biomedical variant catalogue based on whole genome sequences of 582 dogs and eight wolves. *Anim. Genet.* (2019) 50:695–704. doi: 10.1111/age.12834

16. Au KS, Ashley-Koch A, Northrup H. Epidemiologic and genetic aspects of spina bifida and other neural tube defects. *Dev Disabil Res Rev.* (2010) 16:6–15. doi: 10.1002/ddrr.93

17. Thomson C, Hahn C (editors). Neuroembriology. In: *Veterinary Neuroanatomy: A Clinical Approach*. St Louis: Saunders Elsevier Press (2012). p. 11–13.

18. Martín Muñiz L, Del Magno S, Gandini G, Pisoni L, Menchetti M, Foglia A, et al. Surgical outcomes of six bulldogs with spinal lumbosacral meningomyelocele or meningocele. *Vet Surg.* (2020) 49:200–6. doi: 10.1111/vsu.13342

19. Bertram S, Ter Haar G, De Decker S. Congenital malformations of the lumbosacral vertebral column are common in neurologically normal French bulldogs, English bulldogs, and pugs, with breed-specific differences. *Vet Radiol Ultrasound.* (2019) 60:400–8. doi: 10.1111/vru.12753

20. Song RB, Glass EN, Kent M. Spina bifida, meningomyelocele, and meningocele. *Vet Clin North Am Small Anim Pract.* (2016) 46:327–45. doi: 10.1016/j.cvsm.2015.10.007

21. Balioglu MB, Akman YE, Ucpunar H, Albayrak A, Kargin D, Atici Y, et al. Sacral agenesis: evaluation of accompanying pathologies in 38 cases, with analysis of long-term outcomes. *Childs Nerv Syst.* (2016) 32:1693–702. doi: 10.1007/s00381-016-3022-5

22. Ladino Torres MF, DiPietro MA. Spine ultrasound imaging in the newborn. *Semin Ultrasound CT MR.* (2014) 35:652–61. doi: 10.1053/j.sult.2014.08.001

23. Kylat RI, Bader M. Caudal regression syndrome. *Children.* (2020) 7:211. doi: 10.3390/children7110211

24. Singh SK, Singh RD, Sharma A. Caudal regression syndrome–case report and review of literature. *Pediatr Surg Int.* (2005) 21:578–81. doi: 10.1007/s00383-005-1451-4

25. Akhaddar A. Caudal regression syndrome (spinal thoraco-lumbo-sacro-coccygeal agenesis). *World Neurosurg.* (2020) 142:301–2. doi: 10.1016/j.wneu.2020.07.055

26. Dewberry L, Peña A, Mirsky D, Ketzer J, Bischoff A. Sacral agenesis and fecal incontinence: how to increase the index of suspicion. *Pediatr Surg Int.* (2019) 35:239–42. doi: 10.1007/s00383-018-4402-6

27. Macedo M, Martins JL, Freitas Filho LG. Sacral ratio and fecal continence in children with anorectal malformations. *BJU Int.* (2004) 94:893–4. doi: 10.1111/j.1464-410X.2004.05053.x

28. Garcia-Barceló MM, Chi-Hang Lui V, Miao X, So MT, Yuk-yu Leon T, Yuan ZW, et al. Mutational analysis of SHH and GLI3 in anorectal malformations. *Birth Defects Res A Clin Mol Teratol.* (2008) 82:644–8. doi: 10.1002/bdra.20482

29. Emans PJ, Kootstra G, Marcelis CL, Beuls EA, van Heurn LW. The Currarino triad: the variable expression. *J Pediatr Surg.* (2005) 40:1238–42. doi: 10.1016/j.jpedsurg.2005.05.004

30. Bevanda K, MemidŽan I, Boban-RaguŽ A. Caudal regression syndrome (Currarino syndrome) with chromosome mutation 9. *Radiology Case Rep.* (2020) 15:1184–8. doi: 10.1016/j.radcr.2020.05.023

31. Martucciello G, Torre M, Belloni E, Lerone M, Pini Prato A, Cama A, et al. Currarino syndrome: proposal of a diagnostic and therapeutic protocol. *J Pediatr Surg.* (2004) 39:1305–11. doi: 10.1016/j.jpedsurg.2004.05.003

32. Dworschak GC, Reutter HM, Ludwig M. Currarino syndrome: a comprehensive genetic review of a rare congenital disorder. *Orphanet J Rare Dis.* (2021) 16:167. doi: 10.1186/s13023-021-01799-0

33. Hybki GC, Murphy LA, Marchi JP, Patlogar JE, Brisson JO, Nakamura RK. Lumbosacral agenesis in a cat. *JFMS Open Rep.* (2016) 2:2055116916628555. doi: 10.1177/2055116916628555

34. Patrick T, Gonzalez O, Dick EJ, Jr, Kumar S. Perosomus elumbis in a stillborn rhesus macaque (Macaca mulatta): a case report. *J Med Primatol.* (2020) 49:110–2. doi: 10.1111/jmp.12459

35. Avedillo LJ, Camón J. Perosomus elumbis in a pig. *Vet Rec.* (2007) 160:127–9. doi: 10.1136/vr.160.4.127

36. Dennis SM. Perosomus elumbis in sheep. *Aust Vet J.* (1975) 51:135–6. doi: 10.1111/j.1751-0813.1975.tb09436.x

37. Jones CJ. Perosomus elumbis (vertebral agenesis and arthrogryposis) in a stillborn Holstein calf. *Vet Pathol.* (1999) 36:64–70. doi: 10.1354/vp.36-1-64

38. Balamurugan B., Pridhavidhar ReddyYV, Jyothi K. Surgical management of dystocia due to Perosomus elumbis in a nondescript buffalo. *J Entomol Zool Stud.* (2018) 6:2472–4.

39. Agerholm JS, Holm W, Schmidt M, Hyttel P, Fredholm M, McEvoy FJ. Perosomus elumbis in Danish Holstein cattle. *BMC Vet Res.* (2014) 10:227. doi: 10.1186/s12917-014-0227-2

40. Gerhauser I, Geburek F, Wohlsein P. Perosomus elumbis, cerebral aplasia, and spina bifida in an aborted thoroughbred foal. *Res Vet Sci.* (2012) 92:266–8. doi: 10.1016/j.rvsc.2010.11.009

41. Piegari G, D'Anza E, Costanza D, Prisco F, Meomartino L, d'Aquino I, et al. Perosomus elumbis in piglets: Pathological, radiological and cytogenetic findings. *Animals*. (2021) 11:1132. doi: 10.3390/ani11041132

42. Gentile A, Testoni S. Inherited disorders of cattle: a selected review. *Slov Vet Res.* (2006) 43:17–29.

43. Ehlers K, Stürje H, Merker HJ, Nau H. Valproic acid-induced spina bifida: a mouse model. *Teratology.* (1992) 45:145–54. doi: 10.1002/tera.1420450208

44. Shen ZY, Zhang J, Bai YZ, Zhang SC. Diagnosis and management of fecal incontinence in children and adolescents. *Front Pediatr.* (2022) 10:1034240. doi: 10.3389/fped.2022.1034240

45. Sinha S, Shah MA, Babu DM. Symptomatic lower urinary tract dysfunction in sacral agenesis: Potentially high risk? *Indian J Urol.* (2018) 34:56–61. doi: 10.4103/iju.IJU_184_17

46. Siroky MB. Electromyography of the perineal floor. *Urol Clin North Am.* (1996) 23:299–307. doi: 10.1016/S0094-0143(05)70312-8

frontiers | Frontiers in Veterinary Science

TYPE Original Research
PUBLISHED 13 July 2023
DOI 10.3389/fvets.2023.1183412

OPEN ACCESS

EDITED BY
Theresa Elizabeth Pancotto,
Virginia Tech, United States

REVIEWED BY
Giovanni Mogicato,
Ecole Nationale Vétérinaire de Toulouse (ENVT), France
Jean-Marie Graïc,
University of Padua, Italy

*CORRESPONDENCE
Hakyoung Yoon
✉ hyyoon@jbnu.ac.kr

RECEIVED 10 March 2023
ACCEPTED 27 June 2023
PUBLISHED 13 July 2023

CITATION
Kim J, Kwon D, Kim S-S, Lee K and Yoon H (2023) Measurement of brainstem diameter in small-breed dogs using magnetic resonance imaging.
Front. Vet. Sci. 10:1183412.
doi: 10.3389/fvets.2023.1183412

Measurement of brainstem diameter in small-breed dogs using magnetic resonance imaging

Jihyun Kim[1], Danbee Kwon[2], Sung-Soo Kim[3], Kichang Lee[1] and Hakyoung Yoon[1]*

[1]Department of Veterinary Medical Imaging, College of Veterinary Medicine, Jeonbuk National University, Iksan, Republic of Korea, [2]Bundang Leaders Animal Medical Center, Seongnam-si, Republic of Korea, [3]VIP Animal Medical Center, Seoul, Republic of Korea

Measurement of brainstem diameters (midbrain, pons, and medulla oblongata) is of potential clinical significance, as changes in brainstem size may decrease or increase due to age, neurodegenerative disorders, or neoplasms. In human medicine, numerous studies have reported the normal reference range of brainstem size, which is hitherto unexplored in veterinary medicine, particularly for small-breed dogs. Therefore, this study aims to investigate the reference range of brainstem diameters in small-breed dogs and to correlate the measurements with age, body weight (BW), and body condition score (BCS). Herein, magnetic resonance (MR) images of 544 small-breed dogs were evaluated. Based on the exclusion criteria, 193 dogs were included in the midbrain and pons evaluation, and of these, 119 dogs were included in the medulla oblongata evaluation. Using MR images, the height and width of the midbrain, pons, and medulla oblongata were measured on the median and transverse plane on the T1-weighted image. For the medulla oblongata, two points were measured for each height and width. The mean values of midbrain height (MH), midbrain width (MW), pons height (PH), pons width (PW), medulla oblongata height at the fourth ventricle level (MOHV), medulla oblongata height at the cervicomedullary (CM) junction level (MOHC), rostral medulla oblongata width (RMOW), and caudal medulla oblongata width (CMOW) were 7.18 ± 0.56 mm, 17.42 ± 1.21 mm, 9.73 ± 0.64 mm, 17.23 ± 1.21 mm, 6.06 ± 0.53 mm, 5.77 ± 0.40 mm, 18.93 ± 1.25 mm, and 10.12 ± 1.08 mm, respectively. No significant differences were found between male and female dogs for all the measurements. A negative correlation was found between age and midbrain diameter, including MH ($p < 0.001$) and MW ($p = 0.002$). All brainstem diameters were correlated positively with BW ($p < 0.05$). No significant correlation was found between BCS and all brainstem diameters. Brainstem diameters differed significantly between breeds ($p < 0.05$), except for MW ($p = 0.137$). This study assessed linear measurements of the brainstem diameter in small-breed dogs. We suggest that these results could be useful in assessing abnormal conditions of the brainstem in small-breed dogs.

KEYWORDS

canine, brainstem, midbrain, pons, medulla oblongata, size, age, body weight

1. Introduction

The brainstem—the caudoventral part of the cranial cavity, located between the diencephalon, cerebellum, and spinal cord (1, 2)—is composed of the midbrain (mesencephalon), pons (ventral metencephalon), and medulla oblongata (myelencephalon), and most of the cranial nerves originate from nuclei located in the midbrain through the medulla oblongata (1–6). The brainstem is the caudoventral part of the cranial cavity, located between the diencephalon, cerebellum, and spinal cord (1, 2). The brainstem plays an important role in the regulation of posture, consciousness, respiratory, and cardiovascular coordination (3–6). Therefore, clinical signs associated with brainstem dysfunction include disturbances of consciousness, gait abnormalities, cranial nerve deficits, postural abnormalities, abnormal respiratory activities, and autonomic dysfunction (3).

Magnetic resonance imaging (MRI) is a non-invasive modality that is widely used to detect brain lesions, including in the brainstem (7, 8). MRI provides accurate and detailed quantitative morphological information about the brainstem (5, 6, 9, 10). In previous human studies, linear measurement has been suggested as a reliable and rapid method for evaluating brainstem size, and a multitude of studies measuring the brainstem quantitatively have been reported (6, 9–16).

Studies establishing normal reference ranges of brainstem diameters in humans through linear measurements using MRI have been carried out (5, 9–15). Brainstem size has been found to decrease with the normal aging process (5, 9, 11–14). Furthermore, brainstem diameters decrease with neurodegenerative diseases, such as Parkinson's disease, progressive supranuclear palsy, or other atrophic processes (6, 16). Contrastingly, some diffusely infiltrating brain tumors increase the diameter of the brainstem with no marked signal change in the MR images (16). Consequently, knowledge of the morphology of the normal brainstem is crucial, not only to understand normal age-related degeneration but also to compare the pathophysiology of neurodegenerative disorders and detect neoplastic changes (11, 16).

Quantitative measurement of brainstem diameters in dogs using MRI has not yet been studied in veterinary medicine, and thus, there is a lack of normative data pertaining to the brainstem, particularly for small-breed dogs. Consequently, the aim of this study is to: (i) establish a reference range for brainstem diameters (midbrain, pons, and medulla oblongata) in small-breed dogs; (ii) analyze the statistical differences in brainstem diameters between sex and different breeds; and (iii) analyze the correlation between brainstem diameters and body weight (BW), body condition score (BCS), and age.

Abbreviations: BW, body weight; BCS, body condition score; MR, magnetic resonance; MRI, magnetic resonance imaging; MH, midbrain height; MW, midbrain width; PH, pons height; PW, pons width; MOHV, medulla oblongata height at the fourth ventricle level; MOHC, medulla oblongata height at the cervicomedullary junction level; RMOW, rostral medulla oblongata width; CMOW, caudal medulla oblongata width; CM, cervicomedullary; ICC, intraclass correlation coefficient; CI, confidence interval.

2. Materials and methods

2.1. Animals

This was a retrospective multicenter study. The medical records and brain MR images of 544 small-breed dogs who visited the Leaders Animal Medical Center and VIP Animal Medical Center from June 2019 to December 2022 were collected. Additionally, detailed medical information about each dog, including breed, sex, age, and BW, was collected. The following exclusion criteria were applied: presence of lesions in the parenchyma of the brainstem, any lesion in the brain parenchyma associated with neoplasia, inflammation, edema, hemorrhage, or infarction, clinically significant Chiari-like malformation or abnormalities at the craniocervical junction with or without syringomyelia, severe ventriculomegaly, or hydrocephalus. Consequently, 193 dogs were included for midbrain and pons measurement. Of these, 74 dogs with mild abnormalities at the craniocervical junctions were excluded, and 119 dogs were included for medulla oblongata measurement.

For the 193 dogs included in the midbrain pons measurement, the sex distribution was castrated males ($n = 99$), intact males ($n = 6$), spayed females ($n = 74$), and intact females ($n = 14$); the breed distribution was Chihuahua ($n = 12$), Maltese ($n = 59$), Mixed ($n = 18$), Pomeranian ($n = 35$), Poodle ($n = 33$), Shih Tzu ($n = 20$), and Yorkshire Terrier ($n = 16$); the mean age was 8.30 ± 3.95 (0.58–17.00) years; and the mean BW was 4.11 ± 1.67 kg (1.45–9.55 kg). For the 119 dogs included in the medulla oblongata measurement, the sex distribution was castrated males ($n = 63$), intact males ($n = 5$), spayed females ($n = 41$), and intact females ($n = 10$); the breed distribution was Chihuahua ($n = 9$), Maltese ($n = 35$), Mixed ($n = 11$), Pomeranian ($n = 14$), poodle ($n = 22$), Shih Tzu ($n = 19$), and Yorkshire Terrier ($n = 9$); the mean age was 8.47 ± 4.06 (0.67–17.00) years; and the mean BW was 4.53 ± 1.75 (1.45–9.55) kg. This study was approved by the Institutional Animal Care and Use Committee of Jeonbuk National University (Approval No. NON 2022-086).

2.2. Measurements

MR images of the brain were acquired using 1.5 Tesla MRI machines (GoldSeal Signa HDxt 1.5T, GE Healthcare, United States, and Signa Creator 1.5T, GE Healthcare, United States). In the study, the median and transverse planes of T1-weighted images (slice thickness: 2.5 or 3 mm, repetition time: TR = 400–1,790 ms, TE = 9–25 ms) were used for measurement. The median plane of the T1-weighted image was used for height measurement and the transverse plane of the T1-weighted image was used for width measurement.

Linear measurements of height and width of each of the following were performed: midbrain, pons, and medulla oblongata (Figure 1). For the midbrain, midbrain height (MH) was measured from the midpoint of the interpeduncular fossa to the margin of the cerebral aqueduct, perpendicular to the line of the interpeduncular fossa (Figure 1A). Midbrain width (MW) was measured by connecting both bilateral commissures of the medial geniculate body and brachium of the caudal colliculus (Figure 1B). For the pons, pons height (PH) was measured from the ventral margin of the pons to the margin of the fourth ventricle, perpendicular to the tangent line of the most ventral

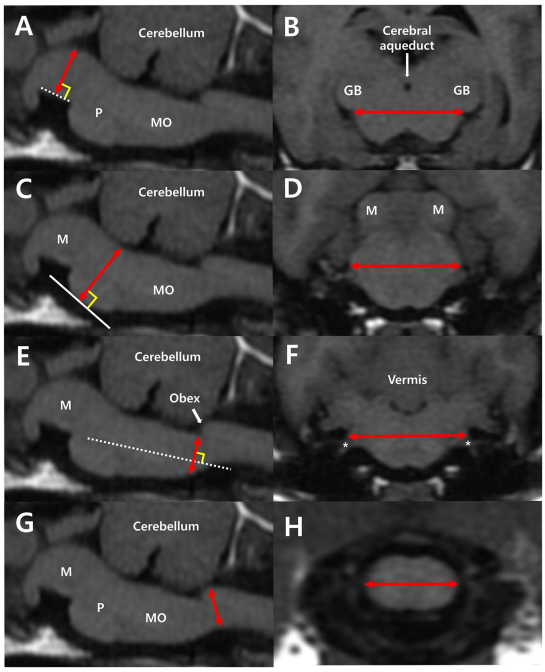

FIGURE 1
Median plane of the brainstem **(A,C,E,G)** and transverse plane of the midbrain **(B)**, pons **(D)**, and medulla oblongata **(F,H)** in T1-weighted MRI images. **(A)** Midbrain height (MH) was measured from the midpoint of the interpeduncular fossa to the margin of the cerebral aqueduct, perpendicular to the interpeduncular fossa (dotted line). **(B)** Midbrain width (MW) was measured by connecting both bilateral commissures of the medial geniculate body and the brachium of the caudal colliculus. **(C)** Pons height (PH) was measured from the ventral margin of the pons to the margin of the fourth ventricle, perpendicular to the tangent line (white line) of the most ventral point of the pons. **(D)** Pons width (PW) is the maximum width connecting both bilateral middle cerebellar peduncles. **(E)** Medulla oblongata height at the fourth ventricle level (MOHV) was measured from the kinking point at the level of the obex to the ventral margin of the medulla, perpendicular to the long axis of the medulla. **(F)** Rostral medulla oblongata width (RMOW) was measured from one end to the other of the bilateral cochlear nuclei. CN VIII (asterisk), the vestibulocochlear nerve, extends from the cochlear nuclei. **(G)** Medulla oblongata height at the CM junction (MOHC) is the diameter measured at the level of the CM junction. **(H)** Caudal medulla oblongata width (CMOW) is the widest width of the medulla at the level of the CM junction. M, midbrain; P, pons; MO, medulla oblongata; GB, geniculate body.

point of the pons (Figure 1C). Pons width (PW) was calculated by measuring the maximum width connecting both bilateral middle cerebellar peduncles (Figure 1D). The diameter of the medulla oblongata was measured at two different levels, one for height and one for width. The height of the medulla oblongata was measured at the fourth ventricle level and cervicomedullary (CM) junction level. The medulla oblongata height at the fourth ventricle level (MOHV) was measured from the kinking point at the level of the obex to the ventral margin of the medulla, perpendicular to the long axis of the medulla (Figure 1E). Medulla oblongata height at the CM junction (MOHC) was measured at the level of the CM junction (Figure 1G). The width of the medulla oblongata was measured at the rostral region and caudal region. Rostral medulla oblongata width (RMOW) was measured from end to end of the bilateral cochlear nuclei at the trapezoid level (Figure 1F). Caudal medulla oblongata width (CMOW) was obtained by measuring the greatest width of the medulla at the level of the CM junction (Figure 1H).

For intra-observer reliability analysis, measurements of all brainstem diameters (193 dogs for the midbrain and pons and 119 dogs for the medulla oblongata) were repeated twice by observer A (JK), and the mean values were used for all statistical analysis. For inter-observer reliability analysis, all brainstem diameters (193 dogs for the midbrain and pons; and 119 dogs for the medulla oblongata) were measured by observers A and B (Residents of the Veterinary Medical Imaging Department of the Teaching Hospital of Jeonbuk National University).

2.3. Statistics

All brainstem diameters are presented as mean ± standard deviation (SD). Linear regression analysis was used to analyze the correlation between brainstem diameter and "age, BW, and BCS." An Independent *t*-test was used to analyze the mean differences in brainstem diameter between sexes. One-way ANOVA was used to analyze the differences in brainstem diameter between breeds. Intra-observer and inter-observer reliability for all measurements was assessed using an absolute agreement-type intraclass correlation coefficient (ICC) with 95% confidence intervals (CI). IBM SPSS Statistics (version 27.0; IBB Corp., Armonk, NY, United States) was used for all the statistical analyses, and all experimental values were considered to be statistically significant at $p < 0.05$.

3. Results

Mean ± standard deviations of MH, MW, PH, PW, MOHV, MOHC, RMOW, and CMOW are summarized in Table 1.

3.1. Differences in brainstem diameter between sexes

The dogs were divided into two groups of males and females [for the midbrain and pons, males ($n = 105$), females ($n = 88$); for the medulla oblongata, males ($n = 68$), females ($n = 51$)]. Mean ± SD values of all brainstem diameters for each sex and the analysis of difference of each value between sexes are summarized in Table 2. There was no statistically significant difference between sex in MH ($p = 0.076$), MW ($p = 0.320$), PH ($p = 0.065$), PW ($p = 0.056$), MOHV ($p = 0.603$), MOHC ($p = 0.549$), RMOW ($p = 0.054$), and CMOW ($p = 0.702$).

3.2. Correlation between brainstem diameter and "age, BW, and BCS"

Correlations between brainstem diameter and "age, BW, and BCS" were analyzed through simple linear regression analysis. Scatter plots and the results of linear regression analysis are presented in Figures 2–4. All the brainstem diameters positively correlated with BW: MH ($p = 0.023$), MW ($p = 0.033$), PH ($p = 0.010$), PW ($p < 0.001$), MOHV ($p < 0.001$), MOHC ($p < 0.001$), RMOW ($p < 0.001$), and

TABLE 1 Mean and standard deviations of brainstem diameters.

Variables	*N*	Age (years)	BW (kg)	Mean±SD (mm) (range)
MH	193	8.30 ± 3.95 (0.58–17.00)	4.11 ± 1.67 (1.45–9.55)	7.18 ± 0.56 (4.80–8.70)
MW				17.42 ± 1.21 (12.30–20.10)
PH				9.73 ± 0.64 (7.76–11.60)
PW				17.23 ± 1.21 (13.65–20.60)
MOHV	119	8.47 ± 4.06 (0.67–17.00)	4.53 ± 1.75 (1.45–9.55)	6.06 ± 0.53 (4.80–7.44)
MOHC				5.77 ± 0.40 (4.95–6.98)
RMOW				18.93 ± 1.25 (15.9–23.95)
CMOW				10.12 ± 1.08 (8.17–14.05)

BW, body weight; SD, standard deviation; MH, midbrain height; MW, midbrain width; PH, pons height; PW, pons width; MOHV, medulla oblongata height at the fourth ventricle level; MOHC, medulla oblongata height at the CM junction; RMOW, rostral medulla oblongata width; CMOW, caudal medulla oblongata width.

TABLE 2 Mean and standard deviation of all brainstem diameter values by sex and analysis of the difference in each value between sexes using an independent *t*-test.

	N	Mean±SD (mm)		*p*-value
		Male	Female	
MH	Male ($n = 105$)	7.11 ± 0.61	7.25 ± 0.48	0.076
MW		17.50 ± 1.26	17.33 ± 1.14	0.320
PH	Female ($n = 88$)	9.65 ± 0.62	9.82 ± 0.67	0.065
PW		17.38 ± 1.22	17.04 ± 1.19	0.056
MOHV	Male ($n = 68$)	6.04 ± 0.46	6.09 ± 0.62	0.603
MOHC		5.79 ± 0.42	5.75 ± 0.38	0.549
RMOW	Female ($n = 51$)	19.12 ± 1.15	18.68 ± 1.35	0.054
CMOW		10.15 ± 0.98	10.07 ± 1.21	0.702

SD, standard deviation; MH, midbrain height; MW, midbrain width; PH, pons height; PW, pons width; MOHV, medulla oblongata height at the fourth ventricle level; MOHC, medulla oblongata height at the cervicomedullary junction; RMOW, rostral medulla oblongata width; CMOW, caudal medulla oblongata width.

CMOW ($p = 0.003$). On the other hand, none of the parameters correlated significantly with BCS. However, there was a significantly positive correlation between brainstem diameter and the BW/BCS index in all brainstem diameters, in contrast to the correlation between BCS alone. In the correlation between age and brainstem diameter, MH ($p < 0.001$) and MW ($p = 0.002$) were negatively correlated with age. PH, PW, MOHV, MOHC, RMOW, and CMOW were not significantly correlated with age.

3.3. Differences in brainstem diameters between breeds

Differences in brainstem diameters were analyzed in seven small breeds (Chihuahua, Maltese, Mixed, Pomeranian, Poodle, Shih Tzu, and Yorkshire Terrier). Apart from MW ($p = 0.137$), the remaining values, including MH ($p < 0.001$), PH ($p = 0.006$), PW ($p = 0.003$), MOHV ($p < 0.001$), MOHC ($p < 0.001$), RMOW ($p = 0.004$), and CMOW ($p = 0.008$), had significant differences between breeds (Figure 5). Mean ± standard deviations of brainstem diameters categorized by breed are summarized in Tables 3, 4.

3.4. Intra-observer and inter-observer reliability

Observer A measured all values of the brainstem diameter twice. There was excellent reliability for the two measurements in all the brainstem diameters. The ICC for each brainstem diameter was: 0.992 (95% CI: 0.990–0.994) in MH; 0.981 (95% CI: 0.975–0.986) in MW; 0.992 (95% CI: 0.990–0.994) in PH; 0.983 (95% CI: 0.977–0.987) in PW; 0.997 (95% CI: 0.995–0.998) in MOHV; 0.992 (95% CI: 0.995–0.998) in MOHC; 0.984 (95% CI: 0.977–0.989) in RMOW; and 0.991 (95% CI: 0.987–0.994) in CMOW. The *p*-value for all values was <0.001.

All values were measured by two clinicians, observers A and B. There was excellent reliability for the two measurements in all the brainstem diameters. The ICC for each brainstem diameter was 0.945 (95% CI: 0.922–0.960) in MH; 0.942 (95% CI: 0.923–956) in MW; 0.959 (95% CI: 0.945–969) in PH; 0.968 (95% CI: 0.958–0.976) in PW; 0.886 (95% CI: 0.833–0.922) in MOHV; 0.907 (95% CI: 0.863–0.936) in MOHC; 0.946 (95% CI: 0.922–0.962) in RMOW; and 0.910 (95% CI: 0.836–0.946) in CMOW. The *p*-value for all values was <0.001.

4. Discussion

In this present study, we aimed to perform linear measurements of brainstem diameters, including the height and width of the midbrain, pons, and medulla oblongata. MR images of 193 dogs were evaluated and reference ranges of brainstem size in small-breed dogs were obtained. We present reference ranges of width and height for the midbrain, pons, and medulla oblongata for small-breed dogs.

This study found there was no significant difference between sexes in terms of brainstem diameters and this finding is in agreement with previous human studies (5, 10–14, 17, 18). In some human studies, there was only a difference in brainstem size between sexes in the age group of 50 or older (15, 19); another study demonstrated differences in midbrain or pons size; however, they did not categorize the groups by age (9, 20). In humans, differences in brainstem size between sexes may be attributed to the correlation with the larger total intracranial volume in males (15, 17). Significant brainstem shrinkage may be owing to intrinsic or extrinsic factors such as hormones, hypertension, or interactions with environmental factors, however, it has not been clarified thoroughly (15, 19). In the present study, mean values of MH, PH, and MOHV were slightly higher in females, whereas mean values of MW, PW, MOHC, RMOW, and CMOW were slightly higher in males, but this difference was not statistically significant. There was a significant difference in mean BW between males and females (larger in males). It was considered that there might be differences in the structure of the calvarium between the various breeds included in the sample population of this study (21, 22).

Results of the present study showed a positive correlation with BW; this is similar to the findings of previous studies of brain area

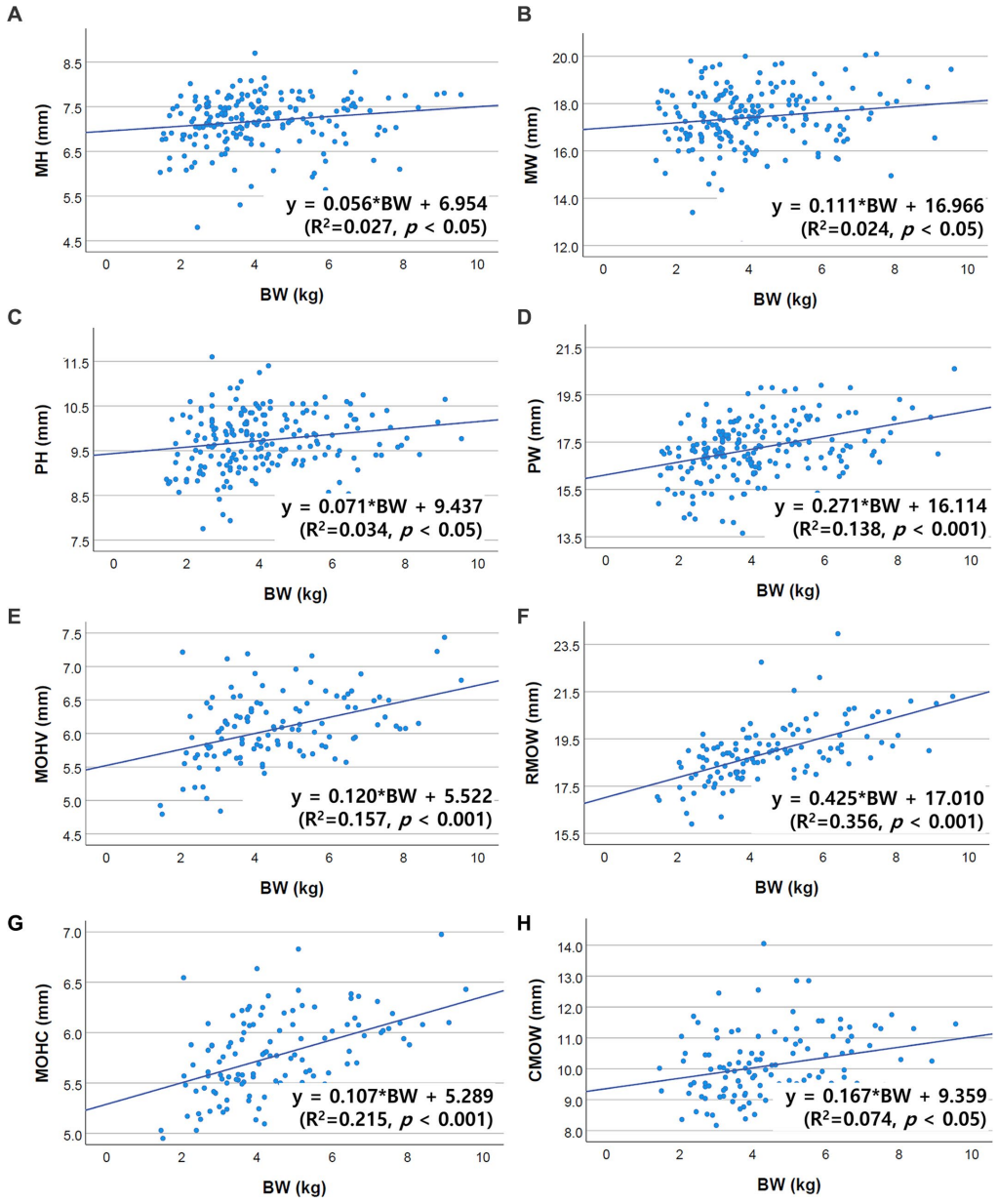

FIGURE 2
Scatter plots of the linear regression analysis of the relationship between BW and brainstem diameter. All brainstem diameters showed significant positive correlations with BW. **(A)** Positive correlation between MH and BW (R^2=0.027, p<0.05). **(B)** Positive correlation between MW and BW (R^2=0.024, p<0.05). **(C)** Positive correlation between PH and BW (R^2=0.034, p<0.05). **(D)** Positive correlation between PW and BW (R^2=0.138, p<0.001). **(E)** Positive correlation between MOHV and BW (R^2=0.157, p<0.001). **(F)** Positive correlation between RMOW and BW (R^2=0.356, p<0.001). **(G)** Positive correlation between MOHC and BW (R^2=0.215, p<0.001). **(H)** Positive correlation between CMOW and BW (R^2=0.074, p<0.05).

(including the brainstem) in dogs (22, 23). The relationship between BCS and brainstem diameter was also considered in this study. BCS alone had no significant correlation with brainstem diameter. However, BW/BCS showed a positive correlation with brainstem diameter. The BCS may correlate negatively with brainstem diameter as obesity has a negative correlation with an index of physique (24). It is assumed that the reason for the lack of correlation between brainstem diameter and the BCS is the BCS of the dogs included for the measurement was mostly between four and six and the proportion of the dogs with extreme BCS was relatively low. As the BW/BCS index positively correlated with brainstem diameter, it could be more accurate to use the BW/BCS index in dogs with extreme BCS to evaluate normal ranges of brainstem size; however, using BW alone could be also accurate in dogs with an ideal BCS.

Only midbrain diameter (MH, MW) was negatively correlated with age, and no other values (PH, PW, MOHV, MOHC, RMOW, and CMOW) were significantly correlated with age. Several human imaging studies have reported a variation in the changes in different brain regions with age and volume loss with age depending on the brain area (5, 9–20, 25–28). Particularly in the human brainstem, a significant age-related decrease in midbrain area was confirmed (5,

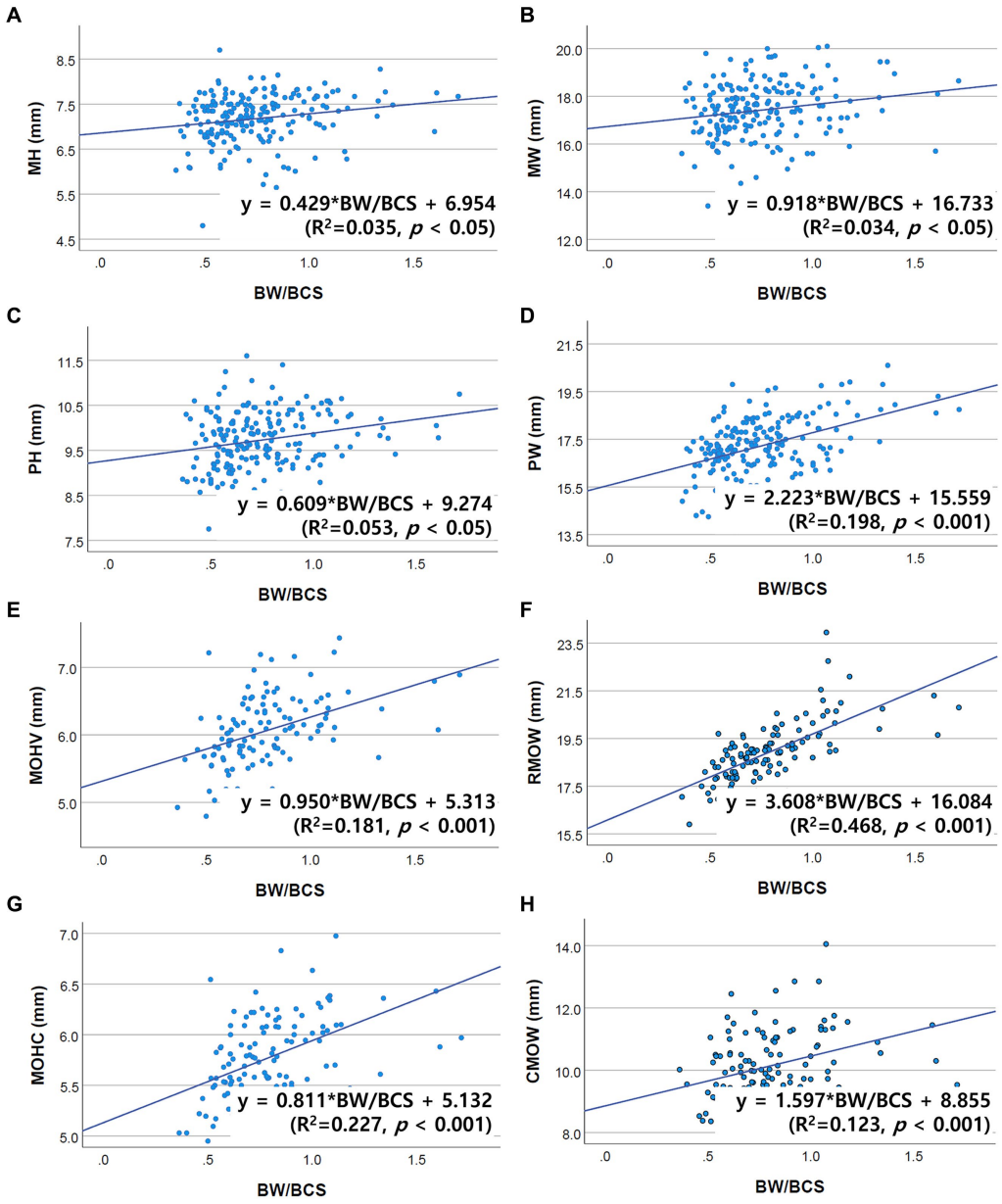

FIGURE 3
Scatter plots of the linear regression analysis of the relationship between the BW/BCS index and brainstem diameter. All brainstem diameters were significantly positively correlated with the BW/BCS index. **(A)** Positive correlation between MH and BW/BCS (R^2=0.035, p<0.05). **(B)** Positive correlation between MW and BW/BCS (R^2=0.034, p<0.05). **(C)** Positive correlation between PH and BW/BCS (R^2=0.053, p<0.05). **(D)** Positive correlation between PW and BW/BCS (R^2=0.198, p<0.001). **(E)** Positive correlation between MOHV and BW/BCS (R^2=0.181, p<0.001). **(F)** Positive correlation between RMOW and BW/BCS (R^2=0.468, p<0.001). **(G)** Positive correlation between MOHC and BW/BCS (R^2=0.227, p<0.001). **(H)** Positive correlation between CMOW and BW/BCS (R^2=0.123, p<0.001).

9, 11–14, 16, 17, 19, 20, 29). For the pons and medulla, no significant correlation with age was identified (9–11, 13, 17–19, 27–29). Additionally, a minimal decline in the pons and medulla oblongata with aging was found in a few studies but the significance was not clear (5, 12). These aforementioned findings are in accordance with our results.

Physiological or pathological changes of the brain in aging dogs resemble the changes found in humans (21, 22, 30, 31). In dogs, cerebral atrophy, including findings such as widening of the cerebral sulci, ventriculomegaly, a decrease in frontal lobe volume, a decrease in interthalamic adhesion, and a decrease in the hippocampus, can be found in normal aging dogs (22, 23, 29–31). These changes may have multifactorial etiopathogenesis associated with β amyloid deposition, oxidative damage, decreased glycosphingolipids, neuronal shrinkage, neurotransmitter deficits, or decreased neurogenesis (21, 23, 30, 32). Although age changes of the brainstem have not been broadly studied in dogs, it has been demonstrated that hypointensity of the substantia nigra in the T2-weighted image is

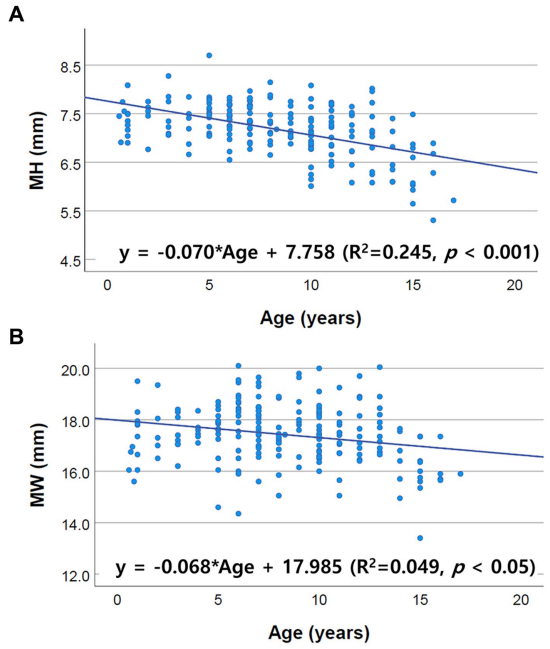

FIGURE 4
Scatter plots of the linear regression analysis of the relationship between age and brainstem diameter. Only MH and MW correlated negatively with age. The other values, including PH, PW, MOHV, MOHC, RMOW and CMOW, had no significant correlation with age. **(A)** Negative correlation between MH and age (R^2=0.245, p<0.001). **(B)** Negative correlation between MW and age (R^2=0.049, p<0.05).

TABLE 3 Mean and standard deviations of midbrain and pons diameter values in groups divided by breed (Chihuahua, Maltese, Mixed, Pomeranian, Poodle, Shih Tzu, Yorkshire Terrier).

Breed	MH	MW	PH	PW
Chihuahua (n=12)	7.25 ± 0.29	17.61 ± 1.07	9.97 ± 0.68	16.71 ± 0.73
Maltese (n=59)	7.00 ± 0.58	17.52 ± 1.24	9.84 ± 0.68	17.02 ± 1.32
Mixed (n=18)	7.25 ± 0.46	17.15 ± 1.00	9.67 ± 0.70	17.86 ± 1.47
Pomeranian (n=35)	7.34 ± 0.37	16.93 ± 1.15	9.35 ± 0.57	16.90 ± 1.00
Poodle (n=33)	7.42 ± 0.55	17.70 ± 1.09	9.85 ± 0.62	17.81 ± 1.15
Shih Tzu (n=20)	6.71 ± 0.70	17.60 ± 1.54	9.69 ± 0.59	17.07 ± 0.96
Yorkshire Terrier (n=16)	7.41 ± 0.35	17.51 ± 1.14	9.83 ± 0.48	17.38 ± 1.13

MH, midbrain height; MW, midbrain width; PH, pons height; PW, pons width.

TABLE 4 Mean and standard deviations of medulla oblongata diameter values in groups divided by breed (Chihuahua, Maltese, Mixed, Pomeranian, Poodle, Shih Tzu, Yorkshire Terrier).

Breed	MOHV	MOHC	RMOW	CMOW
Chihuahua (n=9)	5.95 ± 0.72	5.83 ± 0.38	18.61 ± 0.67	9.96 ± 1.25
Maltese (n=35)	5.87 ± 0.52	5.60 ± 0.38	18.39 ± 0.79	9.68 ± 0.84
Mixed (n=11)	6.49 ± 0.30	5.92 ± 0.40	19.43 ± 1.47	10.16 ± 0.74
Pomeranian (n=14)	6.07 ± 0.49	5.58 ± 0.38	18.66 ± 1.25	9.87 ± 1.20
Poodle (n=22)	6.39 ± 0.35	6.07 ± 0.41	19.52 ± 1.45	10.83 ± 1.25
Shih Tzu (n=19)	6.02 ± 0.51	5.79 ± 0.31	19.44 ± 1.47	10.27 ± 1.04
Yorkshire Terrier (n=9)	5.69 ± 0.47	5.76 ± 0.34	18.67 ± 0.91	10.23 ± 0.80

MOHV, medulla oblongata height at the fourth ventricle level; MOHC, medulla oblongata height at the CM junction; RMOW, rostral medulla oblongata width; CMOW, caudal medulla oblongata width.

associated with iron accumulation resulting from the metabolism of neurotransmitters (31, 33–35). In the human brainstem, prominent age-related decline of midbrain size has been reported (5, 9, 11–14, 16, 17, 19, 20, 29), consistent with the present study. The midbrain has fibers and numerous nuclear masses in the tegmentum and a decrease in midbrain size has been attributed to neuronal death or degeneration (6, 15, 17, 29). Shrinkage of the substantia nigra with a decrease in the number of neurons has also been reported (12, 15, 17, 36). These aging changes in humans can be suggested as the reason for the result in this study, i.e., that the midbrain diameter shrinks with aging in dogs. Besides changing with age, brainstem size can decrease or increase depending on pathological changes. The size or diameter of the brainstem decreases through atrophy associated with neurodegenerative disorders, and these structural measurements play an important role in diagnosis in humans (6, 9, 37). Furthermore, some diffusely infiltrating tumors, such as gliomas, may be detected through an increase in size, without observable differences in signal intensities due to changes in relaxation times (16).

In the present study, there were significant differences in brainstem diameters between breeds. All values, except MW, were significantly different between breeds. There were a number of breeds that presented significant differences for each measurement, as shown in Figure 4. The shape or volume of the skull and brain structure vary depending on the breed or size of the dog (21, 22, 32, 38–40). Particularly, the Maltese differed from other breeds in most measurements, and most of the mean values, except PH, were significantly smaller than other breeds. This would have contributed to BW distribution, as the mean BW of the Maltese was relatively low compared with that of other breeds.

ICC with 95% CI was used in intra-observer and inter-observer reliability analyses. Interclass correlation was interpreted by criteria according to Fleiss (41): values <0.40 were considered poor agreement, values between 0.40 and 0.75 were considered fair to good agreement, and values >0.75 were considered excellent agreement (41). Intra-and inter-observer reliability analysis showed excellent agreement in all of the measurements in this study, indicating that there was no significant error in the measurement method of brainstem diameter.

Our study has some considerable limitations. First, owing to the limitations of retrospective study, the dogs used for measurement were not completely clinically healthy. However, we used brain MR images of patients with minimal brain lesions that were not clinically important and no brainstem lesions. Second, as this was a multicenter study, the location of the slice for the transverse plane was relatively diverse depending on the radiologist. Additionally, a particular anatomical structure was not used for the numerous measurement points. Therefore, the measurement points may not be perfectly accurate. Third, there was also a difference of 2.5 or 3 mm in slice thickness between the two local animal hospitals. The definitive MRI slice thickness in

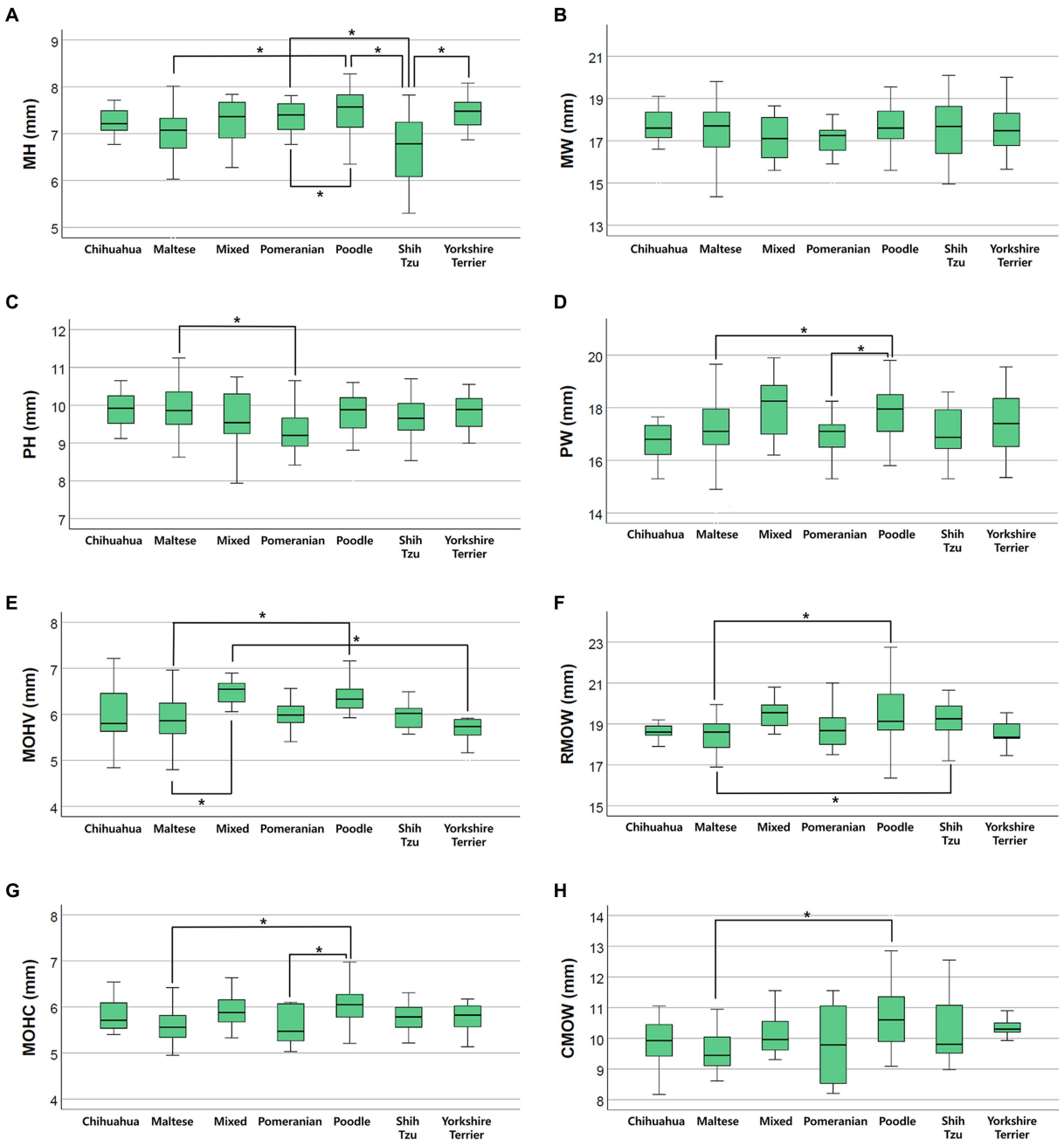

FIGURE 5
Box plots of the difference in brainstem diameters between breeds. There were statistically significant differences between breeds in **(A)** MH ($p<0.001$), **(C)** PH ($p=0.006$), **(D)** PW ($p=0.003$), **(E)** MOHV ($p<0.001$), **(F)** RMOW ($p=0.004$), **(G)** MOHC ($p<0.001$), and **(H)** CMOW ($p=0.008$). There were no statistically significant differences between breeds in **(B)** MW ($p=0.137$).

small animals has not yet been determined (30, 42). However, as a thinner slice allows better contour and less volume averaging than a thicker slice (30, 42, 43), measurements may not be precise as the availability of high-field MRI increased in veterinary medicine and high-quality neurological imaging is possible at 3.0 Tesla MRI (44, 45), using higher-field MRI could improve the accuracy of the measuring points. Fourth, the sample size was small for the comparison between breeds. Evaluation with a larger sample size may be required for each breed.

In conclusion, we assessed linear measurements of the brainstem diameter using MRI in small-breed dogs. Midbrain diameter and age were significantly negatively correlated. There was no significant difference between sexes in terms of brainstem diameter. In some breeds, there was a significant mean difference in brainstem diameters, except MW. Knowledge of brainstem diameters with normal variations related to aging and breeds can be valuable in determining pathological variations, such as neurodegenerative diseases and tumors.

Data availability statement

The original contributions presented in the study are included in the article/supplementary material, further inquiries can be directed to the corresponding author.

Ethics statement

The animal study was reviewed and approved by IACUC NON 2022-086. Written informed consent was obtained from the owners for the participation of their animals in this study.

Author contributions

JK and HY: conception and design, drafting the article, and revising the article for intellectual content. JK, DK, S-SK, KL, and HY: data acquisition. JK: analysis and interpretation of data. JK, KL, and HY: final approval of the completed article. All authors contributed to the article and approved the submitted version.

Funding

This research was supported by National University Development Project a Jeonbuk National University in 2022.

Conflict of interest

The authors declare that the research was conducted in the absence of any commercial or financial relationships that could be construed as a potential conflict of interest.

Publisher's note

All claims expressed in this article are solely those of the authors and do not necessarily represent those of their affiliated organizations, or those of the publisher, the editors and the reviewers. Any product that may be evaluated in this article, or claim that may be made by its manufacturer, is not guaranteed or endorsed by the publisher.

References

1. Evans HE, De Lahunta A. *Miller's anatomy of the dog*. Saint Louis, MO: Elsevier Health Sciences (2013). 658–671.

2. Sciacca S, Lynch J, Davagnanam I, Barker R. Midbrain, pons, and medulla: anatomy and syndromes. *Radiographics*. (2019) 39:1110–25. doi: 10.1148/rg.2019180126

3. Dewey CW, Da Costa RC. *Practical guide to canine and feline neurology*. Hoboken, NJ: John Wiley & Sons (2015). 29–52.

4. Konig HE, Liebich HG. *Veterinary anatomy of domestic animals*. Stuttgart, Germany: Thieme (2020). 520–526.

5. Elameen RAAE. *Measurement of normal brainstem diameter in Sudanese population using MRI*. Diss: Sudan University of Science and Technology (2016).

6. Rajagopal KV, D'Souza AS, Verma A, Mamatha H, Prasanna LC. Comparative morphometric evaluation of the brainstem in neurodegenerative diseases with healthy individuals using magnetic resonance imaging. *J Taibah Univ Med Sci*. (2022) 17:87–95. doi: 10.1016/j.jtumed.2021.06.012

7. Joslyn S, Hague D. Magnetic resonance imaging of the small animal brain. *In Pract*. (2016) 38:373–85. doi: 10.1136/inp.i4183

8. Kim B, Kim H, Kim S, Hwang Y. A brief review of non-invasive brain imaging technologies and the near-infrared optical bioimaging. *Appl Microsc*. (2021) 51:9. doi: 10.1186/s42649-021-00058-7

9. Debnath J, Sharma V, Patrikar S, Krishna S, Shijith KP, Keshav RR. Normal measurements of brainstem and related structures for all ages: an MRI-based morphometric study. *Med J Armed Forces India*. (2022) 79:428–38. doi: 10.1016/j.mjafi.2022.06.002

10. Sjh OJ, Joo YG, Suh SJ. MR measurement of normal brainstem diameter in Korean adults. *J Korean Radiol Soc*. (1990) 26:653–7. doi: 10.3348/jkrs.1990.26.4.653

11. Singh S, Sharma BR, Bhatta M, Poudel N. Measurement of anteroposterior diameters of normal brainstem by magnetic resonance imaging. *J Gandaki Med Coll-Nepal*. (2019) 12:53–8. doi: 10.3126/jgmcn.v12i2.27210

12. Elhussein N, Alkhathami AHA, Ayad CE. Norms for brain stem: a morphometric MRI based study. *IOSR J Dent Med Sci*. (2017) 6:74–91. doi: 10.9790/0853-1606047479

13. Raininko R, Autti T, Vanhanen SL, Ylikoski A, Erkinjuntti T, Santavuori P. The normal brainstem from infancy to old age. *Neuroradiology*. (1994) 36:364–8. doi: 10.1007/BF00612119

14. Doraiswamy PM, Na C, Husain MM, Figiel GS, McDonald WM, Ellinwood EH Jr, et al. Morphometric changes of the human midbrain with normal aging: MR and stereologic findings. *AJNR Am J Neuroradiol*. (1992) 13:383–6.

15. Musrshed KA, Ziylan T, Seker M, Cicekcibasi AE, Acikgozoglu S. Morphometric assessment of brain stem and cerebellar vermis with midsagittal MRI: the gender differences and effects of age. *Neuroanatomy*. (2003) 2:35–8.

16. Koehler PR, Haughton VM, Daniels DL, Williams AL, Yetkin Z, Charles HC, et al. MR measurement of normal and pathologic brainstem diameters. *AJNR Am J Neuroradiol*. (1985) 6:425–7.

17. Luft AR, Skalej M, Schulz JB, Welte D, Kolb R, Bürk K, et al. Patterns of age-related shrinkage in cerebellum and brainstem observed *in vivo* using three-dimensional MRI volumetry. *Cereb Cortex*. (1999) 9:712–21. doi: 10.1093/cercor/9.7.712

18. Chida K, Goto N, Kamikura I, Takasu T. Quantitative evaluation of pontine atrophy using computer tomography. *Neuroradiology*. (1989) 31:13–5. doi: 10.1007/BF00342022

19. Oguro H, Okada K, Yamaguchi S, Kobayashi S. Sex differences in morphology of the brainstem and cerebellum with normal ageing. *Neuroradioloy*. (1998) 40:788–92. doi: 10.1007/s002340050685

20. Sohmiya M, Tanaka M, Aihara Y, Hirai S, Okamoto K. Age-related structural changes in the human midbrain: an MR image study. *Neurobiol Aging*. (2001) 22:595–601. doi: 10.1016/S0197-4580(01)00227-5

21. Head E. Neurobiology of the aging dog. *Age*. (2011) 33:485–96. doi: 10.1007/s11357-010-9183-3

22. Thames RA, Robertson ID, Flegel T, Henke D, O'Brien DP, Coates JR, et al. Development of a morphometric magnetic resonance image parameter suitable for distinguishing between normal dogs and dogs with cerebellar atrophy. *Vet Radiol Ultrasound*. (2010) 51:246–53. doi: 10.1111/j.1740-8261.2009.01655.x

23. Tapp PD, Siwak CT, Gao FQ, Chiou JY, Black SE, Head E, et al. Frontal lobe volume, function, and β-amyloid pathology in a canine model of aging. *J Neurosci*. (2004) 24:8205–13. doi: 10.1523/JNEUROSCI.1339-04.2004

24. Khosla T, Lowe C. Indices of obesity derived from body weight and height. *Br J Prev Soc Med*. (1967) 21:122–8. doi: 10.1136/jech.21.3.122

25. Murphy DG, DeCarli C, Schapiro MB, Rapoport SI, Horwitz B. Age-related differences in volumes of subcortical nuclei, brain matter, and cerebrospinal fluid in healthy men as measured with magnetic resonance imaging. *Arch Neurol*. (1992) 49:839–45. doi: 10.1001/archneur.1992.00530320063013

26. Jernigan TL, Archibald SL, Fennema-Notestine C, Gamst AC, Stout JC, Bonner J, et al. Effects of age on tissues and regions of the cerebrum and cerebellum. *Neurobiol Aging*. (2001) 22:581–94. doi: 10.1016/S0197-4580(01)00217-2

27. Lee NJ, Park IS, Kho IS, Jung TW, Rhyu IJ. No volume difference of medulla oblongata between young and old Korean people. *Brain Res*. (2009) 1276:77–82. doi: 10.1016/j.brainres.2009.04.027

28. Sullivan EV, Rosenbloom M, Serventi KL, Pfefferbaum A. Effects of age and sex on volumes of the thalamus, pons, and cortex. *Neurobiol Aging*. (2004) 25:185–92. doi: 10.1016/S0197-4580(03)00044-7

29. Shah S, Doraiswamy P, Husain M, Figiel G, Boyko O, Mcdonald W, et al. Assessment of posterior fossa structures with midsagittal MRI: the effects of age. *Neurobiol Aging*. (1991) 12:371–4. doi: 10.1016/0197-4580(91)90025-F

30. Mai W. *Diagnostic MRI in dogs and cats*. Boca Raton, FL: CRC Press (2018). 88–323.

31. Kimotsuki T, Nagaoka T, Yasuda M, Tamahara S, Matsuki N, Ono K. Changes of magnetic resonance imaging on the brain in beagle dogs with aging. *J Vet Med Sci*. (2005) 67:961–7. doi: 10.1292/jvms.67.961

32. Hasegawa D, Yayoshi N, Fujita Y, Fujita M, Orima H. Measurement of interthalamic adhesion thickness as a criteria for brain atrophy in dogs with and without cognitive dysfunction (dementia). *Vet Radiol Ultrasound*. (2005) 46:452–7. doi: 10.1111/j.1740-8261.2005.00083.x

33. Bizzi A, Brooks RA, Brunetti A, Hill JM, Alger JR, Miletich RS, et al. Role of iron and ferritin in MR imaging of the brain: a study in primates at different field strengths. *Radiology*. (1990) 177:59–65. doi: 10.1148/radiology.177.1.2399339

34. Drayer B, Burger P, Darwin R, Riederer S, Herfkens R, Johnson GA. MRI of brain iron. *Am J Roentgenol*. (1986) 147:103–10. doi: 10.2214/ajr.147.1.103

35. Hill JM, Switzer RC 3rd. The regional distribution and cellular localization of iron in the rat brain. *Neuroscience*. (1984) 11:595–603. doi: 10.1016/0306-4522(84)90046-0

36. McGeer PL, McGeer EG, Suzuki JS. Aging and extrapyramidal function. *Arch Neurol*. (1977) 34:33–5. doi: 10.1001/archneur.1977.00500130053010

37. Chelban V, Bocchetta M, Hassanein S, Haridy NA, Houlden H, Rohrer JD. An update on advances in magnetic resonance imaging of multiple system atrophy. *J Neurol*. (2019) 266:1036–45. doi: 10.1007/s00415-018-9121-3

38. Kii S, Uzuka Y, Taura Y, Nakaichi M, Takeuchi A, Inokuma H, et al. Magnetic resonance imaging of the lateral ventricles in beagle-type dogs. *Vet Radiol Ultrasound*. (1997) 38:430–3. doi: 10.1111/j.1740-8261.1997.tb00866.x

39. Vite CH, Insko EK, Schotland HM, Panckeri K, Hendricks JC. Quantification of cerebral ventricular volume in English bulldogs. *Vet Radiol Ultrasound*. (1997) 38:437–43. doi: 10.1111/j.1740-8261.1997.tb00868.x

40. Dehaan CE, Kraft SL, Gavin PR, Wendling LR, Griebenow ML. Normal variation in size of the lateral ventricles of the Labrador Retriever dog as assessed by magnetic resonance imaging. *Vet Radiol Ultrasound*. (1994) 35:83–6. doi: 10.1111/j.1740-8261.1994.tb00191.x

41. Fleiss JL, Levin B, Paik MC. *Statistical methods for rates and proportions*. Hoboken, NJ: John Wiley & Sons (2003). 598-626.

42. Packer RA, Rossmeisl JH, Kent MS, Griffin JF IV, Mazcko C, LeBlanc AK. Consensus recommendations on standardized magnetic resonance imaging protocols for multicenter canine brain tumor clinical trials. *Vet Radiol Ultrasound*. (2018) 59:261–71. doi: 10.1111/vru.12608

43. Thrower SL, Al Feghali KA, Luo D, Paddick I, Hou P, Briere T, et al. The effect of slice thickness on contours of brain metastases for stereotactic radiosurgery. *Adv Radiat Oncol*. (2021) 6:100708. doi: 10.1016/j.adro.2021.100708

44. Ivan D, Ohlerth S, Richter H, Verdino D, Rampazzoz A, Pot S. 3T high-resolution magnetic resonance imaging, conventional ultrasonography and ultrasound biomicroscopy of the normal canine eye. *BMC Vet Res*. (2022) 18:67–13. doi: 10.1186/s12917-021-03108-0

45. Frayne R, Goodyear BG, Dickhoff P, Lauzon ML, Sevick RJ. Magnetic resonance imaging at 3.0 tesla: challenges and advantages in clinical neurological imaging. *Invest Radiol*. (2003) 38:385–402. doi: 10.1097/01.rli.0000073442.88269.c9

frontiers | Frontiers in Veterinary Science

TYPE Original Research
PUBLISHED 17 July 2023
DOI 10.3389/fvets.2023.1156870

OPEN ACCESS

EDITED BY
Adriano Wang-Leandro,
University of Veterinary Medicine Hannover, Germany

REVIEWED BY
Giovanni Mogicato,
Ecole Nationale Vétérinaire de Toulouse (ENVT), France
Francesca Del Chicca,
University of Zürich, Switzerland

*CORRESPONDENCE
Junghee Yoon
✉ heeyoon@snu.ac.kr

RECEIVED 02 February 2023
ACCEPTED 03 July 2023
PUBLISHED 17 July 2023

CITATION
Je M, Yang S, Lee D, Choi J and Yoon J (2023) Single-slab 3D double inversion recovery for magnetic resonance brain imaging in clinically healthy dogs.
Front. Vet. Sci. 10:1156870.
doi: 10.3389/fvets.2023.1156870

Single-slab 3D double inversion recovery for magnetic resonance brain imaging in clinically healthy dogs

Miseong Je, Sunho Yang, Dongjae Lee, Jihye Choi and Junghee Yoon*

College of Veterinary Medicine and the Research Institute for Veterinary Science, Seoul National University, Seoul, Republic of Korea

Introduction: In veterinary medicine, magnetic resonance imaging (MRI) is widely utilized for brain imaging. But the complex structures of brain tissues can give rise to artifacts such as partial volume averaging in conventional sequences. To address this issue, several studies about double inversion recovery (DIR) sequences have been conducted in human medicine. However, published clinical studies about brain MRI using DIR sequences in dogs are currently lacking. The purpose of this study was to evaluate the magnetic resonance features of single-slab 3D DIR sequences in the normal canine brain.

Methods: Five healthy Beagle dogs were examined and the following pulse sequences were acquired for each: (1) spin-echo T2-weighted (T2W), (2) fluid attenuated inversion recovery (FLAIR), (3) gray matter (GM) selective, and (4) white matter (WM) selective single-slab 3D DIR sequence. For qualitative analysis, the distinction between gray and white matter of the cerebral cortex, presence and severity of the image artifacts were assessed for each pulse sequence. In addition, reconstructed images of single-slab 3D DIR sequences were qualitatively evaluated. For quantitative analysis, contrast ratios (CRs), signal-to-noise ratios (SNRs), and contrast-to-noise ratios (CNRs) of the GM, WM and cerebrospinal fluid (CSF) were measured for each pulse sequence.

Results and Discussion: GM selective 3D DIR was superior to T2W and FLAIR in delineating the boundaries between GM and WM in the overall brain area. Whereas WM selective 3D DIR provided better gray-white matter distinction of the cerebral cortex than T2W and FLAIR at the level of the medulla oblongata, where T2W and FLAIR images exhibited severe partial volume averaging artifacts. In general, the 3D DIR images demonstrated fewer artifacts compared to other sequences, and the reconstructed sagittal and dorsal images of these sequences maintained same spatial resolution as the original transverse images without any image degradation. Both gray and white matter selective 3D DIR sequences effectively suppressed unwanted signals, thereby providing high contrast between gray and white matter. Findings from this study could serve as a foundation for further studies on DIR sequences for the evaluation of brain diseases in dogs.

KEYWORDS

brain, dog, double inversion recovery, gray matter, magnetic resonance imaging, white matter

1. Introduction

Given the high soft tissue resolution and utility of specialized sequences, MRI is the preferred modality for brain imaging (1, 2). However, it should be considered that complicatedly folded brain structure may cause some imaging artifacts. One of the most common artifacts encountered in clinical situation is partial volume averaging artifact, which easily occurs at the curved interface between different brain structures, and it can be manifested as pseudolesions (3). Conversely, true lesions might be obscured by partial volume averaging, especially in lesions adjacent to cerebrospinal fluid (CSF) (4). Consequently, errors in interpreting MR images could occur with conventional MRI sequences such as T2-weighted (T2W) and fluid attenuated inversion recovery (FLAIR) (5, 6). To complement these sequences, double inversion recovery (DIR) sequence has been introduced in several human studies (5–7). In the DIR sequence, two different 180° inversion radiofrequency (RF) pulses are applied before a classic fast or turbo spin-echo acquisition, allowing two different signals to be nulled simultaneously (8). Thus, DIR can selectively depict gray matter (GM) by suppressing white matter (WM) and CSF signals, or WM by suppressing GM and CSF signals, and was known for providing markedly high contrast resolution between gray and white matter with superior delineation in human patients (4, 8). Especially, GM selective DIR, which selectively images GM by suppressing the signals from both WM and CSF, has been reported to provide better conspicuity of cortical and subcortical lesions in various central nervous system (CNS) diseases than other MR techniques (9).

DIR imaging was initially introduced using two-dimensional (2D) multislice sequences at 1.5-Tesla (T) (4, 8, 10). However, due to the complex morphology of the brain, three-dimensional (3D) MR imaging with high spatial resolution is preferred over 2D MR imaging. Some studies have reported that a multislab 3D DIR sequence improves the spatial resolution and detection of intracortical lesions, but the presence of flow artifacts and signal intensity differences between slabs cannot be resolved with multislab 3D sequence (6, 11, 12). On the other hand, single-slab 3D DIR sequence has a long echo train and variable flip angles for refocusing RF pulses, which covers whole brain with high quality and without flow artifacts from CSF or blood (12). Consequently, multislab 3D DIR sequence has been replaced by single-slab 3D DIR sequence (9).

In human medicine, DIR sequences have been widely used to evaluate various neurologic diseases including multiple sclerosis, epilepsy, and Alzheimer's disease, all of which exhibit cortical lesions or changes in cortical thickness or volume (9, 13, 14). However, to the authors' knowledge, published clinical studies about brain MRI using DIR sequences in dogs are currently lacking. The purpose of this study was to evaluate the magnetic resonance features of single-slab 3D DIR sequences in the normal canine brain. Authors hypothesized that single-slab 3D DIR sequences, either gray or white matter selective, would provide higher tissue contrast resolution than conventional T2W and FLAIR sequences, and would identify the exact boundary between brain tissues with fewer artifacts in clinically healthy dogs.

2. Materials and methods

2.1. Study design and description of dogs

This investigation was a prospective, methods comparison, exploratory study. Five purpose-bred healthy, intact male Beagle dogs were used in the study. The median age was 4 years (range, 4–5 years) and the median weight was 14 kg (range, 12.8–15.5 kg). For each dog, the screening tests including physical and neurological examination, thoracic radiographs and abdominal ultrasonographic examination were done prior to the procedures by a veterinarian (MJ) with 2 years of radiology experience. The dogs are owned by College of Veterinary Medicine, Seoul National University and all the procedures performed in the study were approved by the Seoul National University Institutional Animal Care and Use Committees (SNU-220807-1).

2.2. Data recording: brain MRI protocol

Magnetic resonance imaging examinations were performed with the dogs under general anesthesia, using a 1.5-T MR scanner (GE Signa, 1.5T, GE healthcare). Anesthetic protocols were the following: medetomidine (0.01 mg/kg IM, Domitor, Zoetis) was used for premedication, alfaxalone (2.0 mg/kg IV, Alfaxan, Jurox Pty Ltd) for induction, and isoflurane (Ifran, Hana Pharm) for maintenance. Noninvasive blood pressure, oxygen saturation, heart rate, body temperature, and end-tidal carbon dioxide concentration were monitored during the anesthesia.

The dogs were positioned in sternal recumbency on an 8-channel phased-array knee coil. Spin-echo T2W, FLAIR, GM and WM selective single-slab 3D DIR images were obtained in transverse plane from each dog. Table 1 details the parameters that were used for each sequence. To reduce the acquisition time for 3D DIR sequences,

TABLE 1 Pulse sequence parameters used for brain magnetic resonance imaging in dogs.

Parameter	T2W	FLAIR	GM selective 3D DIR	WM selective 3D DIR
TR (ms)	5,904	8,000	5,000	5,000
TE (ms)	80	100	80	80
TI (ms)	–	2,433	2,562/605	2,290/419
ETL	20	20	140	140
ST (mm)	3	3	2	2
Locs per slab	–	–	50	50
FOV (mm)	200	200	200	200
Matrix	288 × 224	256 × 192	176 × 176	176 × 176
NEX	4	2	2	2
Acquisition time (min:sec)	4:49	8:1	5:24	5:23

TR, repetition time; TE, echo time; TI, inversion time; ETL, echo train length; ST, slice thickness; FOV, field-of-view; NEX, number of excitations; T2W, T2-weighted; FLAIR, fluid attenuated inversion recovery; DIR, double inversion recovery; 3D, three-dimensional; GM, gray matter; WM, white matter.

number of excitations (NEX) was adjusted from 4 to 2. The acquisition time for each sequence was automatically recorded. After the examination, complications related to the anesthesia were monitored for 5 days in each dog.

2.3. Data analysis

The qualitative and quantitative analysis of brain images were conducted using a DICOM viewer software (RadiAnt DICOM Viewer, version 4.6.9, free evaluation edition, Medixant, Poznan, Poland). The qualitative analysis was performed by one veterinarian (MJ) with 2 years of radiology experience, under the supervision of a veterinarian (JY) with more than 30 years of diagnostic imaging expertise. The quantitative measurements were performed by three other veterinarians (MJ, SY, and DL) with 1–2 years of radiology experience. Because of obvious signal differences, the readers could not be entirely blinded to the type of the sequences.

In qualitative assessment, the images of each sequence were compared in the same transverse planes. The images were evaluated in six different anatomical regions; at the level of the frontal lobe, optic chiasm, interthalamic adhesion, mesencephalic aqueduct, pons, and medulla oblongata. For each plane, distinction between gray and white matter of the cerebral cortex was assessed using a four-point scale: (1) not visualized at all; (2) poorly visualized but possible to detect; (3) clearly visualized with blurry junction; and (4) clearly visualized with sharp junction. In addition, the readers assessed the image quality according to the artifacts, including motion, partial volume averaging, and flow artifacts. This evaluation was also conducted using a four-point scale: (1) "poor": pronounced artifacts present, limiting diagnostic capability; (2) "fair": artifacts do not prevent diagnostic capability but degrade image quality; (3) "good": minor artifacts present without significant impact on image quality; and (4) "excellent": no artifacts observed. Meanwhile, transverse images of gray and white matter selective 3D DIR sequences were reconstructed using multiplanar reconstruction, then sagittal and dorsal planes were assessed to determine the presence of signal intensity variations along the slab direction.

In quantitative assessment, contrast ratios (CRs), signal-to-noise ratios (SNRs), and contrast-to-noise ratios (CNRs) of the GM, WM and CSF were calculated as follows:

$$CR_{tissue1,2} = \frac{SI_{tissue1} - SI_{tissue2}}{SI_{tissue1} + SI_{tissue2}}$$

$$SNR_{tissue} = \frac{SI_{tissue}}{SD_{air}}$$

$$CNR_{tissue1,2} = \frac{SI_{tissue1} - SI_{tissue2}}{SD_{air}}$$

where SI_{tissue} is the mean tissue signal intensity measured in arbitrary units; SD_{air} the standard deviation of background signal. The CRs and CNRs are calculated using the absolute value because a positive or a negative contrast between the two tissues is considered to be equal (15). All values are given as mean ± SD. Signal intensities of individual types of tissues were assessed by region of interest (ROI) measurements with the ROI placed identically on each sequence (Figure 1). The gray and white matter ROI was chosen from the thickest and most uniform area possible, the CSF measurement was taken within the lateral ventricles. Standard deviation (SD) of background was determined by measuring the SD of the pixel intensities in a background air containing no image artifacts.

2.4. Statistical analysis

All statistical analysis was conducted by one author with diagnostic imaging expertise and statistical training (MJ) using commercially available software (SPSS statistical program, IBM SPSS Statistics 25, IBM Corporation, NY). The ordinal data were presented as medians and ranges, while the continuous data were presented as means and SD. All the parameters were compared using the Kruskal-Wallis *H* test and *post hoc* test with Bonferroni correction. Interobserver agreements between the three observers were assessed using the intraclass correlation coefficient (ICC) test. Variables with *P*-values of <0.05 were considered statistically significant.

3. Results

Brain MR images were attained with each sequence in all dogs without any anesthetic complications. No significant abnormalities were identified in brain MR images of all dogs. The total scan time was between 25 and 30 min in each dog. The acquisition time of each sequence is presented in Table 1.

The score of gray-white matter distinction is displayed for each pulse sequence and each location (Table 2). In all six locations from the frontal lobe to the medulla oblongata level, gray-white matter distinction of the cerebral cortex was more clearly visualized on GM selective 3D DIR than T2W and FLAIR. GM selective 3D DIR also had statistically higher distinction score than WM selective 3D DIR at the level of the mesencephalic aqueduct and pons. WM selective 3D DIR did not have significant difference with T2W and FLAIR from the frontal lobe to the pons level, but showed significantly higher distinction score than T2W and FLAIR at the level of the medulla oblongata. T2W and FLAIR tended to blur gray-white matter distinction of the occipital lobe at the medulla oblongata level, and in three of five dogs, the border of gray and white matter of the occipital cortex was even not visible at all in FLAIR images at the level of the medulla oblongata. On the other hand, both GM and WM selective 3D DIR sequences clearly visualized gray-white matter distinction in that region (Figure 2). FLAIR generally showed poor gray-white matter distinction of the cerebral cortex except at the interthalamic adhesion level, and the distinction was particularly poor at the medulla oblongata level.

The image quality according to the artifacts are displayed for each pulse sequence (Table 3). Motion and flow artifacts were absent, regardless of the sequence in all dogs. On the other hand, partial volume averaging artifacts were detected in all sequences. These artifacts were usually identified at the narrow sulci and gyri region. The severity of partial volume averaging artifacts was significantly

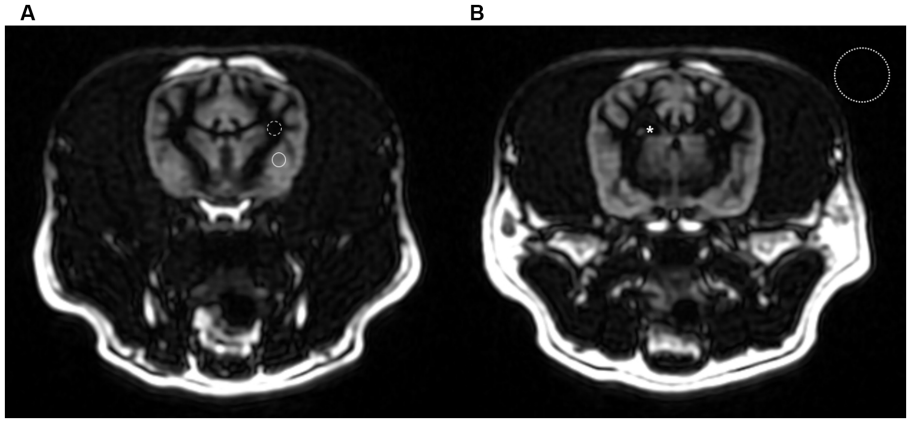

FIGURE 1
Transverse gray matter selective three-dimensional double inversion recovery images at the level of the optic chiasm **(A)** and interthalamic adhesion **(B)** in a dog. The region of interest (ROI) of gray and white matter were chosen from the thickest and most uniform area possible (solid line and dashed line). The ROI for CSF measurement was taken within the lateral ventricles (asterisk). Standard deviation of background was measured in a background air containing no image artifacts (dotted line).

TABLE 2 Comparison of MR sequences for gray-white matter distinction score at six different locations.

	T2W [median (range)]	FLAIR [median (range)]	GM selective 3D DIR [median (range)]	WM selective 3D DIR [median (range)]	*P*-value
Frontal lobe	3 (0)[a]	2 (1.0)[b]	4 (0)[a, b]	3 (1.0)	0.002
Optic chiasm	3 (0)[a]	2 (1.0)[b]	4 (0)[a, b]	3 (1.0)	0.002
Interthalamic- adhesion	3 (0)[a]	3 (1.0)[b]	4 (0)[a, b]	3 (1.0)	0.002
Mesencephalic- aqueduct	3 (0)[a]	2 (1.0)[b]	4 (0)[a, b, c]	3 (1.0)[c]	0.001
Pons	3 (1.0)[a]	2 (0)[b]	4 (0)[a, b, c]	3 (1.0)[c]	0.002
Medulla- oblongata	2 (0)[a, b]	1 (1.0)[c, d]	4 (1.0)[a, c]	3 (0)[b, d]	0.001

T2W, T2-weighted; FLAIR, fluid attenuated inversion recovery; DIR, double inversion recovery; 3D, three-dimensional; GM, gray matter; WM, white matter.
[a, b, c, d] Within a row, the same superscript indicated statistically significant differences between two groups using a Bonferroni correction (significance level of P-value < 0.0083).

lower at 3D DIR images, compared to T2W and FLAIR. In the images of conventional sequences, it was found that the gray-white matter junctions were blurred due to severe artifacts (Figure 3).

By the single-slab excitation, which simultaneously excites the entire slab, 3D DIR images had homogeneous signal intensity along the slab direction. Thus, the reconstructed sagittal and dorsal images of GM and WM selective 3D DIR sequences had same spatial resolution as the original transverse images, without any visible image degradation (Figure 4).

For the measurements of quantitative parameters including CRs, SNRs, and CNRs, the intraclass correlation among the three readers showed excellent interobserver agreement (Table 4). The mean and SD for CR, SNR, and CNR of the GM, WM and CSF are displayed for each pulse sequence (Table 5). $CR_{GM\text{-}WM}$ was markedly higher for GM and WM selective 3D DIR than T2W and FLAIR, and FLAIR had the lowest $CR_{GM\text{-}WM}$ than other three sequences. $CNR_{GM\text{-}WM}$ of GM and WM selective 3D DIR sequences were significantly higher than FLAIR. Although the mean values of $CNR_{GM\text{-}WM}$ of both 3D DIRs were measured to be higher than T2W, differences were not statistically significant. There were no significant differences in $CR_{GM\text{-}WM}$ and $CNR_{GM\text{-}WM}$ between GM and WM selective 3D DIR. $CR_{GM\text{-}CSF}$ of GM selective DIR was significantly higher than T2W, but there was no significant difference with FLAIR. $CR_{WM\text{-}CSF}$ was significantly higher in WM selective DIR than both T2W and FLAIR. $CNR_{GM\text{-}CSF}$ of GM selective DIR and $CNR_{WM\text{-}CSF}$ of WM selective DIR have no statistical differences with T2W and FLAIR. No significant difference was found between sequences for SNR_{GM} except WM selective DIR, which suppressed GM signals. Likewise, no significant difference was found between sequences for SNR_{WM} except GM selective DIR, which suppressed WM signals.

4. Discussion

Based on the author's literature review, this is the first published study of the utility of 3D DIR sequences for brain imaging in clinically healthy dogs. In this study, we compared the brain images obtained by single-slab 3D DIR sequences with those of conventional sequences, T2W and FLAIR, qualitatively and quantitatively.

Our findings demonstrated that GM selective 3D DIR is superior to conventional T2W and FLAIR in delineating the boundaries between gray and white matter of the cerebral cortex in all six locations from the frontal lobe to the medullar oblongata level. These results are consistent with previous human studies, which have shown that GM selective DIR provides superior gray-white differentiation compared to T2W or FLAIR (4, 8). Whereas WM selective 3D DIR had no significant difference from the conventional sequences in visualization of gray-white matter distinction of the cerebral cortex, from the

frontal lobe to the pons level. However, at the level of the medulla oblongata, where T2W and FLAIR images showed severe blurring of the gray-white matter junction of the cerebral cortex, not only GM selective 3D DIR but also WM selective 3D DIR provided much better visualization of the boundaries between gray and white matter. The narrow and tapered shape of the cerebral parenchyma at the level of the medulla oblongata resulted in severe partial volume averaging artifacts in conventional sequences. However, the utilization of two 3D DIR sequences with thin continuous slices effectively reduced the impacts of partial volume averaging artifacts, thereby resulting in improved distinction between gray and white matter of the cerebral cortex at the level of the medulla oblongata.

In a previous study, it has been reported that nonselective excitation of the single-slab 3D DIR can effectively prevent the occurrence of artifacts from blood flow or CSF pulsation (12). In our study, artifacts such as motion or flow artifacts were not visually apparent on 3D DIR images, except for mild partial volume averaging artifacts. But motion and flow artifacts were not visible in T2W and FLAIR images as well. In terms of the severity of artifacts, the only significant difference between conventional sequences and two 3D DIR sequences was observed in relation to partial volume averaging artifacts. The image quality of both two 3D DIR sequences was significantly less affected by partial volume averaging artifacts than T2W and FLAIR, because 3D DIR sequences obtained volumetric data and effectively overcame the artifacts.

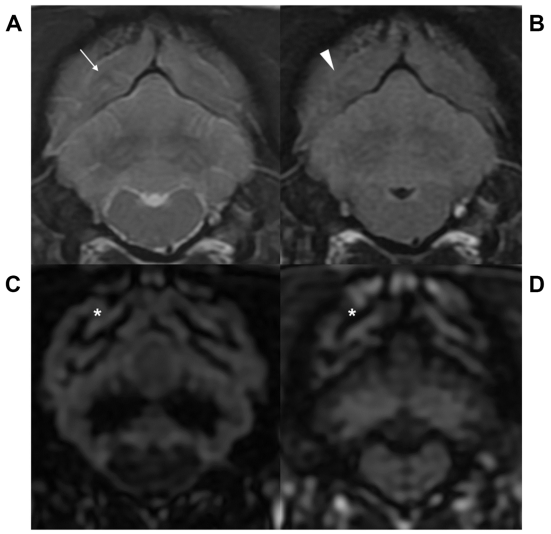

FIGURE 2
Transverse T2-weighted (T2W, **A**), fluid attenuated inversion recovery (FLAIR, **B**), gray matter selective three-dimensional double inversion recovery (GM selective 3D DIR, **C**), and white matter selective three-dimensional double inversion recovery (WM selective 3D DIR, **D**) images at the level of the medulla oblongata in a dog. T2W and FLAIR images showed blurry gray-white matter distinction (arrow and arrowhead), while GM and WM selective 3D DIR images clearly visualized the border of gray and white matter (asterisk) at the level of the medulla oblongata.

An additional advantage of 3D DIR sequences is the isotrophic resolution, which enables the original images to be reconstructed in any orientation with same spatial resolution. This characteristic eliminates the need to repeat MR examinations with the same region in different planes.

In quantitative analysis, GM selective 3D DIR had significantly higher $CR_{GM\text{-}WM}$ than other conventional sequences, T2W and FLAIR. In addition, GM selective 3D DIR had higher mean value of $CR_{GM\text{-}CSF}$ than T2W and FLAIR, but showed no statistical difference with FLAIR, a sequence that suppresses the CSF signal. WM selective 3D DIR showed significantly higher $CR_{GM\text{-}WM}$ and $CR_{WM\text{-}CSF}$ than other conventional sequences. These results revealed that good degrees of unwanted signal suppression were achieved with both two 3D DIR sequences.

CNR, a parameter which takes into account the background noise, is regarded as clinically the most relevant parameter, and the ability to detect brain anatomy depends on CNR (16, 17). In our study, both GM and WM selective 3D DIR had significantly higher $CNR_{GM\text{-}WM}$ than FLAIR. It suggests that both two 3D DIR sequences provide better contrast resolution between gray and white matter than FLAIR. In addition, the mean values of $CNR_{GM\text{-}WM}$ of two 3D DIR sequences were higher than that of T2W, but differences were statistically non-significant. FLAIR showed significantly the lowest $CR_{GM\text{-}WM}$ and $CNR_{GM\text{-}WM}$, which suggests that the ability of gray-white matter differentiation would be the worst. $CNR_{GM\text{-}CSF}$ of GM selective 3D DIR and $CNR_{WM\text{-}CSF}$ of WM selective 3D DIR had no significant differences with other sequences, and even T2W had higher mean values of $CNR_{GM\text{-}CSF}$ and $CNR_{WM\text{-}CSF}$ than 3D DIR sequences. Therefore, it should be noted that 3D DIR sequences may not be superior for delineating the boundary between CSF regions such as ventricles or subarachnoid space and brain parenchyma. In this aspect, it is unlikely that 3D DIR sequences will completely replace conventional sequences. However, they can serve as a valuable supplement, particularly in the assessment of the gray-white matter junction.

Previous studies have stated that long scan time of DIR sequences may limit their routine clinical use (4, 8). In our current study, the parameters of 3D DIR sequences were adjusted for the acquisition time to be clinically acceptable. During the initial

TABLE 3 Comparison of MR sequences for image quality according to the artifacts.

	T2W [median (range)]	FLAIR [median (range)]	GM selective 3D DIR [median (range)]	WM selective 3D DIR [median (range)]	*P*-value
Motion artifacts	4 (0)	4 (0)	4 (0)	4 (0)	1.000
Flow artifacts	4 (0)	4 (0)	4 (0)	4 (0)	1.000
Partial volume averaging artifacts	2 (1.0) [a, b]	1 (1.0) [c, d]	3 (0) [a, c]	3 (0) [b, d]	0.001

T2W, T2-weighted; FLAIR, fluid attenuated inversion recovery; DIR, double inversion recovery; 3D, three-dimensional; GM, gray matter; WM, white matter.
[a, b, c, d] Within a row, the same superscript indicated statistically significant differences between two groups using a Bonferroni correction (significance level of P-value < 0.0083).

examination conducted on a Beagle dog, it was found that reducing the number of excitations (NEX) from 4 to 2 did not result in a noticeable difference in image quality. As a result, the scan time was reduced by the half and both GM and WM selective 3D DIR acquired shorter scan time (5 min 24 s in GM selective 3D DIR and 5 min 23 s in WM selective 3D DIR) than FLAIR (8 min 1 s). We assumed that adjustment of the parameters for reducing the scan time might lead to a substantial loss of SNR. But in our study, SNR_{GM} of GM selective 3D DIR and SNR_{WM} of WM selective 3D DIR had no statistical difference with other sequences. This finding differs from previous studies that reported relatively low SNRs for DIR sequences (4, 12).

Our study had some limitations. First, the dogs in the study were considered as normal based on only few MR sequences, physical and

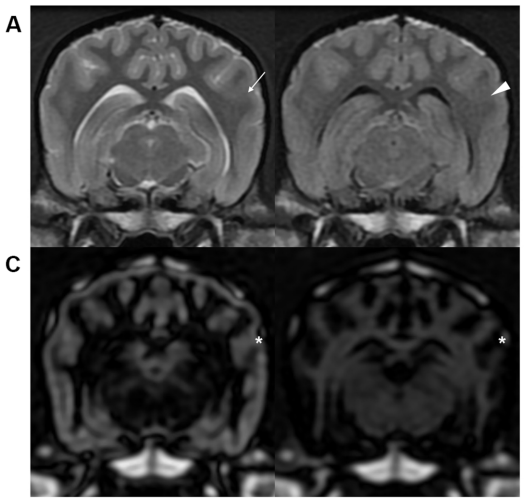

FIGURE 3
Transverse T2-weighted (T2W, **A**), fluid attenuated inversion recovery (FLAIR, **B**), gray matter selective three-dimensional double inversion recovery (GM selective 3D DIR, **C**), and white matter selective three-dimensional double inversion recovery (WM selective 3D DIR, **D**) images at the level of the mesencephalic aqueduct in a dog. Partial volume averaging artifacts at the gray-white matter junctions were more severe in T2W (arrow) and FLAIR (arrowhead) than GM and WM selective 3D DIR (asterisk) images, resulting in blurred gray-white matter distinction.

TABLE 4 Intraclass correlation coefficient values for interobserver reliability of quantitative analysis.

Evaluation factors		ICC	95% confidence interval
CR	GM-WM	0.998	0.996–0.999
	GM-CSF	0.987	0.972–0.994
	WM-CSF	0.992	0.984–0.997
SNR	GM	0.940	0.875–0.975
	WM	0.952	0.899–0.979
	CSF	0.979	0.955–0.991
CNR	GM-WM	0.987	0.973–0.995
	GM-CSF	0.986	0.970–0.994
	WM-CSF	0.984	0.967–0.993

CR, contrast ratio; SNR, signal to noise ratio; CNR, contrast to noise ratio; GM, gray matter; WM, white matter; CSF, cerebrospinal fluid; ICC, intraclass correlation coefficient.

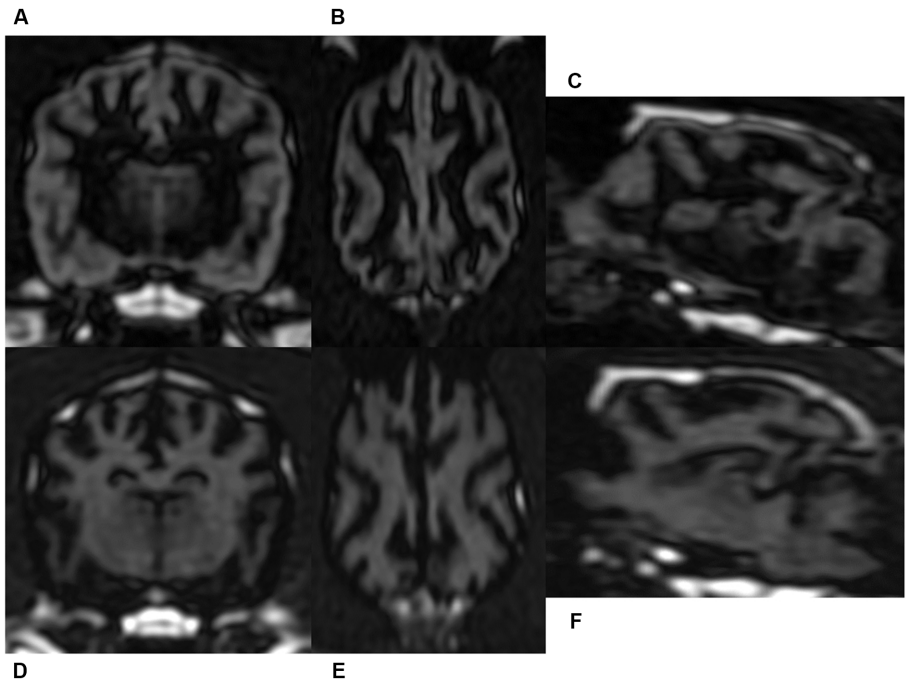

FIGURE 4
Gray matter selective three-dimensional double inversion recovery (GM selective 3D DIR, **A–C**) and white matter selective three-dimensional double inversion recovery (WM selective 3D DIR, **D–F**) images in a dog. Because of the nearly isotrophic resolution, reconstructed dorsal and sagittal images of GM selective 3D DIR **(B,C)** and WM selective 3D DIR **(E,F)** had identical image quality with the original transverse magnetic resonance images **(A,D)**.

TABLE 5 Comparison of MR sequences for contrast between brain tissues.

	Ratio	T2W (mean±SD)	FLAIR (mean±SD)	GM selective DIR (mean±SD)	WM selective DIR (mean±SD)	*P*-value
GM	SNR	183.28 ± 43.383[a]	122.22 ± 32.306[b]	137.04 ± 54.595[c]	17.95 ± 4.712[a, b,c]	0.004
WM	SNR	114.27 ± 26.308[a]	83.77 ± 24.002[b]	15.01 ± 6.413[a, b, c]	146.43 ± 46.560[c]	0.004
CSF	SNR	315.05 ± 81.312[a, b, c]	21.30 ± 5.609[a]	16.00 ± 7.239[b]	19.90 ± 4.693[c]	0.007
GM-WM	CR	0.23 ± 0.018[a, b]	0.19 ± 0.020[a, b]	0.80 ± 0.042[a]	0.77 ± 0.044[b]	0.001
	CNR	69.02 ± 17.952[a]	38.45 ± 9.305[a, b, c]	122.03 ± 49.147[b]	128.48 ± 43.405[c]	0.002
GM-CSF	CR	0.26 ± 0.028[a, b]	0.70 ± 0.047[a]	0.79 ± 0.030[b]	0.10 ± 0.052[a, b]	0.001
	CNR	131.77 ± 40.783[a]	100.91 ± 27.695[b]	121.03 ± 47.701[c]	3.87 ± 2.199[a, b, c]	0.009
WM-CSF	CR	0.47 ± 0.011[a]	0.59 ± 0.064[a]	0.12 ± 0.076[a]	0.75 ± 0.043[a]	0.000
	CNR	200.78 ± 55.178[a]	62.46 ± 19.417[a]	3.45 ± 1.897[a, b]	126.53 ± 42.889[b]	0.001

SNR, signal to noise ratio; CR, contrast ratio; CNR, contrast to noise ratio; T2W, T2-weighted; FLAIR, fluid attenuated inversion recovery; DIR, double inversion recovery; 3D, three-dimensional; GM, gray matter; WM, white matter.
[a, b, c] Within a row, the same superscript indicated statistically significant differences between two groups using a Bonferroni correction (significance level of *P*-value < 0.0083).

neurological examination and absence of clinical signs. To reduce anesthetic time, a complete MRI protocol including pre- and post-contrast T1-weighted (T1W) sequences or CSF analysis could not be conducted. Second, the signal intensities of each brain tissue were measured in arbitrary units without the use of a phantom for reference. Since the signal intensity is dependent on several factors such as imaging parameters, scanner settings, and acquisition techniques, the values obtained are not directly calibrated to a specific physical quantity. Third, the assessment of the clinical feasibility of 3D DIR sequences was limited as clinical patients with brain lesions were not included. The parameters measured in this study were not lesion-related values, but rather aimed to evaluate the contrast between brain tissues within each sequence. Therefore, in order to assess the lesion conspicuity in 3D DIR sequences, additional parameters should be evaluated in further studies.

Several CNS diseases in human are known to cause changes in GM, and numerous studies have reported the utility of 3D DIR sequences in evaluating these diseases (11). Likewise, in veterinary medicine, there are diseases that cause changes in GM, and the representative one is epilepsy (18). A study found the reduction of GM in dogs with idiopathic and structural epilepsy, by using voxel based morphometry (VBM) analysis (18). For VBM to function properly, the MRI image should have good contrast between the different brain tissues. However, the tissue distinction is not accurate especially in the sulcus region where the contrast between GM and adjacent WM can be reduced. Another problem is that the voxels containing several tissues may not be interpreted accurately, because the VBM model assumes that each voxel contains only one type of tissue (19). Considering the characteristics of 3D DIR sequences, which provide high contrast between gray and white matter with less partial volume averaging, the utilization of 3D DIR images for VBM analysis could potentially resolve these problems. In addition, 3D DIR sequences are expected to provide superior conspicuity of brain lesions located at the gray-white matter junction, and the diagnostic efficacy of 3D DIR sequences for brain lesions such as meningoencephalitis should be studied further.

In conclusion, both GM and WM selective single-slab 3D DIR sequences provided higher contrast between gray and white matter with fewer imaging artifacts than conventional sequences, including T2W and FLAIR. Therefore, the addition of a single-slab 3D DIR sequences to a standard MR brain imaging protocol could enhance the depiction of anatomical contrast. This study can also provide valuable background data for further studies about DIR sequences for evaluating brain diseases in dogs, and further studies are warranted using dogs with brain lesions.

Data availability statement

The original contributions presented in the study are included in the article/supplementary material, further inquiries can be directed to the corresponding author.

Ethics statement

The animal study was reviewed and approved by Seoul National University Institutional Animal Care and Use Committees (SNU-220807-1).

Author contributions

MJ, JC, and JY contributed to the conception and design of the study. MJ, SY, and DL contributed to data acquisition. MJ and JY performed the data interpretation and drafted the manuscript. MJ performed the statistical data analysis and the interpretation. All authors revised the manuscript and gave their final approval.

Conflict of interest

The authors declare that the research was conducted in the absence of any commercial or financial relationships that could be construed as a potential conflict of interest.

Publisher's note

References

1. Hecht S, Adams WH. MRI of brain disease in veterinary patients part 1: basic principles and congenital brain disorders. *Vet Clin N Am Small Anim Pract*. (2010) 40:21–38. doi: 10.1016/j.cvsm.2009.09.005

2. Kraft SL, Gavin PR, Wendling LR, Reddy VK. Canine brain anatomy on magnetic resonance images. *Vet Radiol*. (1989) 30:147–58. doi: 10.1111/j.1740-8261.1989.tb00767.x

3. Mai W. (2018). *Diagnostic MRI in dogs and cats*. *1st*. CRC Press: Boca Raton, FL, pp. 75–700.

4. Turetschek K, Wunderbaldinger P, Bankier AA, Zontsich T, Graf O, Mallek R, et al. Double inversion recovery imaging of the brain: initial experience and comparison with fluid attenuated inversion recovery imaging. *Magn Reson Imaging*. (1998) 16:127–35. doi: 10.1016/s0730-725x(97)00254-3

5. Almutairi AD, Hassan HA, Suppiah SA, Alomair OI, Alshoaibi A, Almutairi H, et al. Lesion load assessment among multiple sclerosis patient using DIR, FLAIR, and T2WI sequences. *Egypt J Radiol Nucl Med*. (2020) 51:209. doi: 10.1186/s43055-020-00312-0

6. Geurts JJG, Pouwels PJW, Uitdehaag BMJ, Polman CH, Barkhof F, Castelijns JA. Intracortical lesions in multiple sclerosis: improved detection with 3D double inversion-recovery MR imaging. *Radiology*. (2005) 236:254–60. doi: 10.1148/radiol.2361040450

7. Hamed W, Fathi W, Mahmoud W, Elhawary G. Diagnostic accuracy of double inversion recovery in delineation of multiple sclerosis lesions and its clinical correlation with expanded disability scoring system. *Egypt J Radiol Nucl Med*. (2019) 50:114. doi: 10.1186/s43055-019-0057-0

8. Redpath TW, Smith FW. Technical note: use of a double inversion recovery pulse sequence to image selectively grey or white brain matter. *Br J Radiol*. (1994) 67:1258–63. doi: 10.1259/0007-1285-67-804-1258

9. Umino M, Maeda M, Ii Y, Tomimoto H, Sakuma H. 3D double inversion recovery MR imaging: clinical applications and usefulness in a wide spectrum of central nervous system diseases. *J Neuroradiol*. (2019) 46:107–16. doi: 10.1016/j.neurad.2018.06.002

10. Bedell BJ, Narayana PA. Implementation and evaluation of a new pulse sequence for rapid acquisition of double inversion recovery images for simultaneous suppression of white matter and CSF. *J Magn Reson Imaging*. (1988) 8:544–7. doi: 10.1002/jmri.1880080305

11. Boulby PA, Symms MR, Barker GJ. Optimized interleaved whole-brain 3D double inversion recovery (DIR) sequence for imaging the neocortex. *Magn Reson Med*. (2004) 51:1181–6. doi: 10.1002/mrm.20088

12. Pouwels PJW, Kuijer JPA, Mugler JP, Guttmann CRG, Barkhof F. Human gray matter: feasibility of single-slab 3D double inversion-recovery high-spatial-resolution MR imaging. *Radiology*. (2006) 241:873–9. doi: 10.1148/radiol.2413051182

13. Jahng GH, Lee DK, Lee JM, Rhee HY, Ryu CW. Double inversion recovery imaging improves the evaluation of gray matter volume losses in patients with Alzheimer's disease and mild cognitive impairment. *Brain Imaging Behav*. (2016) 10:1015–28. doi: 10.1007/s11682-015-9469-2

14. Sun K, Yu T, Yang D, Ren Z, Qiao L, Ni D, et al. Fluid and white matter suppression imaging and voxel-based morphometric analysis in conventional magnetic resonance imaging - negative epilepsy. *Front Neurol*. (2021) 12:651592. doi: 10.3389/fneur.2021.651592

15. Usamentiaga R, Ibarra-Castanedo C, Maldague X. More than fifty shades of grey: quantitative characterization of defects and interpretation using SNR and CNR. *J Nondestruct Eval*. (2018) 37:25. doi: 10.1007/s10921-018-0479-z

16. Duyn JH, Van Gelderen P, Li TQ, De Zwart JA, Koretsky AP, Fukunaga M. High-field MRI of brain cortical substructure based on signal phase. *Proc Natl Acad Sci U S A*. (2007) 104:11796–801. doi: 10.1073/pnas.0610821104

17. Runge V. M., Nitz W. R., Schmeets S. H. (2009). *The physics of clinical MR taught through images*. *2nd*. Thieme, New York, USA, pp. 26–29.

18. Frank L, Lüpke M, Kostic D, Löscher W, Tipold A. Grey matter volume in healthy and epileptic beagles using voxel-based morphometry - a pilot study. *BMC Vet Res*. (2018) 14:50. doi: 10.1186/s12917-018-1373-8

19. Ashburner J, Friston KJ. Voxel-based morphometry - the methods. *Neuroimage*. (2000) 11:805–21. doi: 10.1006/nimg.2000.0582

frontiers | Frontiers in Veterinary Science

TYPE Original Research
PUBLISHED 13 September 2023
DOI 10.3389/fvets.2023.1248024

OPEN ACCESS

EDITED BY
Adriano Wang-Leandro,
University of Veterinary Medicine Hannover, Germany

REVIEWED BY
Marco Bernardini,
University of Padua, Italy
Yael Merbl,
Cornell University, United States
Philippa Johnson,
Cornell University, United States

*CORRESPONDENCE
Robert Clark
✉ rob.clark@willows.uk.net

RECEIVED 26 June 2023
ACCEPTED 10 August 2023
PUBLISHED 13 September 2023

CITATION
Clark R, Ferreira A and Behr S (2023) Significance of intramedullary T2* signal voids in the magnetic resonance imaging of paraplegic deep pain-negative dogs following intervertebral disc extrusion at short-term follow-up. *Front. Vet. Sci.* 10:1248024. doi: 10.3389/fvets.2023.1248024

Significance of intramedullary T2* signal voids in the magnetic resonance imaging of paraplegic deep pain-negative dogs following intervertebral disc extrusion at short-term follow-up

Robert Clark[1]*, Amy Ferreira[2] and Sebastien Behr[1]

[1]Neurology and Neurosurgery, Willows Veterinary Centre and Referral Service, Part of Linnaeus Veterinary Limited, Solihull, United Kingdom, [2]Diagnostic Imaging, Willows Veterinary Centre and Referral Service, Solihull, United Kingdom

Introduction: Dogs presenting as paraplegic without nociception due to a thoracolumbar intervertebral disc extrusion provide a difficult decision to both the clinician and the owner. The prognosis when performing surgical decompression remains guarded. Aside from significant extradural compression, these dogs often have a significant secondary spinal cord injury, which has shown to be an important factor in determining both the likelihood of developing progressive myelomalacia and the return to ambulation.

Materials and methods: This is a retrospective, observational, single centre study including 82 dogs presenting as paraplegic with absent nociception diagnosed with an intervertebral disc extrusion. Patients underwent MRI of the thoracolumbar spine, including a gradient echo sequence which was evaluated for the presence of intramedullary signal void artefacts. Decompressive surgery was performed, and patients were evaluated for the presence of nociception at short term follow up (at least four weeks post-surgery).

Results: Overall, 59.8% of patients regained nociception within the study period. This number was significantly reduced to 33.3% when multiple gradient echo signal voids were present (compared to 67.3% of dogs without signal voids). There was no significant difference in the rate of developing progressive myelomalacia between groups.

Conclusions: This paper adds to the existing literature and suggests that the gradient echo sequence may be of use when assessing acute spinal cord injury in the context of intervertebral disc extrusion and how it relates to prognosis.

KEYWORDS

myelomalacia, nociception, gradient echo, intervertebral disc extrusion, magnetic resonance imaging

Introduction

Paraplegic deep pain-negative dogs and the possibility of progressive myelomalacia (PMM) provide a unique decision-making challenge to the veterinary surgeon and the client. The prognosis in dogs presenting as paraplegic with absent nociception remains guarded, with recovery rates reported to range from 30 to 75%, with an overall recovery rate of 61% (1–7). Previously, no correlation between the degree of compression and the initial neurological grade or eventual outcome had been found (8–10). This suggests that the degree of compression observed in dogs following an acute intervertebral disc extrusion (IVDE) may not be the most significant factor affecting the outcome. Research should therefore focus

on intramedullary MRI changes in pre-surgery patients to better understand the probability of a positive or negative outcome.

PMM was first described clinically and histopathologically as the "ascending syndrome" in 1972. The authors identified extensive necrosis and ischaemic changes associated with marked extra and intramedullary haemorrhage of the spinal cords of eight dogs (11). PMM is characterised by progressive haemorrhagic necrosis of the spinal cord that ascends/descends over several spinal cord segments (12). More recently, dogs developing PMM have been demonstrated to exhibit an increase in biomarkers associated with oxidative stress (8-isoprostane F2α and acrolein), as well as decreased endogenous antioxidation of glutathione, thus suggesting that PMM may be the end point of cascading secondary injury that is unable to be regulated by the body following an acute spinal cord injury such as an IVDE (12). However, these tests are not available on the patient's side and thus cannot assist the clinician in decision-making prior to surgery.

Clinically, this condition is of great importance as PMM invariably proves fatal and can develop even after surgical decompression, with the majority of dogs being euthanised within 3 days of presentation (13).

PMM has been demonstrated to develop in dogs graded 3 (non-ambulatory paraparesis), 4 (paraplegic with intact nociception), and 5 (paraplegic with absent nociception) following an IVDE with a prevalence of 0.6, 2.7, and 14.5%, respectively (14). The prevalence of paraplegic deep pain-negative dogs developing PMM is generally accepted to be ∼9–17.5% (4, 5, 15–17), although rates as high as 33% are reported in the French bulldog (2). Clinical factors associated with an increased risk of developing PMM in dogs include being <6 years of age, L5–L6 disc herniations, and rapidly progressive onset of clinical signs (2).

Despite the importance of identifying this condition prior to surgical decompression, few studies exist that assess the possible risk factors that may be identified on preoperative MRI. At present, the length of the T2-weighted hyperintensity within the spinal cord or the length of spinal cord swelling with the use of a HASTE sequence have been identified as risk factors for the development of PMM on preoperative MRI of the spinal cord. Initially, a T2-weighted hyperintensity longer than six times the length of the body of L2 was believed to be a characteristic of PMM (18). However, a more recent study concluded that a T2-weighted hyperintensity of more than 4.57 times the length of L2 was found in 84.6% of dogs with myelomalacia, and dogs with a T2-weighted hyperintensity over this length were 17.2 times more likely to develop myelomalacia (14). Dogs with a loss of CSF signal ratio of >7.4 times the length of L2 on HASTE sequences were shown to be more likely to develop PMM (19). Currently, to the authors' knowledge, one case report links the appearance of gradient echo signal void to histopathologically confirmed PMM post-mortem (20), and the presence of GRE signal void on preoperative MRI has not been evaluated in the context of short-term outcomes following surgery.

The pathology of naturally occurring acute spinal cord injury and PMM has previously been assessed, with varying degrees of intramedullary haemorrhage being identified (21). Gradient echo MRI creates a contrast between tissues based on T2*relaxation, which refers to the decay of transverse magnetisation caused by a combination of T2 decay (spin-spin relaxation) and the rate of net magnetization vector dephasing caused by external and local magnetic field inhomogeneities. Therefore, gradient echo or T2*-weighted imaging is able to highlight local inhomogeneities that can go undetected on spin echo sequences. T2*-weighted imaging is particularly sensitive to haemorrhage because certain haemoglobin breakdown products are paramagnetic and create local magnetic field inhomogeneities (22). Given that the main clinical application of the T2*-weighted GRE sequence is the identification of haemorrhage (23), it would stand to reason that this sequence would be useful when assessing haemorrhagic intramedullary spinal cord injury. The usefulness of GRE sequences has been evaluated retrospectively in canine and feline spinal cord diseases (24). This study did not evaluate intramedullary change, instead stating that the T2*-weighted GRE sequence may be useful in differentiating extradural haemorrhage from spinal cord parenchyma.

The presence of a GRE signal void within the spinal cord parenchyma has been shown to have a negative correlation with a successful outcome when managing an acute non-compressive intervertebral disc extrusion. However, this correlation was only significant when considering all dogs included in the study and became insignificant when grouping dogs by neurological grade (25). This highlights the possible importance of the GRE sequence as a measure of secondary spinal cord injury severity and its potential usefulness in assessing the risk of PMM.

Hence, this study aimed to evaluate the presence or absence of either single or multiple GRE signal voids on the preoperative MRI of patients presenting as paraplegic with absent nociception and their relationship to short-term outcomes. The hypothesis is that patients with single or multiple intramedullary GRE signal voids would be more likely to develop PMM and less likely to recover nociception.

Materials and methods

Study population

This was a retrospective, observational, single-centre study. Subjects were selected from dogs evaluated at Willows Veterinary Referral Hospital, Solihull between 2009 and 2021. The inclusion criteria were dogs referred for acute-onset paraplegia with absent nociception, as confirmed on neurological examination by an ECVN-certified or eligible veterinary neurologist or neurology resident under the supervision of an ECVN-certified or eligible veterinary neurologist. The sample size was determined by the number of patients evaluated during the study period. Patients must have undergone an MRI of the thoracolumbar spine, including at least T2-weighted sagittal, T2-weighted transverse, and T2*/GRE transverse sequences. Patients must have been diagnosed with intervertebral disc extrusions managed surgically via a hemilaminectomy or mini-hemilaminectomy. A follow-up period of at least 4 weeks with re-examination was required to confirm the presence or absence of PMM or nociception. The exclusion criteria were an incomplete MRI protocol (absence of the aforementioned sequences), the presence of MRI artefacts or a low-quality study, or insufficient follow-up information. Subject inclusion or exclusion decisions were made by an ECVN-certified veterinary neurologist (S.B.) and a resident in veterinary neurology (R.C.).

Patient demographics and clinical assessment at presentation and re-examination

Individual medical records were reviewed, and the following data were recorded: age, breed, sex, presenting complaints and neurological examination findings, neuroanatomical localisation, and outcome following surgical intervention with a follow-up period of at least 4 weeks. The selected patients were divided into subgroups for comparison: patients recovering nociception vs. those not recovering nociception and patients developing suspected PMM vs. those not developing suspected PMM. A diagnosis of suspected PMM was made based on the following previously described clinical findings: loss of pelvic limb reflexes (patellar and withdrawal) and loss of perineal reflex when distant from the site of extrusion, poor abdominal wall tone, and cranial advancement of the cutaneous trunci reflex more than four sites cranial to the site of extrusion. Evidence of progressive-onset thoracic limb weakness, Horner's syndrome, or respiratory compromise was also considered consistent with PMM (13, 14, 16, 18, 19, 26). Loss of pelvic limb reflexes was differentiated from spinal shock when there was a loss of both the patella and withdrawal reflexes in extrusions cranial to L4–S1 spinal cord segments at the time of the initial examination.

Image acquisition

Patients were anaesthetised as per protocols provided by the attending anaesthetist. All dogs were scanned using a standardised MRI protocol. Dogs were placed in dorsal recumbency for an MRI of the thoracolumbar spine using a 1.5-T system (Magentom Sola, Siemens Healthcare Limited, Erlangen, Federal Republic of Germany, or Signa HD, GE Healthcare, United States). Images were acquired in three standard planes, always including T2-weighted sagittal and transverse sequences and T2*-weighted GRE transverse sequences. In each case, a multichannel high-resolution spinal coil was used. When signal quality was considered poor, a multichannel high-resolution surface coil was used to improve image quality. Slice thickness ranged from 2.0 mm to 2.5 mm for T2-weighted sequences and from 2.0 mm to 3.5 mm for GRE sequences. The decision on which slice thickness to use was made by the attending radiographer at the time of imaging based on patient size (thicker slices for larger patients) and on the length of the spinal cord to be imaged (thicker slices for longer sections of the spinal cord).

Image review

Images were reviewed by a European College of Veterinary Diagnostic Imaging (ECVDI) board-certified veterinary radiologist (A.F.) on DICOM viewing software (OsiriX, Pixmeo, Switzerland). The reviewer was aware that patients presented for paraplegia with absent nociception but was blinded to the outcome data. Hyperintensity of the spinal cord on T2-weighted sequences was defined as higher than that of the standard signal intensity of the spinal cord parenchyma at a distant and unaffected site. When a linear T2-weighted hyperintensity was visible on the mid-sagittal image, its longitudinal length was measured and expressed as a ratio when compared to the length of the L2 vertebral body (T2HI: L2 ratio). T2*/GRE signal void was defined as a region of susceptibility artefact that was hypointense to the standard signal intensity of the spinal cord parenchyma at an adjacent portion of the spinal cord. The GRE signal voids were denoted as being either single or multiple. Single GRE signal voids were defined as occupying a single area on a single transverse slice. Please see Figure 1 for two representative case examples of patients with a single GRE signal void. Multiple GRE signal voids were determined as two or more separate areas of signal void on one transverse image and/or GRE signal voids that were present on more than one transverse image (i.e., present at more than one level or large enough to occupy multiple slices). Figure 2 represents a single patient that was considered to have GRE signal voids occupying both different areas of the spinal cord on a single transverse slice but also having GRE signal voids present on multiple transverse slices.

Statistical analysis

Statistical analyses were performed by one author (R.C.) using commercially available statistical analysis software (SPSS, IBM Corp., Released 2020. IBM SPSS Statistics for Macintosh, Version 27.0. Armonk, NY: IBM Corp). Individual datasets were compared using the chi-squared test or Fisher's exact test with statistical significance set at a P-value of <0.05. Binary regression was used when assessing the T2HI: L2 ratio's significance in relation to the recovery of nociception or the development of PMM. For all data, averages were expressed as a median with an interquartile range (IQR). Receiver operating characteristic (ROC) curves were performed to assess the correlation and most optimal sensitivity and specificity of T2HI: L2 when compared to the outcome. The data were then categorised based on this calculation to allow for categorical comparison and odds ratio calculations.

Results

Patient demographics

A total of 116 paraplegic dogs without nociception that had an MRI of the thoracolumbar spine presented within the study period. Of these, 31 were excluded due to immediate euthanasia following MRI (and hence insufficient follow-up information) and 3 due to a lack of GRE sequence available for analysis, leaving a total study population of 82 dogs. Breeds included Miniature Dachshunds [33], French Bulldogs (10), small cross breeds (9), Cocker Spaniels (6), Yorkshire Terriers (3), two each of Standard Dachshunds, Chihuahuas, Staffordshire Bull Terriers, Shih Tzus, Jack Russell Terriers, and one each of medium cross breeds, Toy Poodles, German Shepherds, Nova Scotia Duck Tolling Retrievers, Border Collies, Basset Blue de Gascoignes, Cockapoos, Chinese Crested dogs, Basset Hounds, Border Terriers, and Papillons. The median age of presentation was 4.8 years (IQR = 2.3 years). A total of 52 were male dogs (28 neutered) and 30 were female dogs (24 neutered).

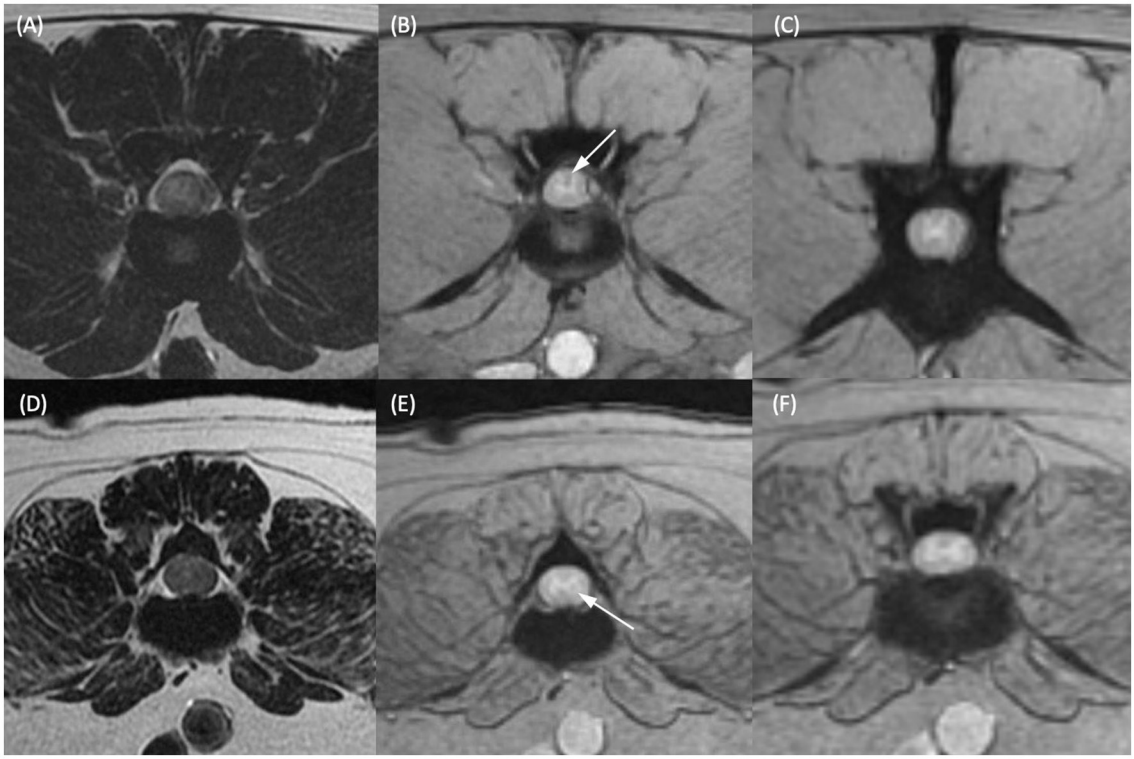

FIGURE 1
T2-weighted transverse **(A, D)** and T2*-weighted gradient echo (GRE) transverse **(B, C, E, F)** MR images of the vertebral column of two different dogs. **(A, B)** Dog 1 at the level of the L2–L3 intervertebral disc and **(C)** at the level of the cranial vertebral body of L4. **(D, E)** Dog 2 at the level of the caudal vertebral body of L3 and **(F)** at the level of the L3–L4 intervertebral disc. Within the dorsal funiculus **(B)** and left lateral funiculus **(E)** there are single, small, subtle, T2*-weighted GRE signal voids (white arrows). **(C, F)** Are given as regions of spinal cord considered not to have T2*-weighted GRE signal voids present in the same patients for comparison.

Prevalence of GRE signal voids

Within the study population, 21 dogs (25.6%) displayed multiple GRE signal voids, 12 dogs (14.6%) displayed single GRE signal voids, and 49 dogs (59.8%) did not display GRE signal voids.

Recovery of nociception

A total of 59.8% (49 out of 82) of patients recovered nociception within the study period. Patients exhibiting multiple intramedullary GRE signal voids were significantly less likely to regain nociception within the study period ($P = 0.004$). A total of 33.3% of patients with multiple signal voids recovered nociception vs. 67.3% of those without signal voids. Patients with a single signal void recovered nociception in 75% of cases, though this did not reach statistical significance ($P = 0.608$) when compared to patients without GRE signal voids.

Development of PMM

Moreover, 13.4% (11/82) of the total study population developed suspected PMM postoperatively. The presence of GRE signal voids (singular or multiple) was not significantly associated with the development of suspected PMM (P = 0.099 for multiple and $P = 0.143$ for single).

Assessment of the T2HI:L2 ratio

The ROC analysis produced a cutoff value of 5.2 to produce a sensitivity of 81.8% and a specificity of 70% for the development of PMM, with the area under the curve measured at 0.712, deeming the predictive value acceptable. When this cutoff was used, dogs with a T2W length ratio of >5.2 were 2.35 times more likely (95% CI 0.736–3.667) to develop PMM.

Discussion

Providing accurate prognostic information when evaluating paraplegic deep pain-negative dogs due to an IVDE represents a clinical challenge. The outcome following surgery for this cohort of dogs is consistent with previous results published in the literature based on the severity of the clinical examination (1, 3–7, 15). Reliable information pertaining to prognosis as determined by changes on an MRI is limited. The relative sensitivity and specificity of T2wHI:L2 and SSTSE sequence evaluation are considered low (18, 19), and new imaging features that inform on prognosis would

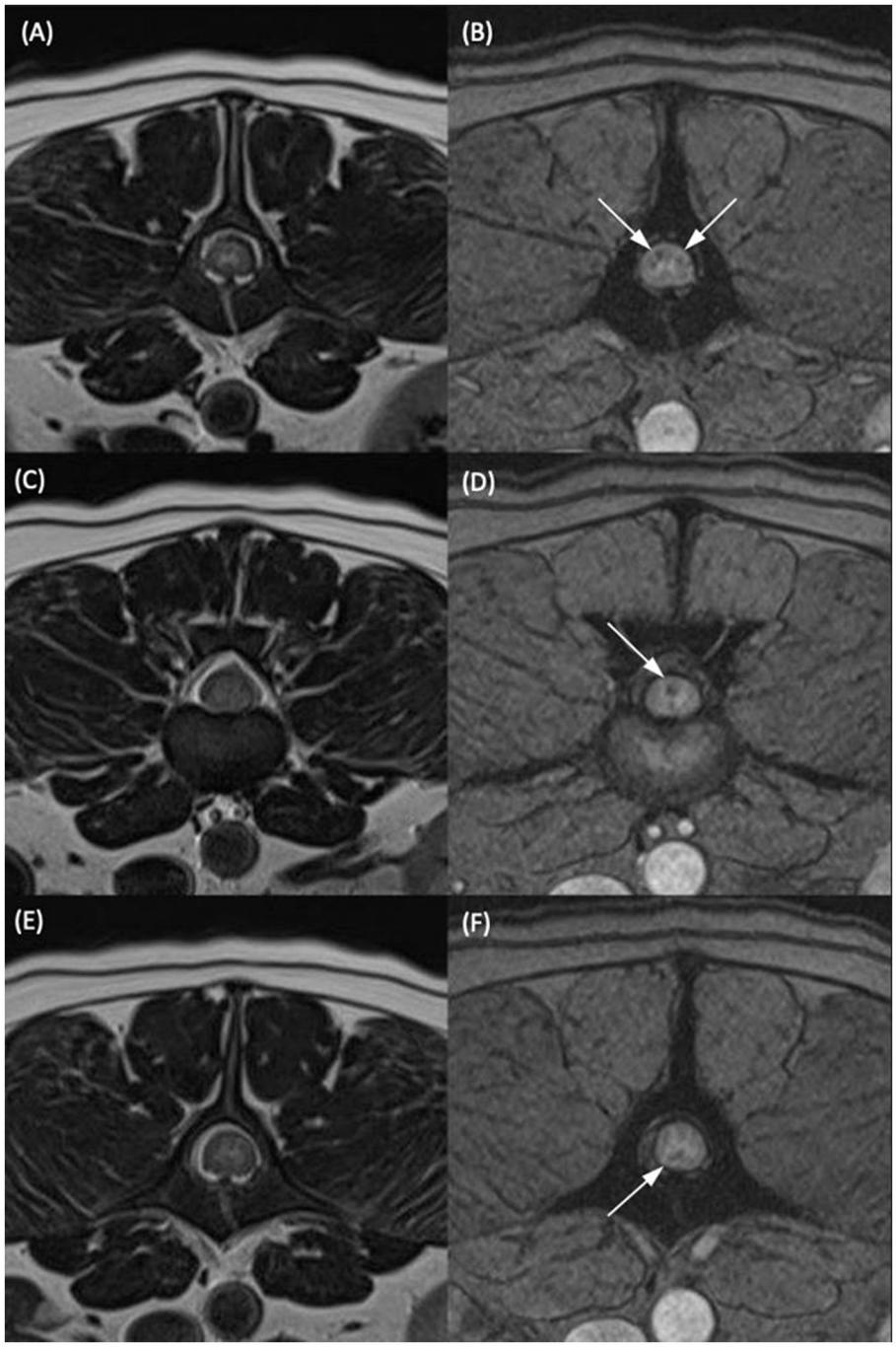

FIGURE 2
T2-weighted transverse **(A, C, E)** and T2*-weighted gradient echo (GRE) transverse **(B, D, F)** MR images of the vertebral column of the same dog classified as having multiple T2*-GRE signal voids. **(A, B)** At the level of the mid vertebral body of L2. **(C, D)** At the L2–L3 intervertebral disc space. **(E, F)** At the level of the cranial portion of the L3 vertebral body. Within the dorsal and both lateral funiculi **(B)**, the dorsal funiculus **(D)** and the ventral funiculus **(F)** were areas of T2*/GRE signal void. The signal voids were considered multiple as they were present in more than one region on one transverse image and present at several different levels in the same patient.

prove invaluable in the selection of surgical cases and setting client expectations.

In human medicine, the presence of intramedullary spinal cord haemorrhage has been consistently associated with severe spinal cord injury and a worse prognosis (27). This has been investigated in naturally occurring spinal cord injury in dogs in the context of an intramedullary T2-weighted hypointensity representing haemorrhage and demonstrating a worse prognosis in dogs with intramedullary haemorrhage (28). The usefulness of GRE sequences in the imaging of canine and feline spines has been previously investigated. However, there were no cases in which intramedullary signal voids in the acute stages following

an intervertebral disc extrusion were demonstrated (24). Only one published case report assesses the appearance of PMM when performing GRE sequences (20). The MRI appearance (including eight dogs with T2*-weighted GRE sequences) of the spinal cord in dogs with incomplete recovery after severe spinal cord injury has been assessed. There was no evidence of intramedullary haemorrhage (as identified by signal voids) present, though all the dogs included had MRIs at least 3 months following the initial injury (29). To the authors' knowledge, this is the first publication documenting the use of the GRE sequence in the context of acute spinal cord injury due to IVDE in dogs prior to surgery.

In the context of severe, acute spinal cord injury, there is little evidence comparing the appearance of the spinal cord on the GRE sequence to histopathological changes. In one case of a dog suffering from PMM, MRI demonstrated a severe and diffuse intramedullary GRE signal void artefact. When evaluated histopathologically, there was extensive liquefactive necrosis of the white matter with multifocal areas of haemorrhage at the junction between malacic and degenerated white matter (20). Although this represents an extreme example, given the noted histopathological appearance of areas displaying the GRE signal voids described, it would stand to reason that a similarly damaging process would occur in our dog populations, worsening their prognosis.

Multiple GRE signal voids were associated with a worsening prognosis, with only 33.3% of patients with multiple signal voids regaining nociception in comparison with 67.3% of patients without GRE signal voids in this study. Although this figure may not be used individually to predict the outcome, in the context of other previous imaging findings demonstrated to be associated with poor prognosis (6, 13), it may assist the clinician in setting client expectations. The presence of GRE signal voids failed to reach significance in the context of predicting PMM, though this may be due to a type II statistical error arising from low case numbers ($n = 11$). As per our previously outlined exclusion criteria, a number of dogs ($n = 31$) were excluded due to immediate euthanasia following an MRI. Had these patients not been euthanised, their inclusion may have altered the results.

One potential weakness in the way in which GRE signal voids were assessed in this study was that the classification did not allow for assessing the true extent of the voids reported (either in cross-sectional area or longitudinal length). When using GRE to identify small lesions (microbleeds) in human medicine, there was poor to moderate interobserver agreement (30). By differentiating single vs. multiple signal voids, an attempt was made to reduce the subjectivity present in the interpretation of the MRI studies and to identify lesions more objectively. Due to the potential implications of a patient being identified as having intramedullary haemorrhage (i.e., euthanasia following MRI in the clinical setting), it felt appropriate to differentiate the patients with more objective change and presumably more severe spinal cord injury.

The retrospective nature of the study was considered to have several limitations, including the accurate acquisition of data and patient enrolment. Paramount to this was the euthanasia of 31 patients under general anaesthesia following MRI. Within this population may have been patients considered to have the most severe MRI changes (as measured by T2-weighted hyperintensity, swelling of the spinal cord, and intramedullary GRE signal voids), with the inclusion of these patients perhaps altering our results. Unfortunately, the outcome of this population could not be assessed and was hence excluded from the current study.

When considering previously assessed MRI characteristics within our study population, it was found that a longer T2-weighted hyperintensity to L2 length ratio was significantly associated with developing PMM, as has been previously described. This prior publication considered dogs of all neurological grades and was performed on low field MRI images (14).

When assessing the outcome of this study, it was decided to use the recovery of nociception in the short term, although, ultimately, this does not mean the return of ambulation for all patients. In a previous study, 15% of patients regaining nociception failed to regain ambulation within a 12-week period. However, all were reported to have good voluntary movements (17). The selected outcome did allow for a greater number of patients to be included and for more objective data collection. The postoperative assessment of nociception and clinical presentation of PMM was always performed by an ECVN-certified or board-eligible neurologist or a neurology resident under the supervision of an ECVN-certified or board-eligible neurologist. A further prospective study in this area may generate adequate data to analyse the return to ambulation and gait analysis over long-term follow-up.

In conclusion, paraplegic dogs with absent nociception due to an IVDE were significantly less likely to recover nociception by short-term follow-up when multiple intramedullary GRE signal voids were identified. Based on these results, the authors would recommend the addition of this sequence in paraplegic deep pain-negative dogs due to IVDE to the standard T2-weighted sagittal, dorsal, and transverse sequences typically acquired to allow for a more accurate assessment of severe secondary spinal cord injury. Although no significant link was drawn between the presence of intramedullary GRE signal voids and the development of PMM, further prospective studies that include a more objective assessment of the nature of the intramedullary GRE signal voids with a larger number of dogs developing PMM may provide further insights.

Data availability statement

The raw data supporting the conclusions of this article will be made available by the authors, without undue reservation.

Ethics statement

Ethical approval was not required for the studies involving animals in accordance with the local legislation and institutional requirements because the study was retrospective and owners were not contacted. Written informed consent was obtained from the owners for the participation of their animals in this study.

Author contributions

RC: study design, data acquisition, statistics calculation, and manuscript preparation. AF: study design, image review, data acquisition, and review of the final manuscript. SB: study design, data acquisition, and review of the manuscript. All authors contributed to the article and approved the submitted version.

Funding

Linnaeus Veterinary Limited supported the costs of the Open Access Publication Charges.

Conflict of interest

The authors declare that the research was conducted in the absence of any commercial or financial relationships that could be construed as a potential conflict of interest.

Publisher's note

References

1. Aikawa T, Fujita H, Kanazono S, Shibata M, Yoshigae Y. Long-term neurologic outcome of hemilaminectomy and disk fenestration for treatment of dogs with thoracolumbar intervertebral disk herniation: 831 cases (2000–2007). *J Am Vet Med Assoc.* (2012) 241:1617–26. doi: 10.2460/javma.241.12.1617

2. Aikawa T, Shibata M, Asano M, Hara Y, Tagawa M, Orima H. A comparison of thoracolumbar intervertebral disc extrusion in french bulldogs and dachshunds and association with congenital vertebral anomalies. *Vet Surg.* (2014) 43:301–7. doi: 10.1111/j.1532-950X.2014.12102.x

3. Ruddle TL, Allen DA, Schertel ER, Barnhart MD, Wilson ER, Lineberger JA, et al. Outcome and prognostic factors in nonambulatory Hansen Type I intervertebral disc extrusions: 308 cases. *Vet Comparat Orthopaed Traumatol.* (2006) 19:29–34. doi: 10.1055/s-0038-1632970

4. Scott HW, McKee WM. Laminectomy for 34 dogs with thoracolumbar intervertebral disc disease and loss of deep pain perception. *J Small Anim Pract.* (1999) 40:417–22. doi: 10.1111/j.1748-5827.1999.tb03114.x

5. Jeffery ND, Barker AK, Hu HZ, Alcott CJ, Kraus KH, Scanlin EM, et al. Factors associated with recovery from paraplegia in dogs with loss of pain perception in the pelvic limbs following intervertebral disk herniation. *J Am Vet Med Assoc.* (2016) 248:386–94. doi: 10.2460/javma.248.4.386

6. Olby NJ, da Costa RC, Levine JM, Stein VM. Prognostic factors in canine acute intervertebral disc disease. *Front Vet Sci.* (2020) 7:59. doi: 10.3389/fvets.2020.596059

7. Olby NJ, Moore SA, Brisson B, Fenn J, Flegel T, Kortz G, et al. ACVIM consensus statement on diagnosis and management of acute canine thoracolumbar intervertebral disc extrusion. *J Vet Intern Med.* (2022) 36:1570–96. doi: 10.1111/jvim.16480

8. Penning V, Platt SR, Dennis R, Cappello R, Adams V. Association of spinal cord compression seen on magnetic resonance imaging with clinical outcome in 67 dogs with thoracolumbar intervertebral disc extrusion. *J Small Anim Pract.* (2006) 47:644–50. doi: 10.1111/j.1748-5827.2006.00252.x

9. Levine JM, Fosgate GT, Chen AV, Rushing R, Nghiem PP, Platt SR, et al. Magnetic resonance imaging in dogs with neurologic impairment due to acute thoracic and lumbar intervertebral disk herniation. *J Vet Intern Med.* (2009) 23:1220–6. doi: 10.1111/j.1939-1676.2009.0393.x

10. Ryan TM, Platt SR, Llabres-Diaz FJ, McConnell JF, Adams VJ. Detection of spinal cord compression in dogs with cervical intervertebral disc disease by magnetic resonance imaging. *Vet Rec.* (2008) 163:11–5. doi: 10.1136/vr.163.1.11

11. Griffiths IR. The extensive myelopathy of intervertebral disc protrusions in dogs ('the ascending syndrome'). *J Small Anim Pract.* (1972) 13:425–37. doi: 10.1111/j.1748-5827.1972.tb06870.x

12. Marquis A, Packer RA, Borgens RB, Duerstock BS. Increase in oxidative stress biomarkers in dogs with ascending-descending myelomalacia following spinal cord injury. *J Neurol Sci.* (2015) 353(1–2):63–9. doi: 10.1016/j.jns.2015.04.003

13. Castel A, Olby NJ, Mariani CL, Muñana KR, Early PJ. Clinical characteristics of dogs with progressive myelomalacia following acute intervertebral disc extrusion. *J Vet Intern Med.* (2017) 31:1782–9. doi: 10.1111/jvim.14829

14. Balducci F, Canal S, Contiero B, Bernardini M. Prevalence and risk factors for presumptive ascending/descending myelomalacia in dogs after thoracolumbar intervertebral disk herniation. *J Vet Intern Med.* (2017) 31:498–504. doi: 10.1111/jvim.14656

15. Olby N, Levine J, Harris T, Muñana K, Skeen T, Sharp N. Long-term functional outcome of dogs with severe injuries of the thoracolumbar spinal cord: 87 cases (1996–2001). *J Am Vet Med Assoc.* (2003) 222:762–9. doi: 10.2460/javma.2003.222.762

16. Muguet-Chanoit AC, Olby NJ, Lim JH, Gallagher R, Niman Z, Dillard S, et al. The cutaneous trunci muscle reflex: a predictor of recovery in dogs with acute thoracolumbar myelopathies caused by intervertebral disc extrusions. *Vet Surg.* (2012) 41:200–6. doi: 10.1111/j.1532-950X.2011.00921.x

17. Olby NJ, Muguet-Chanoit AC, Lim J -H., Davidian M, Mariani CL, Freeman AC, et al. A placebo-controlled, prospective, randomized clinical trial of polyethylene glycol and methylprednisolone sodium succinate in dogs with intervertebral disk herniation. *J Vet Intern Med.* (2016) 30:206–14. doi: 10.1111/jvim.13657

18. Okada M, Kitagawa M, Ito D, Itou T, Kanayama K, Sakai T. Magnetic resonance imaging features and clinical signs associated with presumptive and confirmed progressive myelomalacia in dogs: 12 cases (1997-2008). *J Am Vet Med Assoc.* (2010) 237:1160–5. doi: 10.2460/javma.237.10.1160

19. Gilmour LJ, Jeffery ND, Miles K, Riedesel E. Single-shot turbo spin echo pulse sequence findings in dogs with and without progressive Myelomalacia. *Vet Radiol Ultrasound.* (2017) 58:197–205. doi: 10.1111/vru.12463

20. Platt SR, McConnell J, Bestbier M. Magnetic resonance imaging characteristics of ascending hemorrhagic myelomalacia in a dog. *Vet Radiol Ultrasound.* (2006) 47:78–82. doi: 10.1111/j.1740-8261.2005.00109.x

21. Spitzbarth I, Moore SA, Stein VM, Levine JM, Olby NJ, Gjessing KM, et al. Current insights into the pathology of canine intervertebral disc extrusion-induced spinal cord injury. *Front Vet Sci.* (2020) 7:96. doi: 10.3389/fvets.2020.595796

22. Hodshon AW, Hecht S, Thomas WB. Use of the t2*-weighted gradient recalled echo sequence for magnetic resonance imaging of the canine and feline brain. *Vet Radiol Ultrasound.* (2014) 55:599–606. doi: 10.1111/vru.12164

23. Chavhan GB, Babyn PS, Thomas B, Shroff MM, Mark Haacke E. Principles, techniques, and applications of T2*-based MR imaging and its special applications. *Radiographics.* (2009) 29:1433–49. doi: 10.1148/rg.295095034

24. Hammond LJ, Hecht S. Susceptibility artifacts on t2*-weighted magnetic resonance imaging of the canine and feline spine. *Vet Radiol Ultrasound.* (2015) 56:398–406. doi: 10.1111/vru.12245

25. De Risio L, Adams V, Dennis R, McConnell FJ. Association of clinical and magnetic resonance imaging findings with outcome in dogs with presumptive acute noncompressive nucleus pulposus extrusion: 42 cases (2000–2007). *J Am Vet Med Assoc.* (2009) 234:495–504. doi: 10.2460/javma.234.4.495

26. Castel A, Olby NJ, Ru H, Mariani CL, Muñana KR, Early PJ. Risk factors associated with progressive myelomalacia in dogs with complete sensorimotor loss following intervertebral disc extrusion: a retrospective case-control study. *Vol. 15, BMC Vet Res.* (2019) 9:86 doi: 10.1186/s12917-019-2186-0

27. Tarawneh AM, D'Aquino D, Hilis A, Eisa A, Quraishi NA. Can MRI findings predict the outcome of cervical spinal cord Injury? a systematic review. *Euro Spine J.* (2020) 9:2457–64. doi: 10.1007/s00586-020-06511-7

28. Boudreau E, Otamendi A, Levine J, Griffin JF, Gilmour L, Jeffery N. Relationship between machine-learning image classification of t2-weighted intramedullary hypointensity on 3 tesla magnetic resonance imaging and clinical outcome in dogs with severe spinal cord injury. *J Neurotrauma.* (2021) 38:725–33. doi: 10.1089/neu.2020.7188

29. Lewis MJ, Cohen EB, Olby NJ. Magnetic resonance imaging features of dogs with incomplete recovery after acute, severe spinal cord injury. *Spinal Cord.* (2018) 56:133–41. doi: 10.1038/s41393-017-0004-8

30. Cheng AL, Batool S, McCreary CR, Lauzon ML, Frayne R, Goyal M, et al. Susceptibility-weighted imaging is more reliable than T2*-weighted gradient-recalled echo mri for detecting microbleeds. *Stroke.* (2013) 44:2782–6. doi: 10.1161/STROKEAHA.113.002267

frontiers | Frontiers in Veterinary Science

TYPE Original Research
PUBLISHED 27 September 2023
DOI 10.3389/fvets.2023.1265665

OPEN ACCESS

EDITED BY
Adriano Wang-Leandro,
University of Veterinary Medicine
Hannover, Germany

REVIEWED BY
Christina Precht,
University of Bern, Switzerland
Daniel Sanchez-Masian,
Hospital Veterinario de Referencia
Veterios, Spain

*CORRESPONDENCE
Emma Gilbert
✉ emma.gilbert@cvsvets.com

RECEIVED 23 July 2023
ACCEPTED 31 August 2023
PUBLISHED 27 September 2023

CITATION
Gilbert E, Rose J, Arrol L and Driver CJ (2023) Comparison of standard T2-weighted turbo spin echo and volumetric interpolated breath-hold examination magnetic resonance imaging sequences in the assessment of articular process dysplasia in Pug dogs with thoracolumbar myelopathy.
Front. Vet. Sci. 10:1265665.
doi: 10.3389/fvets.2023.1265665

Comparison of standard T2-weighted turbo spin echo and volumetric interpolated breath-hold examination magnetic resonance imaging sequences in the assessment of articular process dysplasia in Pug dogs with thoracolumbar myelopathy

Emma Gilbert*, Jeremy Rose, Lorna Arrol and Colin J. Driver

Neurology Department, Lumbry Park Veterinary Specialists, Alton, United Kingdom

Introduction: A retrospective study to compare the classification, as normal, hypoplastic or aplastic, of thoracic (T10-T13) caudal articular process (CAP) morphology in Pug dogs with a thoracolumbar myelopathy as normal, hypoplastic or aplastic, between T2 weighted Turbo Spin Echo (T2W-TSE), in sagittal and transverse planes, and Volumetric Interpolated Breath-hold Examination (VIBE) Magnetic Resonance Imaging (MRI) sequences, in comparison to Computed Tomography (CT). We hypothesized a stronger agreement for VIBE in comparison to T2W-TSE.

Results: Diagnostic accuracy of T2W-TSE was inferior to VIBE for aplastic (60%, 95% CI 0.561–0.639 vs. 78%, 95%CI 0.744–0.815) hypoplastic (44%, 95%CI 0.427–0.452 vs. 62.5%, 95%CI 0.595–0.655) and normal CAP (70%, 95%CI 0.655–0.744 vs. 87%, 95%CI 0.848–0.892). Superior accuracy of classification using VIBE vs. T2W-TSE sequences using the McNemar Chi squared test was significant for aplastic ($p = 0.0002$) and normal CAP ($p = 0.004$). VIBE sequences had a sensitivity of 96% and specificity of 75% to detect CAP abnormality and with T2W-TSE imaging sensitivity 81% and specificity of 75%.

Discussion: Three-dimensionally reconstructable VIBE sequences were significantly more accurate than traditional T2W-TSE MRI sequences in classifying CAP morphology, which should reduce the need for CT for pre-operative assessment.

KEYWORDS

Pug dog, CAP dysplasia, VIBE sequence, thoracolumbar myelopathy, T2W turbo spin echo

1. Introduction

Pug dogs are a screw-tailed dog breed over-represented for thoracic vertebral malformations, including caudal articular process (CAP) dysplasia in the caudal thoracic region (1). CAP morphology classification has previously been defined, with hypoplasia being the partial absence of the CAP and aplasia as the complete absence of the CAP (2). These malformations are implicated in the development of pia-arachnoid fibrosis,

sub-arachnoid diverticula, and constrictive myelopathy in the thoracolumbar region of T10-L1 (3, 4). Vertebral stabilization has been recommended in the management of these diseases, given the need to remove the dorsal lamina and interarcuate ligament to access the vertebral canal for spinal cord durotomy (5). Traditionally, a complete assessment of articular process morphology and *in silico* surgical planning requires computed tomography (CT) scans following magnetic resonance imaging (MRI). CT imaging prolongs anesthetic time, has financial implications, increases the number of transfers under anesthesia, requires the availability of two cross-sectional imaging modalities in one hospital, and administers a radiation dose to dogs. MRI is more sensitive at evaluating the primary spinal cord disease process, showing parenchymal detail that cannot be evaluated with CT. Therefore, we considered whether MRI sequences could be used for CAP classification and surgical planning so that the requirement for CT in these patients could be reduced/eliminated.

Three-dimensional (3D) volumetric MRI acquisitions have the advantage of improving through plane spatial resolution and generating high-quality reformatting to yield multiplanar images from the original dataset. Volumetric interpolated breath-hold examination (VIBE) is a form of volumetric imaging using fast 3D gradient-echo sequences that produces T_1 images and was first introduced by Rofsky in 1999 (6). It has the advantage of improving Z-axis resolution, which makes it possible to obtain high-quality multiplanar and 3D reconstruction images. VIBE has been effectively used in breast (7), human abdominal (8), and musculoskeletal imaging (9), with use in veterinary medicine limited to assessing facial neuritis (10) and skull fractures (11). Hecht et al. (11) found that VIBE imaging was highly accurate in identifying animal postmortem skull fractures. MRI of the vertebral column for fracture identification has been previously compared with CT and moderate interobserver agreement was found, but up to 79% of fractures in some vertebrae were not recognized; however, this was using only single-plane MRI sequences (12).

The aim of this study was to quantify the accuracy of two MRI sequences, VIBE and T2W-TSE, when compared to the current gold standard of CT. The null hypothesis is: there will be stronger agreement between VIBE sequences and CT in comparison to standard T2W-TSE and CT, in the assessment of CAP dysplasia in the T10-T13 region.

2. Materials and methods

An estimated *a priori* sample size for this study indicated that between 60 and 120 observations (8–15 dogs) were required, with a significance level of 5% and a power of 80%. This calculation assumed a proportion of agreement under the null hypothesis between 0.80 and 0.85, and the expected difference between two proportions of agreement of the null and alternative hypothesis to be between 0.10 and 0.15.

An ethics proposal of protocols was submitted to and approved by the CVS internal ethical review board (Number CVS-2022-016) prior to the commencement of the study. Data were collected as part of clinical investigations into Pug dogs presenting with signs of T3-L3 myelopathy and consent was gained from their caregivers prior to these investigations. Informed owner consent was received for all diagnostic procedures prior to commencement for all animals and these were carried out in accordance with best practice veterinary care and following RCVS guidelines.

This was a retrospective comparative accuracy study. The practice electronic patient database (Robovet, Covetrus, v.5.53) was searched for Pug dogs presenting with thoracolumbar myelopathy from 2020 to 2022. These were then each searched for the inclusion criteria of MRI T2W-TSE sequences in sagittal and transverse plains, VIBE sequences, and CT, including CAP from T10-L1. Patients were excluded if they had an imaging diagnosis affecting articular process morphology, i.e., osteolytic/productive lesions related to suspected spinal neoplastic, inflammatory, or infectious disease, or if there were vertebral body malformations resulting in significant kyphoscoliosis in the caudal thoracic region.

MRI sequences were randomized and patient details blinded to the observer. There were four observers: one ECVN resident, two boarded veterinary neurologists, and one boarded veterinary diagnostic imager. Each observer received training on the definition of normal, hypoplastic, and aplastic CAP and was shown example CT images, as shown in Figure 1; they then classified each CAP in T2W-TSE and VIBE sequences as normal, hypoplastic, or aplastic, as shown in Figure 2. The primary observer then reviewed CT imaging and classified each CAP, and this was used as the control. This was provided to observers prior to MRI assessment as an example of normal, hypoplastic, and aplastic CAPs. An open-source DICOM viewer (HorosTM, version 3.3.) was used for image review (Apple Mac with macOS 11.5.1, Apple Inc., Cupertino, California), with sequence-linked transverse and sagittal planes being evaluated at the same time. The time taken for the review of sequences was not recorded; however, all observers commented on the increased evaluation time of T2W sequences compared with VIBE.

All MRI sequences were obtained using a high field system (1.5 Tesla Siemens Magnetom Essenza), with patients anesthetized and positioned in dorsal recumbency. The following settings were applied for T2W-TSE: a sequence slice thickness of 3 mm, a resolution of 0.33 × 0.72 × 0.62 mm, a matrix of 384 × 218, and a field of view of 129 × 159. The following settings were applied for VIBE: a slice thickness of 1 mm, a resolution of 0.74 × 0.82 × 0.82 mm, a matrix of 256 × 230, a field of view of 190 × 190, a phase field of view of 100, a slice oversampling of 100, a flip angle of 12, and averages of 2.

CT of the entire spine was performed using a 16-slice Siemens Somatom scope CT scanner with patients under anesthesia in sternal recumbency. A bone algorithm window was used for the reconstruction of images in 3D for control analysis of the caudal articular process. The following settings were applied: a total mAs of 5,580, a kVp of 130, a DLP of 486, a tube rotation time of 0.8 s, and a slice thickness of 0.75 mm.

2.1. Statistical analysis

Overall percentage agreement and percentage agreement by category was reported and compared using a McNemar chi-square test (SPSS 27.0, SPSS Inc., Chicago, IL, USA), and

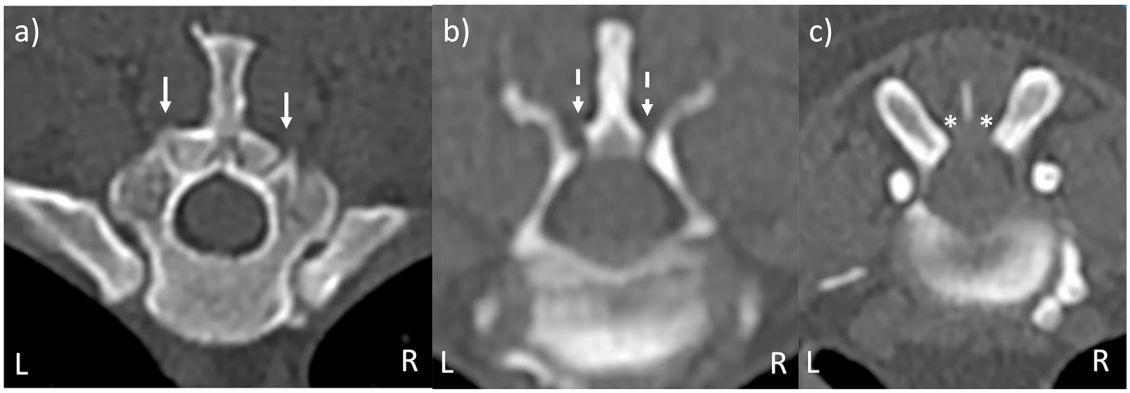

FIGURE 1
CT images of vertebral morphology. **(a)** Bilaterally normal CAP (solid arrows). **(b)** Bilaterally hypoplastic CAP (dashed arrows). **(c)** Bilaterally aplastic CAP (asterisks). Images are taken from more than one dog.

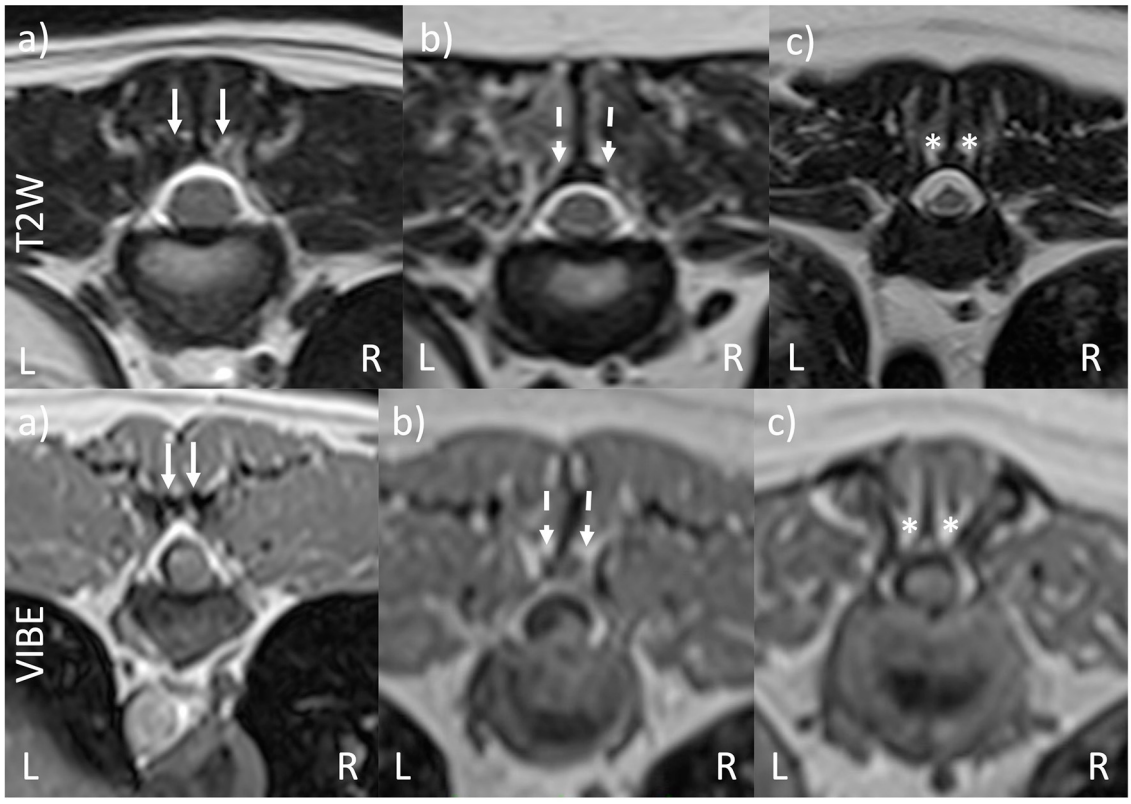

FIGURE 2
VIBE and T2W-TSE transverse images of vertebral morphology. **(a)** Bilaterally normal CAP (solid arrows). **(b)** Bilaterally hypoplastic CAP (dashed arrows). **(c)** Bilaterally aplastic CAP (asterisks). The T2W and VIBE images are from the same pug dog, although the slices are different due to the differing slice thicknesses for the two sequences. The images in **(a–c)** are taken from different dogs.

a *P*-value of <0.05 was accepted as significant. The kappa statistic was calculated using an Online Kappa Calculator (RRID:SCR_021770) and used to assess the agreement of observer categorizations of the two MRI sequences. A zero value of kappa indicates no agreement above that expected by chance, a value of 1 indicates perfect agreement, and a negative value indicates agreement worse than that expected by chance.

The sensitivity and specificity of the two MRI methods to identify abnormal CAP classifications have been reported, with respect to CT as the gold standard. Qualitative/descriptive data will be presented as count numbers and percentages.

TABLE 1 Reviewer number and percentage agreement with CT using T2W-TSE and VIBE sequences.

Reviewer	CT classification of CAP	MRI sequence	
		VIBE	T2W-TSE
1	Normal	13 (81%)	7 (43%)
	Hypoplastic	7 (58%)	5 (41%)
	Aplastic	39 (88%)	42 (95%)
2	Normal	14 (87%)	12 (75%)
	Hypoplastic	9 (75%)	6 (50%)
	Aplastic	41 (93%)	31 (70%)
3	Normal	16 (100%)	13 (81%)
	Hypoplastic	6 (50%)	5 (41%)
	Aplastic	40 (90%)	17 (38%)
4	Normal	13 (81%)	13 (81%)
	Hypoplastic	8 (66%)	5 (41%)
	Aplastic	19 (43%)	19 (43%)

TABLE 2 Percentage accuracy of reviewers regarding the classification of CAP using T2W-TSE and VIBE sequences.

	Percentage accuracy of the classification of CAP		
	Normal	Hypoplastic	Aplastic
VIBE	87*, CI 95% (±2.193)	62.5, 95% CI (±3.03)	78*, CI 95% (±3.531)
T2W-TSE	70*, CI 95% (±4.464)	44, CI 95% (±1.273)	60*, CI 95% (±3.899)

*Denotes a significant difference between T2W-TSE and VIBE accuracy by reviewers for CAP classification.

3. Results

Eleven pugs fit the inclusion criteria, contributing a total of 72 CAPs for classification by observers. The mean age of the pugs was 96 months (range, 52–140). The mean weight was 8.1 kg (range, 4.5–11.5).

Sixteen CAPs were classified as normal, with 12 hypoplastic and 44 aplastic CAPs identified using CT. Table 1 shows each reviewer's number and percentage agreement with CT for both VIBE and MRI sequences of each classification of CAP. Reviewer 1 correctly classified (VIBE/T2W-TSE) 13/7 normal (81%/43%), 7/5 hypoplastic (58%/41%), and 39/42 aplastic CAPs (88%/95%). Reviewer 2 correctly classified 14/12 normal (87%/75%), 9/6 hypoplastic (75%/50%), and 41/31 aplastic CAPs (93%/70%). Reviewer 3 correctly classified 16/13 normal (100%/81%), 6/5 hypoplastic (50%/41%), and 40/17 aplastic CAPs (90%/38%). Reviewer 4 correctly classified 13/13 normal (81%/81%), 8/5 hypoplastic (66%/41%), and 19/19 aplastic CAPs (43%/43%).

As summarized in Table 2, the mean accuracy for T2W-TSE sequences between all reviewers was 60.7%; for individual categories, the mean accuracy was 70% for normal (CI 95% 0.655–0.744), 44% for hypoplastic (CI 95% 0.427–0.452), and 60% for aplastic (CI 95% 0.561–0.639). The mean accuracy between all reviewers for VIBE was 80.5%; for individual categories, the mean accuracy was 87% for normal (CI 95% 0.848–0.892), 62.5% for hypoplastic (CI 95% 0.595–0.655), and 78% for aplastic (CI 95% 0.744–0.815).

The McNemar chi-squared test revealed an overall test statistic of 23.7 with an odds ratio of 0.3 and p-value of 0. For aplastic CAPs, the test statistic was 12.44 with an odds ratio of 0.369 and $p = 0.0002$. For hypoplastic CAPs, the test statistic was 1.7 with an odds ratio of 0.5 and p-value of 0.09. For normal CAPs, the test statistic was 6.66667, with an odds ratio of 0.15 and p-value = 0.004.

Kappa statistics for T2W-TSE interobserver agreement for aplastic, hypoplastic, and normal were, respectively, 0.06 95% CI for free-marginal kappa (−0.12, 0.24), 0.00 95% CI for free-marginal kappa (−0.34, 0.34), and −0.08 95% CI for free-marginal kappa (−0.35, 0.18). These results are interpreted as slight, slight, and no agreement for the respective categories.

Kappa statistics for VIBE interobserver agreement for aplastic, hypoplastic, and normal were, respectively, 0.61 95% CI for free-marginal kappa (0.42, 0.79), 0.11 95% CI for free-marginal kappa (−0.26, 0.48), 0.75 95% CI for free-marginal kappa (0.49, 1.00). These results are interpreted as substantial, slight, and substantial agreement for their respective categories.

Comparing sensitivity and specificity to identify abnormal CAP classifications, CAP on VIBE sequences were classified with a sensitivity of 96% and specificity of 75%, whereas T2W-TSE sequences had a sensitivity of 81% and specificity of 75%. The time taken for each observer to review the T2W and VIBE sequences and reach a decision was not recorded.

4. Discussion

This study allows us to accept the hypothesis that "there would be stronger agreement between VIBE sequences and CT in comparison to standard T2W-TSE and CT, in the assessment of articular process malformations in the T10–T13 region". Additionally, it confirmed a higher accuracy and interobserver repeatability of VIBE studies than T2W-TSE for the correct classification of caudal articular processes. This is consistent with previous findings in the assessment of other small animal bony changes, such as Hecht et al. (11) who found a 93.9% agreement of skull fracture identification of VIBE with CT; this also shows the transferrable use of MRI in observing bone morphology. Our findings suggest that VIBE sequences could potentially be considered in place of CT to identify CAP abnormalities. Considering the superior sensitivity of VIBE sequences (sensitivity of 96% and specificity of 75%) abnormal CAPs are unlikely to be misdiagnosed.

The McNemar statistical test shows a significant difference in the accuracy of classification of normal and aplastic CAPs; however, for the categorization of hypoplastic CAPs, there is no significant difference between VIBE and T2W-TSE sequences despite a higher accuracy of identification of hypoplastic facets with VIBE than with T2W-TSE. The lack of significance in the hypoplastic group may be due to the smaller number of hypoplastic CAPs in the study causing this number to fail to reach significance. Additionally, hypoplastic

CAPs are more difficult to define, as a small number of CAPs can be challenging to identify in any sequence.

Our finding of 77.7% CAP abnormalities in the T10-L1 region in our study is also consistent with previous studies (1). Only one patient contributed only normal CAPs in our study, with the remaining eight normal facets coming from three of our other patients.

Limitations of this study include its retrospective nature, meaning that imaging protocols were not standardized and therefore the orientation angle of sequence to the CAP may affect the ability to correctly interpret T2W-TSE sequences, which cannot undergo 3D reconstruction. However, it is standard for transverse MRI sequences to be obtained perpendicular to the spinal cord in our hospital and therefore this effect was hopefully minimized. The number of CAPs could be increased to strengthen the power of this study. Of the observers in this study, two were ECVN-diploma-holding specialists, one was an ECVN resident, and one was an ECVDI-diploma-holding specialist who uses MRI frequently in clinical practice; this means extrapolation to others with experience in MRI interpretation would be highly likely.

Pug dogs were selected for this study, given their known propensity for CAPs in the thoracic spine. A limitation of this study is that thoracolumbar myelopathy in Pug dogs can be recognized more cranially in the thoracic spine than in the studied region, and therefore, imaging assessment for the surgical management of these areas would need further studies for evaluation. The application of the principle to other breeds was also not investigated in this study and may be more challenging for smaller breeds; therefore, further studies are needed to understand the value of different imaging sequences in these patients.

Our CAP reviewers subjectively commented that they had spent longer deciding the categorization of CAPs with T2W-TSE than with VIBE images, and this could be an important variable to be assessed in future studies as it would add weight to the benefits of using VIBE sequences.

Further investigations will help us to determine whether VIBE sequences could be used for *in silico* surgical planning, notably in the production of patient-specific 3D surgical drill guides, as is the case in total knee arthroplasty in humans, where studies have shown no significant difference in the accuracy of implant placement using MRI and CT imaging for *in silico* planning (13, 14). This would further negate the need for CT, reducing anesthesia time, transfers under anesthesia, and the radiation exposure of these patients.

The current study showed that three-dimensionally reconstructible VIBE sequences were significantly more accurate than traditional T2W-TSE MRI sequences in classifying CAP morphology, which could support the use of MRI assessment of CAPs for decisions on the necessity for stabilization and reduce the need for CT as part of the pre-operative assessment.

Data availability statement

The raw data supporting the conclusions of this article will be made available by the authors, without undue reservation.

Ethics statement

The animal studies were approved by CVS Internal Ethical Review Board. The studies were conducted in accordance with the local legislation and institutional requirements. Written informed consent was obtained from the owners for the participation of their animals in this study.

Author contributions

EG: Data curation, Formal Analysis, Investigation, Writing—original draft, Writing—review and editing. JR: Conceptualization, Investigation, Writing—review and editing. LA: Investigation, Writing—review and editing. CD: Conceptualization, Investigation, Supervision, Writing—review and editing.

Funding

The author(s) declare that no financial support was received for the research, authorship, and/or publication of this article.

Conflict of interest

The authors declare that the research was conducted in the absence of any commercial or financial relationships that could be construed as a potential conflict of interest.

Publisher's note

References

1. Bertram S, Ter Haar G, De Decker S. Caudal articular process dysplasia of thoracic vertebrae in neurologically normal French bulldogs, English bulldogs and pugs: prevalence and characteristics. *Vet Radiol Ultrasound.* (2018) 59:396–404. doi: 10.1111/vru.12609

2. Bouma JL. Congenital malformation of vertebral articular processes in dogs. *Vet Clin North Am Small Anim Pract.* (2016) 46:307–26. doi: 10.1016/j.cvsm.2015.10.006

3. Fisher SC, Shores A, Simpson ST. Constrictive myelopathy secondary to hypoplasia or aplasia of the thoracolumbar caudal articular processes in pugs: 11 cases (1993-2009). *J Am Vet Med Assoc.* (2013) 242:223–9. doi: 10.2460/javma.242.2.223

4. Driver CJ, Rose J, Tauro A, Fernandes R, Rusbridge C. Magnetic resonance image findings in pug dogs with thoracolumbar myelopathy and concurrent caudal articular process dysplasia. *BMC Vet Res.* (2019) 15:182. doi: 10.1186/s12917-019-1866-0

5. Tauro A, Jeremy Rose, Clare Rusbridge, Driver CJ. Surgical management of thoracolumbar myelopathies in pug dogs with concurrent articular facet dysplasia. *VCOT Open*. (2019) 2:e60–e72. doi: 10.1055/s-0039-1692147

6. Rofsky NM, Lee VS, Laub G, Pollack MA, Krinsky GA, Thomasson D, et al. Abdominal MR imaging with a volumetric interpolated breath-hold examination. *Radiology*. (1999) 212:876–84. doi: 10.1148/radiology.212.3.r99se34876

7. Nakayama S, Kakizaki D, Kaise H, Kusama M, Ishikawa A, Amino M, et al. Three-dimensional volumetric interpolated breath-hold magnetic resonance imaging for the diagnosis of breast tumours. *Nihon Rinsho*. (2004) 62:790–8.

8. Vogt FM, Antoch G, Hunold P, Maderwald S, Ladd ME, Debatin JF, et al. Parallel acquisition techniques for accelerated volumetric interpolated breath-hold examination magnetic resonance imaging of the upper abdomen: assessment of image quality and lesion conspicuity. *J Magn Reson Imaging*. (2005) 21:376–82. doi: 10.1002/jmri.20288

9. Koh E, Walton ER, Watson P. VIBE MRI: an alternative to CT in the imaging of sports-related osseous pathology? *Br J Radiol*. (2018) 91:20170815. doi: 10.1259/bjr.20170815

10. Smith PM, Gonçalves R, McConnell JF. Sensitivity and specificity of MRI for detecting facial nerve abnormalities in dogs with facial neuropathy. *Vet Rec*. (2012) 171:349. doi: 10.1136/vr.100877

11. Hecht S, Anderson KM, Castel A, Griffin JF IV, Hespel AM, Nelson N, et al. Agreement of magnetic resonance imaging with computed tomography in the assessment for acute skull fractures in a canine and feline cadaver model. *Front Vet Sci*. (2021) 8:603775. doi: 10.3389/fvets.2021.603775

12. Gallastegui A, Davies E, Zwingenberger AL, Nykamp S, Rishniw M, Johnson PJ. MRI has limited agreement with CT in the evaluation of vertebral fractures of the canine trauma patient. *Vet Radiol Ultrasound*. (2019) 60:533–42. doi: 10.1111/vru.12785

13. Schotanus MGM, Sollie R, van Haaren EH, Hendrickx RPM, Jansen EJP, Kort NP. A radiological analysis of the difference between MRI- and CT-based patient-specific matched guides for total knee arthroplasty from the same manufacturer: a randomised controlled trial. *Bone Joint J*. (2016) 98-B:786–92. doi: 10.1302/0301-620X.98B6.36633

14. Asada S, Mori S, Matsushita T, Nakagawa K, Tsukamoto I, Akagi M. Comparison of MRI- and CT-based patient-specific guides for total knee arthroplasty. *Knee*. (2014) 21:1238–43. doi: 10.1016/j.knee.2014.08.015

frontiers | Frontiers in Veterinary Science

TYPE Case Report
PUBLISHED 05 October 2023
DOI 10.3389/fvets.2023.1260719

OPEN ACCESS

EDITED BY
Adriano Wang-Leandro,
University of Veterinary Medicine Hannover, Germany

REVIEWED BY
Pia M. Vidal,
Catholic University of the Most Holy Conception, Chile
Sam Long,
Veterinary Referral Hospital, Australia

*CORRESPONDENCE
Koen M. Santifort
koen.santifort@evidensia.nl

RECEIVED 18 July 2023
ACCEPTED 21 September 2023
PUBLISHED 05 October 2023

CITATION
Santifort KM, Carrera I and Platt S (2023) Case report: Traumatic hemorrhagic cervical myelopathy in a dog.
Front. Vet. Sci. 10:1260719.
doi: 10.3389/fvets.2023.1260719

Case report: Traumatic hemorrhagic cervical myelopathy in a dog

Koen M. Santifort[1,2]*, Ines Carrera[3] and Simon Platt[3]

[1]IVC Evidensia Small Animal Referral Hospital Arnhem, Neurology, Arnhem, Netherlands, [2]IVC Evidensia Small Animal Referral Hospital Hart van Brabant, Neurology, Waalwijk, Netherlands, [3]Vet Oracle Teleradiology, Norfolk, United Kingdom

A 1.5-year-old female entire French bulldog was referred for neurological evaluation, further diagnostic tests, and treatment 24 h after a road traffic accident. Initial emergency treatment, diagnostic tests, and stabilization had been performed by the referring veterinarian. Neurological examination revealed severe spastic non-ambulatory tetraparesis and was consistent with a C1-5 myelopathy. A magnetic resonance imaging (MRI) study revealed an irregular to elongated ovoid intramedullary lesion centered over the body of C2. The lesion showed marked signal heterogeneity with a central T2W and T2* hyperintense region, surrounded by a hypointense rim on both sequences. The lesion appeared heterogeneously T1W hypointense. The lesion was asymmetric (right-sided), affecting both white and gray matter. The C2-3 intervertebral disk appeared moderately degenerate with a Pfirrmann grade of 3. No evidence of vertebral fracture or luxation was found on radiographs or MRI of the vertebral column. Additional soft tissue abnormalities in the area of the right brachial plexus were suggestive of brachial plexus and muscle injury. A diagnosis of traumatic hemorrhagic myelopathy at the level of C2 and concurrent brachial plexus injury was formed. Conservative treatment was elected and consisted of physiotherapy, bladder care with an indwelling urinary catheter, repeated IV methadone based on pain scoring (0.2 mg/kg), oral meloxicam 0.1 mg/kg q24h, and oral gabapentin 10 mg/kg q8h. The dog was discharged after 4 days, with an indwelling urinary catheter and oral medication as described. The catheter was replaced two times by the referring veterinarian and finally removed after 10 days. Thereafter, voluntary urination was seen. During the 2 months after the road traffic accident, slow recovery of motor function was seen. The right thoracic limb recovery progressed more slowly than the left limb, also showing some lower motor neuron signs during follow-up. This was judged to be consistent with a right-sided brachial plexus injury. The dog was reported ambulatory with mild residual ataxia and residual monoparesis of the right thoracic limb at the last follow-up 3 months post-injury. This case report highlights the MRI-based diagnosis of traumatic hemorrhagic myelopathy in a dog. A fair short-term outcome was achieved with conservative treatment in this case.

KEYWORDS

hemorrhage, hematomyelia, spinal cord, recovery, durotomy, short-term outcome

Introduction

Hemorrhagic myelopathy, also called hematomyelia, in dogs can be due to various etiologies. These include trauma associated with vertebral fractures/luxation [e.g., due to road traffic accidents (RTA)], trauma associated with congenital anomalies of the craniocervical region (e.g., odontoid process malformation and atlantoaxial instability), iatrogenic trauma (e.g., due to spinal cord puncture during cerebrospinal fluid taps), vascular malformations (e.g., arteriovenous malformation), intervertebral disk disease (e.g., intervertebral disk extrusion), neoplasia (e.g., metastatic hemangiosarcoma or lymphoma), inflammatory disease (e.g., steroid-responsive meningitis arteritis), and hemorrhagic diathesis (e.g., related to *Angiostrongylus vasorum* infections) (1–9). When no causes are identified, the terms primary hematomyelia or idiopathic hemorrhagic myelopathy may be applicable (9, 10).

In human medical literature, hemorrhages can be found in the spinal cord in cases of spinal cord injury (SCI) without radiographic abnormalities (SCIWORA) (11–15). This is defined as SCI without evidence of vertebral fractures or dislocation based on radiographic studies. Since this is a fairly rare clinical entity, much of its exact pathophysiology remains unknown. Clinically, human patients (often children) are presented with various degrees of neurological dysfunction (12–14). In one systematic review, "complete" SCI defined as a lack of motor and sensory function "below" the level of the lesion in the spinal cord was reported at initial presentation in almost 20% of patients (12). Recent studies have provided evidence for improved outcomes following early surgical intervention (15). No such studies are available regarding clinical canine patients.

In this case report, we describe the magnetic resonance imaging (MRI) based diagnosis of traumatic hemorrhagic cervical myelopathy in a dog without evidence of vertebral fractures or luxation.

Case description

A 1.5-year-old female entire French bulldog was referred for neurological evaluation, further diagnostic tests, and treatment 24 h after a road traffic accident (RTA). The dog was chasing a cat and collided with a moving vehicle head-on, hitting the side of that vehicle. Bystanders reported that the dog immediately collapsed. The dog was rushed to the nearest veterinary practice. The dog was presented there in lateral recumbency with increased extensor tone of all four limbs. Mucous membranes were noted to be slightly blueish. No voluntary movement of limbs was recorded at that time, consistent with spastic tetraplegia. The dog was noted to show reduced responsiveness, and a modified Glasgow coma scale (MGCS) score of 9 was recorded without further details. Initial emergency treatment, diagnostic tests, and stabilization were performed. This included an IV bolus of 15 mL/kg 0.9% sodium chloride, followed by 20 mL/kg/h Ringers solution, and a single IV bolus of 1 g/kg mannitol [based on concerns for increased intracranial pressure (ICP)]. For analgesia, several boluses of methadone (0.2 mg/kg IV) had been administered. Heart rate increased to 70–90 beats/min over the next hour and the dog became more responsive, with a MGCS score of 13, increasing to 18 during the rest of the day on repeat examinations. Pulse oximetry consistently showed a SpO_2 of 99–100%. Further diagnostic tests included hematology (no significant abnormalities), biochemistry [hyperglycemia (11.72 mmol/L, reference range 4.11–7.95)] and increased blood lactate (5.26 mmol/L, reference range 0.50–2.50), ultrasound of the thorax and abdomen (possible signs of right-sided lung contusion), laterolateral radiographs of the thorax (signs suggestive of lung contusion), cervical vertebral column (Figure 1), and thoracolumbar vertebral column, and non-invasive blood pressure measurements (80–115 mmHg). Repeat testing of blood lactate showed values within the reference range. When the patient was stable the next day, the owners opted for a referral for further neurological examination, diagnostic testing, and treatment.

During the 2-h drive to the referral hospital, the dog had become hyperthermic (rectal temperature of 40.5 degrees Celsius) and was stabilized by the emergency department. Treatment at that point included active cooling, oxygen supplementation via nasal catheter and flow-by. After achieving normothermia, neurological examination revealed severe spastic non-ambulatory tetraparesis, worse in the thoracic limbs than the pelvic limbs. There was some voluntary movement of the limbs, more so in the pelvic limbs than the thoracic limbs. Spinal reflexes were intact in the pelvic limbs but decreased in the thoracic limbs on both sides. These findings were deemed consistent with a C1-5 myelopathy (likely involving the central cord). After discussion with the owners, an MRI study of the cervical spinal cord was performed, including bilateral brachial plexus regions. Additional imaging studies including an MRI of the brain and computed tomography (CT) of the vertebral column, thorax, and abdomen were declined due to financial restrictions. MRI sequences included T2-weighted (T2W) fast-spin echo (FSE) sagittal plane, T1W FSE sagittal plane, short-tau inversion recovery (STIR) sagittal plane, STIR dorsal plane, 3D fast gradient echo combined with water excitation technique (FFE3D combined with WET), T2W FSE transverse plane, T1W FSE transverse plane, T2*W gradient echo transverse plane, and 3D T1W magnetization prepared—rapid gradient echo (MPRAGE) sagittal plane post-contrast.

The MRI study revealed an irregular to elongated ovoid intramedullary lesion centered over the body of C2 (Figure 2). The lesion showed marked signal heterogeneity with a central T2W and T2* hyperintense region, surrounded by a hypointense rim on both sequences. The lesion appeared heterogeneously T1W hypointense. The lesion was predominantly right-sided and dorsolateral within the spinal cord, affecting both white and gray matter. The C2-3

FIGURE 1
Radiograph (laterolateral, right-sided recumbency) of the cervical vertebral column.

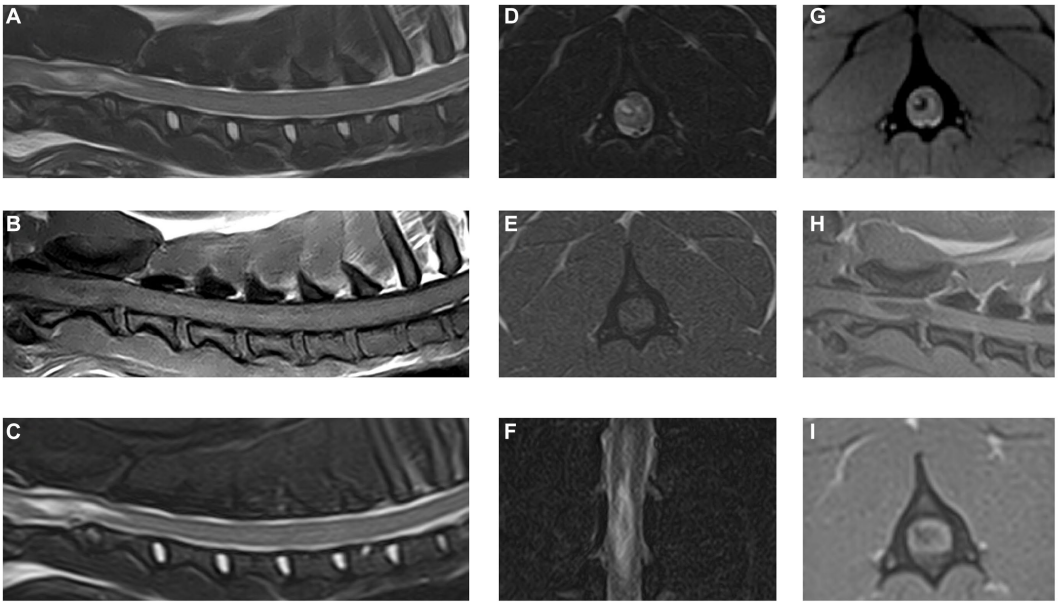

FIGURE 2
Magnetic resonance images of the cervical spinal cord and surrounding structures. **(A)** T2W sagittal plane, **(B)** T1W sagittal plane, **(C)** STIR sagittal plane, **(D)** T2W transverse plane at the level of C2 vertebral body, **(E)** T1W transverse plane at the level of C2 vertebral body, **(F)** STIR dorsal plane, **(G)** T2*W transverse plane at the level of C2 vertebral body, **(H)** 3D T1W MPRAGE sagittal plane, and **(I)** 3D T1W MPRAGE transverse reconstruction at the level of C2 vertebral body.

intervertebral disk appeared moderately degenerate with a Pfirrmann grade of 3. No evidence of vertebral fracture or luxation was found on radiographs of the vertebral column or the MRI study. Additional findings in the area of the right brachial plexus were suggestive of brachial plexus and muscular injury. A diagnosis of traumatic hemorrhagic myelopathy at the level of C2 and concurrent brachial plexus injury was formed.

Coagulation tests (activated partial-thromboplastin time and prothrombin time) were within the reference range. Repeated clinical examinations, focusing on signs or evidence of hemorrhagic diatheses (e.g., hemorrhages in mucous membranes) did not reveal any abnormalities. Conservative treatment was elected and consisted of fluid therapy, physiotherapy, an indwelling urinary catheter, repeated non-invasive blood pressure measurements, repeated IV methadone boluses based on pain scoring (0.2 mg/kg), oral meloxicam 0.1 mg/kg q24h, and oral gabapentin 10 mg/kg q8h.

Over the next 4 days, progressive signs of recovering motor function were observed in the left thoracic limb, both pelvic limbs, and, to a lesser degree, the right thoracic limb. Withdrawal reflexes were normal in the left thoracic and both pelvic limbs at that point but decreased in the right thoracic limb. Extensor muscle tone in all limbs had decreased, most notably in the right thoracic limb. The dog was discharged after 4 days, with an indwelling urinary catheter and oral medication as described. The catheter was replaced twice by the referring veterinarian and finally removed after 10 days. Thereafter, voluntary urination was seen. Meloxicam was discontinued a week later, and gabapentin was tapered and discontinued 2 weeks later. During the 2 months after the road traffic accident, slow recovery of motor function was seen. The right thoracic limb recovery progressed more slowly than the left limb, also showing some lower motor neuron signs (e.g., flaccid paresis) during follow-up at the referring veterinarian and was also visible on videos sent by the owners for remote evaluation by the neurology department of the referral hospital. The recovery was judged to be consistent with right-sided lateralization of the spinal cord hemorrhage and involvement of the brachial plexus on the right. The dog was reported to be ambulatory with mild residual ataxia and moderate to severe monoparesis of the right thoracic limb at the last follow-up 3 months post-injury. Physiotherapy including hydrotherapy had been commenced by the owners and is being continued long-term with the aid of orthopedic braces for the right thoracic limb. The owners were happy with the outcome at the time of writing and the patient remains under the care and supervision of the referring veterinarian.

Discussion

This case report describes the neurological presentation, MRI findings, conservative management, and short-term outcome of traumatic hemorrhagic cervical myelopathy in a French bulldog. Although the presenting clinical signs were severe directly after the traumatic event (RTA in this case), emergency treatment followed by conservative treatment for the cervical myelopathy and suspected brachial plexus injury resulted in a fair short-term outcome.

For the treatment of traumatic SCI in dogs, it is of vital importance to account for basic support measures and general stabilization before focusing on neurological signs and prognostication (15). In the case reported here, initial stabilization was performed by the referring veterinarian. The dog was transported for further work-up when it was deemed to be stabilized. However, hyperthermia developed during the drive to the referral hospital, and measures needed to be taken to stabilize the patient. Fortunately, there did not seem to

have been any neurological deterioration as determined by the results of the neurological examination vs. the descriptions of the referring veterinarian.

As emphasized in several veterinary texts, maintaining adequate tissue (spinal cord) perfusion is a key factor in the treatment of traumatic SCI in dogs (16–18). Spinal cord perfusion pressure (SCPP) is not routinely clinically measured [i.e., calculated from measurements of intradural or "intraspinal" pressure (ISP) and mean arterial blood pressure (MAP)] in canine traumatic SCI cases. Human literature, reporting results in clinical patients, has shown that such measurements can contribute to guiding more efficient and objective treatment measures (19, 20). Even if SCPPs are not performed, maintaining blood pressure (MAP) within the reference range can be and is regarded as a cornerstone of treatment (16, 17). This makes good sense, as low blood pressure will be detrimental to SCPP. High blood pressure is also to be avoided, as the blood-spinal cord barrier (BSCB) and local vascular autoregulation in the injured spinal cord is affected (16–23).

Numerous other possible avenues of treatment are discussed in veterinary as well as human literature (16–18, 23). These include, but are not limited to stem cell therapy, hypothermia, pharmacological treatment (e.g., the dubious role of corticosteroids), and surgery. The role of the latter deserves specific attention based on recent veterinary literature and human literature. As an option for maintaining or increasing SCPP, surgery would provide a way of removing restrictions to the expansion of the spinal cord parenchyma and/or removing compressive lesions. That is to say, surgical opening of the vertebral column and durotomy can provide the spinal cord with space to expand in case of swelling, causing a direct decrease in ISP. Indeed, the role of durotomy in canine spinal cord injury due to intervertebral disk extrusion (IVDE) is the subject of recent studies (24–27). These studies have reported positive effects on outcomes in dogs with severe grades of thoracolumbar spinal cord dysfunction. Durotomy and duraplasty has been studied in humans with SCIWORA as well (15, 20, 28). Myelotomy has also been described in animal models of SCI and is sporadically reported with positive effects in humans (28). Other types of surgery, including stabilization procedures, are reported for the management of SCIWORA in humans as well (29).

With regard to pharmacological treatment, the dog reported here received a variety of intravenous medications and fluids as emergency treatment which included mannitol and methadone. At that point in time, the diagnosis of traumatic hemorrhagic cervical myelopathy had not yet been reached. Importantly, and justly, treatment was focused on stabilizing the trauma patient (16). After the diagnosis of traumatic hemorrhagic cervical myelopathy and concurrent traumatic brachial plexus injury was determined, treatment consisted of fluid therapy, physiotherapy, an indwelling urinary catheter, repeated non-invasive blood pressure measurements, repeated IV methadone boluses based on pain scoring, oral meloxicam, and oral gabapentin. The latter three medications were used with the aim of providing adequate analgesia. Non-steroidal anti-inflammatory drugs (NSAIDs), or cyclooxygenase (COX) inhibitors are particularly preferred for the treatment of SCIWORA in human patients based on animal models and clinical experience (23). However, there are no large prospective, blinded studies assessing the effect of NSAIDs or COX inhibitors in clinical human patients, let alone canine patients with SCIWORA. Nevertheless, the use of these medications would be supported by the importance of inflammatory cascades in SCI pathophysiology as well as the need for analgesia in trauma patients in general (8, 16, 17, 23). Monitoring for side effects, such as gastrointestinal complications, is always advisable. Specifically when corticosteroids have been administered preceding or concurrently. The use of mannitol for SCI is debatable, but as SCPP would benefit from increased blood volume as well as reduction of spinal cord edema, a beneficial effect is not excluded. Future studies may provide the opportunity to develop more evidence-based guidelines. In this trauma patient, mannitol was administered due to concerns of increased ICP. Finally, the use of opioid receptor agonists may be detrimental for SCI patients. Indeed, the use of opioid receptor antagonists (such as naloxone) has shown some positive results in SCI models (16, 23). However, the use of opioid antagonists is not recommended as it would prevent adequate analgesia for a trauma patient such as reported here, and its effectiveness is not adequately supported by evidence in clinical (human or canine) acute trauma patients.

While hemorrhage is a common feature of traumatic SCI in humans in general (30), it is only reported in a minority of cases of cervical SCIWORA in humans (31–33). Up to 67% of human cases of traumatic SCI have signs compatible with spinal cord hemorrhage on MRI (30). In contrast, one study including 59 patients with SCIWORA described MRI findings consistent with hemorrhage in only two cases (31). The finding of an intramedullary hemorrhagic component is considered a robust indicator of irreversible injury and predictor of injury severity (32). Indeed, intramedullary changes including hemorrhage have been shown to negatively affect prognosis in human SCIWORA patients (12). That being said, conservative management of cervical SCIWORA with hematomyelia may still lead to a positive outcome (33). In our case, conservative management resulted in a fair outcome in the short-term, where most of the remaining deficits affected the right thoracic limb. Those deficits were best explained by a concurrent brachial plexus injury, rather than the traumatic cervical hemorrhagic myelopathy in this dog.

In dogs, the use of T2* gradient echo sequences has been reported of value in assessing hemorrhagic lesions of or affecting the spinal cord (34). In the case reported here, this sequence was instrumental for the identification of an intraparenchymal hemorrhage. No signs of linear tracts extending into the spinal cord were found and the lesion epicenter was located over the C2 vertebral body, making an intradural/intramedullary disk extrusion unlikely. There were no signs of vertebral fractures or dislocation on laterolateral radiographs or the MRI study. However, it has been reported that MRI is less sensitive than CT in the identification of vertebral fractures (35). Orthogonal radiographs also have limited sensitivity (36), let alone single-view radiographs which only provide a two-dimensional evaluation of the vertebral column as was available in this case. Thus, a limitation to this case report is the lack of orthogonal radiographs and CT to definitively exclude vertebral fractures. Still, the lack of extraparenchymal hemorrhage and perivertebral muscle abnormalities makes a concurrent vertebral fracture unlikely in this case.

Other limitations to this case report include the lack of further diagnostic tests for the evaluation of the brachial plexus injury (e.g., electromyography, nerve conduction testing) and lack of histopathological confirmation.

In conclusion, we reported the MRI based diagnosis of traumatic hemorrhagic cervical myelopathy in a dog. Conservative management may be considered in such cases, though the role of surgical treatment (including durotomy) deserves attention and consideration in future studies and cases.

Data availability statement

The original contributions presented in the study are included in the article/supplementary material, further inquiries can be directed to the corresponding author.

Ethics statement

Ethical approval was not required for the studies involving animals in accordance with the local legislation and institutional requirements because the animal was treated in accordance with the local legislation and institutional requirements. Written informed consent was obtained from the owners for the participation of their animals in this study.

Author contributions

KS: Conceptualization, Funding acquisition, Investigation, Visualization, Writing – original draft, Writing – review & editing. IC: Visualization, Writing – review & editing. SP: Conceptualization, Investigation, Visualization, Writing – review & editing.

Funding

The author(s) declare financial support was received for the research, authorship, and/or publication of this article. The publication fee was covered by IVC Evidensia's fund for publication of peer-reviewed scientific articles.

Acknowledgments

The authors would like to thank all involved veterinary staff members of the referring veterinarian as well as the referral hospital for the contributions made to the treatment and follow-up of this patient.

Conflict of interest

IC and SP were employed by Vet Oracle Teleradiology.

The remaining author declares that the research was conducted in the absence of any commercial or financial relationships that could be construed as a potential conflict of interest.

Publisher's note

References

1. Chang Y, Dennis R, Platt SR, Penderis J. Magnetic resonance imaging of traumatic intervertebral disc extrusion in dogs. *Vet Rec*. (2007) 160:795–9. doi: 10.1136/vr.160.23.795

2. Johnson P, Beltran E, Dennis R, Taeymans O. Magnetic resonance imaging characteristics of suspected vertebral instability associated with fracture or subluxation in eleven dogs. *Vet Radiol Ultrasound*. (2012) 53:552–9. doi: 10.1111/j.1740-8261.2012.01959.x

3. Kent M, Eagleson JS, Neravanda D, Schatzberg SJ, Gruenenfelder FI, Platt SR. Intraaxial spinal cord hemorrhage secondary to atlantoaxial subluxation in a dog. *J Am Anim Hosp Assoc*. (2010) 46:132–7. doi: 10.5326/0460132

4. Marr J, Miranda IC, Miller AD, Summers BA. A review of proliferative vascular disorders of the central nervous system of animals. *Vet Pathol*. (2021) 58:864–80. doi: 10.1177/0300985820980707

5. Pancotto TE, Rossmeisl JH Jr, Zimmerman K, Robertson JL, Werre SR. Intramedullary spinal cord neoplasia in 53 dogs (1990-2010): distribution, clinicopathologic characteristics, and clinical behavior. *J Vet Intern Med*. (2013) 27:1500–8. doi: 10.1111/jvim.12182

6. Platt SR, Dennis R, Murphy K, De Stefani A. Hematomyelia secondary to lumbar cerebrospinal fluid acquisition in a dog. *Vet Radiol Ultrasound*. (2005) 46:467–71. doi: 10.1111/j.1740-8261.2005.00085.x

7. Schwab ML, Ferrarin DA, Reginatto Wrzesinski M, Rauber JDS, Ripplinger A, Lamego EC, et al. Clinical and histopathological findings of hemorrhagic progressive Myelomalacia after lumbar tap in 2 dogs: case report. *Top Companion Anim Med*. (2022) 50:100681. doi: 10.1016/j.tcam.2022.100681

8. Spitzbarth I, Moore SA, Stein VM, Levine JM, Kühl B, Gerhauser I, et al. Canine spinal cord injury consortium (CANSORT-SCI). Current insights into the pathology of canine intervertebral disc extrusion-induced spinal cord injury. *Front Vet Sci*. (2020) 7:595796. doi: 10.3389/fvets.2020.595796

9. West N, Butterfield S, Rusbridge C, Fernandez A, Tabanez J, Rudolf NJ, et al. Non-traumatic hemorrhagic myelopathy in dogs. *J Vet Intern Med*. (2023) 37:1129–38. doi: 10.1111/jvim.16694

10. Barker A, Williams JM, Chen A, Bagley R, Jeffery ND. Suspected primary hematomyelia in 3 dogs. *Can Vet J*. (2015) 56:278–84.

11. Atesok K, Tanaka N, O'Brien A, Robinson Y, Pang D, Deinlein D, et al. Posttraumatic spinal cord injury without radiographic abnormality. *Adv Orthop*. (2018) 2018:7060654. doi: 10.1155/2018/7060654

12. Boese CK, Lechler P. Spinal cord injury without radiologic abnormalities in adults: a systematic review. *J Trauma Acute Care Surg*. (2013) 75:320–30. doi: 10.1097/TA.0b013e31829243c9

13. Pang D, Wilberger JE Jr. Spinal cord injury without radiographic abnormalities in children. *J Neurosurg*. (1982) 57:114–29. doi: 10.3171/jns.1982.57.1.0114

14. Pang D. Spinal cord injury without radiographic abnormality in children, 2 decades later. *Neurosurgery*. (2004) 55:1325–43. doi: 10.1227/01.neu.0000143030.85589.e6

15. Zhu F, Yao S, Ren Z, Telemacque D, Qu Y, Chen K, et al. Early durotomy with duroplasty for severe adult spinal cord injury without radiographic abnormality: a novel concept and method of surgical decompression. *Eur Spine J*. (2019) 28:2275–82. doi: 10.1007/s00586-019-06091-1

16. Park EH, White GA, Tieber LM. Mechanisms of injury and emergency care of acute spinal cord injury in dogs and cats. *J Vet Emerg Crit Care*. (2012) 22:160–78. doi: 10.1111/j.1476-4431.2012.00723.x

17. Olby N. The pathogenesis and treatment of acute spinal cord injuries in dogs. *Vet Clin North Am Small Anim Pract*. (2010) 40:791–807. doi: 10.1016/j.cvsm.2010.05.007

18. Saadoun S, Jeffery ND. Acute traumatic spinal cord injury in humans, dogs, and other mammals: the under-appreciated role of the dura. *Front Neurol*. (2021) 12:629445. doi: 10.3389/fneur.2021.629445

19. Werndle MC, Saadoun S, Phang I, Czosnyka M, Varsos GV, Czosnyka ZH, et al. Monitoring of spinal cord perfusion pressure in acute spinal cord injury: initial findings of the injured spinal cord pressure evaluation study*. *Crit Care Med*. (2014) 42:646–55. doi: 10.1097/CCM.0000000000000028

20. Saadoun S, Papadopoulos MC. Acute, severe traumatic spinal cord injury: monitoring from the injury site and expansion Duraplasty. *Neurosurg Clin N Am*. (2021) 32:365–76. doi: 10.1016/j.nec.2021.03.008

21. Jin LY, Li J, Wang KF, Xia WW, Zhu ZQ, Wang CR, et al. Blood-spinal cord barrier in spinal cord injury: a review. *J Neurotrauma*. (2021) 38:1203–24. doi: 10.1089/neu.2020.7413

22. Popa C, Popa F, Grigorean VT, Onose G, Sandu AM, Popescu M, et al. Vascular dysfunctions following spinal cord injury. *J Med Life*. (2010) 3:275–85.

23. Zhang Y, Al Mamun A, Yuan Y, Lu Q, Xiong J, Yang S, et al. Acute spinal cord injury: pathophysiology and pharmacological intervention (review). *Mol Med Rep*. (2021) 23:417. doi: 10.3892/mmr.2021.12056

24. Hirano R, Asahina R, Hirano T, Hyakkoku A, Miura R, Kunihiro T, et al. Outcomes of extensive hemilaminectomy with durotomy on dogs with presumptive progressive myelomalacia: a retrospective study on 34 cases. *BMC Vet Res*. (2020) 16:476. doi: 10.1186/s12917-020-02690-z

25. Jeffery ND, Mankin JM, Ito D, Boudreau CE, Kerwin SC, Levine JM, et al. Extended durotomy to treat severe spinal cord injury after acute thoracolumbar disc herniation in dogs. *Vet Surg*. (2020) 49:884–93. doi: 10.1111/vsu.13423

26. Nakamoto Y, Uemura T, Hasegawa H, Nakamoto M, Ozawa T. Outcomes of dogs with progressive myelomalacia treated with hemilaminectomy or with extensive hemilaminectomy and durotomy. *Vet Surg*. (2021) 50:81–8. doi: 10.1111/vsu.13514

27. Takahashi F, Honnami A, Toki M, Dosaka A, Fujita Y, Hara Y, et al. Effect of durotomy in dogs with thoracolumbar disc herniation and without deep pain perception in the hind limbs. *Vet Surg*. (2020) 49:860–9. doi: 10.1111/vsu.13409

28. Telemacque D, Zhu FZ, Ren ZW, Chen KF, Drepaul D, Yao S, et al. Effects of durotomy versus myelotomy in the repair of spinal cord injury. *Neural Regen Res*. (2020) 15:1814–20. doi: 10.4103/1673-5374.280304

29. Qi C, Xia H, Miao D, Wang X, Li Z. The influence of timing of surgery in the outcome of spinal cord injury without radiographic abnormality (SCIWORA). *J Orthop Surg Res*. (2020) 15:223. doi: 10.1186/s13018-020-01743-1

30. Leypold BG, Flanders AE, Burns AS. The early evolution of spinal cord lesions on MR imaging following traumatic spinal cord injury. *AJNR Am J Neuroradiol*. (2008) 29:1012–6. doi: 10.3174/ajnr.A0962

31. Liu Q, Liu Q, Zhao J, Yu H, Ma X, Wang L. Early MRI finding in adult spinal cord injury without radiologic abnormalities does not correlate with the neurological outcome: a retrospective study. *Spinal Cord*. (2015) 53:750–3. doi: 10.1038/sc.2015.45

32. Talbott JF, Huie JR, Ferguson AR, Bresnahan JC, Beattie MS, Dhall SS. MR imaging for assessing injury severity and prognosis in acute traumatic spinal cord injury. *Radiol Clin N Am*. (2019) 57:319–39. doi: 10.1016/j.rcl.2018.09.004

33. Pillai A, Crane E, Chappell A, Buchan M. Traumatic cervical hematomyelia: report of a rare spinal cord injury without radiographic abnormality. *J Trauma*. (2008) 65:938–41. doi: 10.1097/01.ta.0000197909.10358.0f

34. Hammond LJ, Hecht S. Susceptibility artifacts on T2*-weighted magnetic resonance imaging of the canine and feline SPINE. *Vet Radiol Ultrasound*. (2015) 56:398–406. doi: 10.1111/vru.12245

35. Gallastegui A, Davies E, Zwingenberger AL, Nykamp S, Rishniw M, Johnson PJ. MRI has limited agreement with CT in the evaluation of vertebral fractures of the canine trauma patient. *Vet Radiol Ultrasound*. (2019) 60:533–42. doi: 10.1111/vru.12785

36. Kinns J, Mai W, Seiler G, Zwingenberger A, Johnson V, Cáceres A, et al. Radiographic sensitivity and negative predictive value for acute canine spinal trauma. *Vet Radiol Ultrasound*. (2006) 47:563–70. doi: 10.1111/j.1740-8261.2006.00186.x

frontiers | Frontiers in Veterinary Science

TYPE Original Research
PUBLISHED 08 November 2023
DOI 10.3389/fvets.2023.1219943

OPEN ACCESS

EDITED BY
Philippa Johnson,
Cornell University, United States

REVIEWED BY
Erica Andrews,
Cornell University, United States
Yoshihiko Yu,
Independent researcher, Mitaka, Japan

*CORRESPONDENCE
Lea Carisch
✉ lea.carisch@uzh.ch

RECEIVED 09 May 2023
ACCEPTED 16 October 2023
PUBLISHED 08 November 2023

CITATION
Carisch L, Lindt B, Richter H and Del Chicca F (2023) Regional ADC values of the morphologically normal canine brain. *Front. Vet. Sci.* 10:1219943. doi: 10.3389/fvets.2023.1219943

Regional ADC values of the morphologically normal canine brain

Lea Carisch*, Blanca Lindt, Henning Richter and Francesca Del Chicca

Clinic for Diagnostic Imaging, Department of Diagnostics and Clinical Services, Vetsuisse Faculty, University of Zurich, Zurich, Switzerland

Introduction: Diffusion-weighted magnetic resonance imaging is increasingly available for investigation of canine brain diseases. Apparent diffusion coefficient (ADC) of normal canine brains is reported only in small numbers of subjects. The aim of the study was to investigate the ADC of different anatomical regions in the morphologically normal brain in a large population of canine patients in clinical setting. Additionally, possible influence on the ADC value of patient-related factors like sex, age and body weight, difference between the left and right side of the cerebral hemispheres, and between gray and white matter were investigated.

Methods: Brain magnetic resonance studies including diffusion-weighted images of dogs presented at the Vetsuisse Faculty-University Zurich between 2015 and 2020 were reviewed retrospectively. Only morphologically normal brain magnetic resonance studies of dogs presented with neurological signs or non-neurological signs were included. Apparent diffusion coefficient values of 12 regions of interest (ROIs) in each hemisphere and an additional region in the cerebellar vermis were examined in each dog.

Results: A total of 321 dogs (including 247 dogs with neurological signs and 62 dogs with non-neurological signs) of various breeds, sex and age were included. Apparent diffusion coefficient significantly varied among most anatomical brain regions. A significantly higher ADC was measured in the gray [median 0.79 (range 0.69–0.90) $\times$ 10^{-3} mm^2/s] compared to the white matter [median 0.70 (range 0.63–0.85) $\times$ 10^{-3} mm^2/s]. No significant differences were found between the left and right cerebral hemispheres in most of the regions, neither between sexes, different reproductive status, and not consistently between body weight groups. Age was correlated first with a decrease from dogs <1 year of age to middle-age ($\geq$3 to <8 years) dogs and later with an increase of ADC values in dogs $\geq$8 years.

Discussion: Apparent diffusion coefficient values of 25 ROIs were described in 321 morphologically normal canine brains in clinical setting. Apparent diffusion coefficient differences depending on the brain anatomical region are present. Apparent diffusion coefficient differences among age classes are present, likely consistent with brain maturation and aging. The described data can be a reference for future studies in clinical settings on the canine brain.

KEYWORDS

magnetic resonance imaging, canine, MRI, apparent diffusion coefficient, ADC, DWI, neuroimaging

Introduction

Diffusion-weighted imaging (DWI) is gaining popularity in advanced imaging in veterinary medicine and allows quantification of water molecule movement in tissue based on Brownian motion (1). Two diffusion sensitizing gradients – a dephasing and a rephasing gradient - of the same strength, are used next to a 180° radiofrequency pulse. Missing signal return is the result of moving water molecules not being rephased, causing a quantifiable reduction of the magnetic resonance (MR) signal. Movement of water molecules is anti-proportional to tissue cellularity, therefore signal loss can be used to evaluate water molecule's degree of restricted diffusion (2). The strength of the diffusion sensitizing gradient is defined by its *b*-value (s/mm^2).

Hence, DWI provides information about integrity and to some extent functionality of tissue, and consequently potential pathology (3–5). Based on DWI sequences, apparent diffusion coefficient (ADC) maps can be generated, and the ADC quantified (in mm^2/s) in specific regions of interest (ROIs). Variations in ADC can be used to detect and characterize pathological processes (6).

In human medicine DWI is widely used not only with diagnostic purposes to evaluate infarction (7–10), trauma (11) and infection (12) but also for assessment of different neoplasia and individual treatment response (13–16). Further studies investigate mapping of brain regions for identification of epileptogenic zones (17, 18). Moreover, DWI has been used to describe brain maturation and aging in the human brain (19–23) and ADC is known to vary in different regions of the human brain (24). In veterinary medicine, earlier studies mainly describe the use of DWI investigating cerebrovascular incidents in dogs (25, 26), cats (27), rats (28) and brain edema in cats (29). Potential use of DWI also includes evaluation of neoplastic, inflammatory, and epileptic disorders (30–36). Studies evaluating ADC values in the morphologically normal canine brain are rare, (4, 5, 37) with reported differences depending on the anatomical region and on the side of the cerebral hemisphere (4, 5) in small numbers of dogs.

The present study aimed to investigate regional ADC in selected brain regions in the morphologically normal dog brain in clinical setting. No influence of sex, reproductive status and body weight (BW) on ADC has been hypothesized. Difference in ADC depending on the side of the brain hemisphere, on age of the patients, between gray and white matter, and among anatomical regions have been hypothesized.

Materials and methods

Animals

Clinical records of the small animal clinic, Vetsuisse Faculty of the University of Zurich, were reviewed retrospectively. Dogs that underwent magnetic resonance imaging (MRI) examination of the brain, including DWI sequences (see MRI technique), between January 2015 and February 2020 were reviewed. Only dogs with a morphologically normal brain MR examination (absence of abnormalities in morphology and signal intensity in all provided sequences) were included in the study. The diagnosis of a morphologically normal brain study had been stated by a board-certified radiologist, and the images were reviewed by another board-certified radiologist (FDC) at the time of inclusion in the study. If cerebrospinal fluid (CSF) tap was performed, only dogs with normal CSF tap were included. Mildly blood-contaminated samples that were marked by our laboratory, but considered diagnostic, were also included. The analysis consisted of: cell count (reference value: <5 cells/μL), protein concentration (reference value: ≤30 mg/dL) and cytological analysis of cell type as well as serological analysis if indicated. Dogs with any laboratory records of CSF tap abnormalities were excluded. As of the retrospective nature of this study, there was no need to inquire ethical consent. However, a consent form for the use of the dogs' data for academic purposes was signed by the owners of all dogs included.

Magnetic resonance imaging technique

The MRI examinations of all dogs were performed at the Vetsuisse Faculty, University of Zurich. A 3 T MRI scanner (Philips Ingenia 3.0 T scanner, Philips AG Healthcare, Zurich, Switzerland) and a 32-channel coil (dStream HeadNeck, 32ch MR coil; Philips AG Healthcare) or 16-channel coil (dStream HandWrist, 16ch MR coil; Philips AG Healthcare) for small dogs was used. The dogs were positioned in dorsal recumbency under general anesthesia, using case-by-case anesthetic protocols. Images of the brain including the olfactory lobes to at least the second cervical vertebrae were acquired. The standard brain protocol included the sequences with the parameters listed in Supplementary Table S1. Diffusion-weighted (DW) images were acquired in a transverse plane, setting the two *b*-values at 0 s/mm^2 and 1,000 s/mm^2, respectively, and using sensitivity encoding (SENSE) technique and diffusion gradients in all three planes (*x*-, *y*- and *z*-plane). Contrast medium was injected after the DW sequence (DOTAREM 0.2 mL/kg IV [Gadoteric acid; Guerbet Gmbh, Sulzbach, Germany]) followed by saline solution (NaCl 0.9% 5 mL IV).

Data analysis

The signalment, including breed, sex, reproductive status, age, BW, and the symptomatology at presentation was recorded from the medical records of all dogs. Further, body temperature as well as duration of the MRI examination was recorded. All acquired MR images were assessed using a dedicated software (Philips IntelliSpace Portal version 10.1.1; Philips AG, Amsterdam, NL). After acquisition of the DW images, using the IntelliSpace software diffusion package, if necessary, motion correction has been performed. From the DWI sequence, the B0-treshold was adjusted to exclude background pixels from the functional map calculations. The used b-values were selected, and a new imaging series (ADC iso map) generated. Anatomical co-registration (align registration) with the T2W sequence was performed and visually controlled to ensure quality of registration prior to ROI placement.

A total of 13 anatomical brain regions were defined as ROIs and manually drawn in the transverse plane on the ADC map as follows: caudate nucleus, internal capsule (two locations, one rostral and one caudal), piriform lobe, thalamus, hippocampus, occipital lobe (white and gray matter combined and separate), cerebellar lobe (white and gray matter combined and separate), cerebellar vermis (Figure 1).

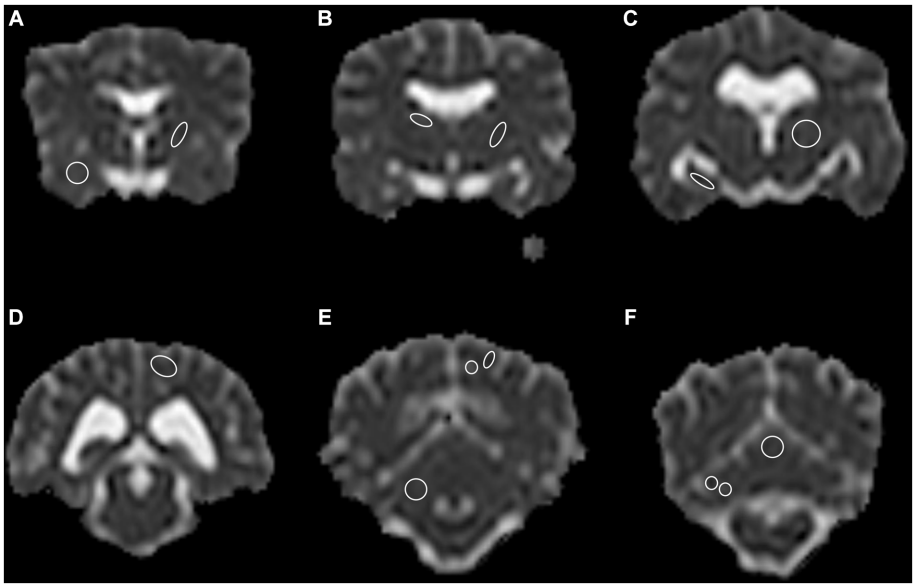

FIGURE 1
A total of 13 anatomical regions were defined as regions of interest (ROI) and drawn on both cerebral hemispheres in the transverse plane, except for the cerebellar vermis, only drawn in the center. **(A)** Right piriform lobe; left rostral internal capsule, **(B)** Right caudate nucleus; left caudal internal capsule, **(C)** Right hippocampus; left thalamus, **(D)** Left occipital lobe, gray and white matter combined, **(E)** Right cerebellum gray and white matter combined; left occipital lobe, gray and white matter separate, **(F)** Right cerebellar hemisphere gray and white matter separate; central vermis, gray and white matter combined. Note the limited spatial resolution of the apparent diffusion coefficient (ADC) map. The left side is on the right side of the image. Border ROI thickness has been increased for representative purposes. Only one side per ROI for representative purposes depicted.

With exception of the cerebellar vermis each ROI was drawn in both left and right hemisphere of the brain, leading to a total of 25 ROIs drawn in each dog. Each ROI was drawn on the slice representing the structure most accurately. Whenever a structure was visible on more than one slice (e.g., thalamus), the slice representing the region with the subjectively largest extent was chosen. Images of all the other sequences and planes and co-registration were used as reference to better identify the anatomy while drawing the ROI. Typically, the ROIs were drawn as follows: on the head of the caudate nucleus; on the rostral and caudal internal capsule (rostral at the level of the head of the caudate nucleus or one slice caudally; and caudal, one or two slices apart from the rostral localization); on the thalamus hemisphere as published in cats (38). The other ROIs were drawn at the level of the best definition and largest extent of the corresponding anatomical structure. ROIs were drawn excluding adjacent brain regions or CSF. ROIs were not drawn in the presence of any kind of artifacts. Considering the different anatomical structures and dogs' sizes, the position and size of the ROI was adapted to each animal. Therefore, the size of the ROI varied strongly among the different brain regions and among dogs. Drawn regions of interest underwent an internal alignment control: in the first 20 cases, all ROIs were drawn by consensus of two of the authors (BL, a veterinarian specifically trained and FDC, an experienced board-certified radiologist). ROIs of the remaining cases were drawn by only one of the authors (BL). In case of uncertainty, the ROIs were placed by consensus of the two authors. ROI ADC values were expressed in 10^{-3} mm^2/s and size in mm^2.

To assess possible influence of age on ADC values, the study population was grouped in four age classes selected to match different dog life stages: <1 year – early and late puppyhood; ⩾1 to <3 years – young adults; ⩾3 to <8 years – mature adults; and ⩾8 years – senior dogs. Depending on BW, animals were grouped into three BW groups: ⩽10 kg, >10 – ⩽25 kg, >25 kg. Dogs were grouped depending on the reason for MR examination at presentation. Dogs presented with neurological signs were compared to dogs presented with non-neurological signs. Dogs with unclear neurological status were excluded for this analysis. Classifications were based on medical records.

Statistical analysis

Data were collected in a spreadsheet software (Microsoft Excel version 16.45; Microsoft, Redmond, WA, United States) and analyzed using statistical software (IBM SPSS Statistics version 27.0; SPSS, IBM Corp, Armonk, NY, United States). Data for ADC values were not normally distributed and analyzed as non-parametrical. Descriptive statistic was performed, data reported as median (range) and mean ± SD was added when appropriate. The ADC values were tested for statistical difference according to sex and reproductive status, BW group and age classes; as well as differences between right and left cerebral hemisphere and between white and gray matter regions. The ADC between ROIs was analyzed using Friedman's test for dependent variables, followed by Bonferroni *post-hoc* correction for multiple pairwise tests. Independent variables were analyzed with the Kruskal–Wallis test (for multiple comparisons) or the Mann–Whitney test (for pairwise comparisons), followed by Bonferroni *post-hoc* correction for multiple pairwise tests. Overall, the level of significance was set at $p < 0.05$.

TABLE 1 Demographic table of dogs included in the study.

Gender	Nr. of dogs	Age (months) median (range)	Weight (kg) median (range)
male intact	82	56.5 (4.4–155.1)	18 (2.6–56.0)
male castrated	115	77.1 (8.7–164)	16.7 (2.0–72.0)
female intact	35	52.0 (4.1–156.2)	7.3 (1.4–33.0)
female spayed	87	100.6 (14.2–194.4)	18.4 (2.1–41.7)
unknown	2	70.4 (38.1–102.8)	7.6 (7.2–7.9)
Breed			
French Bulldog	22	47.2 (11.0–119.1)	12.1 (8.0–27.2)
Labrador Retriever	16	73.1 (35.9–156.2)	30.7 (25.0–41.0)
Chihuahua	13	97.5 (40.9–142.4)	2.7 (2.0–5.2)
Pug	9	96.8 (12.9–151.7)	7.3 (6.0–9.3)
Mixed	64	82.2 (5.2–176.3)	19 (3.1–45.8)
others	197	69.5 (4.1–194.4)	18.3 (1.4–72)
Skull shape			
Brachycephalic	63	72.8 (4.1–151.7)	10.0 (2.0–38.0)
Mesocephalic	145	71 (4.2–194.4)	18.4 (1.4–56.0)
Dolichocephalic	42	69 (9.4–169.3)	24 (4.3–72.0)

Results

A total of 321 dogs met the inclusion criteria and were included in the study (Table 1). Eighty-eight different pure breeds were represented including: French Bulldog ($n = 22$), Labrador Retriever ($n = 16$), Chihuahua ($n = 13$), Pug ($n = 9$), Australian Shepherd ($n = 8$), Border Collie ($n = 7$), German Shepherd ($n = 7$), Dachshund ($n = 6$), Maltese ($n = 6$), Miniature Spitz ($n = 6$), Yorkshire Terrier ($n = 6$), Bernese Mountain Dog ($n = 5$), Golden Retriever ($n = 5$), Jack Russel Terrier ($n = 5$), Beagle ($n = 4$), Cocker Spaniel ($n = 4$), Papillon ($n = 4$), Rhodesian Ridgeback ($n = 4$). Other pure breeds were represented by less than 3 dogs per breed. Sixty-four dogs were of mixed breed and 7 of unknown breed (breed information not disclosed in patient history). Of the pure breeds 63 were brachycephalic, 145 mesocephalic and 42 dolichocephalic (39, 40). One hundred and ninety-seven dogs were male (61.4%) and 122 (38.0%) were female. Eighty-two (25.6%) were intact male dogs, 115 (35.8%) were castrated males. Thirty-five (10.9%) were intact females and 87 (27.1%) were spayed females. Two dogs were of unknown sex (0.6%). Median age was 71.8 months (range 4.1–194.4 months). Dogs were grouped depending on the age as follows: <1 year ($n = 21$); ⩾1 to <3 years ($n = 41$); ⩾3 to <8 years ($n = 142$); and ⩾8 years ($n = 117$). BW was recorded for 320 dogs (median 16.7 kg and range 1.4–72 kg) and grouped as follows: ⩽10 kg ($n = 104$), >10 – ⩽25 kg ($n = 109$), >25 kg ($n = 107$). In one dog the BW was unknown.

The study population included clinical patients and consisted of dogs with neurological signs ($n = 247$) and with clinical signs other than neurological signs ($n = 62$). Dogs were presented for MRI examination with neurological signs ($n = 247$) including seizures (epileptic $n = 114$, non-epileptic $n = 15$), cranial nerve dysfunction ($n = 25$) vestibular dysfunction (peripheral $n = 33$, indistinguishable $n = 6$, central $n = 1$), balance impairment and gait disturbances other than vestibular dysfunction ($n = 39$), and impaired consciousness ($n = 14$). Sixty-two dogs underwent MRI examination for reasons other than neurological signs, including behavioral changes ($n = 27$), ophthalmologic disease ($n = 13$), head/neck pain ($n = 11$), ear disease without neurological deficits ($n = 6$), musculoskeletal disorder ($n = 2$), endocrine disease ($n = 2$) and one dog with nasal discharge. In 12 dogs the neurological status remained unclear, and they were excluded for the analysis of comparison between dogs with neurological signs and those presented for non-neurological signs. In 225 dogs, CSF was tapped from atlanto-occipital ($n = 224$) or lumbar site ($n = 1$). Body temperature was recorded in 253/321 dogs at the time of induction of general anesthesia (median 38.2°C; range 34.5–39.8°C) and at the end of the MR examination (median 37.0°C; range 33.5–40.5°C). The median examination time was 48 min (range 23–121 min). Typically, the DW sequence was performed in the second half of the examination. A total of 7,921 ROIs were drawn. The ADC values (mean ± SD and median and range) and the ROIs size are reported in Table 2. Artifacts prevented the drawing of one or more ROIs in 11 dogs (for a total of 100 ROIs).

The highest ADC values (details in Table 2 and overview in Figure 2) were recorded in the piriform lobe [0.84 (0.70–0.97) $\times 10^{-3}$ mm^2/s], followed by the occipital lobe gray matter [0.83 (0.61–1.06) $\times 10^{-3}$ mm^2/s] and the hippocampus [0.82 (0.63–0.96) $\times 10^{-3}$ mm^2/s]. The lowest ADC value was recorded in the cerebellar white matter region [0.69 (0.57–0.82) $\times 10^{-3}$ mm^2/s]. The largest ROI size was drawn in the thalamus [19.9 (9.5–37.4) mm^2] and the smallest in the white matter of the occipital lobe [8.1 (3.9–14.7) mm^2; Table 2]. For most of the analyzed ROIs, the difference in ADC was statistically significant (Table 3). Significantly higher ADC ($p < 0.001$) were measured in the gray [0.79 (0.69–0.90) $\times 10^{-3}$ mm^2/s] compared to the white matter [0.70 (0.63–0.85) $\times 10^{-3}$ mm^2/s]. Statistically significant difference was present between right and left hemisphere in 5 ROIs ($p < 0.001$–$p = 0.047$): the caudate nucleus [left 0.75 (0.56–0.86) $\times 10^{-3}$ mm^2/s, right 0.77 (0.55–0.91) $\times 10^{-3}$ mm^2/s], internal capsule caudal [left 0.71 (0.60–0.91) $\times 10^{-3}$ mm^2/s, right 0.72 (0.59–0.88) $\times 10^{-3}$ mm^2/s], piriform lobe [left 0.83 (0.71–0.98) $\times 10^{-3}$ mm^2/s, right

TABLE 2 Apparent diffusion coefficient (ADC) and the region of interest (ROI) size in 321 dogs of the right and left hemisphere separately and averaged.

Location	Hemisphere (Nr. of ROI)	Mean ADC mean ± SD	Median	Min.	Max.	ADC hemispheres averaged median (range) mean ± SD	ROI size (mm^2) median (range)
Caudate Nucleus	Right (321)	0.7619 ± 0.0489	0.77	0.55	0.91	0.76 (0.55–0.88) 0.7546 ± 0.05	13.4 (6.8–24.9)
	Left (321)	0.7473 ± 0.0502	0.75	0.56	0.86		
Internal Capsule rostral	Right (320)	0.7072 ± 0.0424	0.71	0.56	0.88	0.71 (0.61–0.89) 0.7068 ± 0.0412	12.8 (4.6–24.7)
	Left (321)	0.7065 ± 0.0401	0.70	0.56	0.91		
Internal Capsule caudal	Right (321)	0.7155 ± 0.0422	0.72	0.59	0.88	0.72 (0.60–0.90) 0.71360 ± 0.0407	15.5 (5.9–31.7)
	Left (321)	0.7117 ± 0.0392	0.71	0.60	0.91		
Piriform Lobe	Right (320)	0.8353 ± 0.0386	0.83	0.68	0.96	0.84 (0.70–0.97) 0.8371 ± 0.0384	18.4 (9.0–37.0)
	Left (320)	0.8390 ± 0.0382	0.83	0.71	0.98		
Thalamus	Right (320)	0.7325 ± 0.0309	0.73	0.63	0.82	0.73 (0.66–0.82) 0.7315 ± 0.0321	19.9 (9.5–37.4)
	Left (320)	0.7305 ± 0.0332	0.73	0.62	0.81		
Hippocampus	Right (318)	0.8202 ± 0.0577	0.82	0.62	0.98	0.82 (0.63–0.96) 0.8160 ± 0.0614	10.5 (4.3–17.5)
	Left (318)	0.8117 ± 0.0647	0.81	0.63	0.97		
Occipital Lobe gray & white matter av.	Right (316)	0.7202 ± 0.0535	0.72	0.59	0.89	0.72 (0.59–0.88) 0.7213 ± 0.0521	17.5 (8.5–32.4)
	Left (317)	0.7224 ± 0.0507	0.72	0.58	0.89		
Occipital Lobe gray matter	Right (314)	0.8228 ± 0.0870	0.83	0.59	1.08	0.83 (0.61–1.06) 0.8262 ± 0.0838	10.2 (4.9–19.7)
	Left (315)	0.8296 ± 0.0805	0.83	0.57	1.06		
Occipital Lobe white matter	Right (314)	0.7063 ± 0.0558	0.70	0.59	0.94	0.71 (0.62–0.87) 0.7081 ± 0.0514	8.1 (3.9–14.7)
	Left (315)	0.7098 ± 0.0467	0.71	0.57	0.86		
Cerebellum gray & white matter av.	Right (314)	0.6951 ± 0.0461	0.69	0.60	0.86	0.69 (0.59–0.83) 0.6967 ± 0.0449	16 (7.6–31.6)
	Left (313)	0.6983 ± 0.0437	0.70	0.57	0.87		
Cerebellum gray matter	Right (313)	0.7299 ± 0.0647	0.73	0.56	0.97	0.73 (0.61–0.96) 0.7343 ± 0.0615	12.3 (5.7–23.0)
	Left (312)	0.7387 ± 0.0582	0.73	0.62	0.95		
Cerebellum white matter	Right (312)	0.6855 ± 0.0529	0.69	0.55	0.87	0.69 (0.57–0.82) 0.6862 ± 0.0506	11.8 (5.7–23.0)
	Left (311)	0.6869 ± 0.0482	0.68	0.56	0.81		
Vermis gray & white matter av.	Middle (314)	0.7196 ± 0.0772	0.71	0.57	1.08	0.71 (0.57–1.08) 0.7196 ± 0.0772	9.8 (4.8–18.3)

ADC values are in ($\times 10^{-3}$ mm^2/s). Max., maximum ADC; Min., minimum ADC; av., averaged.

0.83 (0.68–0.96) × 10^{-3} mm^2/s], hippocampus [left 0.81 (0.63–0.97) × 10^{-3} mm^2/s, right 0.82 (0.62–0.98) × 10^{-3} mm^2/s] and cerebellum gray matter [left 0.73 (0.62–0.95) × 10^{-3} mm^2/s, right 0.73 (0.56–0.91) × 10^{-3} mm^2/s]. No hemisphere side had consistently higher ADC values. No statistically significant difference in ADC values between male and female dogs or depending on reproductive status was present.

Depending on the BW classes, differences were found in 3 ROIs (occipital lobe combined matter, cerebellum gray matter, cerebellar vermis; $p < 0.001$–$p = 0.011$). In 1 ROI (occipital lobe combined matter) the median values were higher within the ⩽10 kg group whereas in 2 ROIs (vermis, cerebellum gray matter) the median values were higher within the >25 kg group. No BW group had consistently higher ADC. Statistically significant differences were mainly but not consistently found between the age class <1 year to the middle-aged class (⩾3 to <8 years) with highest median values within dogs <1 year of age (Figure 3). Overall, median ADC values within gray and white matter decreased from dogs under 1 year of age to middle-aged dogs (⩾3 to <8 years) and increased again in dogs over 8 years of age.

Statistically significant differences were found in the internal capsule (rostral and caudal) in dogs presented with neurological signs compared to dogs presented with non-neurological signs. In both ROIs the ADC values were higher in the group with neurological signs. No difference was found between ADC drawn by consensus and values from the single observer.

Discussion

The study describes the regional ADC values in morphologically normal brains in a large population of canine patients in clinical settings. The highest ADC values were measured in the piriform lobe followed by the occipital lobe and the hippocampus. Other studies report the highest ADC values in the hippocampus followed by the

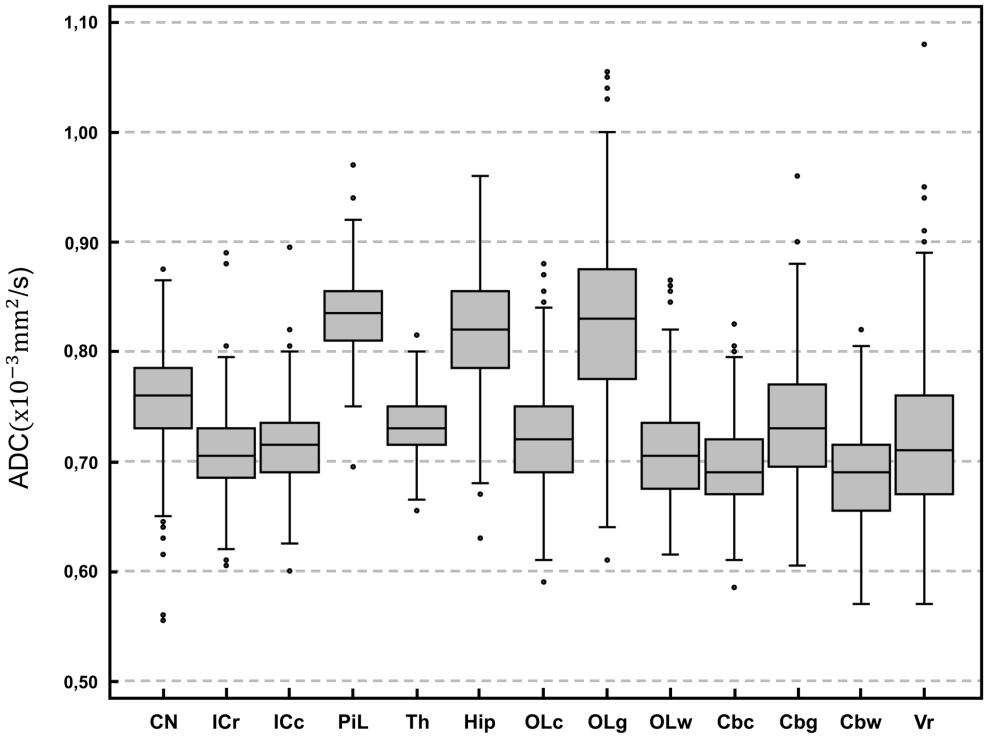

FIGURE 2
Box-plot comparison of apparent diffusion coefficient (ADC; × 10^{-3} mm^2/s) among anatomical regions of interest. For each plot, the box represents the 25th to 75th percentiles, the horizontal line represents the median. Whiskers indicate the highest value within 1.5-times the interquartile range (IQR) and the lowest value within 1.5-times the IQR. Dots represent the outliers. CN, caudate nucleus; ICr, internal capsule rostral; ICc, internal capsule caudal; PiL, piriform lobe; Th, thalamus; Hip, hippocampus; OLc, Occipital lobe combined; OLg, occipital lobe gray matter; OLw, occipital lobe white matter; Cbc, cerebellum combined; Cbg, Cerebellum gray matter; Cbw, cerebellum white matter; Vr, vermis. Except for vermis, right and left hemisphere values are averaged.

TABLE 3 Statistical comparison (Friedman test with *post-hoc* test Bonferroni correction for multiple testing) of ADC values among anatomical regions of interest.

	CN	ICr	ICc	PiL	Th	Hip	OLc	OLg	OLw	Cbc	Cbg	Cbw	Vr
CN													
ICr	#												
ICc	#	1.000											
PiL	#	#	#										
Th	#	#	#	#									
Hip	#	#	#	0.093	#								
OLc	#	0.029*	1.000	#	0.575	#							
OLg	#	#	#	0.024*	#	1.000	#						
OLw	#	1.000	1.00	#	#	#	0.131	#					
Cbc	#	1.000	0.007*	#	#	#	#	#	0.611				
Cbg	#	#	0.004*	#	1.000	#	1.000	#	#	#			
Cbw	#	0.008*	#	#	#	#	#	#	0.002*	1.000	#		
Vr	#	1.000	1.000	#	0.005*	#	1.000	#	1.000	0.001*	0.036*	#	

Values marked with * are statistically significant ($p < 0.05$) and values below 0.001 are indicated by #. CN, caudate nucleus; ICr, internal capsule rostral; ICc, internal capsule caudal; PiL, piriform lobe; Th, thalamus; Hip, hippocampus; OLc, Occipital lobe combined; OLg, occipital lobe gray matter; OLw, occipital lobe white matter; Cbc, cerebellum combined; Cbg, Cerebellum gray matter; Cbw, cerebellum white matter; Vr, vermis.

piriform lobe (4); in the cortex of the frontal and parietal lobes followed by the occipital lobe and hippocampus (5). The lowest ADC value was found in the cerebellar white matter, similar to findings in cats (3). As shown in Table 4, ADC values of the present study were substantially similar as reported (5), except for the gray matter of the cerebellum. Higher regional ADC values have also been reported (4).

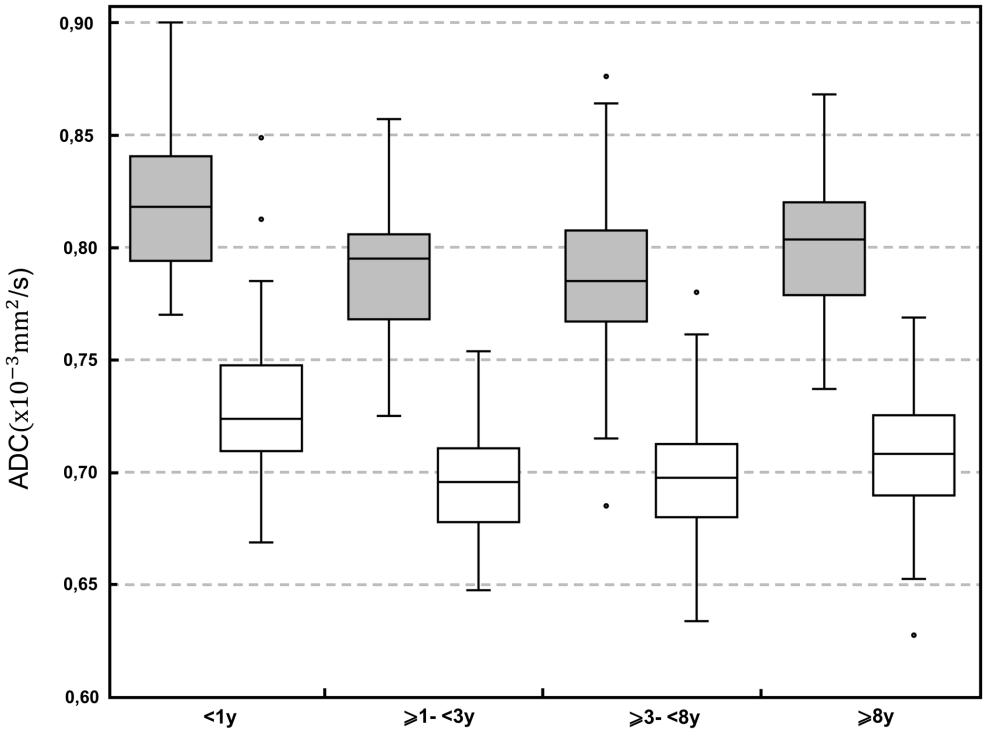

FIGURE 3
Boxplot of the apparent diffusion coefficient (ADC; × 10^{-3} mm^2/s) in the different age classes: <1; ⩾1 to <3 years; ⩾3 to <8 years; and ⩾8 years. Grey boxes represent gray matter; white boxes represent white matter. For each plot, the box represents the 25th to 75th percentiles, the horizontal line represents the median. Whiskers represent the highest value within 1.5-times the interquartile range (IQR) and the lowest value within 1.5-times the IQR. Dots represent the outliers.

However, different ADC values of different studies should be compared cautiously because they are strongly influenced by differences in equipment and technology used. This includes the system type, the strength of the magnet and the applied scanning protocol. Even using the same coil, variations in ADC values are reported (41). To minimize these variations, the same magnet, coils, and protocol were used in the present study. Similar ADC values were reported with identical magnet strength and *b*-values (5).

Apparent diffusion coefficient values of white matter regions were significantly lower compared to gray matter. This is expected since white matter, contrary to gray matter, mainly consists of myelinated axons, which act as diffusion barriers and lead to lower ADC values (5). Moreover, myelinated axons are responsible for a directional diffusion pattern, parallel to the axonal pathways, called anisotropy (5, 42). This finding is reproducible in dogs and humans (4, 5, 23, 43) and has been recently described also in cats (3).

The median ADC significantly differed in 5 ROIs between right and left cerebral hemisphere. Apparent diffusion coefficient was not consistently higher on one hemisphere side: significantly higher ADC was found in the right caudate nucleus, internal capsule and hippocampus, and in the left piriform lobe and cerebellum gray matter. Statistically higher ADC values in the left cerebral hemisphere have been reported (4), as well as higher, but not significantly different values in the right hemisphere (5) in a smaller number of dogs. Asymmetry in ADC values in several regions has been described in humans, with some correlation to age and gender (44). One of the most accredited explanations is that asymmetry in cerebral structures or neuronal density could influence cell density and therefore diffusivity, causing differences in ADC depending on the side. Higher neuronal density leads to lower diffusion and the right canine brain hemisphere has been reported being heavier than the left (45). Handedness is a discussed explanation for laterality in human brains (46) influencing cell density and therefore diffusivity, causing differences in ADC depending on the side (47). Pawedness in dogs and associated brain asymmetry is also described. However, in studies on dogs that do show pawedness, no overrepresentation of the left or right paw was found (48–50) This could support the lack of consistency for higher ADC values in one side of the hemispheres in our study.

Similarly, to our results, no difference in ADC values depending on the sex has been found in cats (3). Studies in canines and humans showed an effect of age on diffusivity in the brain. In humans ADC values decrease until adulthood and increase during the senescence period. Myelination during adolescence and, inversely, loss of extracellular volume and demyelination during senescence have been discussed as underlying causes. (5, 44, 51, 52) In our study, median ADC values decreased from dogs younger than 1 year of age to middle aged dogs (⩾3 to <8 years) and increased again in the age class of dogs older than 8 years. The changes in myelination would support our results, considering the different life span between humans and dogs, and likely according to different pace of age-relating changes of the brain.

Similarly, as reported (5), no consistent differences between BW groups and median ADC values were found in our study. There is no convincing explanation for the described difference in three ROIs

TABLE 4 Comparison of ADC values between current and previous studies.

Equipment				
		Current study	MacLellan et.al.	Hartmann et.al
MR equipment		Philips Ingenia 3.0 T scanner. Philips AG Healthcare. Zurich. Switzerland	GE Signa HDx 3.0-T MRI scanner. GE Medical Systems. Milwaukee. WI. USA	Philips Intera Gyroscan. Philips Healthcare. Hamburg. Germany
Field strength b-value		3 Tesla 0 and 1′000 s/mm^2	3 Tesla 0 and 1′000 s/mm^2	1 Tesla 0 and 800 s/mm^2
Coils		dStream HeadNeck. 32ch MR coil; dStream HandWrist. 16ch MR coil	HD T/R quad extremity. Invivio, Pewaukee. Wis.	SENSE-flex M coil
Sample size		321 dogs	13 dogs	10 dogs
ADC				
Location	Hemisphere	Current study mean±SD (× 10^{-3} mm^2/s)	MacLellan mean±SD (× 10^{-3} mm^2/s)	Hartmann mean±SD (× μm^2/s)
Caudate Nucleus	Right	0.7619 ± 0.0489		843.3 ± 94.3
	Left	0.7473 ± 0.0502		962.4 ± 103.2
Internal Capsule rostral	Right	0.7072 ± 0.0424		
	Left	0.7065 ± 0.0401		
Internal Capsule caudal	Right	0.7155 ± 0.0422		
	Left	0.7117 ± 0.0392		
Piriform Lobe	Right	0.8353 ± 0.0386		895.0 ± 50.6
	Left	0.8390 ± 0.0382		935.9 ± 37.8
Thalamus	Right	0.7325 ± 0.0309	0.7766 ± 0.0368	792.2 ± 31.0
	Left	0.7305 ± 0.0332	0.7804 ± 0.0426	823.4 ± 30.1
Hippocampus	Right	0.8202 ± 0.0577	0.8776 ± 0.0737 (averaged)	1052.9 ± 109.7
	Left	0.8117 ± 0.0647		1035.7 ± 109.0
Occipital Lobe gray & white matter averaged	Right	0.7202 ± 0.0535	0.7982 ± 0.0363	
	Left	0.7224 ± 0.0507	0.7885 ± 0.0391	
Occipital Lobe gray matter	Right	0.8228 ± 0.0872	0.8866 ± 0.0376	
	Left	0.8296 ± 0.0805	0.8632 ± 0.0580	
Occipital Lobe white matter	Right	0.7063 ± 0.0558	0.6936 ± 0.0413	
	Left	0.7098 ± 0.0467	0.6897 ± 0.0272	
Cerebellum gray & white matter averaged	Right	0.6951 ± 0.0461	0.7196 ± 0.0573	
	Left	0.6983 ± 0.0437	0.7038 ± 0.0573	
Cerebellum gray matter	Right	0.7299 ± 0.0647	0.8369 ± 0.0654	
	Left	0.7387 ± 0.0582	0.8349 ± 0.0552	
Cerebellum white matter	Right	0.6855 ± 0.0529	0.7196 ± 0.0573	
	Left	0.6869 ± 0.0482	0.7038 ± 0.0573	

MacLellan et al. (5) and Hartmann et al. (4).

depending on the BW. Two of these ROIs (caudal internal capsule and gray matter of the cerebellum) were among the smaller sized ROIs. It can be speculated that through limited spatial resolution in the ADC maps, further decreasing in smaller animals, ROI placement in smaller dogs may be more inaccurate than in larger animals. In smaller dogs, pixels may represent a larger proportion of the optically resolved patient anatomy and a mismatch between morphological sequences, with higher spatial resolution, might lead to inaccurate ROI placement. Therefore, differences to smaller sized dogs may simply be an inaccuracy effect.

The majority of the dogs were, as expected, presented with neurological signs ($n = 247$), less than the half of them with epileptic seizures. In dogs diagnosed with idiopathic epilepsy, the ADC values during the interictal phase are described to be higher in the piriform lobe and the semioval center, compared to values of healthy dogs. This fact might be explained by cell loss and an increased intercellular space (35). During ictus the opposite is found, and regional ADC decreases in human patients and canine experimental model of status epilepticus (53, 54). Our data did not confirm this variation in the ADC of the piriform lobe in dogs depending on the clinical signs. No ADC differences were found between dogs presented with neurological signs vs. dogs presented with non-neurological signs in all ROI, except for the internal capsule. In our patient population,

dogs presented with neurological sings included highly heterogeneous etiology and the difference in ADC in the internal capsule cannot be clearly interpreted. It can be only speculated if the different ADC could suggest a possible link between neurological signs and region integrity or if this variation could represent a cause or the sequela of the neurological signs. Since a final histological diagnosis was not available in these dogs, caution should be used in the interpretation of these results.

Many other patient related factors can influence the ADC. In rats and mice, ADC is described to correlate positively with body temperature (55, 56). The patient temperature was recorded when available and was maintained in the physiological range. The exact temperature at the time of the acquisition of the DW images was not recorded though, and its influence on the ADC remains unknown. Anesthesia and its effect on neuronal activity can also influence water diffusivity. This phenomenon may cause increased ADC in specific brain regions, reflecting decreased neuronal activity (57). In our study, anesthesia was not standardized, and the anesthetic protocol elected on case-by-case evaluation by the anesthetist in charge. The possible influence of anesthesia was therefore not investigated.

The major limitation of this study is the examined population, consisting of clinical patients. Even though only dogs with morphologically normal MR brain studies were included, non-visible or microstructural pathological processes cannot be ruled out since most of the dogs were presented with neurological signs and obviously, no histopathological examination was possible. Pathologies of different nature beyond the optical resolution of the standard morphological MR images might go undetected (58, 59) but could potentially affect the ADC. Moreover, the analyzed population suffers the selection bias of a clinical population. The age groups are unequal in size, being older dogs presented more often for MRI examination. This disproportionate distribution of age group size could have had an impact on the results.

Another limitation consists in the retrospective nature of the study. Individual case management and the time between MRI examination and presence of clinical signs was neither investigated nor standardized and could influence ADC values in relation to the onset of the clinical signs. Apparent diffusion coefficient values were analyzed in the context of the clinical patient work-up. The influence of technically related factors potentially affecting the ADC, phantom reference values or signal-to-noise ratio in every single examination, as well as influence of non-optically visible artifacts were not investigated. The reported ADC based on the images acquired with described technique does not allow quantification of the anisotropy, particularly marked in the white matter of the brain. ADC ROI placement was largely performed by a single observer and no repetition of measurements was performed. Possible inter-observer variabilities should be therefore considered a limitation.

Conclusion

The present study investigates the ADC in different regions of canine brain with morphologically normal MRI examination. Three-hundred and twenty-one dogs of varying breeds, sex, reproductive status, and age were included in the study. Apparent diffusion coefficient significantly varies among most anatomical brain regions. Apparent diffusion coefficient was significantly lower in the white than in the gray matter. The left and right cerebral hemispheres had similar ADC values in most of the regions, and no differences depending on sex or reproductive status were observed. No consistent correlation between body-weight groups and ADC values was found. Age was correlated first with a decrease and later increase of ADC values, likely consistent with brain maturation and aging. The described data can be reference for future studies in clinical settings on the canine brain.

Data availability statement

The original contributions presented in the study are included in the article/Supplementary material, further inquiries can be directed to the corresponding author.

Ethics statement

A consent form for the use of the dogs' data for academic purposes was signed by the owners of all dogs included.

Author contributions

Conception and design done by FC and LC. Acquisition of data done by BL. Statistical analysis done by HR. Drafting of the article done by LC. All authors contributed to the article and approved the submitted version.

Acknowledgments

Part of the study was presented at the ECVDI annual meeting (Edinburgh in 2022) as an oral presentation.

Conflict of interest

The authors declare that the research was conducted in the absence of any commercial or financial relationships that could be construed as a potential conflict of interest.

Publisher's note

Supplementary material

The Supplementary material for this article can be found online at: https://www.frontiersin.org/articles/10.3389/fvets.2023.1219943/full#supplementary-material

References

1. Feynman R. The Brownian movement In: R Feynman, R Leighton and M Sands, editors. *The Feynman lectures on physics*. Boston, MA: Addison-Wesley (1963). 41.

2. Guo A, Cummings T, Dash R, Provenzale J. Lymphomas and high-grade astrocytomas: comparison of water diffusibility and histologic characteristics. *Radiology*. (2002) 224:177–83. doi: 10.1148/radiol.2241010637

3. Lindt B, Richter H, Del Chicca F. Investigated regional apparent diffusion coefficient values of the morphologically normal feline brain. *J Feline Med Surg*. (2022) 24:e214–22. doi: 10.1177/1098612X221101535

4. Hartmann A, Söffler C, Failing K, Schaubmar A, Kramer M, Schmidt M. Diffusion-weighted magnetic resonance imaging of the normal canine brain. *Vet Radiol Ultrasound*. (2014) 55:592–8. doi: 10.1111/vru.12170

5. McLellan M, Ober C, Feeney D, Jessen C. Diffusion-weighted magnetic resonance imaging of the brain of neurologically normal dogs. *Am J Vet Res*. (2017) 78:601–8. doi: 10.2460/ajvr.78.5.601

6. Le Bihan D, Breton E. MR imaging of Intravoxel incoherent motions: application to diffusion and perfusion in neurologic disorders. *RSNA*. (1986) 161:401–7. doi: 10.1148/radiology.161.2.3763909

7. Olivot J, Marks M. Magnetic resonance imaging in the evaluation of acute stroke. *Top Magn Reson Imaging*. (2008) 19:225–30. doi: 10.1097/RMR.0b013e3181aaf37c

8. Fiebach J, Schellinger P, Jansen O, Meyer M, Wilde P, Bender J, et al. CT and diffusion-weighted MR imaging in randomized order: diffusion-weighted imaging results in higher accuracy and lower interrater variability in the diagnosis of hyperacute ischemic stroke. *Stroke*. (2002) 33:2206–10. doi: 10.1161/01.STR.0000026864.20339.CB

9. Kucinski T, Väterlein O, Glauche V, Fiehler J, Klotz E, Eckert B, et al. Correlation of apparent diffusion coefficient and computed tomography density in acute ischemic stroke. *Stroke*. (2002) 33:1786–91. doi: 10.1161/01.STR.0000019125.80118.99

10. Mullins M, Schaefer P, Sorensen A, Halpern E, Ay H, He J, et al. CT and conventional and diffusion-weighted MR imaging in acute stroke: study in 691 patients at presentation to the emergency department. *Radiology*. (2002) 224:353–60. doi: 10.1148/radiol.2242010873

11. Liu A, Maldjian J, Bagley L, Sinson G, Grossman R. Traumatic brain injury: diffusion-weighted MR imaging findings. *AJNR Am J Neuroradiol*. (1999) 20:1636–41.

12. Dmytriw A, Sawlani V, Shankar J. Diffusion-weighted imaging of the brain: beyond stroke. *Can Assoc Radiol J*. (2017) 68:131–46. doi: 10.1016/j.carj.2016.10.001

13. Provenzale J, Mukundan S, Barboriak D. Diffusion-weighted and perfusion MR imaging for brain tumor characterization and assessment of treatment response. *Radiology*. (2006) 239:632–49. doi: 10.1148/radiol.2393042031

14. Barboriak DP. Imaging of brain tumors with diffusion-weighted and diffusion tensor MR imaging. *Magn Reson Imaging Clin N Am*. (2003) 11:379–401. doi: 10.1016/S1064-9689(03)00065-5

15. Guzman R, Altrichter S, El-Koussy M, Gralla J, Weis J, Barth A, et al. Contribution of the apparent diffusion coefficient in perilesional edema for the assessment of brain tumors. *J Neuroradiol*. (2008) 35:224–9. doi: 10.1016/j.neurad.2008.02.003

16. Perrone A, Guerrisi P, Izzo L, D'Angeli I, Sassi S, Mele L, et al. Diffusion-weighted MRI in cervical lymph nodes: differentiation between benign and malignant lesions. *Eur J Radiol*. (2011) 77:281–6. doi: 10.1016/j.ejrad.2009.07.039

17. Diehl B, Najm I, Ruggieri P, Tkach J, Mohamed A, Morris H, et al. Postictal diffusion-weighted imaging for the localization of focal epileptic areas in temporal lobe epilepsy. *Epilepsia*. (2001) 42:21–8. doi: 10.1046/j.1528-1157.2001.19500.x

18. Engel J, McDermott M, Wiebe S, Langfitt J, Stern J, Dewar S, et al. Early surgical therapy for drug-resistant temporal lobe epilepsy: a randomized trial. *JAMA*. (2012) 307:922–30. doi: 10.1001/jama.2012.220

19. Nusbaum A, Tang C, Buchsbaum M, Wei C, Atlas S. Regional and global changes in cerebral diffusion with Normal aging. *Am J Neuroradiol*. (2001) 22:136–42.

20. Engelter S, Provenzale J, Petrella J, DeLong D, MacFall J. The effect of aging on the apparent diffusion coefficient of Normal-appearing white matter. *Am J Roentgenol*. (2000) 175:425–30. doi: 10.2214/ajr.175.2.1750425

21. Sotardi S, Gollub R, Bates S, Weiss R, Murphy S, Grant P, et al. Voxelwise and regional brain apparent diffusion coefficient changes on MRI from birth to 6 years of age. *Radiology*. (2021) 298:415–24. doi: 10.1148/RADIOL.2020202279

22. Neil J, Miller J, Mukherjee P, Hüppi P. Diffusion tensor imaging of normal and injured developing human brain - a technical review. *NMR Biomed*. (2002) 15:543–52. doi: 10.1002/nbm.784

23. Helenius J, Soinne L, Perkiö J, Salonen O, Kangasmäki A, Kaste M, et al. Diffusion-weighted MR imaging in Normal human brains in various age groups. *AJNR*. (2002) 23:194–9.

24. Ahlhelm F, Hagen T, Schneider G, Dorenbeck U, Nabhan A, Reith W. ADC mapping of normal human brain. *Med Sci Monit*. (2004) 10:MT121–5.

25. Garosi L, McConnell J, Platt S, Barone G, Baron J, Lahunta A, et al. Clinical and topographic magnetic resonance characteristics of suspected brain infarction in 40 dogs. *J Vet Intern Med*. (2006) 20:311–21. doi: 10.1111/j.1939-1676.2006.tb02862.x

26. McConnell J, Garosi L, Platt S. Magnetic resonance imaging findings of presumed cerebellar cerebrovascular accident in twelve dogs. *Vet Radiol Ultrasound*. (2005) 46:1–10. doi: 10.1111/j.1740-8261.2005.00001.x

27. Moseley M, Kucharczyk J, Mintorovitch J, Cohen Y, Kurhanewicz J, Derugin N, et al. Diffusion-weighted MR imaging of acute stroke: correlation with T2-weighted and magnetic susceptibility-enhanced MR imaging in cats. *AJNR*. (1990) 11:423–9.

28. Liu K, Li F, Tatlisumak T, Garcia J, Sotak C, Fisher M, et al. Regional variations in the apparent diffusion coefficient and the intracellular distribution of water in rat brain during acute focal ischemia. *Stroke*. (2001) 32:1897–905. doi: 10.1161/01.str.32.8.1897

29. Kuroiwa T, Nagaoka T, Ueki M, Yamada I, Miyasaka N, Akimoto H, et al. Correlations between the apparent diffusion coefficient, water content, and ultrastructure after induction of vasogenic brain edema in cats. *J Neurosurg*. (1999) 90:499–503. doi: 10.3171/jns.1999.90.3.0499

30. McLellan M, Ober C, Feeney D, Jessen C. Evaluation of diffusion-weighted magnetic resonance imaging at 3.0 tesla for differentiation between intracranial neoplastic and noninfectious inflammatory lesions in dogs. *JAVMA*. (2019) 255:71–7. doi: 10.2460/javma.255.1.71

31. Wada M, Hasegawa D, Hamamoto Y, Yu Y, Asada R, Fujiwara-Igarashi A, et al. Comparison of canine and feline Meningiomas using the apparent diffusion coefficient and fractional anisotropy. *Front Vet Sci*. (2021) 7:614026. doi: 10.3389/fvets.2020.614026

32. Fages J, Oura T, Sutherland-Smith J, Jennings S. Atypical and malignant canine intracranial meningiomas may have lower apparent diffusion coefficient values than benign tumors. *Vet Radiol Ultrasound*. (2020) 61:40–7. doi: 10.1111/vru.12814

33. Scherf G, Sutherland-Smith J, Uriarte A. Dogs and cats with presumed or confirmed intracranial abscessation have low apparent diffusion coefficient values. *Vet Radiol Ultrasound*. (2022) 63:197–200. doi: 10.1111/vru.13064

34. Carloni A, Bernardini M, Mattei C, De Magistris A, Llabres-Diaz F, Williams J, et al. Can MRI differentiate between ring-enhancing gliomas and intra-axial abscesses? *Vet Radiol Ultrasound*. (2022) 63:563–72. doi: 10.1111/vru.13098

35. Hartmann A, Sager S, Failing K, Sparenberg M, Schmidt M. Diffusion-weighted imaging of the brains of dogs with idiopathic epilepsy. *BMC Vet Res*. (2017) 13:338. doi: 10.1186/s12917-017-1268-0

36. Sutherland-Smith J, King R, Faissler D, Ruthazer R, Sato A. Magnetic resonance imaging apparent diffusion coefficients for histologically confirmed intracranial lesions in dogs. *Vet Radiol Ultrasound*. (2011) 52:142–8. doi: 10.1111/j.1740-8261.2010.01764.x

37. Anaya García M, Hernández Anaya J, Marrufo Meléndez O, Velázquez Ramírez J, Palacios AR. In vivo study of cerebral white matter in the dog using diffusion tensor tractography. *Vet Radiol Ultrasound*. (2015) 56:188–95. doi: 10.1111/vru.12211

38. Vite C, Magnitsky S, Aleman D, O'Donnell P, Cullen K, Ding W, et al. Apparent diffusion coefficient reveals gray and white matter disease, and T2 mapping detects white matter disease in the brain in feline alpha-mannosidosis. *Am J Neuroradiol*. (2008) 29:308–13. doi: 10.3174/ajnr.A0791

39. Reich L, Hartnack S, Fitzi-Rathgen J, Reichler IM. Life expectancy of mesocephalic, dolichocephalic and brachycephalic dog breeds in Switzerland. *Schweiz Arch Tierheilkd*. (2023) 165:235–0. doi: 10.17236/sat00390

40. O'Neill DG, Pegram C, Crocker P, Brodbelt DC, Church DB, Packer RMA. Unravelling the health status of brachycephalic dogs in the UK using multivariable analysis. *Sci Rep*. (2020) 10:17251. doi: 10.1038/s41598-020-73088-y

41. Sasaki M, Yamada K, Watanabe Y, Matsui M, Ida M, Fujiwara S, et al. Variability in absolute apparent diffusion coefficient values across different platforms may be substantial: a multivendor, multi-institutional comparison study. *Radiology*. (2008) 249:624–30. doi: 10.1148/radiol.2492071681

42. Sen P, Basser P. A model for diffusion in white matter in the brain. *Biophys J*. (2005) 89:2927–38. doi: 10.1529/biophysj.105.063016

43. Moraru L, Dimitrievici L. Apparent diffusion coefficient of the normal human brain for various experimental conditions. *AIP conference proceedings*. American Institute of Physics Inc. (2017).

44. Naganawa S, Sato K, Katagiri T, Mimura T, Ishigaki T. Regional ADC values of the normal brain: differences due to age, gender, and laterality. *Eur Radiol*. (2003) 13:6–11. doi: 10.1007/s00330-002-1549-1

45. Tan Ü, Caliskan S. Allometry and asymmetry in the dog brain: the right hemisphere is heavier regarless of paw preference. *Int J Neurosci*. (1987) 35:189–94. doi: 10.3109/00207458708987127

46. Good C, Johnsrude I, Ashburner J, Henson R, Friston K, Frackowiak R. Cerebral asymmetry and the effects of sex and handedness on brain structure: a voxel-based morphometric analysis of 465 normal adult human brains. *Neuroimage*. (2001) 14:685–700. doi: 10.1006/nimg.2001.0857

47. Powell J, Parkes L, Kemp G, Sluming V, Barrick T, García-Fiñana M. The effect of sex and handedness on white matter anisotropy: a diffusion tensor magnetic resonance imaging study. *Neuroscience*. (2012) 207:227–42. doi: 10.1016/j.neuroscience.2012.01.016

48. Aydinlioğlu A, Arslan K, Cengiz N, Rağbetli M, Erdoğan E. The relationships of dog hippocampus to sex and paw preference. *Int J Neurosci*. (2006) 116:77–88. doi: 10.1080/00207450690962433

49. Aydinlioğlu A, Arslan K, Erdogan A, Ragbetli M, Keleh P, Diyarbakırlı S. The relationship of Callosal anatomy to paw preference in dogs. *Eur J Morphol*. (2000) 38:128–33. doi: 10.1076/0924-3860(200004)38:2;1-F;FT128

50. Hackert R, Maes L, Herbin M, Libourel P, Abourachid A. Limb preference in the gallop of dogs and the half-bound of pikas on flat ground. *Laterality*. (2008) 13:310–9. doi: 10.1080/13576500801948692

51. Watanabe M, Sakai O, Ozonoff A, Kussman S, Jara H. Age-related apparent diffusion coefficient changes in the normal brain. *Radiology*. (2013) 266:575–82. doi: 10.1148/radiol.12112420

52. Gross B, Garcia-Tapia D, Riedesel E, Ellinwood N, Jens J. Normal canine brain maturation at magnetic resonance imaging. *Vet Radiol Ultrasound*. (2010) 51:361–73. doi: 10.1111/j.1740-8261.2010.01681.x

53. Chatzikonstantinou A, Gass A, Förster A, Hennerici M, Szabo K. Features of acute DWI abnormalities related to status epilepticus. *Epilepsy Res*. (2011) 97:45–51. doi: 10.1016/j.eplepsyres.2011.07.002

54. Hasegawa D, Orima H, Fujita M, Nakamura S, Takahashi K, Ohkubo S, et al. Diffusion-weighted imaging in kainic acid-induced complex partial status epilepticus in dogs. *Brain Res*. (2003) 983:115–27. doi: 10.1016/S0006-8993(03)03041-5

55. Hasegawa Y, Latour L, Sotak H, Dardzinski B, Fisher M. Temperature dependent change of apparent diffusion coefficient of water in Normal and ischemic brain of rats. *J Cereb Blood Flow Metab*. (1994) 14:383–90. doi: 10.1038/jcbfm.1994.49

56. Bertalan G, Boehm-Sturm P, Schreyer S, Morr A, Steiner B, Tzschätzsch H, et al. The influence of body temperature on tissue stiffness, blood perfusion, and water diffusion in the mouse brain. *Acta Biomater*. (2019) 96:412–20. doi: 10.1016/j.actbio.2019.06.034

57. Abe Y, Tsurugizawa T, Le Bihan D. Water diffusion closely reveals neural activity status in rat brain loci affected by anesthesia. *PLoS Biol*. (2017) 15:e2001494. doi: 10.1371/journal.pbio.2001494

58. Smith E, Schneider J, Wardlaw J, Greenberg S. Cerebral microinfarcts: the invisible lesions. *Lancet Neurol*. (2012) 11:272–82. doi: 10.1016/S1474-4422(11)70307-6

59. Shenton M, Hamoda H, Schneiderman J, Bouix S, Pasternak O, Rathi Y, et al. A review of magnetic resonance imaging and diffusion tensor imaging findings in mild traumatic brain injury. *Brain Imaging Behav*. (2012) 6:137–92. doi: 10.1007/s11682-012-9156-5

frontiers | Frontiers in Veterinary Science

TYPE Original Research
PUBLISHED 23 November 2023
DOI 10.3389/fvets.2023.1302418

OPEN ACCESS

EDITED BY
Adriano Wang-Leandro,
University of Veterinary Medicine Hannover, Germany

REVIEWED BY
Viktor Paluš,
NeuroVet, Slovakia
Ângela Paula Martins,
University of Lisbon, Portugal

*CORRESPONDENCE
Claudia La Rosa
✉ claudia.la.rosa@anicura.it

RECEIVED 26 September 2023
ACCEPTED 09 November 2023
PUBLISHED 23 November 2023

CITATION
La Rosa C, Morabito S, Carloni A, Davini T, Remelli C, Specchi S and Bernardini M (2023) Prevalence, MRI findings, and clinical features of lumbosacral intervertebral disc protrusion in French Bulldogs diagnosed with acute thoracic or lumbar intervertebral disc extrusion. *Front. Vet. Sci.* 10:1302418. doi: 10.3389/fvets.2023.1302418

Prevalence, MRI findings, and clinical features of lumbosacral intervertebral disc protrusion in French Bulldogs diagnosed with acute thoracic or lumbar intervertebral disc extrusion

Claudia La Rosa[1]*, Simona Morabito[1,2], Andrea Carloni[1,2], Tommaso Davini[1], Carlotta Remelli[1], Swan Specchi[1,2] and Marco Bernardini[1,3]

[1]AniCura I Portoni Rossi Veterinary Hospital, Bologna, Italy, [2]Antech Imaging Services, Fountain Valley, CA, United States, [3]Department of Animal Medicine, Productions and Health, University of Padua, Legnaro, Italy

Introduction: Intervertebral disc protrusion (IVDP) is a neurological disorder commonly observed at the lumbosacral junction of old, medium-to-large breeds, non-chondrodystrophic dogs. Although uncommon, lumbosacral IVDP can also be seen in chondrodystrophic dogs, among them French Bulldogs (FBs) and could be associated with congenital vertebral malformations in this breed. This study aims to evaluate the prevalence, clinical features, and MRI characteristics of lumbosacral IVDP and congenital vertebral malformations in FBs diagnosed with thoracic or lumbar intervertebral disc extrusion (IVDE) and to evaluate the possible interference of the neurologic deficits related to chronic IVDP on neurological examination.

Materials and methods: This is a single-center, retrospective case series. A search for FBs diagnosed with IVDE affecting the thoracic or lumbar regions is done on the database of the AniCura I Portoni Rossi Veterinary Hospital (Zola Predosa, Bologna, Italy). Eligible dogs have a complete medical report and a high-field MRI of the lumbosacral junction. MRIs of the lumbosacral junction are evaluated to determine the position of IVDP, cranial intervertebral foraminal stenosis, and signs of nerve root involvement. Radiographs, when available, are reviewed to identify the presence of lumbosacral congenital vertebral malformations.

Results: Eighty FBs are included in the study. The prevalence of lumbosacral IVDP among FBs is 91.3%. Among FBs with lumbosacral IVDP, 45.0% show concurrent cranial intervertebral foraminal stenosis, 28.8% exhibit concurrent nerve root involvement, 56.2% appear to be asymptomatic for lumbosacral changes, while 15.1% manifest a decreased or absent withdrawal reflex as a supposed consequence of chronic lumbosacral IVDP. Congenital vertebral malformations are detected in 10 dogs.

Conclusion: The results of this study support the hypothesis that lumbosacral IVDP is frequent in FBs presenting with thoracic or lumbar IVDE. In over half the dogs lumbosacral IVDP appears to be asymptomatic; however, in other cases, chronic lumbosacral IVDP seems to cause neurological deficits that may lead to erroneous localization of acute IVDE, representing a confounding factor for clinicians.

KEYWORDS

congenital vertebral malformations, chondrodystrophic dogs, intervertebral disc protrusion, intervertebral disc extrusion, lumbosacral junction, magnetic resonance imaging

1 Introduction

Intervertebral disc herniation (IVDH) is a well-documented pathological condition in dogs, encompassing intervertebral disc extrusion (Hansen type I herniation; IVDE) and intervertebral disc protrusion (Hansen type II herniation; IVDP) (1–5). IVDE is most commonly seen in chondrodystrophic (CD) breeds affecting the cervical and thoracolumbar regions (3, 5). French Bulldogs (FBs) are highly prone to developing IVDE, with a reported prevalence of 45.5% among all neurological conditions (6).

In contrast, IVDPs are commonly observed in older, medium-to-large, non-chondrodystrophic (NCD) breeds and broadly represent the most common type of IVDH affecting the lumbosacral (LS) junction (2, 4, 7–10). LS IVDP can result in compressive radiculopathy of the cauda equina and intervertebral foraminal stenosis. Abnormal findings upon neurological examination are LS pain, paresthesia, proprioceptive deficits, lameness of the pelvic limbs, stiffness during physical activity, difficulty in jumping, a depressed withdrawal reflex and muscle atrophy, especially of the gluteal and hamstring muscle groups (8, 11, 12).

Albeit uncommon, IVDP can occur in CD dogs. IVDPs affecting the LS junction are poorly reported in CD dogs (4). A recent study found 72/149 dogs with LS IVDH within a population of neurologically normal FBs, English Bulldogs, and pugs; among FBs alone, the same study recorded a prevalence of 52.8% for LS IVDH (13). Another study reported a prevalence of 77.4% within a population of FBs, both with and without neurological disorders (14).

Furthermore, the LS junction has been reported to be affected by congenital vertebral malformations (CVMs) in CD dogs based on CT examination and a possible association between CVMs and LS IVDP has been suggested (13, 14).

To the best of our knowledge, no studies have focused on MRI characteristics of LS IVDP and the resulting involvement of nerve roots in FBs. It is the authors' opinion that LS IVDP in FBs is a frequent, underdiagnosed, chronic condition that can cause neurological deficits possibly interfering with neurological evaluation when these dogs are presenting with acute thoracic or lumbar IVDE. Therefore, this study aims to evaluate (1) the prevalence and MRI characteristics of LS IVDP, cranial intervertebral foraminal stenosis, root involvement, and CVMs in FBs diagnosed with thoracic or lumbar IVDE and (2) the possible interference of the neurologic deficits related to chronic IVDP on neurological examination performed when dogs are evaluated for acute IVDE.

It is hypothesized that a high prevalence of LS IVDP may be a confounding factor at the time of neuroanatomical localization of acute myelopathy and an association between LS CVM and IVDP may exist.

2 Materials and methods

2.1 Case recruitment criteria

This is a single-center, descriptive, retrospective case series. The database of the AniCura I Portoni Rossi Veterinary Hospital (Zola Predosa, Bologna, Italy) was searched for FBs that were diagnosed through MRI with IVDE affecting the thoracolumbar (T3–L3) or LS (L4–S3) regions between April 2018 and February 2023. All the animals used in the study were client-owned and underwent MRI examinations of the vertebral column as part of their diagnostic workup. Dogs were eligible if they had (1) a medical report including signalment and a neurological examination performed by a European College of Veterinary Neurology (ECVN) board-certified veterinary neurologist or an ECVN resident and (2) an MRI of the vertebral column extended to the LS junction, imaged in the T2-weighted sagittal plane and at least one other plane. If multiple MRI studies of the same dog were performed at different times, only the oldest one including the LS junction was examined. Patients with multiple IVDEs, LS IVDE, or other concurrent pathological conditions affecting the spinal cord or acquired disease processes of the vertebral column between T3 and S3 were excluded. Radiographs of the LS junction were also evaluated when available.

2.2 Medical records review

Details regarding signalment (sex, age, and neutered/spayed status), neurological examination, and location of IVDE were collected. Information obtained from neurological examination included: (1) analysis of the gait graded from 1 (spinal hyperesthesia only) to 5 (paraplegia without deep pain) according to a grading system described elsewhere (15); (2) assessment of the withdrawal reflex of pelvic limbs (normal/increased or reduced/absent); (3) level of cutaneous trunci muscle reflex (CTMR) cut-off; and (4) assessment of thoracic/lumbar or LS pain (present or absent). Dogs were divided into two groups based on the localization of IVDE: group A (cranial to the fourth lumbar vertebra [L4]), and group B (caudal to L4). Dogs in both groups were further subdivided into cases with normal withdrawal reflexes and cases with reduced/absent withdrawal reflexes.

2.3 Images analyses

Radiographs and MRI were reviewed by two European College of Veterinary Diagnostic Imaging board-certified radiologists (A.C. and

Abbreviations: CD, chondrodystrophic dogs; CVMs, congenital vertebral malformations; CTMR, cutaneous trunci muscle reflex; FB, French Bulldog; IVDE, intervertebral disc extrusion; IVDP, intervertebral disc protrusion; LS, lumbosacral.

10.3389/fvets.2023.1302418

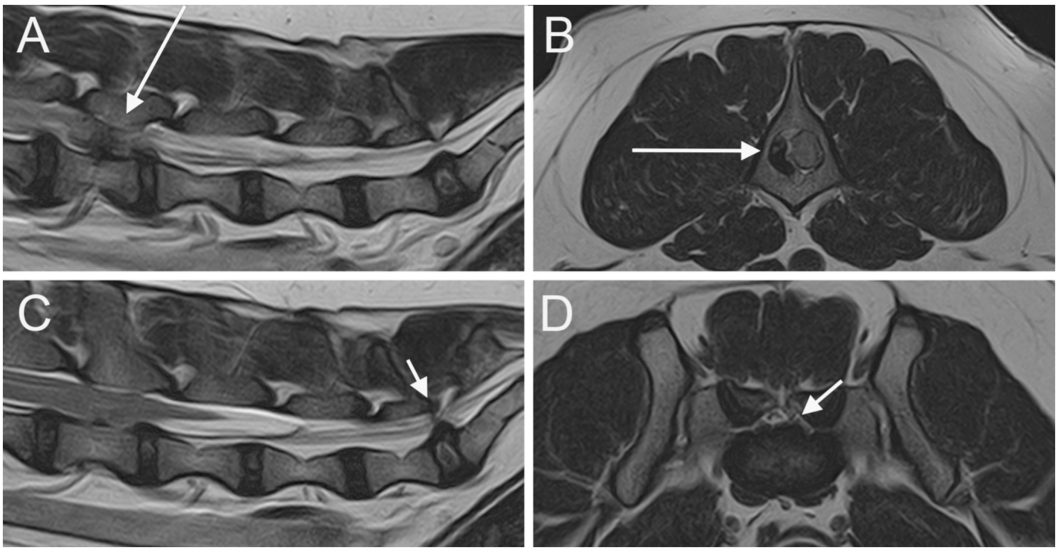

FIGURE 1
Parasagittal **(A)** and sagittal **(C)** T2W images of the lumbar vertebral column and the LS junction; transverse T2W at the level of L4 vertebra **(B)** and at the level of LS junction **(D)**. A severe extrusion of the L4-L5 IVD in seen on the right side of the vertebral canal (long arrow). An IVDP affecting both the vertebral canal and the intervertebral foramina is seen at the LS junction (short arrows).

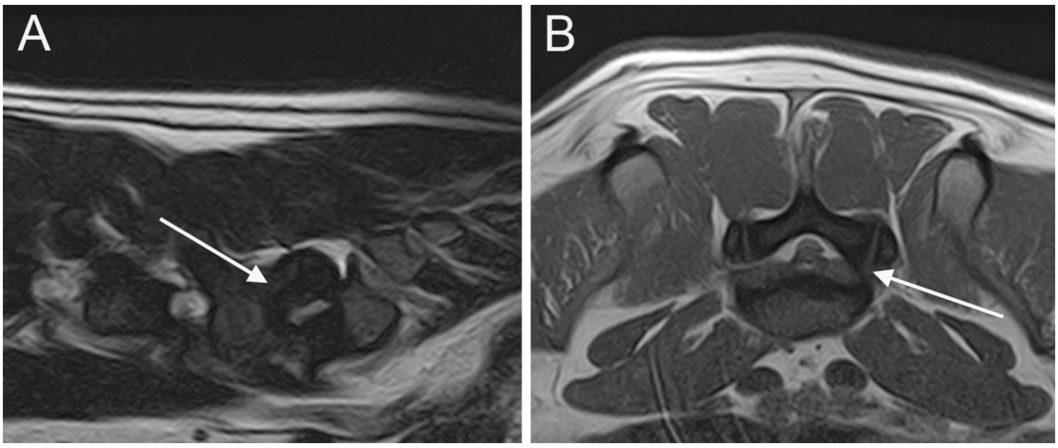

FIGURE 2
Parasagittal **(A)** and transverse **(B)** T2W images of the LS junction showing cranial intervertebral foraminal stenosis (arrows).

S.M.), two interns (C.L.R. and T.D.), and an ECVN board-certified neurologist (M.B.) using a DICOM viewer program (Horos DICOM viewerTM).[1] All the reviewers were blinded about the findings of neurological examinations.

MRI scans of the LS junction were evaluated for LS IVDP, cranial intervertebral foraminal stenosis, and involvement of spinal nerve roots. IVDP was classified as canalar, left or right intervertebral foraminal, bilateral intervertebral foraminal, canalar + right/left intervertebral foraminal, and all positions (canalar + bilateral intervertebral foraminal) (Figure 1). The degree of LS IVDP was scored as grade 1 when obstruction of the spinal canal was <25%, grade 2 when obstruction was 25–50%, and grade 3 when the obstruction was >50% (10, 16). Cranial intervertebral foraminal stenosis was defined as an abnormal conformation and/or signal changes of the edge of the cranial part of the LS intervertebral foramen leading to a reduction in size (Figure 2). Spinal nerve root involvement was defined as occurring when nerve roots were compressed, enlarged, showed MRI signal changes, or were not detected due to the presence of degenerative material along the nerve root path (Figure 3) and estimated as absent, left/right lateral, or bilateral. Radiographs were reviewed for the presence of LS CVM such as butterfly vertebra, transitional vertebra, block vertebrae, and spina bifida. When radiographs were not available, we analyzed MRI for the same alterations. The above

1 www.horosproject.com

10.3389/fvets.2023.1302418

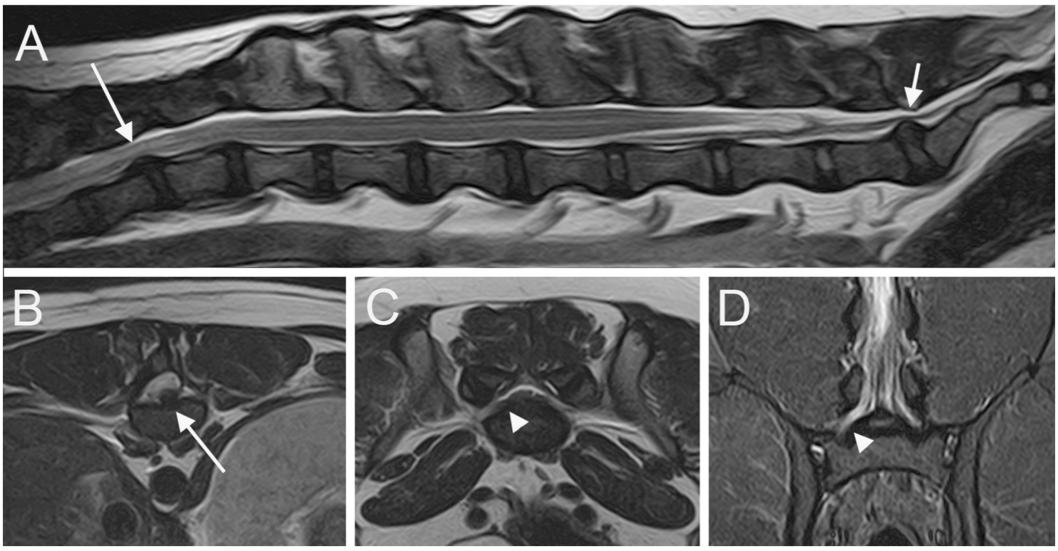

FIGURE 3
Sagittal T2W image **(A)** of the T11-S1 vertebral column; transverse T2W images at the level of L4 caudal epiphysis **(B)** and at the level of LS junction **(C)**; dorsal STIR **(D)** image of the L6-S1 vertebral column. A T12-T13 IVDE is seen (long arrows); a LS IVDP (short arrow) is associated with an enlargement and signal change of the right L7 nerve root (arrowheads).

findings were recorded in a spreadsheet (Microsoft Excel for Mac, Version 16.74). A descriptive analysis was performed by C.L.R. for all these variables: IVDPs at the level of the intervertebral foramina, cranial intervertebral foraminal stenosis, spinal nerve root involvement, and LS CVM were classified as present or absent; IVDPs at the level of spinal canal were classified as absent, grade 1, grade 2 or grade 3 as described above.

3 Results

3.1 Case recruitment criteria and medical records review

Initially, 173 dogs were considered for inclusion. Seven cases were excluded because of an incomplete medical report, 77 cases because the LS junction was either not included in the MRI or not imaged as required, and 9 cases because of concurrent pathological conditions affecting the spinal cord, multiple IVDEs, or LS IVDE. Consequently, 80 FBs fulfilled the inclusion criteria. These FBs comprised 54 males (67.5%) of which 10 were neutered and 26 females (32.5%) of which 21 were spayed. Age at presentation ranged from 15 months to 9 years, with a mean of 2.9 years and a median age of 4 years.

Neurological examination findings and sites of IVDE are summarized in Table 1. Forty-nine out of 80 dogs (61.3%) were diagnosed with an IVDE cranial to the fourth lumbar vertebra L4 (group A), and 31/80 dogs (38.8%) with an IVDE caudal to L4 (group B). Within group A, 34/49 dogs (69.4%) had a normal withdrawal reflex bilaterally and 15/49 dogs (30.6%) had bilateral (12/15; 80%) or unilateral (3/15; 20%) reduced/absent withdrawal reflex. Within group B, 12/31 dogs (38.7%) had bilaterally normal withdrawal reflexes, while 19/31 dogs (61.3%) had either bilateral (16/19; 84.2%) or unilateral (3/19, 15.7%) reduced/absent withdrawal reflex.

3.2 Imaging analysis

Radiographs were available for review in 70/80 cases (87.5%), with both lateral and ventrodorsal projections available in 52/70 cases (74.3%), and only 1 projection in 18/70 cases (25.7%). MRI was conducted under general anesthesia, with dogs placed in dorsal recumbency. All studies were performed with a 1.5T MR scanner (Vantage Elan, Canon Medical Systems Europe B.V., Netherlands) with the best-fitting 16-channel flexible receiving coil from the 2 available. MRI of the LS junction was available in 2 planes in 53 cases (66.3%) (48 cases on sagittal and dorsal planes and 5 cases on sagittal and transverse planes) and in all 3 spatial planes in 27 cases (33.7%). MRI sequences available for review are summarized in Supplementary Table 1.

At least one abnormality (IVDP, cranial intervertebral foraminal stenosis, or nerve root involvement) at the level of the LS junction was observed in 76/80 dogs (95%). Of the 76 dogs, 6 (7.9%) showed all the 3 types of LS abnormalities bilaterally. Seventy-three out of 76 dogs (96.1%) presented with LS IVDP in at least 1 position, and 45% of these dogs (33/73) showed concurrent cranial intervertebral foraminal stenosis while 28.8% of these dogs (21/73) had concurrent nerve root involvement. IVDPs that affect all the positions were observed in most patients (53/73; 72.6%) (Figure 1), less frequently at both the canalar and unilateral intervertebral foraminal level (11/73; 15.1%) and rarely at the intervertebral foraminal position (7/73; 9.6%) or the canalar position (2/73; 2.7%). LS IVDPs were graded 1 in 34/73 dogs (46.6%), 2 in 19/73 dogs (26.0%), and 3 in 20/73 dogs (27.4%). Moreover, 36 out of 76 cases (47.4%) showed cranial intervertebral foraminal stenosis (Figure 2), while 37 cases (48.7%) presented with the involvement of spinal nerve roots in at least 1 side (Figure 3).

In both group A and group B, IVDPs affected at least one position (43/49, 87.8% and 30/31, 96.8%, respectively). In both groups, most

TABLE 1 Distribution of thoracic and lumbar IVDE and clinical neurological findings in all dogs included.

	N = 80 (%)
Neurological findings	
Gait	
Grade 0	5 (6.3%)
Grade 1	6 (7.5%)
Grade 2	42 (52.5%)
Grade 3	15 (18.8%)
Grade 4	8 (10%)
Grade 5	4 (5%)
Spinal reflexes	
Withdrawal reflex	
Reduced/absent	34/80 (42.5%)
Bilateral	28/34 (82.4%)
Left	4/34 (11.8%)
Right	2/34 (5.9%)
CTMR cut-off	21/80 (26.3%)
Pain	54/80 (67.5%)
Thoracic or lumbar	50/54 (92.6%)
Lumbosacral	4/54 (5%)
Neurolocation (IVDE site)	
T11–T12	1 (1.3%)
T12–T13	4 (5%)
T13–L1	4 (5%)
L1–L2	10 (12.5%)
L2–L3	12 (15%)
L3–L4	18 (22.5%)
L4–L5	19 (23.8%)
L5–L6	11 (13.8%)
L6–L7	1 (1.3%)

IVDPs affected all the positions, while IVDPs at both canalar and unilateral intervertebral foraminal level, or bilateral intervertebral foraminal level, or canalar position or unilateral intervertebral foraminal level were seen less frequently. The distribution of IVDP, cranial intervertebral foraminal stenosis, and nerve root involvement within the population and within each group is summarized in Table 2.

CVMs were detected in 10 cases (12.5%). A butterfly vertebra affecting the last lumbar and the first sacral vertebra was seen in 3 and 4 cases, respectively. An LS transitional vertebra was observed in 3 cases. No dogs presented with spina bifida or block vertebrae. All the 10 dogs with CVM had a concurrent LS IVDP.

3.3 Association between clinical and MRI findings

Among the 34 dogs in group A with a bilaterally normal withdrawal reflex, 30 (88.2%) showed LS IVDP with or without concurrent LS alterations. Of the remaining 4 dogs, 2 (5.9%) revealed cranial intervertebral foraminal stenosis without spinal nerve root involvement, and the other 2 (5.9%) displayed no LS abnormalities. Among the 15 dogs in group A with decreased/absent withdrawal reflex, 13 (86.7%) manifested LS IVDP with or without concurrent LS alterations; in this subgroup, 7 dogs were neurologically graded 2, 4 dogs were neurologically graded 3, and 2 dogs were neurologically graded 4. One of the two remaining dogs exhibited only cranial intervertebral foraminal stenosis without spinal nerve root involvement and the other showed no LS abnormalities; these two dogs were neurologically graded four and five, respectively. Among the 12 dogs in group B with bilateral normal withdrawal reflex, 11 (91.6%) showed LS IVDP and 1 showed no LS abnormalities. All 19 dogs in group B with decreased/absent withdrawal reflex showed an LS IVDP with or without concurrent LS abnormalities. Details about LS changes within each group are summarized in Table 3.

Among the 73 dogs with LS IVDP, only 4 (5.5%) were found to have LS spinal pain upon neurological examination. All the 4 dogs revealed bilaterally decreased/absent withdrawal reflex; among these dogs, 3 were in group A and 1 was in group B. Of the remaining 69 dogs, 44 (63.8%) showed hyperesthesia at the caudal thoracic or lumbar levels that matched with the IVDE site upon MRI examination, 20 (29%) revealed no spinal pain and a bilaterally normal withdrawal reflex or a CTMR cutoff that could suggest thoracolumbar localization and 5 (7.2%) exhibited no spinal pain, decreased/absent withdrawal reflexes, and no CTMR cut-off.

4 Discussion

The results of this study support our hypothesis that LS IVDP is frequent in FBs presenting with thoracic or lumbar IVDE. LS IVDP affecting at least 1 position (canalar, intervertebral foraminal, or both) was observed in 91.3% of the FBs in our population, a percentage much higher than that reported in 2 previous studies [77.4%; (14) and 52.8% (13)] and more than half of the FBs in our population were graded ≥2. This difference may be due to several factors. First, the FBs in our population were older (median age = 4 years) than the dogs described in the paper written by Bertram et al. (median age 16 months) (13). Second, the positioning of the patient for MRI may have played a role. Our patients were placed in dorsal recumbency while in the study of Bertram et al. patients were examined under sternal recumbency (13). The supine position has the effect of extending the LS junction, leading to an exacerbation of IVDP with respect to the neutral position (1, 16, 17). Thus, positioning may have partially led to an overestimation of the real severity of LS IVDP in our population. However, in our study, 45% of the FBs with LS IVDP showed concomitant cranial intervertebral foraminal stenosis, a degenerative condition frequently reported with LS IVDP, and 28.8% revealed concurrent nerve root involvement. These findings decrease the likelihood of positioning-related bias (17, 18). Third, the contrast between epidural fat and a degenerated disc is stronger in MRI than in CT, allowing MRI to offer a precise detection of mild IVDPs. This property of the MRI may also be useful in defining the spatial distribution of IVDPs (3, 19). The latter point may explain the greater prevalence (87.6%) of large LS IVDPs affecting both the

TABLE 2 LS changes within the entire population.

LS changes	Entire population n. of dogs (%)	Group A n. of dogs (%)	Group B n. of dogs (%)
IVDP	73 (91.3%)	43 (87.8%)	30 (96.8%)
Canalar IVDP	2 (2.7%)	2 (4.7%)	0 (0%)
Left intervertebral foraminal	2 (2.7%)	1 (2.3%)	1 (3.3%)
Right intervertebral foraminal	0 (0%)	0 (0%)	0 (0%)
Bilateral intervertebral foraminal	5 (6.8%)	3 (7%)	2 (6.7%)
Canalar + left intervertebral foraminal	5 (6.8%)	4 (9.3%)	1 (3.3%)
Canalar + right intervertebral foraminal	6 (8.2%)	2 (4.7%)	4 (13.3%)
All positions	53 (72.6%)	31 (72.1%)	22 (73.3%)
Cranial intervertebral foraminal stenosis	36 (45%)	22 (44.9%)	14 (45.2%)
Left lateral	5 (13.9%)	1 (4.5%)	4 (28.6%)
Right lateral	11 (30.6%)	5 (22.7%)	6 (42.9%)
Bilateral	20 (55.6%)	16 (72.7%)	4 (28.6%)
Nerve root involvement	37 (46.3%)	20 (40.8%)	17 (54.8%)
Left lateral	13 (35.1%)	6 (30%)	7 (41.2%)
Right lateral	7 (18.9%)	4 (20%)	3 (17.6%)
Bilateral	17 (45.9%)	10 (50%)	7 (41.2%)

TABLE 3 Prevalence of LS changes within each group.

	Group A		Group B	
	Normal withdrawal reflexes	Impaired withdrawal reflexes	Normal withdrawal reflexes	Impaired withdrawal reflexes
IVDP	11	3	0	5
Cranial intervertebral foraminal stenosis	2	1	0	0
Nerve root involvement	0	0	0	0
IVDP + cranial intervertebral foraminal stenosis	5	4	3	5
IVDP + nerve root involvement	9	1	5	6
All LS changes	5	5	3	3
No LS changes	2	1	1	0
Total	34	15	12	19

vertebral canal and at least one foramen in our population compared to a previous study (14).

The presence of LS CVMs has been considered to be a predisposing factor for LS IVDH. An association between LS IVDH with both LS transitional vertebra in a population of non-CD dogs (20) and hemivertebra at L7 or S1 (13) has been described. The prevalence of LS CVMs in our population study was much lower (12.5%) than that reported in recent papers based on CT examination (49.1 and 56.3% in neurological and non-neurological FBs, respectively) (13, 14) and similar to that reported in studies based on radiographs (0 to 17.5%) (21–23). We can suppose that LS IVDPs in FBs are a common finding even in absence of LS CVMs. However, MRI and radiography are not the best imaging modalities for diagnosing CVMs. CT is reported to be far more sensitive in the identification of the number of CVMs when compared to both radiography (24, 25) and MRI (1). Therefore, it is likely that the diagnostic modalities used in the present study may have underestimated the real prevalence of CVMs in our population.

The vertebral column outgrows the spinal cord in length, and the degree of elongated growth of spinal cord segments varies regionally (26). Thus, positions of most spinal cord segments reside in the vertebral canal cranial to the vertebra of the same number. This phenomenon is most pronounced in the caudal lumbar and sacrocaudal segments of the spinal cord. Generally, the three sacral spinal cord segments lie within the fifth lumbar

vertebral foramen, albeit with some variation between breeds: in small breeds, these segments extend approximately one vertebra further caudally (2, 26). As a result, the segments involved in the withdrawal reflex of the pelvic limbs (L6–S2) likely reside in the vertebral canal caudal to the L4 vertebra. Therefore, the withdrawal reflex could be decreased/eliminated by an IVDE at the L4–L5 intervertebral space or caudally. For this reason, in order to compare clinical findings (normal, decreased, or absent withdrawal reflexes) with the presence/absence of LS changes, the L4 vertebrae were taken as a cut-off point to classify the population into 2 groups: 61.3% of dogs were diagnosed with an IVDE cranial to L4 (group A) and 38.8% with an IVDE caudal to L4 (group B).

Forty-one out of the 73 FBs with LS IVDP (30 in group A and 11 in group B) had a bilaterally normal withdrawal reflex and none of them showed LS pain upon neurological examination. Therefore, in all these dogs, LS IVDP appears to be asymptomatic. This finding is in accordance with the 52.8% of neurologically normal FBs with LS IVDH reported in the literature (13).

Thirty-two out of 73 dogs with LS IVDP (13 in group A and 19 in group B) had a decreased or absent withdrawal reflex. In group A, 2 dogs were paraplegic (one graded 4 and the other graded 5); and the remaining 11 dogs showed variable degrees of paraparesis. Paraplegic dogs have increased odds of spinal shock, a condition characterized by impaired spinal reflexes and muscle tone caudal to an injury to the spinal cord, compared to dogs with persistent motor function (2, 27). Therefore, the impaired withdrawal reflex in the two paraplegic dogs was likely a consequence of the spinal shock caused by IVDE rather than due to the LS IVDP. In contrast, the 11 paraparetic dogs are more likely to have shown a decreased or absent withdrawal reflex as a consequence of LS IVDP. This is an important fact from a clinical point of view.

When performing a neurological examination in FBs, clinicians should be aware that chronic neurological deficits caused by LS IVDP might interfere with the neurological deficits due to acute IVDE, potentially leading to a wrong localization. In group B, a decreased or absent withdrawal reflex could be due to both acute IVDE and chronic LS IVDP. Both types of IVDH could contribute to a clinical presentation. This fact might not have an important impact in making immediate surgical decisions, since IVDE is likely to play a major role. However, a possible persistent flexor impairment in the follow-up could be erroneously attributed to irreversible spinal cord damage at the level of IVDE rather than to IVDP—especially in dogs where an L7 nerve root involvement has been seen using MRI.

LS pain is reported to be the most frequent and first presenting clinical sign in dogs diagnosed with LS degenerative stenosis (8). Approximately half of the FBs with LS IVDP in our population were graded at least 2 regarding the severity of IVDP, but only 5.5% of the FBs with LS IVDP in our population exhibited LS spinal pain upon neurological examination. One possible explanation could be that most dogs presented with severe thoracic or lumbar hyperesthesia related to acute IVDE and the pain possibly arising at the LS junction could be masked or overlooked under neurological examination. Therefore, it is advisable to carefully evaluate FBs with thoracic or lumbar IVDE for the presence of LS hyperesthesia.

The main limitations of this study are due to its retrospective nature. The first concerns the different MRI protocols used to investigate the LS region. This lack of standardization may have influenced the assessment of LS changes, especially with regard to nerve root involvement. However, as an inclusion criterion, all dogs were at least examined in the sagittal plane, which is considered an accurate approach in evaluating canalar and foraminal involvement. Another limitation is the lack of clinical follow-up. A long-term assessment of the hind limb withdrawal reflex after recovery from IVDE might have allowed for gathering of additional information about the role of LS IVDP in FBs with an IVDE caudal to L4.

In conclusion, LS IVDP is frequently reported in FBs, with or without cranial intervertebral foraminal stenosis, nerve root involvement, or CVMs, which often causes neither deficits upon neurological examination nor evident LS pain. In some dogs, chronic LS IVDP may cause neurological deficits that may lead to incorrect neurolocalization, representing a possible confounding factor for clinicians even in young and middle-aged subjects. Therefore, FBs need to be carefully examined at the level of the LS junction even when a patient is presenting with thoracic or lumbar IVDE.

Data availability statement

The original contributions presented in the study are included in the article/Supplementary material, further inquiries can be directed to the corresponding author.

Ethics statement

Ethical approval was not required for the studies involving animals in accordance with the local legislation and institutional requirements because the animal study was a retrospective study. Written informed consent was not obtained from the owners for the participation of their animals in this study because it was a retrospective study on routine clinical work-up.

Author contributions

CLR: Data curation, Formal analysis, Investigation, Resources, Writing – original draft, Writing – review & editing. SM: Formal analysis, Writing – review & editing. AC: Formal analysis, Writing – review & editing. TD: Formal analysis, Resources, Writing – review & editing. CR: Data curation, Investigation, Writing – review & editing. SS: Writing – review & editing. MB: Conceptualization, Formal analysis, Project administration, Resources, Supervision, Writing – original draft, Writing – review & editing.

Funding

The author(s) declare that no financial support was received for the research, authorship, and/or publication of this article.

Conflict of interest

The authors declare that the research was conducted in the absence of any commercial or financial relationships that could be construed as a potential conflict of interest.

Publisher's note

All claims expressed in this article are solely those of the authors and do not necessarily represent those of their affiliated organizations, or those of the publisher, the editors and the reviewers. Any product that may be evaluated in this article, or claim that may be made by its manufacturer, is not guaranteed or endorsed by the publisher.

Supplementary material

The Supplementary material for this article can be found online at: https://www.frontiersin.org/articles/10.3389/fvets.2023.1302418/full#supplementary-material

References

1. Mai W. *Diagnostic MRI in dogs and cats*. Boca Raton: CRC Press (2018). 766 p.

2. De Lahunta A, Glass E, Kent M. *Veterinary neuroanatomy and clinical neurology*. *5th* ed. Philadelphia: Elsevier (2021).

3. Da Costa RC, De Decker S, Lewis MJ, Volk H. Canine spinal cord injury consortium (CANSORT-SCI). Diagnostic imaging in intervertebral disc disease. *Front Vet Sci*. (2020) 7:588338. doi: 10.3389/fvets.2020.588338

4. Brisson BA. Intervertebral disc disease in dogs. *Vet Clin North Am Small Anim Pract*. (2010) 40:829–58. doi: 10.1016/j.cvsm.2010.06.001

5. Fenn J, Olby NJ. Canine spinal cord injury consortium (CANSORT-SCI). Classification of intervertebral disc disease. *Front Vet Sci*. (2020) 7:579025. doi: 10.3389/fvets.2020.579025

6. Mayousse V, Desquilbet L, Jeandel A, Blot S. Prevalence of neurological disorders in French bulldog: a retrospective study of 343 cases (2002-2016). *BMC Vet Res*. (2017) 13:212. doi: 10.1186/s12917-017-1132-2

7. Smolders LA, Bergknut N, Grinwis GC, Hagman R, Lagerstedt AS, Hazewinkel HA, et al. Intervertebral disc degeneration in the dog. Part 2: chondrodystrophic and non-chondrodystrophic breeds. *Vet J*. (2013) 195:292–9. doi: 10.1016/j.tvjl.2012.10.011

8. Worth A, Meij B, Jeffery N. Canine degenerative lumbosacral stenosis: prevalence, impact and management strategies. *Vet Med*. (2019) 10:169–83. doi: 10.2147/VMRR.S180448

9. Kranenburg HJ, Grinwis GC, Bergknut N, Gahrmann N, Voorhout G, Hazewinkel HA, et al. Intervertebral disc disease in dogs – Part 2: comparison of clinical, magnetic resonance imaging, and histological findings in 74 surgically treated dogs. *Vet J*. (2013) 195:164–71. doi: 10.1016/j.tvjl.2012.06.001

10. Suwankong N, Voorhout G, Hazewinkel HA, Meij BP. Agreement between computed tomography, magnetic resonance imaging, and surgical findings in dogs with degenerative lumbosacral stenosis. *J Am Vet Med Assoc*. (2006) 229:1924–9. doi: 10.2460/javma.229.12.1924

11. Dewey CW, da Costa RC. *Canine and Feline Neurology*. *3rd* edn. Ames: John Wiley & Sons (2016).

12. De Risio L, Thomas WB, Sharp NJ. Degenerative lumbosacral stenosis. *Vet Clin North Am Small Anim Pract*. (2000) 30:111–32, vi. doi: 10.1016/s0195-5616(00)50005-9

13. Bertram S, Ter Haar G, De Decker S. Congenital malformations of the lumbosacral vertebral column are common in neurologically normal French bulldogs, English bulldogs, and pugs, with breed-specific differences. *Vet Radiol Ultrasound*. (2019) 60:400–8. doi: 10.1111/vru.12753

14. Lecourtois C, Baudin-Tréhiou C, Blond L. Lumbosacral endplate contour defect is frequently observed concurrent with other lumbosacral abnormalities on spinal CT of French bulldogs. *Vet Radiol Ultrasound*. (2023) 64:813–22. doi: 10.1111/vru.13271

15. Balducci F, Canal S, Contiero B, Bernardini M. Prevalence and risk factors for presumptive ascending/descending myelomalacia in dogs after thoracolumbar intervertebral disk herniation. *J Vet Intern Med*. (2017) 31:498–504. doi: 10.1111/jvim.14656

16. Lampe R, Foss KD, Hague DW, Oliveira CR, Smith R. Dynamic MRI is reliable for evaluation of the lumbosacral spine in healthy dogs. *Vet Radiol Ultrasound*. (2020) 61:555–65. doi: 10.1111/vru.12891

17. Jones JC, Davies SE, Werre SR, Shackelford KL. Effects of body position and clinical signs on L7-S1 intervertebral foraminal area and lumbosacral angle in dogs with lumbosacral disease as measured via computed tomography. *Am J Vet Res*. (2008) 69:1446–54. doi: 10.2460/ajvr.69.11.1446

18. Schwarz T, Saunders J. *Veterinary computed tomography*. *1st* ed. Chichester: John Wiley & Sons Ltd (2011).

19. Robertson I, Thrall DE. Imaging dogs with suspected disc herniation: pros and cons of myelography, computed tomography, and magnetic resonance. *Vet Radiol Ultrasound*. (2011) 52:S81–4. doi: 10.1111/j.1740-8261.2010.01788.x

20. Flückiger MA, Damur-Djuric N, Hässig M, Morgan JP, Steffen F. A lumbosacral transitional vertebra in the dog predisposes to cauda equina syndrome. *Vet Radiol Ultrasound*. (2006) 47:39–44. doi: 10.1111/j.1740-8261.2005.00103.x

21. Lackmann F, Forterre F, Brunnberg L, Loderstedt S. Epidemiological study of congenital malformations of the vertebral column in French bulldogs, English bulldogs and pugs. *Vet Rec*. (2022) 190:e509. doi: 10.1002/vetr.509

22. Gong H, Slunsky P, Klass LG, Brunnberg L. Prevalence of lumbosacral transitional vertebrae in dogs in Berlin. *Pol J Vet Sci*. (2020) 23:261–5. doi: 10.24425/pjvs.2020.133641

23. Kuricová M, Ledecký V, Kvetková J, Lipták T. Vertebral malformations in French bulldogs. *J Fac Vet Med Istanbul Univ*. (2017) 43:1–153. doi: 10.16988/iuvfd.322981

24. Brocal J, De Decker S, José-López R, Guevar J, Ortega M, Parkin T, et al. Evaluation of radiography as a screening method for detection and characterisation of congenital vertebral malformations in dogs. *Vet Rec*. (2018) 182:573. doi: 10.1136/vr.104388

25. Corlat L, Blanco B, Lucena R, Pj G, Mirò F, Novales M. Congenital vertebral malformations in French bulldogs: X-ray vs computed tomography. *Bull UASVM Vet Med*. (2017) 74:11508. doi: 10.15835/buasvmcn-vm

26. Evans HE, De Lahunta A. *Miller's anatomy of the dog*. *4th* ed. St. Louis: Elsevier (2013).

27. McBride R, Parker E, Garabed RB, Olby NJ, Tipold A, Stein VM, et al. Developing a predictive model for spinal shock in dogs with spinal cord injury. *J Vet Intern Med*. (2022) 36:663–71. doi: 10.1111/jvim.16352

frontiers | Frontiers in Veterinary Science

TYPE Original Research
PUBLISHED 06 December 2023
DOI 10.3389/fvets.2023.1302399

OPEN ACCESS

EDITED BY
Adriano Wang-Leandro,
University of Veterinary Medicine Hannover, Germany

REVIEWED BY
Hakyoung Yoon,
Jeonbuk national University, Republic of Korea
Giovanni Mogicato,
Ecole Nationale Vétérinaire de Toulouse (ENVT), France

*CORRESPONDENCE
Tommaso Davini
✉ tommaso.davini@anicura.it

RECEIVED 26 September 2023
ACCEPTED 22 November 2023
PUBLISHED 06 December 2023

CITATION
Davini T, Mattei C, La Rosa C, Remelli C, Specchi S, Lionello E, Dell'Era E and Bernardini M (2023) Are postnatal traumatic events an underestimated cause of porencephalic lesions in dogs and cats? *Front. Vet. Sci.* 10:1302399. doi: 10.3389/fvets.2023.1302399

Are postnatal traumatic events an underestimated cause of porencephalic lesions in dogs and cats?

Tommaso Davini[1]*, Chiara Mattei[1,2], Claudia La Rosa[1], Carlotta Remelli[1], Swan Specchi[1,2], Elena Lionello[3], Elena Dell'Era[1] and Marco Bernardini[1,3]

[1]Anicura I Portoni Rossi Veterinary Hospital, Zola Predosa, Bologna, Italy, [2]Antech Imaging Service, Fountain Valley, CA, United States, [3]Department of Animal Medicine, Productions and Health, University of Padua, Legnaro, Italy

Introduction: Porencephaly is defined as a fluid-filled cavity of variable size in the brain cortex. It is regarded as a congenital condition and is typically considered a developmental or an encephaloclastic defect. Our hypothesis is that postnatal traumatic events in the first few months of life may represent a cause of canine and feline porencephaly that is more common than generally suspected. The aims of this study were to retrospectively investigate porencephaly in a large population of dogs and cats, detect MRI features that might be useful to differentiate postnatal acquired traumatic forms from congenital/perinatal porencephaly, and define the prevalence of seizure activity in porencephalic patients.

Materials and methods: This is a double-center, descriptive, retrospective case series. Databases were searched for cases within a 17-year time span that involve dogs and cats with an MRI-based diagnosis of cerebral cavitary lesions. Animals were included if a complete signalment and an exhaustive MRI of the brain were available. Besides the porencephalic lesions, MRIs of the head were reviewed to detect concomitant musculoskeletal abnormalities.

Results: Thirty-two cases involving nine cats and twenty-three dogs were selected. Of all the cases, 21.9% were aged six years or older at the time of diagnosis. All patients in which the neuroanatomical localization was available showed clinical signs of a prosencephalic disorder. Epileptic seizures were observed in 71.8% of cases. A single porencephalic cavity was found in 78.1% of cases. The most affected cerebral lobe was the parietal lobe ($n = 20$). The defects involved both the grey and white matter in 78.1% of cases. Twenty cases showed concomitant musculoskeletal abnormalities overlying the porencephalic cavities. Fourteen of twenty cases showed evidence of fractures, of which thirteen showed depression of the calvarium and twelve masticatory muscle abnormalities. Of these, seven of fourteen had a history consistent with a head trauma in the first period of life.

Conclusion: The recognition of skull fractures and muscular abnormalities closely associated with the porencephalic cavity may support a diagnosis of a postnatal traumatic origin of porencephaly. Therefore, this study highlights the importance of evaluating musculoskeletal structures in the MRIs of the heads of porencephalic cases.

KEYWORDS

Porencephaly, cavitary lesions, cyst-like lesions, congenital brain disease, cerebrospinal fluid (CSF), trauma, magnetic resonance imaging (MRI)

1 Introduction

Cerebral cystic lesions have been described in humans as well as large and small animals. By definition, these brain lesions include extensive lesions such as hydranencephaly, where the neopallium is reduced to a thin, nearly transparent pial-glial-membrane with no associated parenchyma (1), and focal lesions, such as porencephaly. Porencephaly is a less extensive defect, usually represented by a single, cystic, fluid-filled cavity of varying size in the wall of the cerebral hemispheres and typically involves mainly the white matter; connections between the defect and both or either the ventricular and subarachnoid space (2, 3) may be present. In veterinary literature, hydranencephaly and porencephaly are often considered together (4, 5) since parameters for differentiation are not defined, and subjective criteria are sometimes used (6). From an etiopathogenetic point of view, porencephaly is regarded as a congenital disorder and can be classified as a developmental or an encephaloclastic defect. Developmental porencephaly represents a neuronal migration disorder that leaves a defect in the developing cerebral parenchyma. Encephaloclastic porencephaly is a cerebral cavity that results from a destructive process of various etiologies including cerebral ischemia, trauma, and infection (7). Porencephaly is known since decades in veterinary medicine and most of the literature focuses on infectious and metabolic diseases, such as Border disease and copper deficiency, during the fetal life of ruminants and laboratory animals (2, 3, 8–10). In recent years, a few retrospective papers and case reports have been published on canine and feline porencephaly and its diagnosis through magnetic resonance imaging (MRI) (6, 7, 11–14). Certain acquired conditions, including traumatic insults to the brain parenchyma, may also result in focal loss of brain tissue, resulting in cavities that are filled with cerebrospinal fluid (CSF) ("ex vacuo" lesions) and that share the same imaging features as the truly congenital lesions (15). The authors' hypothesis is that traumatic events in the first weeks or months of life may constitute a cause of canine or feline porencephaly that is more common than generally suspected. The aims of this retrospective study were to (1) investigate a large population of dogs and cats with MRI diagnosis of porencephaly, (2) detect MRI features that might be useful to differentiate presumed postnatal, acquired traumatic from congenital, and (3) define the prevalence of seizure activity.

2 Materials and methods

This is a double-center, descriptive, retrospective case series. The medical record databases of the neurology units of two referral veterinary hospitals (AniCura I Portoni Rossi Veterinary Hospital, Zola Predosa, Italy, and Veterinary Teaching Hospital, University of Padua, Legnaro, Italy) were searched for cases between February 2007 and January 2023 of dogs and cats with an MRI-based diagnosis of cerebral cavitary lesions. Terms such as "cysts," "cavitary lesions," "ex-vacuo lesions," "porencephaly," and "hydranencephaly" were used for the search.

To be eligible for inclusion, dogs and cats needed to have a complete signalment and an MRI of the brain available for reviewing. Data from history and neurological examination, performed by either an ECVN board-certified neurologist or an ECVN neurology resident, were collected when available. In particular, information extracted from the medical records included neuroanatomic localization and neurological signs.

MRIs of the brain were acquired under general anesthesia with either a low-field MRI scanner (0.22 Tesla MrVet, Paramed Medical Systems, Genoa, Italy) or a high-field MRI scanner (1.5 Tesla Vantage Elan, Canon Medical Systems Europe B.V., Netherlands).

All MRI studies were reviewed independently by a European College of Veterinary Diagnostic Imaging (ECVDI) board certified radiologist (C.M.), an American College of Veterinary Radiology (ACVR) board certified radiologist (S.S.), two neurology interns (T.D. and C.L.R.), and a European College of Veterinary Neurology (ECVN) board certified neurologist (M.B.) using a dedicated Digital Imaging and Communications in Medicine viewer program (2020 Horos Project TM). Any discrepancies among observers were resolved by discussion to reach a consensus. Criteria for exclusion from the study were as follows: 1) MRI studies lacking images in all the spatial planes and 2) evidence in the MRI studies of other concomitant brain diseases.

All cases were classified as affected by porencephalic cavities (PCs) when a presumed CSF-filled cystic cavity was located in the wall of a cerebral hemisphere and surrounded at least partially by brain parenchyma (white matter, grey matter, or both). If loss of brain parenchyma for an extension of at least two lobes, associated with a partial loss in other lobes, for an entire hemisphere, or for both hemispheres (6), was identified, the lesion was defined as hydranencephaly and not further considered.

MRI images were assessed for the following: PC number (single, multiple); lateralization (left, right, bilateral); lobar involvement (olfactory, frontal, parietal, piriform, temporal, occipital); communication with CSF spaces (lateral ventricle, subarachnoid space, both, none); involvement of white matter (WM), grey matter (GM), or both; and contrast enhancement (CE – present, absent). When present, concomitant musculoskeletal abnormalities were noted: fractures, thickening or thinning of the overlying calvarium, depression of the calvarium, and ipsilateral masticatory muscle changes (atrophy and fat infiltration). Based on these abnormalities, patients with musculoskeletal abnormalities were classified into two categories: 1) presumed acquired traumatic forms, when fractures and other musculoskeletal changes were visualized, and 2) non-traumatic forms.

When present, further concomitant parenchymal abnormalities were reported. If performed, additional diagnostic tests, such as CSF examination, were registered.

All the findings were entered into a spreadsheet software (Microsoft Excel for Mac, Version 16.74). Descriptive statistics were performed by one of the neurology interns (T. D.).

3 Results

Thirty-eight patients were selected after the first search in the medical records. Of these, one case was excluded because it was classified as hydranencephaly, and five cases were excluded because

Abbreviations: PC, Porencephalic cavity; CSF, cerebrospinal fluid; WM, white matter; GM, grey matter; CE, contrast enhancement; T2W, T2 weighted; T1W, T1 weighted; SE, spin echo; FLAIR, Fluid-Attenuated Inversion Recovery; MC, meningocele; MEC, meningoencephalocele; GSF, growing skull fracture.

MRIs showed evidence of other concomitant disorders (three suspected necrotizing meningoencephalitis and two neoplasias). Thirty-two cases met the inclusion criteria and were then considered porencephalic cases.

3.1 Signalment

Twenty-three cases were dogs, and nine were cats. There were fifteen different dog breeds, with mixed breeds being the most common (8/23). All canine breeds included in the study are listed in Table 1. Thirteen dogs were females (6 neutered), and ten were males (3 neutered). The mean age of the dogs was forty-one months (range 3–142 months), and the median age was twenty-four months. All of the nine cats were domestic shorthairs. Six were neutered females, and three were neutered males. The mean age of the cats was thirty months (range 9–98 months), and the median age was twenty-one months.

3.2 Medical records review

The neuroanatomical localization was available in 28/32 cases. A forebrain localization was made in 28/28 cases, of which it was the only localization in 25/28 cases; in 3/28 cases, it was part of a multifocal localization (peripheral vestibular due to otitis media/interna (n = 2) and T3-L3 spinal cord segments due to spinal cord compression secondary to severe congenital malformations (n = 1)). Sixteen of 28 patients (9 dogs and 7 cats) showed both seizure activity and other neurological deficits. Seven of 28 patients (6 dogs and 1 cat) had a normal neurological examination, and the forebrain localization was hypothesized on the history of seizure activity. Five of 28 cases (4 dogs and 1 cat) were seizure free but showed abnormalities at neurological examination. Table 2 lists all the neurological abnormalities detected in the porencephalic patients. The mean age of the patients at the time of seizure onset was 26.1 months.

CSF was collected in 11/32 cases and found within normal range (< 5 cell/μL, protein <30 mg/dL) in all cases but one. This was a 9-year-old Pekingese dog showing an albuminocytological dissociation.

3.3 MRI features

Twenty-one of 32 patients were examined with a low-field MR scanner and 11/32 with a high-field MR scanner. At least a T2 weighted (T2W) or a T1 weighted (T1W) spin echo (SE) sequence was available in all spatial planes for each MRI study. T1W SE sequences after intravenous administration of 0.2 mL/kg of gadoteric acid were available in all cases. Fluid-Attenuated Inversion Recovery (FLAIR) sequences were available in 27/32 cases. The MRI features of the PCs and musculoskeletal changes are presented in Table 3. A total of thirty-nine PCs were seen. All cases showed either one or two PCs. A single PC was found in 25 (78.1%) cases. In this group, a clear communication with both the ventricular system and the subarachnoid space was seen in 16/25 cases and with the subarachnoid space alone or the ventricular system alone in 7/25 and 2/25 cases, respectively. Two PCs were found in 7 (21.9%) cases (Figure 1), of which both lesions showed a communication with both the ventricular system and the subarachnoid space in four of seven cases. In each of the remaining 3/7 cases, there was a lesion communicating with both the CSF spaces and the other lesion communicating with the subarachnoid space alone (1 case), the ventricular system alone (1 case), or showing no communication at all (1 case). The PCs were confined in a single lobe (6/39) or involved multiple lobes (33/39). The most affected cerebral lobe was the parietal lobe (n = 20), and the least affected was the olfactory lobe (n = 10). The defects involved both the GM and WM in 25/32 cases (78.1%). Contrast enhancement was absent in 27/32 cases and present in 5/32 cases.

Musculoskeletal changes were observed in 20/32 cases. Fourteen of 20 cases showed evidence of fractures. All these abnormalities were closely related to the PCs.

All fourteen cases with fractures presented at least two further musculoskeletal changes and then were classified as presumed acquired traumatic forms (Figure 2). Thinning of the calvarium overlying the PC was seen in 3 cases (Figure 3). None of them presented further musculoskeletal abnormalities. Depression of the calvarium was seen in 13 cases, all but one of which were associated with fractures. Thirteen cases showed masticatory muscle changes, all but one of which were associated with fractures.

Four of five patients where CE was observed have been classified into the presumed trauma category.

In seven of fourteen cases classified as presumed acquired traumatic forms in MRI, there was a history reporting a head trauma in the first weeks or few months of life: hit by a car (n = 2), bitten/crushed by the mother (n = 1), fell from a height (n = 1), horse kick (n = 1), or clinical evidence of head trauma of unknown origin (n = 2). Two of fourteen cases had no history of trauma, and five of fourteen patients were adopted in adulthood; therefore, history related to the first period of life was not available.

Concurrent abnormalities are listed in Table 3. Meningocele (MC) or meningoencephalocele (MEC) was seen in four cases, all located at the level of the parietal lobe (Figure 4).

TABLE 1 Breeds included in the study.

Dog breeds	Number (%)
Mixed breeds	8 (34.8%)
Border Collie	2 (8.7%)
Bull terrier, Cane Corso, Dobermann, Golden Retriever, Labrador Retriever, Maremma Sheepdog, Pekingese, Pitbull Terrier, German Shepherd, Maltese, Podenco Ibicenco, Chihuahua, French Bulldog	1 (4.3%)

4 Discussion

This study describes porencephaly in a large population of dogs and cats. Porencephaly is frequently described together with hydranencephaly (5, 6). However, the loss of brain parenchyma in hydranencephaly is severe and differentiates from porencephaly, which is a cavitary lesion with smooth and well-defined borders surrounded by brain tissue (16). Establishing a clear demarcation between these two conditions is challenging, and different definitions have been proposed in both human and veterinary literature in the last decades (4, 17–21). In this study, dogs were considered hydranencephalic when presented with a total parenchymal loss

TABLE 2 Main clinical signs among the porencephalic patients.

Clinical sign	Number
Seizures	23
Visual deficits	10
Compulsive circling	9
Abnormal behavior	6
Head turn	3
Head tilt	2
Ataxia	2
Horner's syndrome	1
Inappropriate urination	1
Nystagmus	1
Paraparesis	1

involving at least two lobes and a partial loss in other lobes, as proposed in a recent paper (6).

Porencephaly is poorly described in small animal medicine, especially in cats, with only five cases reported for this species in literature (7, 11, 22, 23). In this study population, 28.1% of the patients were cats, most of them two years old or younger at the time of diagnosis, suggesting that porencephaly should be considered a differential diagnosis in young cats with neurological signs, especially with history of seizure activity.

Moreover, in our population, 21.9% of the patients were 6-year-old or older at the time of diagnosis. Then, independently of the pathogenesis of porencephaly in each of our cases (congenital versus acquired), the related clinical signs could appear late in life (5). Porencephaly may simply represent an incidental finding, as supposed in a previous paper, mainly when the neurological localization of the clinical signs does not match the localization of the PCs (6, 7). However, all twenty-eight patients with an available neuroanatomical localization showed clinical signs of a prosencephalic disorder; in addition, all animals with concurrent neurological disease were previously excluded from this study. This lowers the likelihood that PCs may be an incidental finding.

The main clinical manifestation observed in our population was epileptic seizures (71.8%), as reported in veterinary literature (6, 7, 13, 22). This percentage could even be underestimated since in four cases, information about neurological status was not available. Among the epileptic patients, almost one third had a normal neurological examination, and all but one were aged between twenty-one and seventy-two months. Therefore, our study suggests the importance of considering an MRI of the brain even in patients with an age between six months and six years at seizure onset and a normal neurological examination, for which the first differential diagnosis is idiopathic epilepsy.

Porencephaly is regarded as a congenital anomaly, but it could actually result from a focal injury (vascular accident or trauma) having caused complete loss of a part of the cerebral hemispheres during the perinatal period (16). The World Health Organization defines the perinatal period in human beings as the time frame from twenty-two completed weeks of pregnancy to the first seven days of life (24). A similar definition is lacking in canine and feline medicine. Half of the

TABLE 3 Counts and percentages (in brackets) of the evaluated MRI features within the population study.

MRI features	*n*. (%)
Cases with multiple porencephalic cavities	7/32 (21.9%)
Asymmetrical	7/7 (100%)
Symmetrical	0/7 (0%)
Cases with a single porencephalic cavity	25/32 (78.1%)
Right hemisphere	12/25 (48%)
Left hemisphere	13/25 (52%)
Affected cerebral lobes	
Olfactory lobe	10
Frontal lobe	16
Parietal lobe	20
Temporal lobe	18
Piriform lobe	11
Occipital lobe	17
GM/WM involvement	
Both	25/32 (78.1%)
GM	7/32 (21.9%)
WM	0/32 (0%)
Contrast enhancement	
No	27/32 (84.4%)
Yes	5/32 (15.6%)
Concomitant musculoskeletal abnormalities	
Fractures	14/32 (43.8%)
Thinning	3/32 (9.4%)
Thickening	13/32 (40.6%)
Depression of the calvarium	13/32 (40.6%)
Masticatory muscles changes	13/32 (40.6%)
None	12/32 (37.5%)
Other features	
Meningocele	2/32 (6.2%)
Meningoencephalocele	2/32 (6.2%)
Ipsilateral ventriculomegaly	26/32 (81.2%)
Hydrocephalus internus	10/32 (31.2%)
Absence of septum pellucidum	6/32 (18.7%)
Intracranial arachnoid diverticulum associated with the quadrigeminal cistern/supracollicular fluid accumulation	3/32 (9.4%)

fourteen patients in our population with MRI abnormalities suggestive of skull fractures had a history of a severe head trauma between the third week and fifth month of life. Concomitant depression of the calvarium was appreciated in all patients but one, and adjacent masticatory muscle lesions were seen in all but two of them, supporting the traumatic etiopathogenesis. These data may be potentially underestimated due to the fact that in this category, the remote history was not available for five of the fourteen cases. On the basis of these findings, if one week of life is accepted as the limit of perinatal conditions in small animals as is the case with humans, then

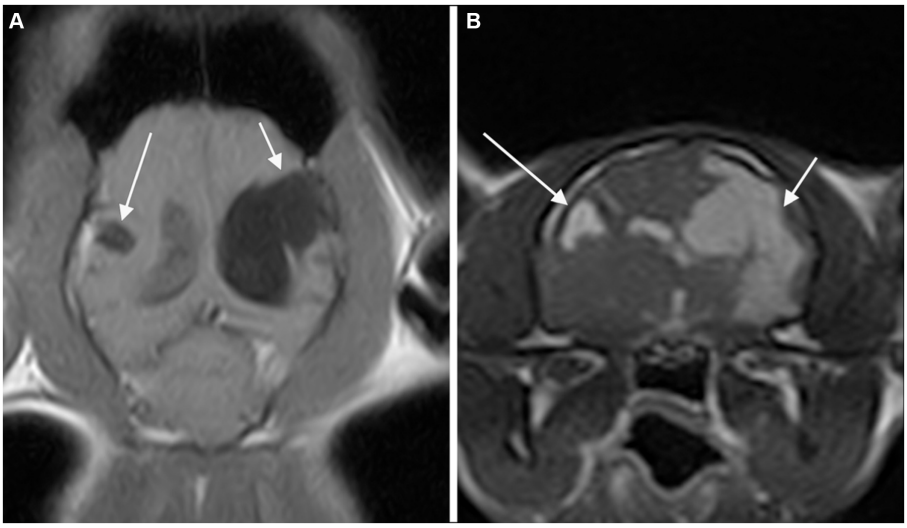

FIGURE 1
Dorsal T1-weighted **(A)** and transverse 3D-Gradient Echo in Steady State at the level of the thalamus **(B)** MR-images of the brain of a cat revealed two CSF-filled cavities consistent with bilateral porencephaly. A focal lesion located in the right parietal lobe (long arrow) showed communication with neither the ipsilateral lateral ventricle nor the sub-arachnoid space. A second, extensive lesion extending from the left lateral ventricle to the cortical surface at the level of the parietal and temporal lobes (short arrow) is seen.

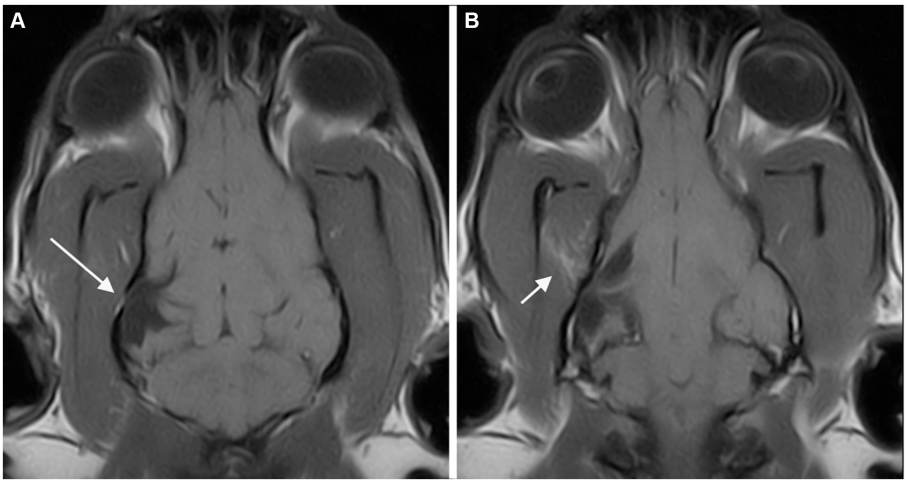

FIGURE 2
Dorsal T1-weighted MR-images of the brain of a dog showing a porencephalic cavity in the right temporal lobe at level of the caudal collicoli **(A)** and a slice below **(B)**. A temporal bone fracture (long arrow) associated with a mild depression of the overlying calvarium is appreciated. Abnormal signal of the right temporal muscle (fat infiltration) is also present (short arrow).

postnatal traumatic events should be considered a possible etiology of this condition.

The association between skull fractures and porencephaly seen in this population could be comparable to the growing skull fractures (GSFs) seen in children as a consequence of head trauma. The pulsatile force of the growing brain causes the skull fracture to enlarge; in addition, interposition of neural tissue prevents healing, inhibiting the migration of osteoblasts to the fracture site. The resorption of the adjacent bone by the continuous pressure from brain tissue herniation through the bone gap adds to the progression of the fracture line; this is the reason why in human medicine, this complication must be corrected early. Porencephaly has been described as a late radiological and surgical finding in patients affected by GSFs (25–27). The same pathogenetic mechanism could explain the relationship between PCs and MC or MEC, as seen in four patients in our study. The congenital lack of the calvarial bone could act as a least resistant point similarly to the skull fracture, allowing the herniation of brain tissue and the developing of the PC. All these malformations occurred at the level of the parietal region; this finding is in accordance with a previous study (28) in which porencephaly was seen in all cases with parietal MC in dogs and with a case report (23) describing a cat with frontoparietal MEC. Another finding that supports a strict relationship between postnatal traumatic brain injury and PCs is that four of the five cases where CE was seen have been classified as presumed

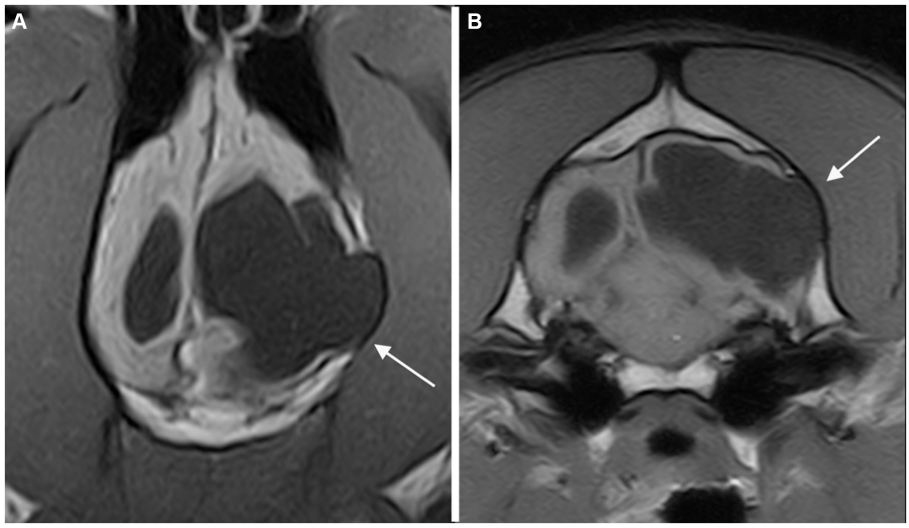

FIGURE 3
Dorsal **(A)** and transverse at the level of the inner ears **(B)** T1-weighted MR-images of the brain of a dog with an extensive unilateral cavity extending from the left lateral ventricle to the cortical surface. A severe mass effect leading to a right midline shift is present. The cranial vault over the porencephalic cyst is stretched and thinned (arrow).

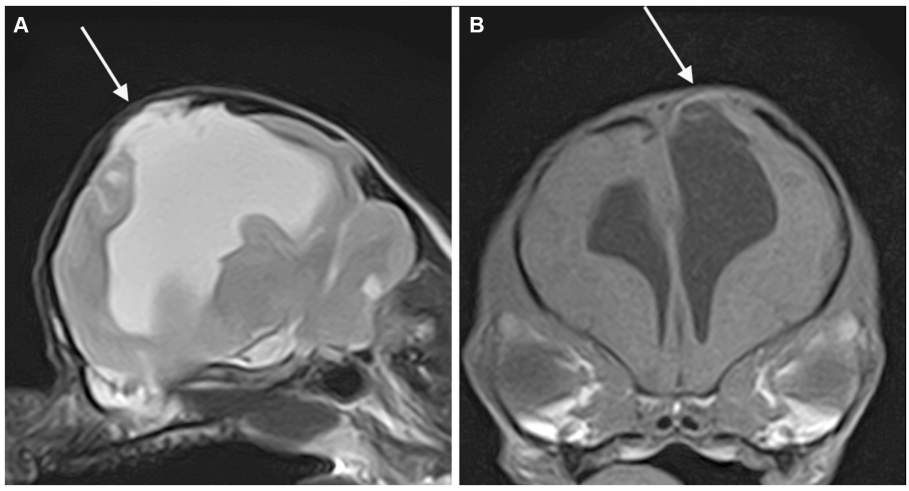

FIGURE 4
Parasagittal T2-weighted **(A)** and transverse T1-weighted **(B)** MR-images of the brain of a dog showing a porencephalic cavity in the left parietal lobe and associated meningoencephalocele (arrow).

acquired traumatic. In these cases, the presence of contrast enhancement could be the result of a chronic blood–brain-barrier dysfunction secondary to traumatic brain injury as reported in both humans and rats in a recent study (29).

The principal limitations of the present study are its retrospective nature and the fact that in almost two thirds of cases, head MRIs were performed with a low field unit. The lack of history for five of the dogs prevents a more exhaustive establishment of a relationship between a possible traumatic event and MRI findings. All the studies were lacking proton density weighted sequences, which are considered the most useful sequences for detecting bone traumatic lesions (30). In addition, the quality of the MRIs obtained with a low field unit could limit the recognition of subtle signs of head trauma, causing one to underestimate the real number of presumed acquired traumatic cases. An additional limitation is the lack of histopathological confirmation in all cases, which might be useful to differentiate congenital from postnatal porencephaly; nonetheless, porencephalic patients are often acceptable pets with a good quality of life, and the diagnosis of porencephaly is generally MRI-based.

In conclusion, this study investigated porencephaly in a large population of dogs and cats. Establishing a possible underlying cause responsible for this condition is often challenging. MRIs can help detect neurological and musculoskeletal abnormalities of the head that support a postnatal, traumatic etiology of the PCs. On the basis of our results, traumatic events are likely to be a more frequent cause of porencephaly than generally reported in literature. Finally, seizure

activity is common in porencephalic dogs and cats; porencephaly might be related to seizure activity even when its onset appears in adulthood.

Data availability statement

The original contributions presented in the study are included in the article/supplementary material, further inquiries can be directed to the corresponding author.

Ethics statement

Ethical approval was not required for the studies involving animals in accordance with the local legislation and institutional requirements because Ethical review and approval was not required for the animal study because retrospective study. Written informed consent was not obtained from the owners for the participation of their animals in this study because Written informed consent for participation was not obtained from the owners because retrospective study on routine clinical work-up.

Author contributions

TD: Data curation, Formal analysis, Investigation, Resources, Writing – original draft, Writing – review & editing. CM: Formal analysis, Writing – review & editing. CL: Formal analysis, Resources, Writing – review & editing. CR: Writing – review & editing. SS: Formal analysis, Writing – review & editing. EL: Investigation, Writing – review & editing. ED: Data curation, Investigation, Resources, Writing – review & editing. MB: Conceptualization, Formal Analysis, Project administration, Resources, Supervision, Writing – original draft, Writing – review & editing.

Funding

The author(s) declare that no financial support was received for the research, authorship, and/or publication of this article.

Conflict of interest

The authors declare that the research was conducted in the absence of any commercial or financial relationships that could be construed as a potential conflict of interest.

Publisher's note

All claims expressed in this article are solely those of the authors and do not necessarily represent those of their affiliated organizations, or those of the publisher, the editors and the reviewers. Any product that may be evaluated in this article, or claim that may be made by its manufacturer, is not guaranteed or endorsed by the publisher.

References

1. De Lahunta A, Glass E, Kent M. *Veterinary neuroanatomy and clinical neurology. 5th* ed. Philadelphia: Elsevier (2021).

2. Vandevelde M, Higgins RJ, Oevermann A. *Veterinary neuropathology: Essentials of theory and practice*. Oxford: John Wiley & Sons (2012).

3. Grant MM. *Jubb, Kennedy & Palmer's pathology of domestic animals*. St. Louis, Missouri: Elsevier health sciences (2015). 1 p.

4. Summers BA, Cummings JF, De Lahunta A. *Veterinary neuropathology*. St. Louis, Mo: Mosby (1995).

5. MacKillop E. Magnetic resonance imaging of intracranial malformations in dogs and cats. *Vet Radiol Ultrasound*. (2011) 52:S42–51. doi: 10.1111/j.1740-8261.2010.01784.x

6. Davies ES, Volk HA, Behr S, Summers B, de Lahunta A, Syme H, et al. Porencephaly and hydranencephaly in six dogs. *Vet Rec*. (2012) 170:179. doi: 10.1136/vr.100109

7. Schmidt MJ, Klumpp S, Amort K, Jawinski S, Kramer M. Porencephaly in dogs and cats: magnetic resonance imaging findings and clinical signs. *Vet Radiol Ultrasound*. (2012) 53:142–9. doi: 10.1111/j.1740-8261.2011.01887.x

8. Golchin D, Sasani F, Moosakhani F, Badiei A, Zafari M, Partovi NM. Congenital cerebral and cerebellar anomalies in relation to bovine viral diarrhoea virus and Akabane virus in newborn calves. *Acta Vet Hung*. (2023) 71:34–40. doi: 10.1556/004.2023.00764

9. Ono K, Nishizawa K, Yamamoto H, Watanabe Y, Aotani H, Yamano T, et al. Neural plasticity after neonatal hypoxic and ischemic insult in rats. *No To Hattatsu*. (1991) 23:453–7.

10. Tsutsui Y, Kashiwai A, Kawamura N, Kadota C, Nagahama M. Postnatal porencephaly induced in mouse by murine cytomegalovirus. *Acta Neuropathol*. (1991) 82:435–41. doi: 10.1007/BF00293377

11. Hori A, Hanazono K, Miyoshi K, Nakade T. Porencephaly in dogs and cats: relationships between magnetic resonance imaging (MRI) features and hippocampal atrophy. *J Vet Med Sci*. (2015) 77:889–92. doi: 10.1292/jvms.14-0359

12. Marenzoni ML, Calò P, Foiani G, Tossici S, Passantino G, Decaro N, et al. Porencephaly and periventricular encephalitis in a 4-month-old puppy: detection of canine parvovirus type 2 and potential role in brain lesions. *J Comp Pathol*. (2019) 169:20–4. doi: 10.1016/j.jcpa.2019.03.005

13. Machado GF, Laranjeira MG, Schweigert A, de Melo GD. Porencephaly and cortical dysplasia as cause of seizures in a dog. *BMC Vet Res*. (2012) 8:246. doi: 10.1186/1746-6148-8-246

14. Hashiguchi O, Yamaguchi Y, Ikezaki S, Saito T, Igura S, Hirai R, et al. Porencephaly with an optic organ abnormality in a beagle dog. *J Toxicol Pathol*. (2022) 35:107–11. doi: 10.1293/tox.2021-0039

15. Mai W. *Diagnostic MRI in dogs and cats*. Boca Raton: CRC Press Taylor & Francis Group (2018).

16. De Risio L, Muñana K. *A practical guide to seizure disorders in dogs and cats. 1st* ed. Palm Beach Gardens, FL: Edra Publishing US LLC (2022).

17. Pavone P, Praticò AD, Vitaliti G, Ruggieri M, Rizzo R, Parano E, et al. Hydranencephaly: cerebral spinal fluid instead of cerebral mantles. *Ital J Pediatr*. (2014) 40:79. doi: 10.1186/s13052-014-0079-1

18. Breedveld G, de Coo IF, Lequin MH, Arts WF, Heutink P, Gould DB, et al. Novel mutations in three families confirm a major role of COL4A1 in hereditary porencephaly. *J Med Genet*. (2006) 43:490–5. doi: 10.1136/jmg.2005.035584

19. Osborn AG, Preece MT. Intracranial cysts: radiologic-pathologic correlation and imaging approach. *Radiology*. (2006) 239:650–64. doi: 10.1148/radiol.2393050823

20. Fortin F. *Radiopaedia. Porencephaly*. (2022). https://radiopaedia.org/articles/porencephaly.

21. McGavin MD, Zachary JF. *Pathologic basis of veterinary disease. 4th* ed. Mosby: Elsevier (2006).

22. Williamson BG, O'Brien DP. What is your neurologic diagnosis? *Porencephaly J Am Vet Med Assoc*. (2013) 242:1641–3. doi: 10.2460/javma.242.12.1641

23. Farré Mariné A, Pumarola M, Luján F-PA. Polysulfone tailor-made implant for the surgical correction of a frontoparietal meningoencephalocoele in a cat. *JFMS Open Rep*. (2022) 8:20551169221098940. doi: 10.1177/20551169221098940

24. World Health Organization. *Perinatal conditions*. https://platform.who.int/mortality/themes/theme-details/topics/topic-details/MDB/perinatal-conditions.

25. Singhal GD, Atri S, Suggala S, Jaluka D, Singhal S, Shrivastava AK. Growing skull fractures; pathogenesis and surgical outcome. *Asian J Neurosurg*. (2021) 16:539–48. doi: 10.4103/ajns.AJNS_183_18

26. Sanford RA. Prevention of growing skull fractures: report of 2 cases. *J Neurosurg Pediatr*. (2010) 5:213–8. doi: 10.3171/2009.9.PEDS09180

27. Singh I, Rohilla S, Siddiqui SA, Kumar P. Growing skull fractures: guidelines for early diagnosis and surgical management. *Childs Nerv Syst*. (2016) 32:1117–22. doi: 10.1007/s00381-016-3061-y

28. Lazzerini K, Gutierrez-Quintana R, José-López R, McConnell F, Gonçalves R, McMurrough J, et al. Clinical features, imaging characteristics, and long-term outcome of dogs with cranial Meningocele or Meningoencephalocele. *J Vet Intern Med*. (2017) 31:505–12. doi: 10.1111/jvim.14638

29. van Vliet EA, Ndode-Ekane XE, Lehto LJ, Gorter JA, Andrade P, Aronica E, et al. Long-lasting blood-brain barrier dysfunction and neuroinflammation after traumatic brain injury. *Neurobiol Dis*. (2020) 145:105080. doi: 10.1016/j.nbd.2020.105080

30. Hecht S, Anderson KM, Castel A, Griffin JF 4th, Hespel AM, Nelson N, et al. Agreement of magnetic resonance imaging with computed tomography in the assessment for acute skull fractures in a canine and feline cadaver model. *Front Vet Sci*. (2021) 8:603775. doi: 10.3389/fvets.2021.603775

frontiers | Frontiers in Veterinary Science

TYPE Original Research
PUBLISHED 18 December 2023
DOI 10.3389/fvets.2023.1325521

OPEN ACCESS

EDITED BY
Daisuke Hasegawa,
Nippon Veterinary and Life Science University, Japan

REVIEWED BY
Philippa Johnson,
Cornell University, United States
Yuji Hamamoto,
Rakuno Gakuen University, Japan

*CORRESPONDENCE
Katrin M. Beckmann
✉ kbeckmann@vetclinics.uzh.ch

†These authors have contributed equally to this work and share last authorship

RECEIVED 21 October 2023
ACCEPTED 23 November 2023
PUBLISHED 18 December 2023

CITATION
Beckmann KM, Wang-Leandro A, Steffen F, Richter H, Dennler M, Bektas R, Carrera I and Haller S (2023) Diffusion tensor-based analysis of white matter in dogs with idiopathic epilepsy. *Front. Vet. Sci.* 10:1325521. doi: 10.3389/fvets.2023.1325521

Diffusion tensor-based analysis of white matter in dogs with idiopathic epilepsy

Katrin M. Beckmann[1,2]*, Adriano Wang-Leandro[3,4], Frank Steffen[1], Henning Richter[3], Matthias Dennler[3], Rima Bektas[5], Ines Carrera[6†] and Sven Haller[7,8†]

[1]Section of Neurology, Department of Small Animals, Vetsuisse Faculty Zurich, University of Zurich, Zurich, Switzerland, [2]Graduate School for Cellular and Biomedical Sciences, University of Bern, Bern, Switzerland, [3]Clinic for Diagnostic Imaging, Department of Diagnostics and Clinical Services, Vetsuisse-Faculty Zurich, University of Zurich, Zurich, Switzerland, [4]Department of Small Animal Medicine and Surgery, University of Veterinary Medicine Hannover, Hannover, Germany, [5]Section of Anaesthesiology, Department of Clinical Diagnostics and Services, Vetsuisse-Faculty Zurich, University of Zurich, Zurich, Switzerland, [6]Vet Oracle Teleradiology, Norfolk, United Kingdom, [7]Department of Surgical Sciences, Radiology, Uppsala University, Uppsala, Sweden, [8]Faculty of Medicine, University of Geneva, Geneva, Switzerland

Introduction: The understanding of epileptic seizure pathogenesis has evolved over time, and it is now generally accepted that not only are cortical and subcortical areas involved but also the connection of these regions in the white matter (WM). Recent human neuroimaging studies confirmed the involvement of the WM in several epilepsy syndromes. Neuroimaging studies investigating WM integrity with diffusion tensor imaging (DTI) in canine idiopathic epilepsy are lacking. This study aimed to test the hypothesis that WM diffusion changes can be found in dogs affected by idiopathic epilepsy.

Method: Twenty-six dogs with idiopathic epilepsy (15 Border Collies and 11 Greater Swiss Mountain dogs) and 24 healthy controls (11 Beagle dogs, 5 Border Collies, and 8 Greater Swiss Mountain dogs) were prospectively enrolled. Most dogs with idiopathic epilepsy (17/26) were enrolled within 3 months after seizure onset. Diffusion tensor imaging of the brain with 32 diffusion directions (low b value = 0 s/mm^2; maximal b value = 800 s/mm^2) was performed in a 3 Tesla scanner. Tract-based spatial statistics (TBSS), a voxel-based approach, was used to investigate changes in fractional anisotropy (FA) and mean diffusivity (MD) in the idiopathic epilepsy group compared to the healthy control group. Additionally, FA and MD were investigated in the region of corpus callosum and cingulate white matter in both groups.

Results: We observed subtle changes in WM DTI between the idiopathic epilepsy group and the healthy control group limited to cingulate WM, with a significantly lower FA in the idiopathic epilepsy group compared to the healthy control group in the region of interest (ROI) approach ($p = 0.027$). No significant changes were found between the idiopathic epilepsy group and the healthy control group in the TBSS analysis and in the corpus callosum in the ROI approach.

Conclusion: This study supports the cingulate area as a target structure in canine epilepsy. The subtle changes only might be explained by the short duration of epilepsy, small sample sizes, and the higher variability in canine brain anatomy. Furthermore, all included dogs showed generalized tonic-clonic seizures, possibly affected by generalized epilepsy syndrome, which are also associated with less pronounced DTI changes in humans than focal epilepsy syndromes.

KEYWORDS

TBSS, white matter integrity, seizures, Border Collie, Greater Swiss Mountain dog, MRI, DTI, canine

1 Introduction

Canine idiopathic epilepsy is diagnosed based on the age of the dog at the onset of the epileptic seizure, unremarkable inter-ictal physical and neurological examination, and exclusion of metabolic, toxic, and structural cerebral disorders by means of diagnostic investigations (1). Magnetic resonance imaging (MRI) of the brain is routinely used as an important diagnostic step for idiopathic epilepsy, and the diagnosis is based on a normal structural brain MRI (2). However, epilepsy is increasingly recognized as a disease of the brain network, involving both gray matter and white matter, which cannot be assessed from conventional MRI sequences, but only with advanced MRI techniques (3–5). Diffusion tensor imaging (DTI) offers a unique opportunity to investigate the white matter structures non-invasively *in vivo* (6).

In order to detect diffusion within tissues, magnetic field gradients are used to create an image that is sensitized to diffusion in a particular direction, and thus, diffusion can be measured by estimating a three-dimensional diffusion model or tensor (7). This tensor is characterized by three orthogonal vectors. The average diffusivity of all three vectors in DTI represents the mean diffusivity (MD) value (8). The MD can be used to measure the microstructural properties of the gray and the white matter and is dependent on the amount of extracellular water (7).

A preferential diffusion in a particular direction is called anisotropic diffusion. White matter is organized in tracts that consist of axonal bundles. The cellular membranes of these axons with some contributions from the myelination and the packing of the axons give a preferential direction of diffusion along the orientation of the axons leading to an anisotropic diffusion within the white matter (7). The most widely used metric for assessing anisotropy is fractional anisotropy (FA), and it is often considered a measure of white matter integrity (7). In cases of compromised white matter integrity, such as demyelination or axonal loss, reduced FA and increased MD values are expected (Figure 1).

In 2020, the ENIGMA Epilepsy study investigated DTI data of 1,249 human patients affected by a variety of epilepsy syndromes, including temporal lobe epilepsy, genetic generalized epilepsy, and non-lesional extratemporal epilepsy (5). Across all these epilepsy syndromes, the FA was lower in most fiber tracts. This effect was most prominent in the corpus callosum, cingulum, and external capsule. The reduction in FA was accompanied by a less robust increase in MD (5).

So far, a single study has been performed in veterinary medicine to investigate diffusion changes in dogs with idiopathic epilepsy. This study focused on apparent diffusion coefficient (ADC) metrics, a technique that describes the overall diffusion within a voxel but lacks a tensor imaging technique (9). Although DTI of the canine brain has been used to detect age-related changes (10), to detect differences between humans and dogs in Krabbe's disease (11), and to investigate the white matter in a compulsive behavioral disorder in dogs (12), the involvement of microstructural white matter changes in canine idiopathic epilepsy remains an unexplored field. Characterizing microstructural white matter changes, which are otherwise undetected in conventional MRI, could release the potential of establishing prognostic non-invasive biomarkers or objective quantitative monitoring parameters for the brain tissue in patients treated with novel treatment strategies such as epilepsy surgery or deep brain stimulation (13, 14).

The study aimed to investigate white matter diffusion changes in dogs affected by idiopathic epilepsy with generalized tonic-clonic seizures. We hypothesized that dogs with idiopathic epilepsy would have lower FA and higher MD in several white matter tracts compared to healthy controls and that this effect would be most pronounced in the corpus callosum and cingulate white matter.

Abbreviations: ADC, apparent diffusion coefficient; DTI, diffusion tensor imaging; FA, fractional anisotropy; IVETF, international veterinary epilepsy task force; MD, mean diffusivity; MRI, magnetic resonance imaging; ROI, region of interest; TBSS, tract-based special statistics.

2 Methods

2.1 Animals

Border Collies and Greater Swiss Mountain dogs diagnosed with idiopathic epilepsy according to the veterinary epilepsy task force criteria (15) and healthy controls of the same breeds were prospectively enrolled in this study during a period of 5 years (2017–2022). Additionally, 11 research Beagles were included in the healthy control group. These Beagle dogs have been part of a preliminary study investigating the feasibility of resting state network detection under general anesthesia (16). Functional MRI and magnetic resonance spectroscopy data from the same scan of most of the Border Collies and Greater Swiss Mountain dogs with idiopathic epilepsy and healthy controls have also been analyzed in previous studies (17–19). This study was approved by the Swiss Federal Veterinary Office Zurich (animal license numbers ZH272/16 and ZH046/20). The authors complied with the Animal Research: Reporting of *In Vivo* (ARRIVE Experiments) guidelines.

A physical and neurological examination was conducted by a board-certified veterinary neurologist in all dogs. Minimum database information was collected as recommended by the international veterinary epilepsy task force (IVETF) for investigations of idiopathic epilepsy, including a seizure history and family seizure history for idiopathic epilepsy, complete blood cell count, and serum biochemistry panel, electrolytes as well as fasted ammonia, bile acids, and urinalysis (1). Information on seizure semiology was collected from all owners in a personal interview based on the questionnaire recommended by the IVETF (1, 15).

Border Collies and Greater Swiss Mountain dogs with idiopathic epilepsy were included only, if they fulfilled the IVETF Tier II criteria and suffered from generalized tonic-clonic seizures (1). Healthy controls were included if they had no history of seizures.

Exclusion criteria were age younger than 1 year [to exclude the influence of incomplete maturation (20)] and older than 10 years [to exclude changes from aging (10)], DTI of insufficient quality, abnormal clinical or neurological examination, abnormal cerebrospinal fluid analyses, and identification of an underlying cause for the epilepsy or structural brain lesion on MRI.

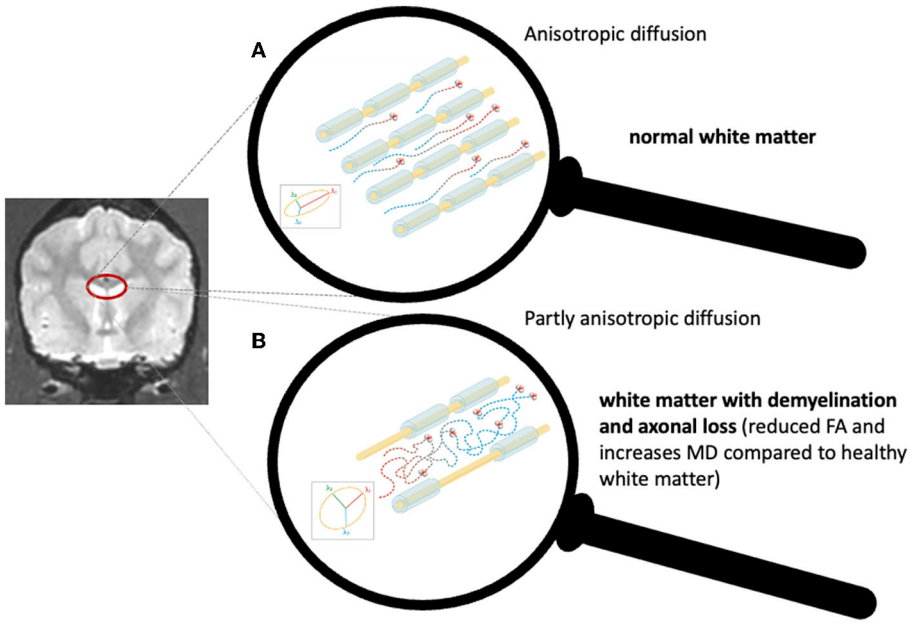

FIGURE 1
Schematic representation of normal water molecule diffusion along the direction of intact axonal bundles **(A)** and reduced anisotropy caused by axonal loss and demyelination **(B)**.

Dogs were divided into two groups: the healthy control group and the idiopathic epilepsy group.

For the region of interest (ROI) analysis, the healthy control group was further subdivided into a healthy control group with a first-degree relative with idiopathic epilepsy and a healthy control group with no family history of idiopathic epilepsy.

2.2 Imaging acquisition

All dogs underwent an MRI scan of the brain with a 3 Tesla MRI (Philips Ingenia scanner, Philips AG, Zurich, Switzerland) and a 16-channel receive–transmit head coil (dStream HeadSpine coil solution, Philips AG, Zurich, Switzerland) under general anesthesia with a standardized anesthetic protocol (16).

Conventional morphological MR images included T2-weighted (T2W) turbo spin-echo sequences in transverse, dorsal, and sagittal planes, a transverse fluid-attenuated inversion recovery (FLAIR), a transverse T2* or a susceptibility-weighted sequence, and a 3D T1W gradient echo sequence.

In the dogs with idiopathic epilepsy, the 3D T1W sequence was repeated after intravenous injection of contrast media [Gadodiamide (Omniscan) GE HealthcareAG, Glattbrugg, Switzerland, or Gadoteric-acid (Dotarem), Guerbet AG, Zürich, Switzerland].

The echo-planar DTI sequence was performed in a transverse plane (TR 8,191 ms; TE 81 ms) with 32 diffusion directions (single low b value = 0 s/mm^2; maximal b value = 800 s/mm^2; isometric voxel size of 1.5 mm, in-plan field of view of 160 × 160 mm, and acquisition matrix of 108 × 105).

2.3 Postprocessing

DICOM images were converted to 4D NIFTI format using dcm2niix (University of South Carolina, South Carolina, USA). Further processing was performed using FSL (FMRIB Software Library v6.0.5.1, Oxford, UK).

Using FSL commands, data were corrected for eddy current and motion distortion, and an automated mask was used to remove extraneural tissues. Then, a diffusion tensor model was fitted to the processed images using the FSL "dtifit" command, which provides a matrix-valued tensor for each voxel. Diffusion tensor maps for each diffusivity parameter were generated for each subject and visually inspected to ensure the quality of the preprocessing, volume registration, and orientation.

2.4 Tract-based spatial statistics

A modified tract-based spatial statistical (TBSS) analysis (21, 22) adapted to dogs (10) was conducted. As previously described by Barry et al. (10), the subjects' FA images were processed according to the human TBSS pipeline until step three (tbss_3_postreg).

Each subject's FA image was registered using a non-linear transformation to the target FA image (the most representative subject identified in step three of the human TBSS pipeline) with FNIRT (23). A mean FA image was created by concatenating the target space FA images into a single 4D file that was then averaged using *fslmaths*. A mean FA skeleton was created by thresholding the mean FA at a lower threshold of 0.2 and an upper threshold of 0.8. This thresholded FA skeleton was then binarized to create an FA skeleton mask. The skeleton mask was then applied to a 4D FA file

TABLE 1 Population characteristics.

	Dogs with idiopathic epilepsy ($n = 26$)	Healthy controls ($n = 24$)	Healthy controls with a first-degree relative with idiopathic epilepsy ($n = 12$)	Healthy controls with no family history of idiopathic epilepsy ($n = 12$)
Breed				
Beagle	0	11	0	11
Border collie	15	5	4	1
Greater Swiss Mountain dog	11	8	8	0
Sex				
Male	14	10	4	6
Male castrated	4			
Female	5	14	8	6
Female spayed	4			
Ratio male:female	2:1	5:7	1:2	1:1
Bodyweight				
Kilograms [median; range]	22.8; 14.0–70.0	19.0; 9.6–54.8	38.3; 16.4–54.8	16.4; 9.6–21.8
Age				
Years [median; range]	3.0; 1.0–8.6	5.6; 1.3–8.6	5.6; 2.5–8.6	5.2; 1.3–7.2

to create a 4D FA skeleton image. MD was processed according to the same steps outlined above and extracted using the FA skeleton. FA and MD values at the location of the FA skeleton mask were then exported for statistical analysis.

2.5 Region of interest analysis

ROI analysis was performed for two regions compromised across all epilepsy syndromes in humans, the corpus callosum and the cingulate white matter (5). The ROIs were selected in the mean FA skeleton mask overlaid with a T1W image of the target dog allowing visualization of the corpus callosum and cingulate white matter. The created mask included the cingulate region bilaterally (Supplementary Figure 1). The corpus callosum mask was created following Barry et al. (10), but with all regions of the corpus callosum in a single mask (Supplementary Figure 2). Using *fslstats*, these ROIs were then applied to the 4D FA skeleton and to the 4D MD skeleton image (24).

2.6 Statistics

For a voxel-based TBSS analysis, permutation testing using FSL's *randomize* tool was used to conduct an independent *t*-test to evaluate differences in diffusion metrics between the idiopathic epilepsy group and the healthy control group using both threshold-free cluster enhancement and family-wise error correction to control for multiple comparisons (25–27).

For the ROI analysis, statistics were performed using R (2023.06.0 in RStudio) (28). In the first step, a Kruskal–Wallis test was performed to investigate differences in FA and MD values in the corpus callosum ROI and the cingulate ROI for two distinct groups: the idiopathic epilepsy group and the healthy control group. In a subsequent step, a Kruskal–Wallis test was conducted to examine the differences in FA and MD values in the corpus callosum ROI and the cingulate ROI across three distinct groups: the idiopathic epilepsy group, the healthy control group with a first-degree relative with idiopathic epilepsy, and the healthy control group with no family history of idiopathic epilepsy. *Post-hoc* pairwise comparisons among the groups were carried out using the Dunn test. To mitigate the issue of multiple comparisons, the Bonferroni correction was applied to adjust the *p*-values. In the event of statistical significance, an effect size (r) was computed to quantify the magnitude of differences observed between the group means. Overall, $p < 0.05$ was considered statistically significant.

3 Results

3.1 Study population

A total of 59 dogs were prospectively enrolled. Nine dogs were excluded because of insufficient imaging quality. A total of 50 dogs were included in the data analysis. Population characteristics are given in Table 1. In the healthy control group, all Greater Swiss Mountain dogs, and all but one Border Collie had a first-degree relative with idiopathic epilepsy. Information regarding the seizure semiology is reported in Table 2. Unfortunately, in cases with focal onset, the owners could not reliably report the side of the focal onset in most cases.

TABLE 2 Seizure semiology.

Medical treatment at the time of MRI		[n]
Phenobarbital		9
Potassium bromide		4
Levetiracetam		3
Imepitoin		1
Type of therapy	Mono	2
	Double	5
	Triple	2
Time between first seizure and MRI		**[n]**
<1 month		5
>1–3 months		12
>3–12 months		6
>12 months		3
Time between last seizure and MRI		**[n]**
>2 days−1 week		11
>1 week−2 weeks		10
>2 weeks−4 weeks		1
>4 weeks		4
Seizures		**[n]**
Status epilepticus		18
Cluster seizures		9
Seizure semiology		
Tonic-clonic		24
Tonic		2
Focal onset secondary generalization		14
Unknown onset		8
Additional focal seizures		10
Autonomic signs	Salivation	9
	Urination	11
	Defecation	5
Postictal aggression		3
Inter-ictal behavioral changes		**[n]**
Anxiety		3

3.2 Voxel-based analysis with TBSS

No significant differences in FA and MD were identified between the idiopathic epilepsy group and the healthy control group using TBSS. The results from TBSS are displayed in Figure 2.

3.3 ROI analysis

The ROI analysis showed a significant difference in the FA of the cingulate white matter in the idiopathic epilepsy group compared to the healthy control group ($p = 0.027$) with lower FA in the idiopathic epilepsy group. The effect size was moderate ($r = -0.313$). No significant differences were found in the FA of the corpus callosum and MD of the corpus callosum and the cingulate white matter between the idiopathic epilepsy group and the healthy control group. The results are displayed in Figure 3.

The Kruskal–Wallis test of FA and MD values of the corpus callosum ROI and the cingulate ROI across the three distinct groups revealed a significant difference in the cingulate FA and MD values ($p = 0.012$ and $p = 0.001$) but not in the callosal FA and MD values ($p = 0.644$ and $p = 0.122$).

For FA of the cingulate white matter, a pairwise comparison of the healthy control group with no familiar history of idiopathic epilepsy and the idiopathic epilepsy group showed a significant difference ($p = 0.009$) with a lower FA in the idiopathic epilepsy group (effect sizes $r = -0.48$).

For MD of the cingulate white matter, a pairwise comparison of the healthy control group with no familiar history of idiopathic epilepsy and the healthy control group with a first-degree relative with idiopathic epilepsy showed significant difference ($p = 0.0007$) with a large effect size ($r = -0.748$) as well as a significance between the healthy control group with a first-degree relative with idiopathic epilepsy and idiopathic epilepsy group ($p = 0.036$) with a moderate effect size ($r = -0.408$). The results are displayed in Figure 4.

4 Discussion

In this single-center prospective study, we investigated white matter integrity in Border Collies and Greater Swiss Mountain dogs with idiopathic epilepsy. We hypothesized that we would find impaired white matter integrity in dogs with idiopathic epilepsy compared to healthy controls manifesting as a decrease in FA and an increase in MD. While a voxel-based analysis (TBSS) did not detect any significant differences between the idiopathic epilepsy group and the healthy control group, the ROI analysis of the corpus callosum and cingulate white matter showed significant differences in the FA in the cingulate white matter between the idiopathic epilepsy group and the healthy control group only, with lower FA values in the idiopathic epilepsy group.

Note that in general voxel-based analysis and ROI analysis in DTI do correlate well, but they do not always provide the same results (29). Automated voxel-based analysis offers the advantage that no prior assumption needs to be performed and the whole brain can be analyzed. However, in our study, the whole brain TBSS includes all 73,713 voxels in the analysis. The analysis is performed with a multiple comparison correction to prevent false-positive results. If the effect is very subtle, these multiple comparison corrections may mask small changes. In contrast, the ROI analysis first combines the signal across multiple voxels within the ROI (645 voxels for the cingulate gyrus ROI and 316 voxels for the corpus callosum ROI) leading to an increased signal-to-noise ratio. Second, as only two analyses are performed in the ROI analysis, the effect of multiple comparisons correction is minimal. Furthermore, voxel-based analysis heavily depends on the exact anatomical registration of each voxel to the study template, and the more diverse shape of the canine brain and a not as well

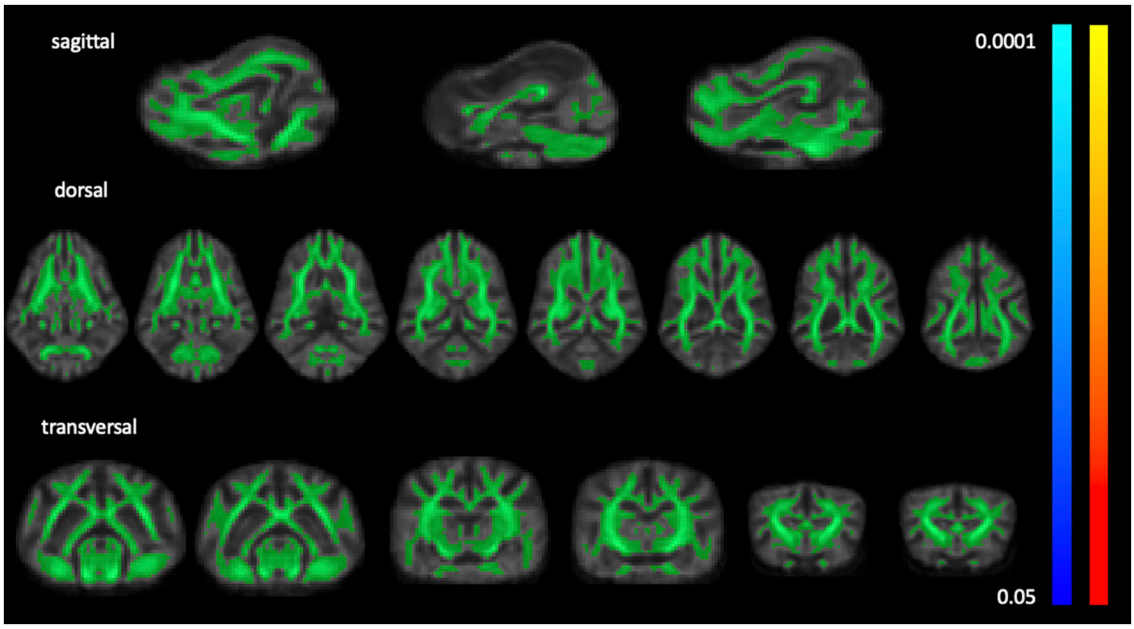

FIGURE 2
Light green overlay of the average white matter mask over sample FA template slices in sagittal, dorsal, and transverse planes. TBSS detected no significant differences from $p < 0.05$ to $p < 0.0001$ for FA (coolmap) and MD (heatmap).

validated processing pipeline might have had an influence on the voxel registration and therefore on the voxel-based analysis (29).

In contrast to canine epilepsy, plenty of DTI studies have been performed in human epilepsy and microstructural compromises of the white matter have been identified in a wide variety of epilepsy syndromes using DTI (5). Decreased FA and increased MD were seen across all epilepsy syndromes in a variety of white matter structures including the corpus callosum and cingulum (5).

While this effect has been very clearly identified in the large-scale ENIGMA human epilepsy study, including more than 1,000 individuals, the results from smaller studies with fewer patients have been less conclusive (5, 30, 31). In smaller studies like ours, with smaller sample sizes, it is more difficult to account for a heterogenic study population and it is more difficult to compensate for additional contributing factors, such as lateralization of the diseases, age, or gender. For example, we did not have information regarding lateralization of the seizure signs in most dogs included in the study, and gender and age were not matched between the idiopathic epilepsy group and the healthy control groups. Furthermore, a stringent classification of epilepsy into a subcategory was lacking in our canine patients. All these factors might have led to the detection of reduced FA in the cingulate white matter only.

In humans, the DTI changes were most pronounced in ipsilateral to mesial temporal lesions and the changes were less pronounced in non-lesional epilepsy (5). We included dogs with generalized epileptic seizures and no visible lesions on MRI, where the effect might be less pronounced compared to focal lesional epilepsy syndromes in humans.

Furthermore, most dogs included in our study were newly diagnosed. In humans, it has been speculated that the white matter changes represent secondary effects, rather than being causal, but large longitudinal studies are lacking (5). Therefore, enrolling dogs with idiopathic epilepsy at the first stages of clinical manifestation of the disease might have had an impact on the ability to detect white matter microstructural abnormalities, and eventually, long-term follow-up examinations could lead to different results.

Previously, inter-ictal brain diffusion in canine idiopathic epilepsy has been investigated with simple diffusion-weighted imaging and a ROI-based approach only. Gray and white matter ROIs have been investigated, but neither the corpus callosum nor the cingulate white matter were included (9). Increased ADC values in dogs with idiopathic epilepsy have been identified in the semioval center and the piriform lobe in this study (9). In contrast to this former study, with our ROI-based approach, we have focused on the white matter structures most commonly involved in human epilepsy (corpus callosum and cingulate white matter). Additionally, we have performed a voxel-based whole-brain approach, which did not depict increased MD in the semioval center or in the piriform lobe.

A more recent retrospective multicentric study focused on peri-ictal imaging findings and found mixed ADC results, including normal, increased, and decreased diffusivity in affected areas (32). The cingulate gyrus was affected in 6/19 cases and had either decreased ADC values in the cortex and increased ADC values in the white matter, or increased ADC values in the white matter only (32). The cingulate gyrus was commonly affected by peri-ictal imaging changes, which supports the cingulate gyrus as a target area in dogs with idiopathic epilepsy. However, in our study, we investigated MD as a measure for overall diffusion and could not detect any significant difference in the MD, but significantly reduced FA in dogs with idiopathic epilepsy compared to healthy

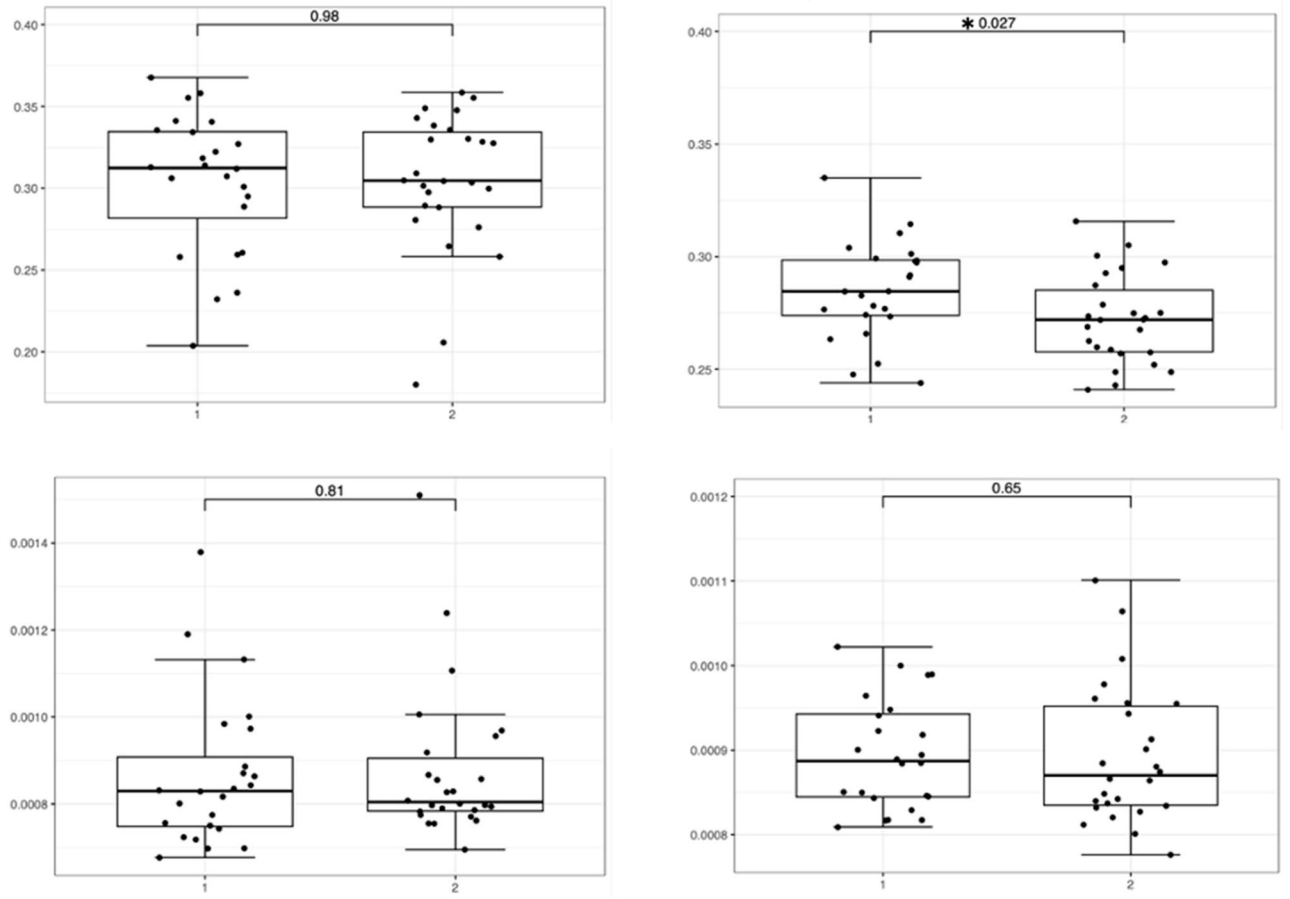

FIGURE 3
Boxplots featuring bilateral FA and MD differences in the corpus callosum and cingulate white matter with significance levels highlighted with an asterisk featuring the relevant *p*-value. The boxes on the **left side** represent the healthy controls (1), and the boxes on the **right side** (2) represent dogs with idiopathic epilepsy.

controls in the cingulate white matter. While both studies suggest the cingulate white matter as a target structure in canine idiopathic epilepsy, the microstructural changes might differ inter-ictally and peri-ictally and longitudinal studies including peri-ictal and inter-ictal time points could give insights into the time course of such changes.

The pathophysiology of white matter changes and its correlation with DTI changes in epilepsy is not well understood. It is still unknown whether the identified white matter abnormalities predate the development of epilepsy or whether they are a secondary effect of ongoing seizures (5). No histological examination was performed to look for a correlation between the reduced FA and possible histological changes in the brains of the dogs with idiopathic epilepsy included in our study. However, various mechanisms have been suggested, including changes related to the underlying epileptogenic process, axonal degeneration, and compensatory white matter reorganization (31, 33). Correlation between histopathological changes and DTI changes in epilepsy is sparse and is derived from rat models and surgically removed brain tissue in humans (34, 35). In the rat model of status epilepticus, myelin staining was reduced in the fimbria of the fornix in correlation with reduced FA 8 weeks after induced status epilepticus (34). In humans with temporal lobe epilepsy, increased extra-axonal fraction, and reduced cumulative axonal membrane circumference and myelin area were found in the surgically extracted fimbria of the fornix (35). Studies investigating histopathological changes in canine epilepsy are sparse (36). In contrast to humans, there is less evidence of temporal lobe involvement in dogs (36). Similar to humans with epilepsy originating from the limbic system, neuronal loss and gliosis were found in the limbic system, including the cingulate gyrus, amygdaloid nucleus, dorsal and ventral parts of the hippocampus, and dorsomedial nucleus of the thalamus in an epileptic Shetland Sheepdog family (37, 38). Involvement of the cingulate cortex would make an effect on the cingulate white matter a reasonable possibility. In contrast, Buckmaster et al. failed to identify any neuropathological changes in the temporal lobe of dogs with medically intractable epilepsy (39). In addition, guidelines for pathological examination of epileptic canine brains have been redefined (40); large studies reporting pathological abnormalities are still lacking.

We investigated idiopathic epilepsy in Border Collies and Greater Swiss Mountain dogs, two dog breeds with a suspected genetic background for epilepsy (41–43). Over the last decade,

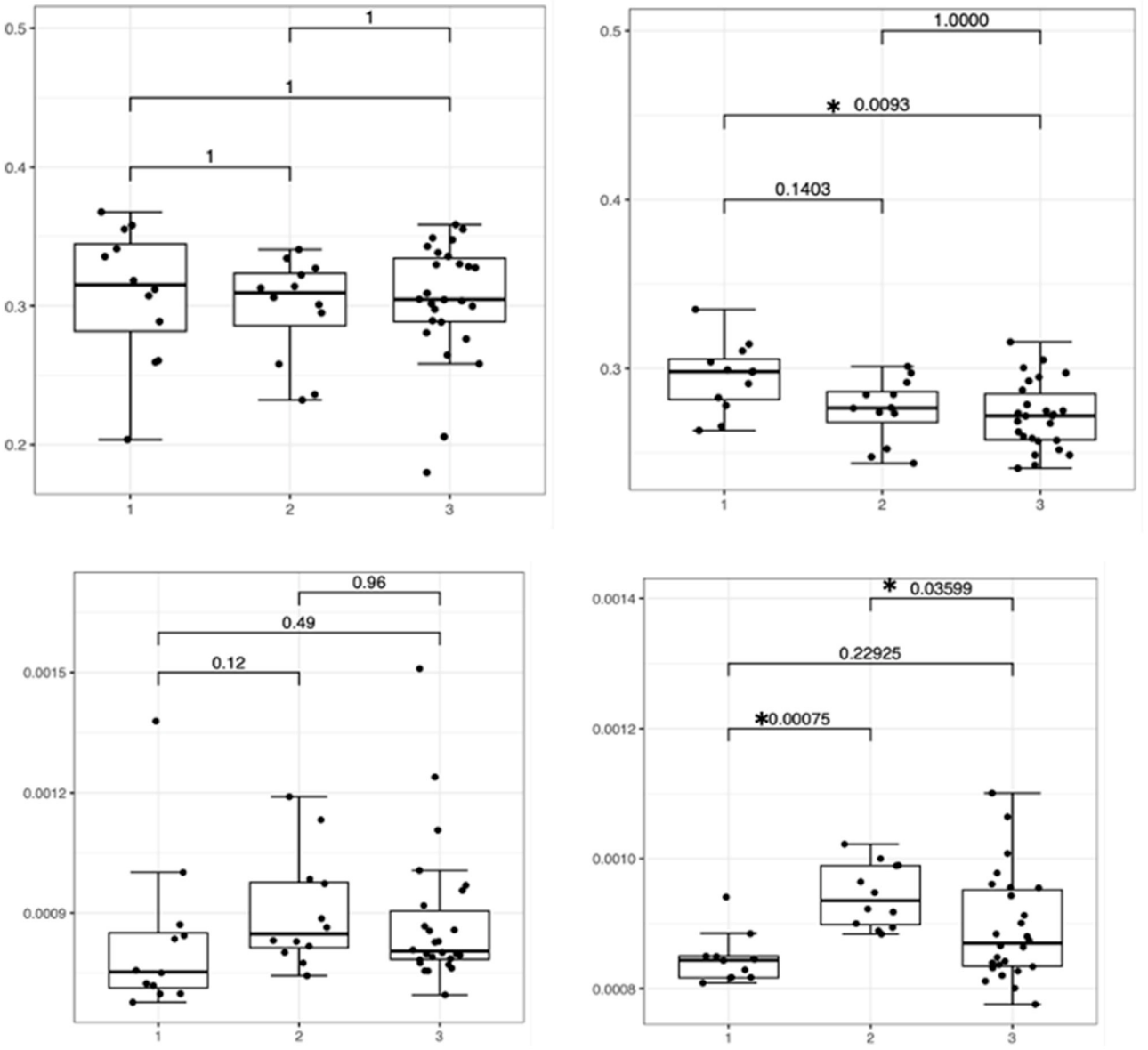

FIGURE 4
Boxplots featuring bilateral FA and MD differences in the corpus callosum and cingulate white matter with significance levels highlighted with an asterisk featuring the relevant *p*-value. Boxes on the **left side** indicate healthy controls with no familiar history of epilepsy (1), boxes in the **middle** indicate healthy controls with a first-degree relative with idiopathic epilepsy (2), and boxes on the **right side** indicate dogs with idiopathic epilepsy (3).

idiopathic epilepsy with a proven or suspected genetic background has been reported for a number of dog breeds with most studies focusing on clinical characteristics and genetic aspects. Nevertheless, most studies have not yet identified causative gene mutations, suggesting that inheritance may be complex (44). We have chosen Border Collies and Greater Swiss Mountain dogs because of their severe form of epilepsy and because these are commonly affected breeds in the author's institution. Choosing dog breeds with well-known epilepsy offered the advantage of more narrowly defined, more similar seizure phenotypes. Furthermore, the true prevalence of epilepsy in these breeds is currently unknown, but based on the literature, it is assumed that it is rather high (42–44). In pursuit of generating comparable data from groups of animals as homogeneous as possible, healthy first-degree relatives from the affected dogs with idiopathic epilepsy were recruited. What seemed to be an advantage when we designed the study might have had a negative impact on our results. Of the healthy Border Collies and Greater Swiss Mountain dogs included in our study, all but one had a first-degree relative with idiopathic epilepsy. In humans, heritability of the white matter microstructure has been demonstrated (45, 46), and in patients with MRI-negative temporal lobe epilepsy, an increase in MD has been identified even in asymptomatic siblings (47). Increased MD was also found in the healthy control dogs with a first-degree relative with idiopathic epilepsy compared to healthy controls without a first-degree relative with idiopathic epilepsy (Figure 4). It

is therefore possible that in close relatives of dogs with suspected genetic idiopathic epilepsy, white matter could be compromised even in unaffected animals. Unfortunately, all but one healthy control dog without a first-degree relative with idiopathic epilepsy were from a different breed (Beagle dogs), and to test the concept of hereditary white matter changes, we would have needed more dogs of the same breed without a family history of epilepsy. Furthermore, the high number of close relatives included in our study may have hidden differences in MD between dogs with idiopathic epilepsy and healthy controls because of heritable white matter changes. Such heritable white matter changes could even turn out to be diffusion-based endophenotypes for epilepsy in dogs. Such diffusion-based endophenotypes might support an imaging-based diagnosis for genetic epilepsy in the future (47).

4.1 Limitations

One of the strongest limitations of our study is the heterogenicity of the study population. We were not able to recruit a control group with the same age and gender profile as the idiopathic epilepsy group. The median age in the control group was almost twice as high as in the idiopathic epilepsy group. Barry et al. have shown significant differences in FA and MD between dogs of <7 years and dogs of >10 years of age (10). We did not include dogs older than 10 years of age, but we cannot rule out that the different ages in both groups had an influence on the results. The gender ratio was reversed between the two groups. The idiopathic epilepsy group included mainly male dogs, while the control group included more females than males. The influence of sex on the microstructure has been proven in humans; for example, one study has shown increased FA in male participants compared to female participants in all subregions of the corpus callosum (48). Such gender-related differences could mask differences due to illness as there was a higher percentage of male dogs in the idiopathic epilepsy group compared to the control group.

We also have different breed distributions in both groups, but to date, it is not known whether there is any regional difference between FA and MD in different dog breeds.

In humans, countless DTI studies have been conducted over the last decade, and post-processing has evolved massively. Well-tested and adapted pipelines exist. In contrast, in veterinary medicine, an adapted version of the TBSS pipeline has just recently been published (10), and although we followed this pipeline in the main, we had to do without the distortion correction due to our imaging acquisition. This might be of even more compromise in dogs than in humans. Dogs have larger frontal sinuses compared to humans, which can cause problems in susceptibility-sensitive sequences (49). In DTI post-processing, it is possible to account for these susceptibility-induced field distortions (50, 51). Unfortunately, the data in our study were acquired with one B0 image only, and at least two B0 images with opposite phase encoding directions are needed for field estimation (50). Therefore, no correction for susceptibility-induced distortions was performed, and diffusion images were displayed with geometric mismatches compared to the structural images. We cannot rule out that the different degrees of distortion in the individual images potentially influenced our results.

5 Conclusion

We aimed to investigate white matter diffusion changes in dogs affected by idiopathic epilepsy with generalized tonic-clonic seizures. We observed subtle changes in DTI between dogs with idiopathic epilepsy and healthy controls limited to cingulate white matter, with a significantly lower FA in dogs with idiopathic epilepsy compared to healthy controls using a ROI approach. No significant changes were found between dogs with idiopathic epilepsy and healthy controls in the TBSS analysis and in the corpus callosum in the ROI approach between both groups. This study supports the cingulate area as a target structure in canine epilepsy. The subtle changes only might be explained by the small sample size and the higher variability in canine brain anatomy. Furthermore, all included dogs showed generalized tonic-clonic seizures, possibly suffering from generalized epilepsy syndrome, which is also associated with less pronounced DTI changes in humans than focal epilepsy syndromes.

Data availability statement

The raw data supporting the conclusions of this article will be made available by the authors, without undue reservation.

Ethics statement

The animal studies were approved by Swiss Federal Veterinary Office Zurich. The studies were conducted in accordance with the local legislation and institutional requirements. Written informed consent was obtained from the owners for the participation of their animals in this study.

Author contributions

KB: Conceptualization, Data curation, Formal analysis, Funding acquisition, Investigation, Methodology, Project administration, Resources, Validation, Visualization, Writing—original draft, Writing—review & editing. AW-L: Methodology, Writing—review & editing, Writing—original draft. FS: Writing—review & editing. HR: Formal analysis, Project administration, Writing—review & editing. MD: Writing—review & editing. RB: Writing—review & editing. IC: Conceptualization, Methodology, Writing—review & editing. SH: Conceptualization, Investigation, Methodology, Supervision, Writing—review & editing.

Funding

The author(s) declare financial support was received for the research, authorship, and/or publication of this article. This research was partially financially supported by the Albert-Heim-Stiftung and the Stiftung für Kleintiere der Vetsuisse-Fakultät Universität Zürich.

Acknowledgments

Preliminary data of these studies were presented at the 35th ECVN Symposium 2023 in Venice by KB. We are grateful for the support of our colleagues from the Department of Neurology and the Clinic for Diagnostic Imaging from the Vetsuisse Faculty Zurich. We also must thank Manuela Wieser (Section of Anesthesiology, Vetsuisse Faculty Zurich) for her assistance in the conduction of the study. We would also like to thank Jeanne Peter (Vetcom team, Vetsuisse Faculty, University of Zurich) for creating Figure 1.

Conflict of interest

IC was employed at Vet Oracle Teleradiology.

The remaining authors declare that the research was conducted in the absence of any commercial or financial relationships that could be construed as a potential conflict of interest.

The author(s) declared that they were an editorial board member of Frontiers, at the time of submission. This had no impact on the peer review process and the final decision.

Publisher's note

Supplementary material

The Supplementary Material for this article can be found online at: https://www.frontiersin.org/articles/10.3389/fvets.2023.1325521/full#supplementary-material

SUPPLEMENTARY FIGURE 1
Sagittal, dorsal, and transverse views of the delineation of the cingulate ROI (blue) overlayed on the average white matter mask (green) over sample FA template.

SUPPLEMENTARY FIGURE 2
Sagittal, dorsal, and transverse views of the delineation of the corpus callosum ROI (purple) overlayed on the average white matter mask (green) over sample FA template.

References

1. De Risio L, Bhatti S, Munana K, Penderis J, Stein V, Tipold A, et al. International veterinary epilepsy task force consensus proposal: diagnostic approach to epilepsy in dogs. *BMC Vet Res.* (2015) 11:148. doi: 10.1186/s12917-015-0462-1

2. Rusbridge C, Long S, Jovanovik J, Milne M, Berendt M, Bhatti SF, et al. International Veterinary Epilepsy Task Force recommendations for a veterinary epilepsy-specific MRI protocol. *BMC Vet Res.* (2015) 11:194. doi: 10.1186/s12917-015-0466-x

3. Kramer MA, Cash SS. Epilepsy as a disorder of cortical network organization. *Neuroscientist.* (2012) 18:360–72. doi: 10.1177/1073858411422754

4. Berg AT, Berkovic SF, Brodie MJ, Buchhalter J, Cross JH, van Emde Boas W, et al. Revised terminology and concepts for organization of seizures and epilepsies: report of the ILAE Commission on Classification and Terminology, 2005-2009. *Epilepsia.* (2010) 51:676–85. doi: 10.1111/j.1528-1167.2010.02522.x

5. Hatton SN, Huynh KH, Bonilha L, Abela E, Alhusaini S, Altmann A, et al. White matter abnormalities across different epilepsy syndromes in adults: an ENIGMA-Epilepsy study. *Brain.* (2020) 143:2454–73. doi: 10.1093/brain/awaa200

6. Beaulieu C. The basis of anisotropic water diffusion in the nervous system - a technical review. *NMR Biomed.* (2002) 15:435–55. doi: 10.1002/nbm.782

7. O'Donnell LJ, Westin C-F. An introduction to diffusion tensor image analysis. *Neurosurg Clin N Am.* (2011) 22:185–96. doi: 10.1016/j.nec.2010.12.004

8. Pierpaoli C, Jezzard P, Basser PJ, Barnett A, Di Chiro G. Diffusion tensor MR imaging of the human brain. *Radiology.* (1996) 201:637–48. doi: 10.1148/radiology.201.3.8939209

9. Hartmann A, Sager S, Failing K, Sparenberg M, Schmidt MJ. Diffusion-weighted imaging of the brains of dogs with idiopathic epilepsy. *BMC Vet Res.* (2017) 13:338. doi: 10.1186/s12917-017-1268-0

10. Barry EF, Loftus JP, Luh WM, de Leon MJ, Niogi SN, Johnson PJ. Diffusion tensor-based analysis of white matter in the healthy aging canine brain. *Neurobiol Aging.* (2021) 105:129–36. doi: 10.1016/j.neurobiolaging.2021.04.021

11. Li JY, Middleton DM, Chen S, White L, Corado CR, Vite C, et al. Quantitative DTI metrics in a canine model of Krabbe disease: comparisons versus age-matched controls across multiple ages. *Neuroradiol J.* (2018) 31:168–76. doi: 10.1177/1971400917733431

12. Ogata N, Gillis TE, Liu X, Cunningham SM, Lowen SB, Adams BL, et al. Brain structural abnormalities in Doberman pinschers with canine compulsive disorder. *Prog Neuropsychopharmacol Biol Psychiatry.* (2013) 45:1–6. doi: 10.1016/j.pnpbp.2013.04.002

13. Hasegawa D, Saito M, Kitagawa M. Neurosurgery in canine epilepsy. *Vet J.* (2022) 285:105852. doi: 10.1016/j.tvjl.2022.105852

14. Nowakowska M, Üçal M, Charalambous M, Bhatti SFM, Denison T, Meller S, et al. Neurostimulation as a method of treatment and a preventive measure in canine drug-resistant Epilepsy: current state and future prospects. *Front Veter Sci.* (2022) 9:889561. doi: 10.3389/fvets.2022.889561

15. Berendt M, Farquhar RG, Mandigers PJ, Pakozdy A, Bhatti SF, De Risio L, et al. International veterinary epilepsy task force consensus report on epilepsy definition, classification and terminology in companion animals. *BMC Vet Res.* (2015) 11:182. doi: 10.1186/s12917-015-0461-2

16. Beckmann KM, Wang-Leandro A, Dennler M, Carrera I, Richter H, Bektas RN, et al. Resting state networks of the canine brain under sevoflurane anaesthesia. *PLoS ONE.* (2020) 15:e0231955. doi: 10.1371/journal.pone.0231955

17. Beckmann KM, Wang-Leandro A, Richter H, Bektas RN, Steffen F, Dennler M, et al. Increased resting state connectivity in the anterior default mode network of idiopathic epileptic dogs. *Sci Rep.* (2021) 11:23854. doi: 10.1038/s41598-021-03349-x

18. Mauri N, Richter H, Steffen F, Zölch N, Beckmann KM. Single-voxel proton magnetic resonance spectroscopy of the thalamus in idiopathic epileptic dogs and in healthy control dogs. *Front Vet Sci.* (2022) 9:885044. doi: 10.3389/fvets.2022.885044

19. Wieser M, Beckmann KM, Kutter APN, Mauri N, Richter H, Zölch N, et al. Ketamine administration in idiopathic epileptic and healthy control dogs: can we detect differences in brain metabolite response with spectroscopy? *Front Veter Sci.* (2023) 9:1093267. doi: 10.3389/fvets.2022.1093267

20. Saksena S, Husain N, Malik GK, Trivedi R, Sarma M, Rathore RS, et al. Comparative evaluation of the cerebral and cerebellar white matter development in pediatric age group using quantitative diffusion tensor imaging. *Cerebellum.* (2008) 7:392–400. doi: 10.1007/s12311-008-0041-0

21. Jbabdi S, Behrens TEJ, Smith SM. Crossing fibres in tract-based spatial statistics. *Neuroimage.* (2010) 49:249–56. doi: 10.1016/j.neuroimage.2009.08.039

22. Smith SM, Jenkinson M, Johansen-Berg H, Rueckert D, Nichols TE, Mackay CE, et al. Tract-based spatial statistics: voxelwise analysis of multi-subject diffusion data. *Neuroimage.* (2006) 31:1487–505. doi: 10.1016/j.neuroimage.2006.02.024

23. Andersson JLR, Jenkinson M, Smith S. Non-linear registration, aka Spatial normalisation. In: *FMRIB* technical report TR07JA2 (2007).

24. Jenkinson M, Beckmann CF, Behrens TE, Woolrich MW, Smith SM. Fsl. *Neuroimage.* (2012) 62:782–90. doi: 10.1016/j.neuroimage.2011.09.015

25. Salimi-Khorshidi G, Smith SM, Nichols TE. Adjusting the effect of nonstationarity in cluster-based and TFCE inference. *Neuroimage.* (2011) 54:2006–19. doi: 10.1016/j.neuroimage.2010.09.088

26. Smith SM, Nichols TE. Threshold-free cluster enhancement: addressing problems of smoothing, threshold dependence and localisation in cluster

inference. *Neuroimage.* (2009) 44:83–98. doi: 10.1016/j.neuroimage.2008.03.061

27. Winkler AM, Ridgway GR, Webster MA, Smith SM, Nichols TE. Permutation inference for the general linear model. *Neuroimage.* (2014) 92:381–97. doi: 10.1016/j.neuroimage.2014.01.060

28. A Language and Environment for Statistical Computing. *R Foundation for Statistical Computing* Available online at: https://www.R-project.org/ (accessed July 20, 2023).

29. Snook L, Plewes C, Beaulieu C. Voxel based versus region of interest analysis in diffusion tensor imaging of neurodevelopment. *Neuroimage.* (2007) 34:243–52. doi: 10.1016/j.neuroimage.2006.07.021

30. Slinger G, Sinke MR, Braun KP, Otte WM. White matter abnormalities at a regional and voxel level in focal and generalized epilepsy: a systematic review and meta-analysis. *Neuroimage Clin.* (2016) 12:902–9. doi: 10.1016/j.nicl.2016.10.025

31. Otte WM, van Eijsden P, Sander JW, Duncan JS, Dijkhuizen RM, Braun KP, et al. A meta-analysis of white matter changes in temporal lobe epilepsy as studied with diffusion tensor imaging. *Epilepsia.* (2012) 53:659–67. doi: 10.1111/j.1528-1167.2012.03426.x

32. Nagendran A, McConnell JF, De Risio L, José-López R, Quintana RG, Robinson K, et al. Peri-ictal magnetic resonance imaging characteristics in dogs with suspected idiopathic epilepsy. *J Veter Internal Med.* (2021) 35:1008–17. doi: 10.1111/jvim.16058

33. Gross DW, Concha L, Beaulieu C. Extratemporal white matter abnormalities in mesial temporal lobe epilepsy demonstrated with diffusion tensor imaging. *Epilepsia.* (2006) 47:1360–3. doi: 10.1111/j.1528-1167.2006.00603.x

34. van Eijsden P, Otte WM, van der Hel WS, van Nieuwenhuizen O, Dijkhuizen RM, de Graaf RA, et al. In vivo diffusion tensor imaging and ex vivo histologic characterization of white matter pathology in a post-status epilepticus model of temporal lobe epilepsy. *Epilepsia.* (2011) 52:841–5. doi: 10.1111/j.1528-1167.2011.02991.x

35. Concha L, Livy DJ, Beaulieu C, Wheatley BM, Gross DW. Diffusion tensor imaging and histopathology of the fimbria-fornix in temporal lobe Epilepsy. *J Neurosci.* (2010) 30:996–1002. doi: 10.1523/JNEUROSCI.1619-09.2010

36. Löscher W. Dogs as a natural animal model of Epilepsy. *Front Veter Sci.* (2022) 9:928009. doi: 10.3389/fvets.2022.928009

37. Yamasaki H, Furuoka H, Takechi M, Itakura C. Neuronal loss and gliosis in limbic system in an epileptic dog. *Vet Pathol.* (1991) 28:540–2. doi: 10.1177/030098589102800614

38. Morita T, Shimada A, Takeuchi T, Hikasa Y, Sawada M, Ohiwa S, et al. Cliniconeuropathologic findings of familial frontal lobe epilepsy in Shetland sheepdogs. *Can J Vet Res.* (2002) 66:35–41.

39. Buckmaster PS, Smith MO, Buckmaster CL, LeCouteur RA, Dudek FE. Absence of temporal lobe epilepsy pathology in dogs with medically intractable Epilepsy. *J Veter Internal Med.* (2002) 16:95–9. doi: 10.1111/j.1939-1676.2002.tb01612.x

40. Matiasek K, Pumarola IBM, Rosati M, Fernandez-Flores F, Fischer A, Wagner E, et al. International veterinary epilepsy task force recommendations for systematic sampling and processing of brains from epileptic dogs and cats. *BMC Vet Res.* (2015) 11:216. doi: 10.1186/s12917-015-0467-9

41. Hulsmeyer V, Zimmermann R, Brauer C, Sauter-Louis C, Fischer A. Epilepsy in Border Collies: clinical manifestation, outcome, and mode of inheritance. *J Veter Internal Med.* (2010) 24:171–8. doi: 10.1111/j.1939-1676.2009.0438.x

42. Sauer-Delhées S, Steffen F, Reichler I, Beckmann K. Clinical characteristics of Idiopathic Epilepsy in greater Swiss mountain dogs in Switzerland. *Schweiz Arch Tierheilkd.* (2020) 162:697–706. doi: 10.17236/sat00279

43. Ostermann TE, Nessler JN, Urankar H, Bachmann N, Fechler C, Bathen-Nöthen A, et al. Phenotype of idiopathic epilepsy in great swiss mountain dogs in germany—a retrospective study. *Front Veter Sci.* (2022) 9:921134. doi: 10.3389/fvets.2022.921134

44. Hulsmeyer VI, Fischer A, Mandigers PJ, DeRisio L, Berendt M, Rusbridge C, et al. International veterinary Epilepsy task force's current understanding of idiopathic epilepsy of genetic or suspected genetic origin in purebred dogs. *BMC Vet Res.* (2015) 11:175. doi: 10.1186/s12917-015-0463-0

45. Chiang MC, Barysheva M, Shattuck DW, Lee AD, Madsen SK, Avedissian C, et al. Genetics of brain fiber architecture and intellectual performance. *J Neurosci.* (2009) 29:2212–24. doi: 10.1523/JNEUROSCI.4184-08.2009

46. Kochunov P, Glahn DC, Lancaster JL, Winkler AM, Smith S, Thompson PM, et al. Genetics of microstructure of cerebral white matter using diffusion tensor imaging. *Neuroimage.* (2010) 53:1109–16. doi: 10.1016/j.neuroimage.2010.01.078

47. Whelan CD, Alhusaini S, O'Hanlon E, Cheung M, Iyer PM, Meaney JF, et al. White matter alterations in patients with MRI-negative temporal lobe epilepsy and their asymptomatic siblings. *Epilepsia.* (2015) 56:1551–61. doi: 10.1111/epi.13103

48. Menzler K, Belke M, Wehrmann E, Krakow K, Lengler U, Jansen A, et al. Men and women are different: diffusion tensor imaging reveals sexual dimorphism in the microstructure of the thalamus, corpus callosum and cingulum. *Neuroimage.* (2011) 54:2557–62. doi: 10.1016/j.neuroimage.2010.11.029

49. Wolfer N, Wang-Leandro A, Beckmann KM, Richter H, Dennler M. Intracranial lesion detection and artifact characterization: comparative study of susceptibility and T2(*)-weighted imaging in dogs and cats. *Front Veter Sci.* (2021) 8:779515. doi: 10.3389/fvets.2021.779515

50. Andersson JLR, Skare S, Ashburner J. How to correct susceptibility distortions in spin-echo echo-planar images: application to diffusion tensor imaging. *Neuroimage.* (2003) 20:870–88. doi: 10.1016/S1053-8119(03)00336-7

51. Smith SM, Jenkinson M, Woolrich MW, Beckmann CF, Behrens TE, Johansen-Berg H, et al. Advances in functional and structural MR image analysis and implementation as FSL. *Neuroimage.* (2004) 23:S208–219. doi: 10.1016/j.neuroimage.2004.07.051

frontiers | Frontiers in Veterinary Science

TYPE Original Research
PUBLISHED 23 January 2024
DOI 10.3389/fvets.2024.1346617

OPEN ACCESS

EDITED BY
Angela Marolf,
The Ohio State University, United States

REVIEWED BY
Marco Bernardini,
University of Padua, Italy
Sam Long,
Veterinary Referral Hospital, Australia

*CORRESPONDENCE
Silke Hecht
✉ shecht@utk.edu

RECEIVED 29 November 2023
ACCEPTED 11 January 2024
PUBLISHED 23 January 2024

CITATION
Simon H, Hecht S, Fazio C and Sun X (2024) Magnetic resonance imaging subtraction vs. pre- and post-contrast 3D gradient recalled echo fat suppressed imaging for evaluation of the canine and feline brain.
Front. Vet. Sci. 11:1346617.
doi: 10.3389/fvets.2024.1346617

Magnetic resonance imaging subtraction vs. pre- and post-contrast 3D gradient recalled echo fat suppressed imaging for evaluation of the canine and feline brain

Heather Simon[1], Silke Hecht[1]*, Constance Fazio[1] and Xiaocun Sun[2]

[1]Department of Small Animal Clinical Sciences, University of Tennessee College of Veterinary Medicine, Knoxville, TN, United States, [2]Office of Information Technology, University of Tennessee, Knoxville, TN, United States

Subtraction magnetic resonance imaging (MRI) has been reported to increase accuracy in the diagnosis of meningeal and inflammatory brain diseases in small animals. 3D T1W gradient recalled echo (GRE) techniques have been proposed as a suitable alternative to conventional spin echo sequences in imaging the canine brain. The aim of this study was to compare subtraction images and paired pre- and post-contrast 3D T1W GRE fat suppressed (FS) images in canine and feline MRI studies using clinical diagnosis as the gold standard. Paired pre- and post-contrast T1W 3D FS GRE images and individual subtraction images of 100 small animal patients were randomized and independently evaluated by 2 blinded observers. Diagnosis categories were "normal," "inflammatory," "neoplastic," and "other." Clinical diagnosis was made in the same categories and served as the gold standard. Image interpretation results were compared to the clinical diagnosis. Interobserver agreement was determined. Clinically, 41 studies were categorized as "normal," 18 as "inflammatory," 28 as "neoplastic," and 13 as "other." The agreement of the pre- and post-contrast GRE images with the gold standard was significantly higher than that of the subtraction images ($k = 0.7491$ vs. $k = 0.5924$; $p = 0.0075$). The largest sources of error were misinterpretation of "other" as "normal" and "normal" as "inflammatory." There was no significant difference between the two observers ($p = 0.8820$). Based on this study, subtraction images do not provide an advantage to paired pre- and post-contrast FS GRE images when evaluating the canine and feline brain.

KEYWORDS

MRI, contrast medium, encephalopathy, dog, cat, central nervous system

1 Introduction

Due to the difficulty of obtaining histopathologic samples for the antemortem diagnosis of canine and feline brain disease, clinicians frequently combine signalment, clinical signs, advanced imaging findings, cerebrospinal fluid analysis results, and treatment response to formulate differential diagnoses and treatment plans. Heavy reliance is placed on non-invasive

measures such as magnetic resonance imaging (MRI) to obtain presumptive diagnoses. Previous studies have shown that MRI is highly sensitive and specific for inflammatory and neoplastic brain lesions in dogs and has high interobserver agreement (1–3).

Subtraction is a post processing procedure performed after MR images have been acquired and involves one image being digitally subtracted from another. This can be done for follow-up studies (e.g., subtracting images obtained at different points in time to assess for disease progression), or during the same scan (e.g., for improved visualization of contrast enhancing structures by subtracting pre- from post-contrast images). Most studies in subtraction techniques are reported in human neuroimaging. Applications include detection of multiple sclerosis plaques and evaluation of changes over time (4–7), evaluation of tumor growth in gliomas and prediction of cleavage planes in surgical resection of meningiomas (8, 9), detection of amyloid-related imaging abnormalities with edema in patients with Alzheimer's disease (10), evaluation of subtle changes in the brains of human infants and children (11), improved delineation of contrast-enhancing tumors adjacent to hemorrhagic lesions (12, 13), improved sensitivity for the detection of ischemic lesions in post-surgical cardiac patients undergoing brain MRI (14), and improved identification of subtle meningeal disease in people (15–17). Added advantages of using subtraction images may include a decrease in image reviewing time (4, 14), and a reduction of intravenous contrast medium dosages in people (18).

Studies on using subtraction techniques in veterinary MRI are limited to date. One study concluded that subtraction images increase the conspicuity of normal canine meninges (19). One case report describes subtraction images being used to differentiate chondroma and squamous cell carcinoma in two beagle dogs (20). Another study reports improved detection of meningeal, articular and muscular contrast enhancement in the spine of dogs afflicted with steroid responsive meningitis arteritis (21). Inflammatory brain diseases in dogs can have variable imaging manifestations including subtle meningeal changes. Granulomatous meningoencephalitis specifically has been likened to multiple sclerosis in people in its leptomeningeal pathophysiology (22). While subtraction images have proven helpful in people with meningeal lesions secondary to multiple sclerosis, reports in canine patients with inflammatory encephalopathies are conflicting. One study found that subtraction images were not superior to T1-weighted post contrast images and that, overall, MRI was poor at detecting meningeal pathology (23). A subsequent study compared subtraction images vs. pre- and post-gadolinium T1-weighted spin echo (SE) image pairs in dogs with intracranial inflammatory conditions. This study concluded that the subtraction images performed better than the pre- and post-contrast imaging pairs, primarily due to their ability to detect intra-axial lesions (24).

Three-dimensional T1-weighted gradient recalled echo (3D T1W GRE) sequences with fat suppression have recently gained popularity as an alternative to standard SE sequences and other techniques (25). Fat suppression alone can increase subtle lesion detection. In a study on meningeal enhancement in dogs, chemical fat suppression significantly increased detection of meningeal enhancement and was associated with the highest inter-observer agreement (26). An added advantage of 3D GRE sequences is their thin slice thickness and lack of an interslice gap. In one study, the 3D T1W GRE images (1 mm slice thickness) had superior anatomic detail when evaluating canine patients for facial nerve pathology compared to conventional T1W SE images (3–3.5 mm slice thickness) (27). In a human study, the same 3D T1W GRE technique, which does not have an inversion recovery pulse, had superior performance in detecting brain tumor enhancement when compared to the more traditional post-contrast inversion recovery fast GRE sequence (28). A canine study found that a 3D T1W GRE sequence is a suitable alternative to the more traditional two-dimensional T1W SE sequence for brain MRI (29).

The aim of this study was to compare subtraction images and paired pre- and post-contrast 3D T1W GRE fat suppressed (FS) images to the gold standard of clinical diagnosis in 100 canine and feline MRI studies. The secondary purpose was to assess inter-observer agreement for both techniques. The hypothesis was that there would be no difference in diagnostic yield and interobserver variability between subtraction images and paired pre- and post-contrast 3D T1W FS GRE images.

2 Materials and methods

2.1 Patients

A retrospective study was performed at The University of Tennessee College of Veterinary Medicine on 100 canine and feline patients receiving a brain MRI study. Medical records were reviewed by the first author (HS), a senior resident in veterinary neurology/neurosurgery. Medical record data recorded were age, gender, breed, weight, clinical history, clinical and neurologic examination findings, cerebrospinal fluid (CSF) analysis results, ancillary test findings, histopathology (if available), treatment response, and follow-up. All patients had current (within 1 month) blood analysis including complete blood count and serum chemistry and a complete neurologic exam within 24 h of imaging. Patients may or may not have had thoracic radiographs, cerebrospinal fluid (CSF) analysis, infectious disease titers, histopathology, or other additional testing. Inclusion criterion was availability of pre- and post-contrast T1W 3D FS GRE sequences and dynamic subtraction images of diagnostic quality. Diagnosis codes were designated for patients by the first author, using all available information (medical record data, clinical history, physical and neurologic examination findings, cerebrospinal fluid analysis results, ancillary test findings, imaging findings, treatment response, follow-up, and histopathology). Diagnosis codes were divided into four groups: 0 for normal, 1 for inflammatory disease, 2 for neoplasia, and 3 for other (any disease entity outside of these categories such as vascular, congenital, toxic/metabolic, etc.). The category of inflammatory disease included infectious and non-infectious causes. The neoplastic category included primary and metastatic disease.

2.2 Imaging protocol

MRI was performed using a 1.5 T MRI system (MAGNETOM Espree TM, Siemens Medical Solutions, Malvern, PA). All patients were anesthetized and positioned in dorsal recumbency. MRI protocols were tailored to individual patients and typically included the following sequences: Sagittal T2W SE; transverse T1W SE, T2W SE, T2*W GRE, T2W 3D TSE with variable flip angle (Sampling Perfection with Application optimized Contrasts using different flip angle Evolution; "SPACE"), T2W Fluid Attenuated Inversion Recovery

(FLAIR), Proton Density-W SE, and diffusion weighted imaging (DWI) with ADC map; transverse pre- and post-contrast 3D T1W gradient recalled echo (GRE) sequence with fat suppression (Volume Interpolated Body/Breath hold Examination; "VIBE") and subtraction; post contrast sagittal and transverse T1W SE; and post contrast dorsal T1W SE with fat saturation. Pre- and post-contrast 3D T1W GRE FS sequences were acquired with 1 mm slice thickness. Contrast medium was administered intravenously at 0.1 mmol/kg (Omniscan TM; Gadodiamide, GE Healthcare Inc., Marlborough, MA 01752, United States).

2.3 Image evaluation

Pre- and post-contrast T1W 3D FS GRE images and subtraction images were separately randomized and anonymized by the first author (HS) and were provided to each reviewer blinded to other imaging sequences and the clinical information. Two experienced board-certified veterinary radiologists (SH, CF) were separately provided with the subtraction images and the pre- and post-contrast T1W 3D FS GRE image pairs and asked to designate a diagnosis code of 0, 1, 2, or 3 (same categories as above) for each scan.

2.4 Statistical analysis

The statistical analysis was performed by a university employed statistician (XS). Chi square test and kappa coefficient test were performed to determine agreement between the subtraction images and the paired pre- and post-contrast T1W 3D FS GRE images, respectively, with the clinical diagnosis. Kappa statistics were also used to determine interobserver agreement. Statistical significance was set at $p < 0.05$. Analyses were conducted in SAS 9.4 TS1M6 for Windows 64× (SAS institute Inc., Cary, NC).

3 Results

To achieve the target of 100 patients to be included in the study, 117 MRI studies were reviewed. Seventeen cases were excluded due to inadequate quality of the subtraction images due to misregistration error (change in patient position between pre- and post-contrast images).

There were 9 cats and 91 dogs. Overall, there were 51 females (45 neutered) and 49 males (34 neutered). The cats were all domestic short hair. The canine breeds included were mixed breed dog ($n = 26$), Chihuahua ($n = 5$), Golden Retriever ($n = 4$), Boxer ($n = 4$), Corgi ($n = 3$), Labrador Retriever ($n = 3$), Australian Shepherd ($n = 3$), Shih Tzu ($n = 3$), Dachshund ($n = 3$), Pug ($n = 3$), English Bull Dog ($n = 2$), Yorkshire Terrier ($n = 2$), Cavalier King Charles Spaniel ($n = 2$), Havanese ($n = 2$), Boston Terrier ($n = 2$), Miniature Schnauzer ($n = 2$), and one each of the following: Australian Kelpie, Bassett Hound, Belgian Malinois, Blue Tick Hound, Border Collie, Cairn Terrier, Australian Cattle Dog, Cocker Spaniel, Coonhound, Dalmatian, French Bulldog, German Shepherd Dog, Otterhound, Maltese, Miniature Pinscher, Pitbull, Pomeranian, Rat Terrier, Rhodesian Ridgeback, German Shorthair Pointer, Staffordshire Terrier and Toy Poodle. Ages ranged from 3 months to 13 years.

Clinical diagnosis codes (gold standard) were as follows: 41/100 normal, 18/100 inflammatory, 28/100 neoplasia, and 13/100 other.

Of the patients in category "normal," the diagnoses were as follows: idiopathic/cryptogenic epilepsy ($n = 20$), idiopathic vestibular disease and/or facial nerve paralysis ($n = 8$), presumed primary cardiac or syncopal episodes ($n = 4$), primary behavioral abnormalities ($n = 2$), otitis media ($n = 2$), and one case each of primary ocular disease, canine cognitive dysfunction, tooth root abscess, portosystemic shunt, and intermittent apnea.

Of the patients in category "inflammatory," the diagnoses were as follows: meningoencephalitis of unknown etiology ($n = 15$), focal meningitis secondary to extension of otitis media/interna ($n = 2$), and idiopathic cerebellitis ($n = 1$).

Of the patients in category "neoplasia," the diagnoses were as follows: extra-axial tumor/presumptive meningioma ($n = 13$), intra-axial tumor/presumptive glioma ($n = 8$), aggressive nasal mass ($n = 2$), pituitary mass ($n = 2$), and one case each of choroid plexus tumor, trigeminal nerve sheath tumor, and infiltrative mass along the carotid artery.

Of the patients in category "other," the diagnoses were as follows: cerebrovascular accidents ($n = 5$), hydrocephalus ($n = 3$), cerebellar hypoplasia ($n = 2$), and one case each of metabolic/toxic bilaterally symmetric brain lesions, multiple skull fractures, and supracollicular fluid accumulation.

The agreement of the pre- and post-contrast T1W GRE images with the gold standard was significantly higher than that of the subtraction images ($k = 0.7491$ vs. $k = 0.5924$; $p = 0.0075$).

There was similar agreement between the pre- and post-contrast T1W GRE and the subtraction images with the clinical diagnosis in patients with intracranial neoplasia (88% vs. 88%; Figure 1). The largest discrepancies between agreement of pre- and post-contrast T1W GRE and subtraction images with the clinical diagnosis were misinterpretation of "other" as "normal" (65% vs. 23%; Figure 2) and "normal" as "inflammatory" (17% vs. 7%; Figure 3). There was no significant difference between the two observers ($p = 0.8820$). Details of the individual interpretation by the two readers can be found in Figures 4, 5 and Supplementary Figures S1–S4.

4 Discussion

With subtraction imaging, tissues that remain static between successive scans will null out, while tissues that have changed will be highlighted. When using subtraction for pre- and post-contrast images, contrast-enhancing tissues will be accentuated. Based on this study, MRI subtraction images did not provide an advantage to paired pre- and post-contrast GRE images when evaluating the canine and feline brain.

One major source of discrepancy between subtraction images and the gold standard was misinterpretation of "normal" studies as "inflammatory." This may be attributable to normal meningeal contrast enhancement being mistaken for pathology. It has been reported that the degree of meningeal enhancement in subtraction images of normal canine brains is greater than expected, and that some degree of enhancement in the pachymeninges and leptomeninges is physiologic due to their lack of a blood-brain-barrier (19). Another less likely explanation may have been instances of false positive identification of intra-axial lesions. 12% of dogs with

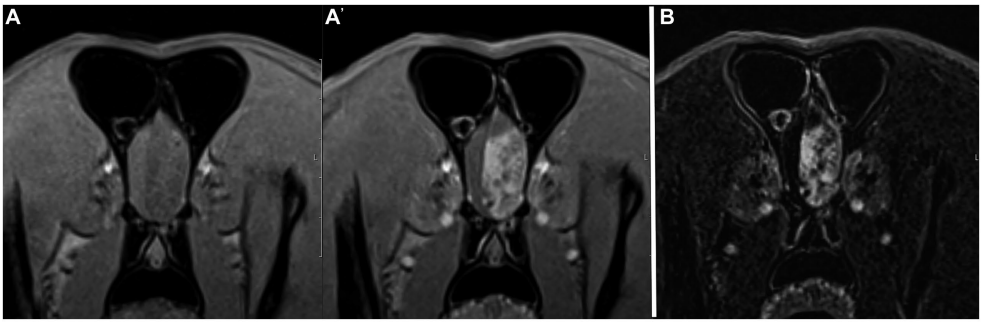

FIGURE 1
Example of good agreement of both the pre- and post-contrast T1W 3D FS GRE images **(A,A')** and the subtraction image **(B)** with the gold standard. This patient was diagnosed with an extra-axial brain tumor (meningioma, presumptive). Both reviewers made the correct diagnosis of "neoplasia" on both image sets. Note the large heterogeneously contrast enhancing mass in the left rostral cranial vault.

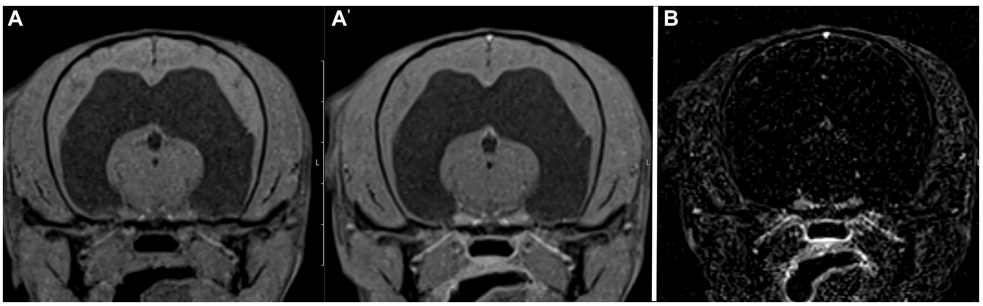

FIGURE 2
Example of good agreement of the pre- and post- contrast T1W 3D FS GRE images **(A,A')** but poor agreement of the subtraction image **(B)** with the gold standard. The pre- and post-contrast GRE images were correctly interpreted as "other" by both reviewers, while a false positive diagnosis of "normal" was made based on the subtraction image. This patient was diagnosed with a hydrocephalus, likely congenital.

idiopathic epilepsy had evidence of intra-axial enhancing lesions on subtraction images in a prior study, attributed to either false positive lesions or possibly representing true pathology (24). A third possibility for false positive results with subtraction images is artifact secondary to large slice thickness (10). However, we feel that this is less likely since our images were created with thin slices and no interslice gap. Finally, even though both radiologists involved in image interpretation in this study have experience in neuroimaging, they did not have enhanced training at interpretation of subtraction images which may have affected the results.

The other major source of error was misinterpretation of "other" as "normal." This can easily be explained by "other" lesions often being static/non-enhancing between scans (e.g., skull defects, intracranial fluid accumulations) and thus being nulled on subtraction images. While it is unlikely that these lesions would be missed in clinical practice where other sequences (e.g., T2-weighted images) are acquired in the frame of a complete brain MRI examination, it is important to recognize the limitations of subtraction images to identify non-contrast-enhancing lesions.

The major limitation of our study is the lack of a definitive diagnosis (histopathology) in most cases. Brain biopsies are not frequently performed in veterinary medicine due to their invasiveness, cost, and potential need for special navigational equipment. The diagnoses in our patient cohort were based on a combination of signalment, history, neurologic exam findings, imaging findings, results of further tests, and follow-up, similar to the methodology used in other studies (30, 31). MRI alone has a sensitivity and specificity of 94.4 and 95.5%, respectively, for the diagnosis of brain disease in dogs (1). The diagnosis of certain brain tumors (e.g., pituitary tumors, nerve sheath tumors, and meningiomas), congenital anomalies (e.g., hydrocephalus), and traumatic lesions can be made with fairly high confidence based on characteristic imaging features. Similarly, even though histopathology is the gold standard in the diagnosis of inflammatory brain lesions, a presumptive diagnosis of meningoencephalomyelitis of undetermined etiology can be made based on a combination of signalment, neurological examination results, magnetic resonance imaging (MRI) findings, cerebrospinal fluid analysis, and negative infectious disease testing results (32). Nevertheless, it is possible that isolated cases in our patient cohort may have been misclassified. In a previous report, 24% of dogs with inflammatory CSF had a normal MRI study (33). It is theoretically possible that some cases of inflammatory disease may have been missed. We believe that this possibility is low, since at our institution patients with a normal brain MR examination almost always have CSF analysis performed as an ancillary diagnostic test. Similarly, even though cerebrovascular lesions may resemble intra-axial brain tumors, diffusion-weighted imaging (DWI), apparent diffusion coefficient (ADC) map, and

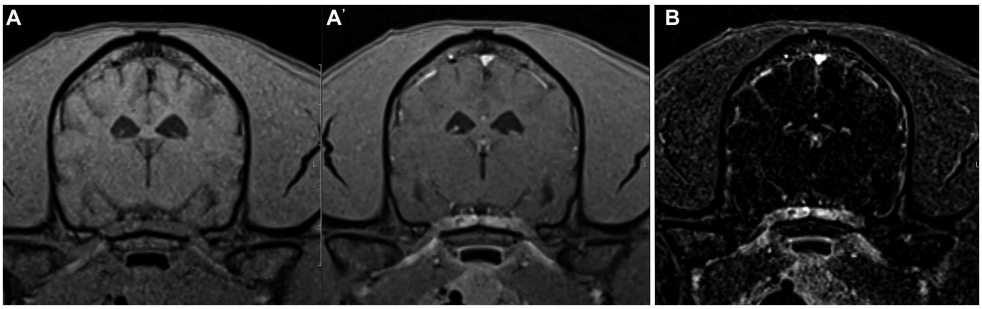

FIGURE 3
Example of good agreement of the pre- and post-contrast T1W 3D FS GRE images **(A,A')** but poor agreement of the subtraction image **(B)** with the gold standard. The pre- and post-contrast GE images were correctly interpreted as "normal" by both reviewers, while a false positive diagnosis of "inflammatory" was made based on the subtraction image which has evidence of meningeal contrast enhancement. This patient was diagnosed with idiopathic vestibular disease.

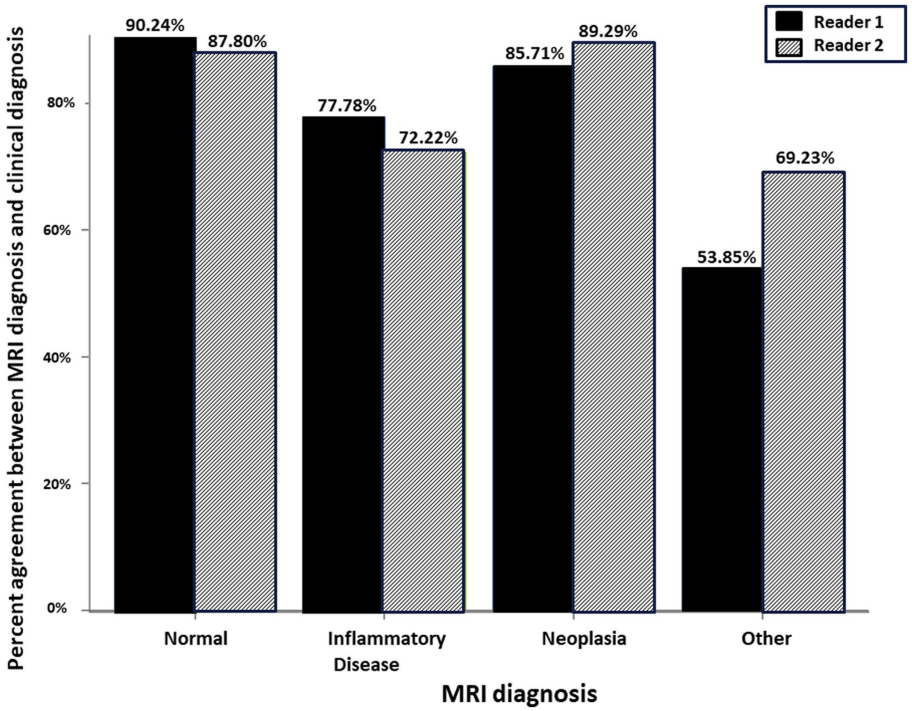

FIGURE 4
Schematic representation of the percent agreement between the MRI Diagnosis based on paired pre- and post-contrast T1W FS GRE and the gold standard clinical diagnosis. There was no significant difference between the two readers.

T2*W GRE sequence are included in our standard MRI brain protocol, increasing confidence in the diagnosis of ischemic and hemorrhagic intra-cranial events (34). Another study limitation is that there was no requirement to have patient follow-up for a specific length of time. It is possible that the clinical diagnosis may have been different for some cases if extended follow-up had been available.

In previous studies that included histopathology, there may have been a bias for patients that had more severe disease and had to be euthanized or died. Without the inclusion criterion of histopathology, our study cohort was more representative of the spectrum of encephalopathies and of the caseload routinely imaged. Furthermore, since the categories were kept broad (i.e., radiologists did not have to specify the tumor type in the "neoplasia" category or the type of brain disease in the "other" category), this allowed for simplified categorization, decreased the number of variables, and helped keep the numbers in each category amenable to statistical analysis. In previous studies where radiologists were asked to interpret brain MRI studies in dogs, they may not have agreed with specific imaging features, however, they satisfactorily agreed on the category of brain disease (3).

Our study included both dogs and cats. It is difficult to draw specific conclusions for cats given their small number in our patient cohort. However, we felt that including all patients as they presented

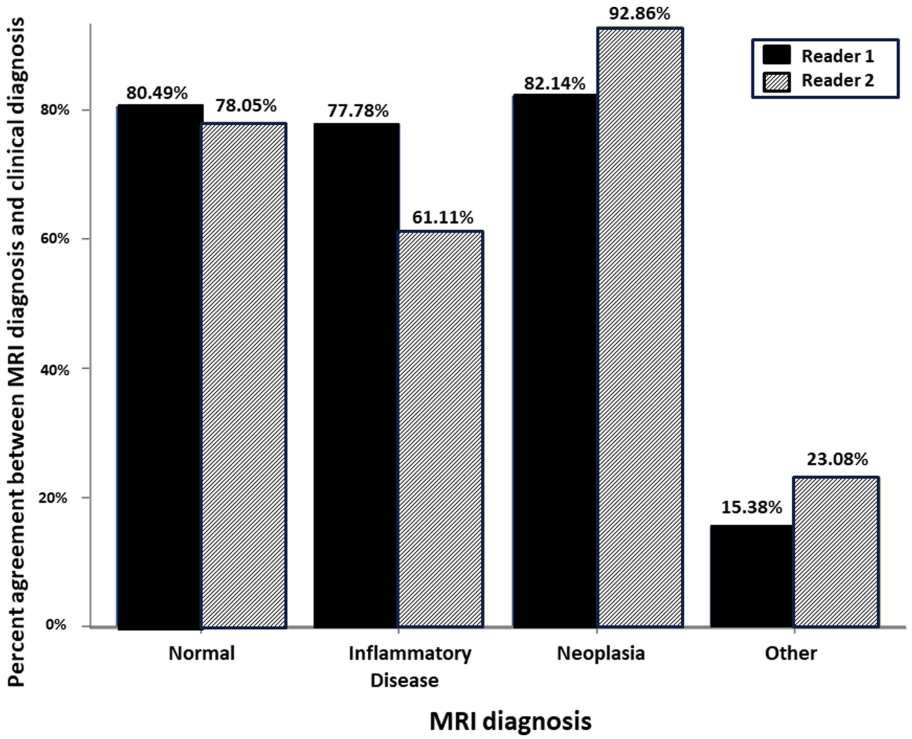

FIGURE 5
Schematic representation of the percent agreement between the MRI Diagnosis based on subtraction MR image and the gold standard clinical diagnosis. There was no significant difference between the two readers.

to the hospital for advanced imaging was a better representation of the natural population without bias.

Another possible source of bias may have been if the attending radiologist at the time of study interpretation would have had access to one of the MRI techniques under investigation (e.g., pre- and post-contrast T1W GRE images) but not the other (e.g., subtraction images), and that thus one of the two actors might have contributed more than the other to the MRI diagnosis and ultimately clinical diagnosis. We believe that this was not a significant factor in our study. Subtraction images were generated by the MRI technologist on the MRI scanning platform while the study was ongoing, and were sent to the reading platform (PACS) at the same time as the post contrast T1-W GRE images. The attending radiologist therefore had access to both and was free to base his/her interpretation on the study sequences and/or the standard pre- and post-contrast spin echo sequences also acquired in all cases.

One last limitation is that the two readers in our study were from the same institution where the MRI studies were originally acquired. A total of eight radiology residents and radiologists share the responsibility for clinical MRI case interpretation at our institution. It cannot be entirely excluded that there may have been isolated cases of re-call bias if a reader was asked to interpret an MRI study of a patient they may have previously seen while on clinical duty. However, we believe that this is negligible as the readers were blinded to patient identity, clinical findings, and other MRI sequences, as the images were randomized, and as there was a time gap of multiple months between presentation of a given patient to the hospital and the image evaluation.

Previous studies investigating the use of subtraction images in the evaluation of canine CNS disease were focused on inflammatory diseases and yielded conflicting results. One study found that subtraction images did not have advantages over T1W post contrast images and that, overall, MRI was poor at detecting meningeal pathology (23). Another study comparing subtraction images vs. pre- and post-gadolinium T1W spin echo (SE) image pairs concluded that the subtraction images performed better than the pre- and post-contrast imaging pairs (24). A possible explanation is that fat within the calvarium is hyperintense on standard SE sequences, which may mimic or obscure adjacent contrast enhancement. Subtraction imaging not only highlights contrast enhancing tissues in these cases, it also results in effective suppression of non-contrast-enhancing fat similar to the effect of chemical fat saturation. Chemical fat suppression resulted in significantly increased detection of meningeal enhancement in a previous study in dogs (26). The GRE sequence used in our study already included fat suppression, possibly negating this positive effect of subtraction images. One study evaluating the utility of MRI in the assessment of dogs with steroid responsive meningitis arteritis found improved depiction of meningeal contrast enhancement in the spine when using subtraction techniques, attributed to effective suppression of non-contrast-enhancing spinal epidural fat similar to the effect of chemical fat saturation (21). The same study found increased conspicuity of contrast enhancement associated with the articular facet joints and paraspinal musculature in some cases. Our study was focused on intracranial pathology only, and, unlike prior studies, included non-inflammatory encephalopathies. MRI subtraction images did not provide an advantage to paired pre- and post-contrast FS GRE images.

Misinterpretation of "other" encephalopathies as "normal" is unlikely to represent a clinical problem as those diseases are likely going to be identified on other MRI sequences. However, misinterpretation of physiologic meningeal enhancement as abnormal, yielding an erroneous diagnosis of meningitis and inflammatory brain disease, represents a clinical pitfall.

This study leaves room for future investigation. In clinical practice, presence or absence of contrast enhancement would likely not be assessed by choosing pre- and post-contrast images or subtraction images in isolation, but would most likely being done by evaluating both in conjunction with other sequences. Providing reviewers with pre- and post-contrast image pairs first, and with pre-and post-contrast image pairs along with subtraction images later, may provide interesting insight if subtraction imaging provides meaningful additional information to the interpretation of T1W images alone.

5 Conclusion

Based on this study, subtraction images do not provide an advantage to paired pre- and post-contrast T1W FS GRE images when evaluating the canine and feline brain. The study results may not apply to instances where fat suppressed images are not available, when evaluating for concurrent extracranial abnormalities (e.g., muscle lesions), and when evaluating the canine and feline spine.

Data availability statement

The raw data supporting the conclusions of this article will be made available by the authors, without undue reservation.

Ethics statement

Ethical approval was not required for the studies involving animals in accordance with the local legislation and institutional requirements because this was a retrospective study involving image evaluation of MRI studies performed in the frame of the diagnostic work-up of small animal patients. Ethical review and approval is not required for a retrospective study at our institution. Written informed consent was obtained from the owners for the participation of their animals in this study.

Author contributions

HS: Investigation, Data curation, Writing – original draft. SH: Investigation, Conceptualization, Methodology, Project administration, Resources, Supervision, Visualization, Writing – review & editing. CF: Investigation, Writing – review & editing. XS: Formal analysis, Investigation, Visualization, Writing – review & editing.

Funding

The author(s) declare that no financial support was received for the research, authorship, and/or publication of this article.

Acknowledgments

The authors would like to acknowledge the Diagnostic Imaging and Neurology services of the University of Tennessee College of Veterinary Medicine and The Office of Information Technology.

Conflict of interest

The authors declare that the research was conducted in the absence of any commercial or financial relationships that could be construed as a potential conflict of interest.

Publisher's note

Supplementary material

The Supplementary material for this article can be found online at: https://www.frontiersin.org/articles/10.3389/fvets.2024.1346617/full#supplementary-material

References

1. Wolff CA, Holmes SP, Young BD, Chen AV, Kent M, Platt SR, et al. Magnetic resonance imaging for the differentiation of neoplastic, inflammatory, and cerebrovascular brain disease in dogs. *J Vet Intern Med*. (2012) 26:589–97. doi: 10.1111/j.1939-1676.2012.00899.x

2. Young BD, Fosgate GT, Holmes SP, Wolff CA, Chen-Allen AV, Kent M, et al. Evaluation of standard magnetic resonance characteristics used to differentiate neoplastic, inflammatory, and vascular brain lesions in dogs. *Vet Radiol Ultrasound*. (2014) 55:399–406. doi: 10.1111/vru.12137

3. Leclerc MK, d'Anjou MA, Blond L, Carmel EN, Dennis R, Kraft SL, et al. Interobserver agreement and diagnostic accuracy of brain magnetic resonance imaging in dogs. *J Am Vet Med Assoc*. (2013) 242:1688–95. doi: 10.2460/javma.242.12.1688

4. Horsfield MA, Rocca MA, Pagani E, Storelli L, Preziosa P, Messina R, et al. Estimating brain lesion volume change in multiple sclerosis by subtraction of magnetic resonance images. *J Neuroimaging*. (2016) 26:395–402. doi: 10.1111/jon.12344

5. Zivadinov R, Ramasamy DP, Hagemeier J, Kolb C, Bergsland N, Schweser F, et al. Evaluation of leptomeningeal contrast enhancement using pre-and Postcontrast subtraction 3D-FLAIR imaging in multiple sclerosis. *AJNR Am J Neuroradiol*. (2018) 39:642–7. doi: 10.3174/ajnr.A5541

6. Duan Y, Hildenbrand PG, Sampat MP, Tate DF, Csapo I, Moraal B, et al. Segmentation of subtraction images for the measurement of lesion change in multiple sclerosis. *AJNR Am J Neuroradiol*. (2008) 29:340–6. doi: 10.3174/ajnr.A0795

7. Moraal B, van den Elskamp IJ, Knol DL, Uitdehaag BM, Geurts JJ, Vrenken H, et al. Long-interval T2-weighted subtraction magnetic resonance imaging: a powerful new outcome measure in multiple sclerosis trials. *Ann Neurol*. (2010) 67:667–75. doi: 10.1002/ana.21958

8. Sollmann N, Gutbrod-Fernandez M, Burian E, Riederer I, Meyer B, Hock A, et al. Subtraction maps derived from longitudinal magnetic resonance imaging in patients with glioma facilitate early detection of tumor progression. *Cancers (Basel)*. (2020) 12:3111. doi: 10.3390/cancers12113111

9. Thenier-Villa JL, Alejandro Galarraga Campoverde R, Ramon DELALZA, Conde AC. Predictors of morbidity and cleavage plane in surgical resection of pure convexity Meningiomas using cerebrospinal fluid sensitive image subtraction magnetic resonance imaging. *Neurol Med Chir (Tokyo)*. (2017) 57:35–43. doi: 10.2176/nmc.oa.2016-0169

10. Martens RM, Bechten A, Ingala S, van Schijndel RA, Machado VB, de Jong MC, et al. The value of subtraction MRI in detection of amyloid-related imaging abnormalities with oedema or effusion in Alzheimer's patients: an interobserver study. *Eur Radiol*. (2018) 28:1215–26. doi: 10.1007/s00330-017-5022-6

11. Rutherford MA, Pennock JM, Cowan FM, Saeed N, Hajnal JV, Bydder GM. Detection of subtle changes in the brains of infants and children via subvoxel registration and subtraction of serial MR images. *AJNR Am J Neuroradiol*. (1997) 18:829–35.

12. Hanna SL, Langston JW, Gronemeyer SA. Value of subtraction images in the detection of hemorrhagic brain lesions on contrast-enhanced MR images. *AJNR Am J Neuroradiol*. (1991) 12:681–5.

13. Melhem ER, Mehta NR. Dynamic T1-weighted spin-echo MR imaging: the role of digital subtraction in the demonstration of enhancing brain lesions. *J Magn Reson Imaging*. (1999) 9:503–8. doi: 10.1002/(SICI)1522-2586(199904)9:4<503::AID-JMRI1>3.0.CO;2-0

14. Patel N, Horsfield MA, Banahan C, Thomas AG, Nath M, Nath J, et al. Detection of focal longitudinal changes in the brain by subtraction of MR images. *AJNR Am J Neuroradiol*. (2017) 38:923–7. doi: 10.3174/ajnr.A5165

15. McKinney A, Palmer C, Short J, Lucato L, Truwit C. Utility of fat-suppressed FLAIR and subtraction imaging in detecting meningeal abnormalities. *Neuroradiology*. (2006) 48:881–5. doi: 10.1007/s00234-006-0145-5

16. Curati WL, Williams EJ, Oatridge A, Hajnal JV, Saeed N, Bydder GM. Use of subvoxel registration and subtraction to improve demonstration of contrast enhancement in MRI of the brain. *Neuroradiology*. (1996) 38:717–23. doi: 10.1007/s002340050335

17. Tay KL, Yang JL, Phal PM, Lim BG, Pascoe DM, Stella DL. Assessing signal intensity change on well-registered images: comparing subtraction, color-encoded subtraction, and parallel display formats. *Radiology*. (2011) 260:400–7. doi: 10.1148/radiol.11101092

18. Chan JH, Tsui EY, Chan CY, Lai KF, Chau LF, Fong D, et al. Digital subtraction in gadolinium-enhanced MR imaging of the brain: a method to reduce contrast dosage. *Eur Radiol*. (2002) 12:2317–21. doi: 10.1007/s00330-001-1285-y

19. Lamb CR, Lam R, Keenihan EK, Frean S. Appearance of the canine meninges in subtraction magnetic resonance images. *Vet Radiol Ultrasound*. (2014) 55:607–13. doi: 10.1111/vru.12166

20. Yamada K, Miyahara K, Sato M, Furuoka H, Nakagawa M, Shigeno S, et al. Differentiation between chondroma and squamous cell carcinoma: evaluation of subtraction image of MRI. *J Vet Med Sci*. (1998) 60:1149–51. doi: 10.1292/jvms.60.1149

21. Remelli C, Martello A, Valentini A, Contiero B, Bernardini M. Magnetic resonance imaging highlights the meningeal involvement in steroid responsive meningitis-arteritis and suggests the inflammation of the surrounding tissues (70 cases). *Front Vet Sci*. (2022) 9:957278. doi: 10.3389/fvets.2022.957278

22. Church ME, Ceja G, McGeehan M, Miller MC, Farias P, Sanchez MD, et al. Meningeal B cell clusters correlate with submeningeal pathology in a natural model of multiple sclerosis. *J Immunol*. (2021) 207:44–54. doi: 10.4049/jimmunol.2000514

23. Keenihan EK, Summers BA, David FH, Lamb CR. Canine meningeal disease: associations between magnetic resonance imaging signs and histologic findings. *Vet Radiol Ultrasound*. (2013) 54:504–15. doi: 10.1111/vru.12055

24. Dirrig H, Lamb CR. Magnetic resonance imaging of intracranial inflammatory conditions in dogs: sensitivity of subtraction images versus pre- and post-gadolinium T1-weighted image pairs. *Vet Radiol Ultrasound*. (2016) 57:410–6. doi: 10.1111/vru.12371

25. Kataoka M, Ueda H, Koyama T, Umeoka S, Togashi K, Asato R, et al. Contrast-enhanced volumetric interpolated breath-hold examination compared with spin-echo T1-weighted imaging of head and neck tumors. *AJR Am J Roentgenol*. (2005) 184:313–9. doi: 10.2214/ajr.184.1.01840313

26. D'Anjou MA, Carmel EN, Blond L, Beauchamp G, Parent J. Effect of acquisition time and chemical fat suppression on meningeal enhancement on MR imaging in dogs. *Vet Radiol Ultrasound*. (2012) 53:11–20. doi: 10.1111/j.1740-8261.2011.01864.x

27. Smith PM, Goncalves R, McConnell JF. Sensitivity and specificity of MRI for detecting facial nerve abnormalities in dogs with facial neuropathy. *Vet Rec*. (2012) 171:349. doi: 10.1136/vr.100877

28. Danieli L, Riccitelli GC, Distefano D, Prodi E, Ventura E, Cianfoni A, et al. Brain tumor-enhancement visualization and morphometric assessment: a comparison of MPRAGE, SPACE, and VIBE MRI techniques. *AJNR Am J Neuroradiol*. (2019) 40:1140–8. doi: 10.3174/ajnr.A6096

29. Fleming KL, Maddox TW, Warren-Smith CMR. Three-dimensional T1-weighted gradient echo is a suitable alternative to two-dimensional T1-weighted spin echo for imaging the canine brain. *Vet Radiol Ultrasound*. (2019) 60:543–51. doi: 10.1111/vru.12774

30. Pons-Sorolla M, Dominguez E, Czopowicz M, Suñol A, Ordás CM, Moliner CM, et al. Clinical and magnetic resonance imaging (MRI) features, tumour localisation, and survival of dogs with presumptive brain gliomas. *Vet Sci*. (2022) 9:257. doi: 10.3390/vetsci9060257

31. Walsh N, Carney PC, Streu S, Thompson M, Johnson PJ. Prevalence of brain magnetic resonance imaging diagnoses and correlation with Signalment and presenting complaint in dogs. Frontiers in veterinary. *Science*. (2021) 8:8. doi: 10.3389/fvets.2021.768709

32. Cornelis I, Van Ham L, Gielen I, De Decker S, Bhatti SFM. Clinical presentation, diagnostic findings, prognostic factors, treatment and outcome in dogs with meningoencephalomyelitis of unknown origin: a review. *Vet J*. (2019) 244:37–44. doi: 10.1016/j.tvjl.2018.12.007

33. Lamb CR, Croson PJ, Cappello R, Cherubini GB. Magnetic resonance imaging findings in 25 dogs with inflammatory cerebrospinal fluid. *Vet Radiol Ultrasound*. (2005) 46:17–22. doi: 10.1111/j.1740-8261.2005.00003.x

34. Cervera V, Mai W, Vite CH, Johnson V, Dayrell-Hart B, Seiler GS. Comparative magnetic resonance imaging findings between gliomas and presumed cerebrovascular accidents in dogs. *Vet Radiol Ultrasound*. (2011) 52:33–40. doi: 10.1111/j.1740-8261.2010.01749.x

frontiers | Frontiers in Veterinary Science

TYPE Original Research
PUBLISHED 19 March 2024
DOI 10.3389/fvets.2024.1359016

OPEN ACCESS

EDITED BY
Adriano Wang-Leandro,
University of Veterinary Medicine Hannover, Germany

REVIEWED BY
Koen Santifort,
IVC Evidensia Small Animal Referral Hospital Arnhem, Neurology, Netherlands
Hakyoung Yoon,
Jeonbuk National University, Republic of Korea
Frank Steffen,
University of Zurich, Switzerland

*CORRESPONDENCE
Sarah A. Moore
✉ moore.2204@osu.edu

RECEIVED 27 December 2023
ACCEPTED 08 March 2024
PUBLISHED 19 March 2024

CITATION
Agustini D, Heimann MK, Co M, Walter BA, Purmessur D and Moore SA (2024) Modic changes in the lumbar vertebral column of chondrodystrophic and non-chondrodystrophic dogs with intervertebral disc disease.
Front. Vet. Sci. 11:1359016.
doi: 10.3389/fvets.2024.1359016

Modic changes in the lumbar vertebral column of chondrodystrophic and non-chondrodystrophic dogs with intervertebral disc disease

Dyah Agustini[1], Mary K. Heimann[2], Megan Co[2], Benjamin A. Walter[2], Devina Purmessur[2] and Sarah A. Moore[1]*

[1]Department of Veterinary Clinical Sciences, College of Veterinary Medicine, The Ohio State University, Columbus, OH, United States, [2]Department of Biomedical Engineering, College of Engineering, The Ohio State University, Columbus, OH, United States

Introduction: Modic changes (MC) are signs of vertebral pathology visible on magnetic resonance (MR) images that have been associated with low back pain (LBP) and disc degeneration in people. Multiple breeds of dogs also develop MCs and coincident back pain. However, the association between breed, MC, and spinal pathologies has yet to be fully elucidated. This study aimed to identify the prevalence of MC that occur spontaneously in the lumbar vertebral column of dogs diagnosed with intervertebral disc disease (IVDD) and examine their association with demographic criteria and the disc width index (DWI).

Methods: Medical records and lumbar vertebral column MR images were examined from 104 dogs (831 intervertebral disc spaces and adjacent vertebrae), which were divided into three groups: chondrodystrophic dogs (CD; n =54) and non-chondrodystrophic dogs (NCD; n =30) with IVDD as the primary diagnosis, and control dogs (n =20) with other spinal diseases as their primary diagnosis.

Results: Increasing age and a diagnosis of IVDD were significantly associated with MC in dogs ($p < 0.001$ and p =0.0062, respectively). In CD dogs with IVDD, Type 2 MC were most prevalent, whereas, in NCD dogs, Type 3 MC were the most prevalent type. Type 2 MC were distributed nearly equally across the lumbar vertebral column, while Type 3 MC were primarily detected at the level of L7-S1.

Discussion: This study demonstrated that MC developed spontaneously in dogs, are common in dogs diagnosed with IVDD, and the type observed varies by breed. Further research is needed to understand the pathogenesis of MC; however, the increased presence of Type 2 MC in CD dogs, similar to what is found in people with disc degeneration, suggests that CD dogs could serve as models for MC in people.

KEYWORDS

Modic changes, intervertebral disc disease, lumbar, disc height index, MRI

Introduction

Low back pain (LBP) is a worldwide leading cause of disability with a growing socioeconomic impact and rising incidence (1). Intervertebral disc disease (IVDD) is the most common cause of LBP (2, 3). In addition, both IVDD and LBP are some of the most common diseases of the vertebral column in both human and veterinary patients, particularly in dogs (4–6). Given the

high prevalence of these conditions in clinical settings, a better understanding of the pathophysiology of these conditions and drivers of associated pain is needed to help develop new treatment strategies (3). Both people and dogs experience similar degenerative mechanisms that result in nucleus pulposus (NP) and anulus fibrosus (AF) structural alterations and associated IVDD (7). The clinical and biological similarities between people and dogs suggest that what is known about various contributors to LBP in people might have relevance to dogs and, conversely, that dogs with naturally occurring IVDD might serve as a spontaneous canine model for translational research (8).

Modic changes (MC) are pathologies of the vertebral column reflected as abnormalities of vertebral and cartilage endplates, leading to changes in signal intensity on magnetic resonance (MR) imaging studies (Figure 1). In people, MC are classically linked to LBP and IVDD (9). Three types of MC have been described, which are differentiated based on the type of signal changes observed: Type 1 MC are hypointense on a T1-weighted image and hyperintense on a T2-weighted image, Type 2 MC are hyperintense on both T1 and T2-weighted images, and Type 3 MC are hypointense on both T1 and T2-weighted images (10). The pathologic processes associated with the development of MC involve inflammation, fatty marrow infiltration, bone remodeling, and fibrosis (10, 11). These changes are correlated with back pain and putatively associated with chemical and mechanical stimulation of nerve fibers induced by the damaged vertebral body (12, 13). Disruption in the cartilage endplate and subchondral bone also contributes to loss of function and destabilization of the NP, which can lead to nerve compression and cause pain in dogs with IVDD (14).

Few studies have previously evaluated MC in dogs with spontaneous IVDD (15–17). The lumbosacral region has been previously noted as the most prevalent location (15, 17). The presence of hyperintense endplate lesions in T1-weighted and T2-weighted images of the thoracolumbar vertebral column has also been reported, indicating fatty infiltration of bone, a finding consistent with Type 2 MC (15). This finding was particularly prevalent in Dachshunds, raising the question of whether chondrodystrophic breeds might have a higher incidence of certain types of MC (15). Type 2 and Type 3 MC have also been previously reported as the most frequent endplate changes found in the canine vertebral column (16, 17). However, little is written about the influence of breed on types of MC observed in dogs (15–17). Therefore, further research is needed to understand better the etiology, prevalence, and distributions of MC in the canine vertebral column.

The goal of this study was to evaluate the prevalence and types of MC that occur spontaneously in the lumbar vertebral column of both chondrodystrophic (CD) and non-chondrodystrophic (NCD) client-owned dogs presented to a veterinary neurology referral center and ultimately diagnosed with IVDD. We also aimed to examine the association between the presence of MC and age, breed, body weight, sex, and the disc width index (DWI), which is also referred to as disc height index in humans and other animal models (18–20). Studying spontaneously occurring MC in dogs may provide novel insight into potential drivers of IVDD associated back pain and could provide a clinically relevant comparison with the human condition, providing support for future translational efforts.

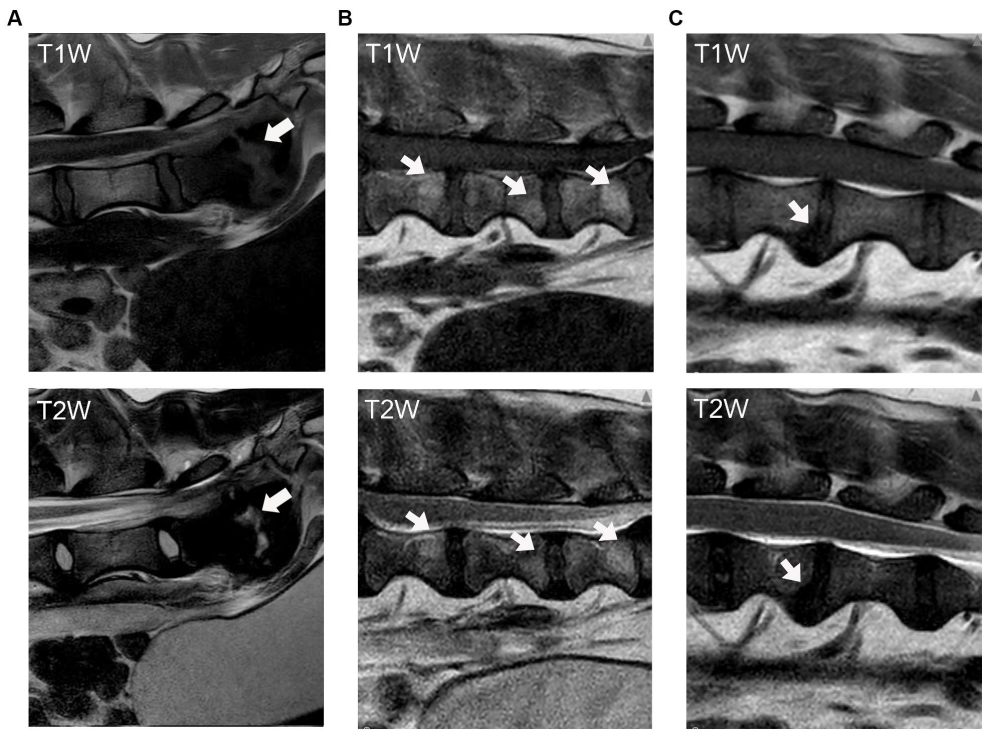

FIGURE 1
Modic changes as seen on T1-weighted and T2-weighted MR images of the canine vertebral column. The arrows indicate the signal changes in the vertebral body and endplate. **(A)** Type 1 MC, hypointensity on T1W and hyperintensity on T2W images. **(B)** Type 2 MC, hyperintensity on both T1W and T2W images; and **(C)** Type 3 MC, hypointensity on both T1W and T2W images.

Materials and methods

This study retrospectively utilized medical records and MRI findings from client-owned dogs admitted to the OSU Veterinary Medical Center with MR imaging of the lumbar vertebral column performed for the clinical diagnosis of spinal disease.

Data collection

Identification of cases

A search of the electronic medical records system of the Ohio State University Veterinary Medical Center was conducted to identify all dogs that had an MRI of the lumbar vertebral column between August 1, 2020, and September 15, 2022. The exclusion criteria were as follows:

1. Dogs had incomplete demographic data in their medical records, including age, body weight, sex, and breed,
2. The sagittal T1-weighted and T2-weighted MR images from T13-S1 were not available for review,
3. Dogs had a history of previous lumbar spinal surgery.

Definitions of groups

Dogs were divided into two main groups: IVDD and control groups. Those with a primary MRI diagnosis of IVD herniation, extrusion, or protrusion served as the IVDD group. Dogs with another primary diagnosis and no evidence of disc herniation, extrusion, or protrusion on their MRI served as the control group.

IVDD group

Dogs in the IVDD group were further divided into chondrodystrophic (CD) and non-chondrodystrophic (NCD) subgroups. Those identified in the medical record as mixed-breed dogs were excluded from the IVDD group due to the inability to characterize the CD status of their breed. Pure breed dogs included in the IVDD group were categorized as CD or non-CD dogs based on the published prevalence of their CFA12 and CFA18 *FGF4* retrogenes expression (21), and 0.10 or 10% frequency of CFA12 *FGF4* retrogene expressed was used as the threshold above which dogs were categorized as CD.

Control group

Dogs with a primary diagnosis other than IVDD (i.e., spinal neoplasia, neuritis, myelitis, etc.) and no secondary diagnosis of IVDD (defined as no evidence of disc protrusion, extrusion, or herniation) or dogs with no remarkable findings on their MRI report were included in the control group regardless of breed.

MRI analysis for Modic changes

Image acquisition

Imaging for all dogs was originally performed by the Radiology Department of the Veterinary Medical Center at the Ohio State University using a Phillips Achieva 3.0 T MRI system (Highland Heights, Ohio 44,143) as part of standard care for diagnosis and management of their clinical complaint. A board-certified veterinary radiologist interpreted the imaging results and provided a final written report on the images. This report was retrieved from the medical record and used to categorize dogs as having a primary diagnosis of IVDD or other (control). Complete MRI studies for all dogs were retrieved and evaluated prospectively by three reviewers (DA, MC, MKH) to document the prevalence and type of MC present throughout the lumbar vertebral column.

Reviewer training

Reviewers underwent a standardized training protocol delivered by a board-certified veterinary neurologist (SM) to review MR images and identify MC. A written protocol for MC evaluation procedures was provided during the training as a step-by-step guide to image examination. Several example images of MC were provided in the protocol to help the reviewers easily identify their appearance. Five cases were initially selected as sample images for training purposes. After each reviewer evaluated the sample images individually, a group training session was conducted to compare interpretations, assess reviewer competence, and further harmonize the approach to review. The reviewers began the interpretation of the entire set of imaging studies only after competence was demonstrated.

Image evaluation

Assessment of Modic changes

Reviewers individually assessed the presence (yes/no) and type of MC (1/2/3) present in each pair of vertebral endplates adjacent to the IVDs from T13-L1 to L7-S1 on the MR images. For vertebral levels where there was no perfect agreement between all three reviewers, an additional assessment by a board-certified veterinary neurologist determined the final judgment.

Imaging studies were evaluated in a randomized fashion using a RocketPACS web-based system (VetRocket, Santa Clara, CA), and reviewers were blinded to the diagnosis and group allocation of each dog. Reviewers were instructed to evaluate the appearance of the cranial and caudal vertebral endplates adjacent to the IVDs from T13-S1 on both T1-weighted and T2-weighted sagittal images to determine the presence and type of MC observed (Figure 1). Definitions of MC applied in this study were taken from Modic et al. (10):

1. Type 1 MC (hypointensity on T1W and hyperintensity on T2W images),
2. Type 2 MC (hyperintensity on T1W and hyperintensity on T2W images),
3. Type 3 MC (hypointensity on both T1W and T2W images).

Disc width index measurement

A mid-sagittal T1W image was used to calculate the DWI for each individual disc width as a potential marker of disc degeneration. The calculation for DWI was based on the ratio of the total caudal-cranial length of the intervertebral disc relative to the vertebral body (20):

$$DWI = \frac{(D+E+F)}{(A+B+C)},$$

10.3389/fvets.2024.1359016

where D, E, and F are the measurements of intervertebral disc width, and A, B, and C are the measurements of the vertebral body (Figure 2). A single reviewer (DA) performed DWI measurements. Five cases were chosen at random from the clinical data set and each case was assessed three different times to evaluate Intra Class Correlation (ICC) analysis to ensure test–retest reliability.

Statistical analysis

Statistical analysis was conducted using STATA/BE 17.0 statistical software. An intra-class correlation test was performed to assess the intra-rater reliability of DWI measurement and inter-rater reliability of MC assessment during reviewer training. Dog breed, age, sex, and body weight were reported using descriptive statistics. Comparison of the number and type of MC present between groups was assessed using cross-tabulation analysis. A logistic regression test assessed the association between MC and age, body weight, sex, and DWI as predictors. Fisher's Exact test was used to test each group's independence (control, CD, and NCD dogs) with the occurrence of MC. The mean differences between DWI of vertebrae with MC and without MC was examined using a two-sample *t*-test. Statistical differences were considered significant if the *p*-value was <0.05.

Results

Case selection

Two hundred thirty dogs with lumbar vertebral column MR images were identified through the initial medical records search. Cases with incomplete demographic information, incomplete MRI studies, or a history of previous spinal surgery were excluded ($n = 14$). Cases with IVDD as the primary diagnosis ($n = 120$) were separated from those with other primary MRI diagnoses or normal MRI ($n = 96$). Only pure-breed dogs were included in the IVDD group ($n = 84$), further divided into CD and NCD groups ($n = 54$ and $n = 30$, respectively). From the group of dogs with normal MR images (no remarkable finding) or other primary diagnoses, dogs with a secondary diagnosis of intervertebral disc herniation, protrusion, or extrusion in their MRI result were excluded ($n = 76$) to obtain a group of dogs with no MRI indication of IVDD that were used as a control group ($n = 20$). Vertebrae with fractures involving the endplate or where the entire disc and endplate were not visible in the sagittal image due to truncation were removed from the image review process ($n = 4$). Two dogs from the IVDD groups and one from the control group had eight lumbar vertebrae, resulting in additional vertebrae for evaluation. In total, 831 intervertebral discs and their adjacent vertebral endplates were evaluated from all three groups (Figure 3).

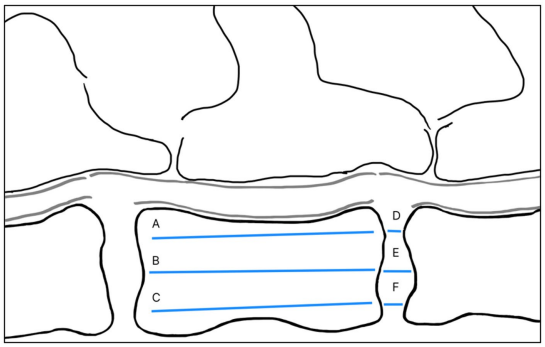

FIGURE 2
Illustration of DWI measurement. A and D refer to the dorsal side of a vertebral body and intervertebral disc, whereas C and F refer to the ventral side. A, B, and C refer to the vertebral body cranial to the adjacent disc. Image and measurement were adapted from Lü et al. (20).

Demographics of the cohort

MRI studies from a total of 104 dogs were evaluated (54 CD dogs, 30 NCD dogs, and 20 control dogs). There was no statistically significant difference in sex distribution between the groups ($p = 0.154$), whereas age and body weight were significantly different ($p < 0.001$ for both). The demographic features of each group are summarized in Table 1.

The control group mainly consisted of mixed breed dogs ($n = 6$), Border Collie ($n = 4$), Australian Shepherd ($n = 3$), and German Shepherd ($n = 2$). Breeds such as American Pitbull Terrier, Belgian Malinois, English Setter, French Bulldog, and German Shorthaired Pointer represented only one of each breed. The most represented breeds in the CD group were Dachshund ($n = 30$), Beagle ($n = 7$), French Bulldog ($n = 6$), and Bichon Frise ($n = 3$). Other breeds included in lesser numbers ($n \leq 2$) in the CD group were American Cocker Spaniel, Basset Hound, Jack Russell Terrier, Pembroke Welsh Corgi, Poodle, and Shih Tzu. The most represented breeds in the NCD group were German Shepherd ($n = 10$), Great Dane ($n = 3$), and Labrador Retriever ($n = 3$). The NCD group also contained one each of the following: Australian Shepherd, Belgian Malinois, Bernese Mountain, Border Collie, English Bulldog, English Coon Hound, Eskimo, Fox Terrier, German Shorthaired Pointer, Golden Retriever, Greyhound, Pomeranian, Shetland Sheepdog, and Shilo Shepherd.

Modic changes in canine lumbar vertebral column

The findings with respect to the presence and type of MC observed are summarized in Table 2. Of all lumbar vertebral levels evaluated, 85.4% showed no MC, 9.5% showed Type 2 MC, and 5.1% showed Type 3 MC. No Type 1 MC changes were observed in any dog included in the present study (Figure 4A). Type 2 MC were found to be presented in CD and NCD dogs but not in control dogs, while Type 3 MC were detected in all dogs, including the control group (Figure 4B). In the IVDD groups, two CD dogs and one NCD dog were found to have both Type 2 MC and Type 3 MC within their lumbar vertebral column, which we refer to as presenting a mixed type of MC (Table 2). In general, Type 2 MC were distributed widely throughout the lumbar vertebral column, whereas Type 3 MC were detected mostly in vertebral endplates adjacent to the L7-S1 disc space ($n = 13$) (Figure 5).

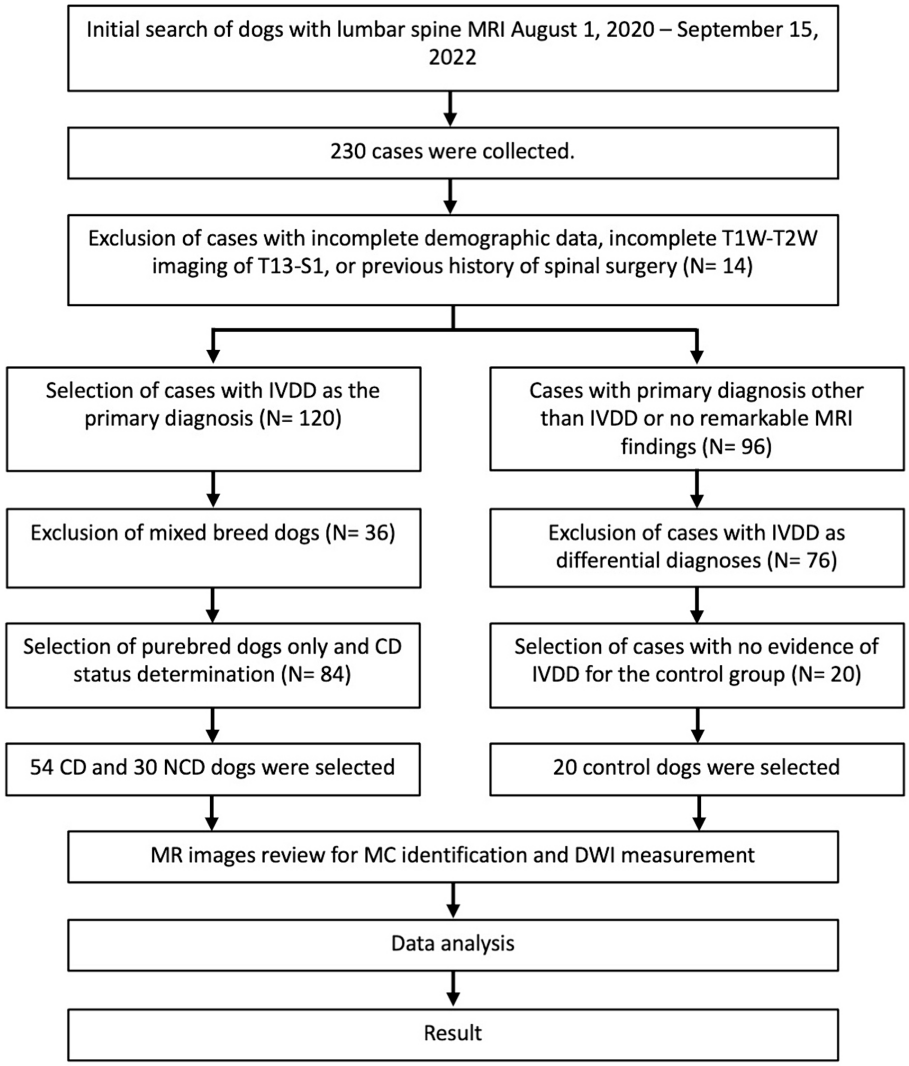

FIGURE 3
Flow chart of the case selection process for 104 dogs with and without intervertebral disc disease.

The presence of MC was not significantly associated with sex ($p = 0.264$) or body weight ($p = 0.263$). Age appeared to be significantly associated with MC ($p < 0.001$). The distribution of MC based on age for all groups are presented in Figure 6. The odds ratio (OR) of having MC in the lumbar vertebral column increased by 1.36 times (95% CIs = 1.174–1.575) for each one-year increase in age. The frequency of MC was higher in by CD and NCD dogs with IVDD compared to controls dogs ($p = 0.0062$), where the odds ratio for the presence of MC in CD dogs was 6.57 (95% CIs = 1.723–25.076) and in the NCD dogs was 5.67 (95% CIs = 1.369–23.462).

The distribution of each MC type and its location by vertebral level are summarized in Figure 7. In the control group, two of six Type 3 MC were found in vertebral endplates adjacent to the T13-L1 intervertebral disc, while the remainder were located at the level of L7-S1. Type 2 MC were more commonly observed than Type 3 MC in the CD dogs ($n = 67$ and $n = 9$, respectively), whereas Type 3 MC were observed more than Type 2 MC in the NCD dogs ($n = 27$ and $n = 12$, respectively). In both CD and NCD dogs, Type 2 MC were distributed throughout the lumbar vertebral column, while Type 3 MC occurred predominantly at the vertebral endplates adjacent to the L7-S1 intervertebral disc space.

Relationship between Modic changes and disc width index

The intraclass-correlation test (ICC) was performed under a two-way mixed-effects model to assess the repeatability of a single observer's measurements of disc width in dogs with and without IVDD as measured at three distinct times. Intra-observer reliability for DWI measurements was 0.99, which can be categorized as excellent (22).

The average ratio of intervertebral disc width was 0.25–0.4 for the disc space adjacent to vertebrae with MC and 0.26–0.35 for the disc space adjacent to vertebrae without MC present. There was no statistically significant difference in DWI between disc adjacent to vertebral endplates that contained MC and those that did not, except at the level of L7-S1, where the DWI was significantly larger in discs adjacent to vertebral endplates with MC ($p = 0.0247$) (Table 3).

10.3389/fvets.2024.1359016

TABLE 1 Demographics of 104 client-owned dogs with and without IVDD.

Demographic criteria	Control group ($n = 20$)	CD group ($n = 54$)	Non-CD group ($n = 30$)	p-value
Age (year)				<0.001*
Median	3	7	8	
Range	1–9	2–13	2–12	
Body weight (kg)				<0.001*
Median	20.4	8.2	36.8	
Range	6.5–57	3–34.6	7.8–69.4	
Sex				
Male-neutered	6	33	22	0.154**
Male intact	4	1	1	
Female-spayed	9	20	7	
Female intact	1	0	0	

*Kruskal-Wallis test. **Fisher's exact test.

TABLE 2 Comparison of Modic changes identified in 104 chondrodystrophic (CD) and non-chondrodystrophic (NCD) dogs with and without IVDD.

Modic changes	Control group ($n = 20$)	CD group ($n = 54$)	Non-CD group ($n = 30$)	p-value (Fisher's exact test)
No MC found	17 (85%)	25 (46.3%)	15 (50%)	< 0.001
Type 1 MC	0	0	0	
Type 2 MC	0	21 (38.9%)	3 (10%)	
Type 3 MC	3 (15%)	6 (11.1%)	11 (36.7%)	
Mixed type (2/3)	0	2 (3.7%)	1 (3.3%)	

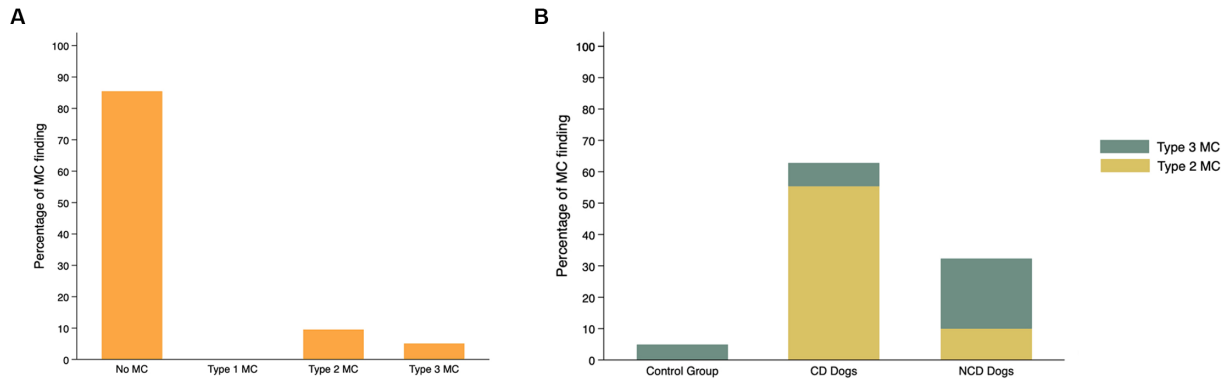

FIGURE 4
Frequency (%) of Modic changes (MC) observed in 831 lumbar vertebral segments from 104 dogs with and without intervertebral disc disease (IVDD) **(A)** by type of MC observed and **(B)** by group and breed chondrodystrophy status.

Discussion

This study represents one of only a few publications evaluating MC in dogs (15–17, 23) and is the first to associate the type and distribution of MC with breed chondrodystrophy status in client-owned dogs. Findings from our study support those recently published by Beukers et al. (17) that dogs can spontaneously develop MC, that MC are commonly observed at the lumbosacral junction, and that the development of MC in dogs is strongly associated with age, a finding observed in people as well.

In our study population, no Type 1 MC were identified and Type 2 MC were the most common type of MC observed. The Type 1 MC images presented in Figure 1A were obtained from another client-owned dog diagnosed with discospondylitis and not included in the current study. It is interesting to note that Beukers et al. (17) also found that Type 1 MC was significantly associated with imaging characteristics of discospondylitis. Type 1 MC are thought to reflect the replacement of normal bone marrow by fibrous and granulation tissue. TNF-α expression in the vertebral endplates of people with Type 1 MC is significantly higher than in those with Type 2 MC (24),

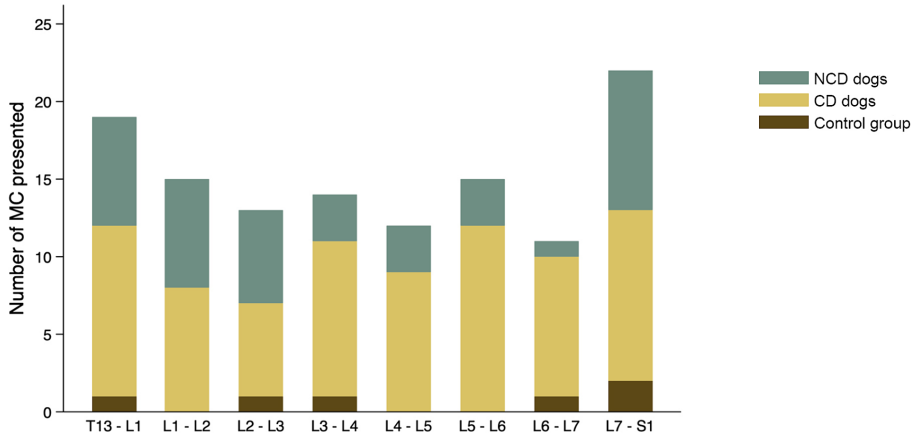

FIGURE 5
Distribution of all Modic changes observed in 831 lumbar vertebral segments from 104 dogs with and without intervertebral disc disease (IVDD). Dogs were divided into a control group with no evidence of IVDD, a group of chondrodystrophic dogs (CD) with IVDD and a group of non-chondrodystrophic dogs (NCD) with IVDD.

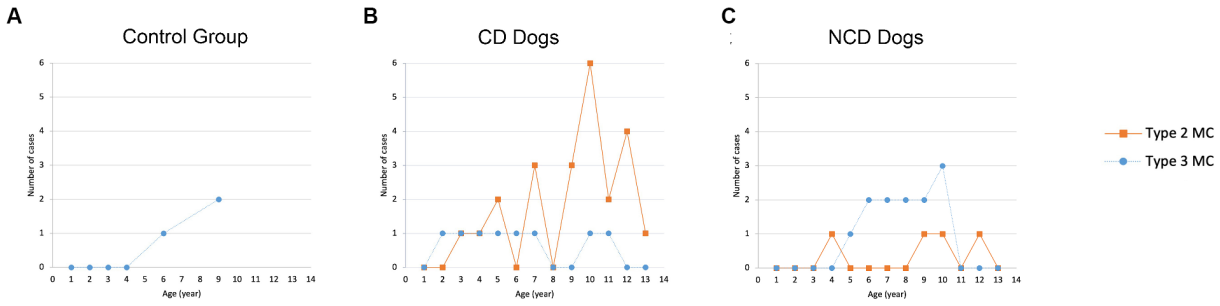

FIGURE 6
Distribution of Modic changes based on age in **(A)** control group, **(B)** CD dogs, and **(C)** NCD dogs.

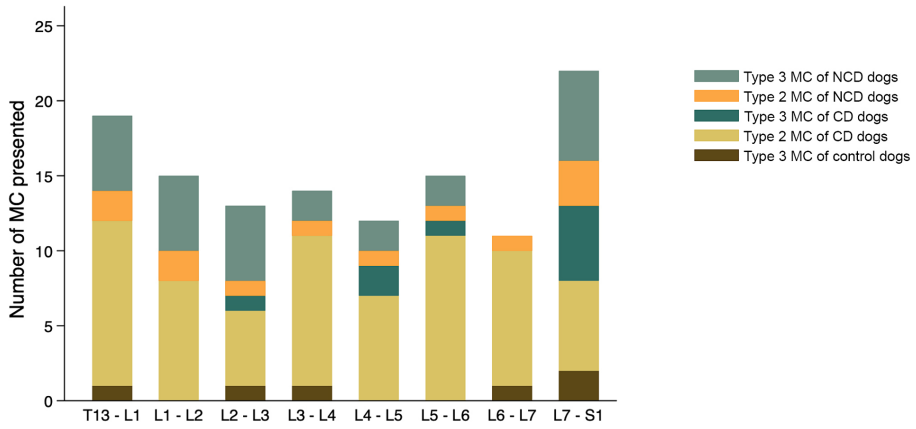

FIGURE 7
Distribution of Modic changes, by type, observed in 831 lumbar vertebral segments from 104 dogs with and without intervertebral disc disease (IVDD). Dogs were divided into a control group with no evidence of IVDD, a group of chondrodystrophic dogs (CD) with IVDD and a group of non-chondrodystrophic dogs (NCD) with IVDD.

TABLE 3 Comparison of mean DWI in each intervertebral disc adjacent to vertebral endplates with and without MC.

Level	Mean disc width index		Two-sample *t*-test (*p*-value)
	Normal (SD)	With MC (SD)	
T13-L1	0.26 (0.05)	0.25 (0.05)	0.8726
L1-L2	0.24 (0.05)	0.25 (0.05)	0.6147
L2-L3	0.26 (0.2)	0.26 (0.05)	0.9521
L3-L4	0.22 (0.05)	0.234 (0.04)	0.4178
L4-L5	0.23 (0.2)	0.21 (0.05)	0.7742
L5-L6	0.22 (0.2)	0.214 (0.04)	0.9497
L6-L7	0.23 (0.05)	0.24 (0.05)	0.5851
L7-S1	0.35 (0.08)	0.4 (0.2)	0.0247

supporting the argument that Type 1 MC are most likely to be associated with active inflammation (9). Type 1 MC have also been significantly associated with the presence of low back pain, and disc herniation appears to be an important risk factor for development (25, 26). Type 1 MC are also considered an interconvertible lesion, as they can develop into Type 2 MC or revert to normal condition (19, 26–28). Given what is known about the underlying pathophysiology and time course for the development of Type 1 MC, we assume it is possible that Type 1 MC were not observed in our population of dogs because they represent very early degenerative changes resulting in more mild clinical signs that could be missed by owners and veterinarians until the process becomes more advanced. In the previous studies, Type 1 MC accounted for a minimal number of dogs (16, 17). The presence of Type 1 MC has also potentially been associated with previous spinal surgery (17). Our study design excluded dogs with previous spinal surgery from evaluation and therefore precluded assessing this relationship. Additionally, it is possible that Type I MC represent an earlier stage of vertebral endplate changes associated with IVDD (11, 15) and that Type I MC can transition to Type 2 MC over time (10, 19, 26, 28); therefore, more subtle signs of lower back pain associated with Type I MC could be missed in dogs who are unable to self-report their back pain.

Another recent study evaluating MC in the canine vertebral column observed Type 3 MC most commonly (17); however, several studies have shown that Type 2 MC are the most commonly observed type of MC in people and are associated with the replacement of normal bone marrow with fat and upregulation of complement-mediated inflammation. Type 3 MC, which represent subchondral bone sclerosis, are reportedly more rare in people (19, 29, 30). An important difference in population between Beukers et al. (17) and the present might drive observed differences in results, specifically the inclusion of a large number of CD dogs in the present study. In our canine IVDD population, 65.4% of MC detected were Type 2 MC, while 34.6% of MC identified were Type 3 MC, suggesting that both types of MC occur relatively frequently in dogs with IVDD. Type 2 MC were detected most frequently in CD dogs, while only 10% of NCD dogs in our cohort had Type 2 MC. In contrast, Type 3 MC were observed more commonly in NCD dogs.

While not an aim of their study, another publication describing MRI findings associated with IVDD in a population composed primarily of CD dogs also reported a high prevalence of Type 2 MC (16), whereas Type 3 MC were most common in a previously reported cohort predominantly composed of NCD (17). Given the increased commonality of Type 2 MC in both people and CD dogs, our results could support the CD dog as a more translationally relevant spontaneous canine model for studying MC as compared to the NCD.

Across all dogs in the current study, MC were observed most frequently in the vertebral endplates at the level of L7-S1, and this finding is similar to previous reports (15, 17). However, we observed distinct patterns of distribution for Type 2 MC and Type 3 MC. Type 2 MC were observed mostly in CD dogs and were distributed almost equally across all lumbar segments, whereas Type 3 MC were observed mostly in NCD dogs and predominated at the vertebrae adjacent to the L7-S1 intervertebral disc space. To our knowledge, our study is the first to report a difference in MC type and distribution between CD and NCD dogs, and these findings might be important in considering causes and clinical implications of MC. We speculate these distinct distribution patterns might be influenced by differences in genetics, pathophysiology or biomechanics underlying IVDD characteristics in CD and NCD dogs. In the CD dogs, the CFA12 *FGF4* retrogene is considered a major risk factor for the IVDD phenotype. Histologically, discs from CD dogs undergo loss of notochordal cells and transformation of nucleus pulposus into chondrocyte-like cells at a young age (21, 31). This predisposes to early disc degeneration, which can occur in a similar manner throughout the vertebral column (32–34). Conversely, in NCD dogs, risk factors for the development of IVDD appear to center more on age, body dimensions, and vertebral column biomechanics (33, 35, 36), where relative ventrodorsal instability make the lumbosacral junction focally and particularly susceptible to high wear and tear and associated age-related disc degeneration (32, 33, 35).

Several studies in people report that vertebral endplates adjacent to the lower lumbar IVDs, L4-L5 and L5-S1, are the most common sites for Type 2 MC (13, 29, 37). This differs from the findings in our cohort of dogs. The differences might be caused by the distinction in biomechanical factors affecting the vertebral column between dogs and people or could be driven by the unique role of *FGF4* retrogene expression as a driver of IVDD in CD dogs (21, 31, 38). Comparably, a mutation in the fibroblast growth factor receptor 3 (*FGFR3*) in people, which causes an achondroplasia phenotype (39) is associated with lumbar spinal stenosis and more diffuse degenerative changes throughout the entire lumbar vertebral column, differing from the high incidence of IVDD focally at the lumbosacral junction in people without an achondroplasia phenotype (40, 41). More studies are

needed to investigate the relationship between *FGF4* retrogene expression and vertebral endplate changes consistent with MC.

Imaging assessment of disc space narrowing through calculation of disc height index (analogous to DWI measured in the present study) is often used as a clinical indicator of IVDD in people (42) since intervertebral disc height is related to age-related degenerative changes (43, 44). A study conducted by Akeda et al. (42) showed that lumbar disc height reduction in elderly people was significantly associated with low back pain conditions. Changes in laminar layers of AF and deposition of chondroid substance that was found particularly in middle-aged and older people have been proposed to contribute to disc space narrowing (43, 45). The reduction of disc height index has also been significantly associated with the presence of MC in people, particularly Type 2 MC (19). In the present study, we did not observe an association between reduced DWI and the presence of MC. Instead, we found an increased ratio of DWI in dogs affected with MC, but only at the level L7 – S1. The lack of association between DWI and MC in our population might be related to the diverse breeds included in our study, leading to variability in vertebral body and disc width measurement. Previous research in the canine cervical vertebral column found that disc to vertebral body area and length ratios differed significantly by breed (46). Further morphometric studies of the canine vertebral column are needed to obtain more information about disc space narrowing association with IVDD and MC in dogs.

The Pfirmann grading system has been used as a tool to assess disc degeneration based on sagittal T2-weighted images in both people and dogs (47–49). A previous study investigating lumbar IVDD in people found that MC were correlated with higher Pfirmann grade (48). The present study did not employ Pfirmann grading as a marker of disc degeneration, as it is not commonly used as part of the clinical image evaluation process for dogs with IVDD. Future studies could prospectively explore the relationship between Pfirrman grade and the presence of MC in dogs with IVDD.

This study represents the first evaluation of the relationship between chondrodystrophy breed status and the presence and distribution of spontaneously developing MC. Our study leveraged a comprehensive set of clinically annotated MRI studies, coupled with dog demographic information, to evaluate associations between these factors and the type of MC developed in a veterinary patient population with potential translational relevance. Given the nature of our population, we were unable to correlate MRI observations with histopathologic findings and were unable to define a control group of dogs with entirely normal vertebral columns for comparison. Additionally, because MR images were obtained from a database of previously imaged veterinary patients, correlation with other parameters, such as semi-quantitative measures of back pain or owner-derived quality of life scores, were not possible in the present study. While this study focused on the presentation of MC in the lumbar region of canine vertebral column, evaluation of MC in the thoracic and cervical region may provide further insight into the MC prevalence and breed-associated distribution in dogs. To address these limitations, prospective longitudinal investigation in dogs, including imaging of the entire vertebral column, will be necessary to better understand the relationship between MC development, degenerative changes to the intervertebral disc, and their association with low back pain.

Conclusion

This study demonstrates that MC occur spontaneously in dogs diagnosed with IVDD of the lumbar vertebral column. Age and diagnosis of IVDD are risk factors for the presence of MC, and older dogs and both CD and NCD dogs with IVDD have an increased odds ratio for MC. Type of MC observed varies with breed where 38.9% of CD dogs in our study population had Type 2 MC, which were distributed almost evenly throughout the lumbar vertebral column, while 36.7% of NCD dogs showed Type 3 MC, which were found mostly in the L7-S1 region. Further research is needed to understand the pathogenesis of MC and their correlation with clinical signs of back pain; however, the increased presence of Type 2 MCs in CD dogs, similar to what is found in people with disc degeneration, suggests that CD dogs might serve as a model for future translation studies of MC.

Data availability statement

The raw data supporting the conclusions of this article will be made available by the authors, without undue reservation.

Author contributions

DA: Conceptualization, Data curation, Formal analysis, Investigation, Methodology, Visualization, Writing – original draft, Writing – review & editing. MH: Investigation, Methodology, Writing – review & editing. MC: Investigation, Methodology, Writing – review & editing. BW: Conceptualization, Formal analysis, Methodology, Supervision, Writing – review & editing. DP: Conceptualization, Formal analysis, Methodology, Supervision, Writing – review & editing. SM: Conceptualization, Formal analysis, Investigation, Methodology, Supervision, Writing – review & editing.

Funding

The author(s) declare financial support was received for the research, authorship, and/or publication of this article. The Fulbright Foreign Scholarship funded DA throughout the graduate school program.

Acknowledgments

We want to thank Rebecca B. Garabed, VMD, MPVM, PhD for her guidance in data analysis and Denise Bailey for the IT support in retrieving the medical records from the database.

Conflict of interest

The authors declare that the research was conducted in the absence of any commercial or financial relationships that could be construed as a potential conflict of interest.

Publisher's note

References

1. Ferreira ML, De Luca K, Haile LM, Steinmetz JD, Culbreth GT, Cross M, et al. Global, regional, and national burden of low back pain, 1990–2020, its attributable risk factors, and projections to 2050: a systematic analysis of the global burden of disease study 2021. *Lancet Rheumatol*. (2023) 5:e316–29. doi: 10.1016/S2665-9913(23)00098-X

2. Luoma K, Vehmas T, Kerttula L, Grönblad M, Rinne E. Chronic low back pain in relation to Modic changes, bony endplate lesions, and disc degeneration in a prospective MRI study. *Eur Spine J*. (2016) 25:2873–81. doi: 10.1007/s00586-016-4715-x

3. Wu PH, Kim HS, Jang IT. Intervertebral disc diseases PART 2: a review of the current diagnostic and treatment strategies for intervertebral disc disease. *IJMS*. (2020) 21:2135. doi: 10.3390/ijms21062135

4. Kent P, Kongsted A, Secher Jensen T, Albert H, Manniche C, Schiøttz-Christensen B. SpineData – a Danish clinical registry of people with chronic back pain. *CLEP*. (2015) 7:369–80. doi: 10.2147/CLEP.S83830

5. Bergknut N, Egenvall A, Hagman R, Gustås P, Hazewinkel HAW, Meij BP, et al. Incidence of intervertebral disk degeneration–related diseases and associated mortality rates in dogs. *J. Am. Vet. Med. Assoc.* (2012) 240:1300–9. doi: 10.2460/javma.240.11.1300

6. Teraguchi M, Yoshimura N, Hashizume H, Muraki S, Yamada H, Minamide A, et al. Prevalence and distribution of intervertebral disc degeneration over the entire spine in a population-based cohort: the Wakayama spine study. *Osteoarthr Cartil*. (2014) 22:104–10. doi: 10.1016/j.joca.2013.10.019

7. Lee NN, Kramer JS, Stoker AM, Bozynski CC, Cook CR, Stannard JT, et al. Canine models of spine disorders. *JOR Spine*. (2020) 3:e1109. doi: 10.1002/jsp2.1109

8. Thompson K, Moore S, Tang S, Wiet M, Purmessur D. The chondrodystrophic dog: a clinically relevant intermediate-sized animal model for the study of intervertebral disc-associated spinal pain. *JOR Spine*. (2018) 1:e1011. doi: 10.1002/jsp2.1011

9. Modic MT. Modic type 1 and type 2 changes. *J Neurosurg Spine*. (2007) 6:150–1. doi: 10.3171/spi.2007.6.2.150

10. Modic MT, Steinberg PM, Ross JS, Masaryk TJ, Carter JR. Degenerative disk disease: assessment of changes in vertebral body marrow with MR imaging. *Radiology*. (1988) 166:193–9. doi: 10.1148/radiology.166.1.3336678

11. Dudli S, Fields AJ, Samartzis D, Karppinen J, Lotz JC. Pathobiology of Modic changes. *Eur Spine J*. (2016) 25:3723–34. doi: 10.1007/s00586-016-4459-7

12. Määttä JH, Rade M, Freidin MB, Airaksinen O, Karppinen J, Williams FMK. Strong association between vertebral endplate defect and Modic change in the general population. *Sci Rep*. (2018) 8:16630. doi: 10.1038/s41598-018-34933-3

13. Chen Y, Bao J, Yan Q, Wu C, Yang H, Zou J. Distribution of Modic changes in patients with low back pain and its related factors. *Eur J Med Res*. (2019) 24:34. doi: 10.1186/s40001-019-0393-6

14. Fenn J, Olby NJ. The canine spinal cord injury consortium (CANSORT-SCI). Classification of intervertebral disc disease. *Front Vet Sci*. (2020) 7:579025. doi: 10.3389/fvets.2020.579025

15. Gendron K, Doherr MG, Gavin P, Lang J. Magnetic resonance imaging characterization of vertebral endplate changes in the dog: MR imaging characterization of vertebral endplate changes. *Vet Radiol Ultrasound*. (2012) 53:50–6. doi: 10.1111/j.1740-8261.2011.01861.x

16. Besalti O, Pekcan Z, Sirin YS, Erbas G. Magnetic resonance imaging findings in dogs with thoracolumbar intervertebral disk disease: 69 cases (1997–2005). *J Am Vet Med Assoc*. (2006) 228:902–8. doi: 10.2460/javma.228.6.902

17. Beukers M, Grinwis GCM, Vernooij JCM, Van Der Hoek L, Tellegen AR, Meij BP, et al. Epidemiology of Modic changes in dogs: prevalence, possible risk factors, and association with spinal phenotypes. *JOR Spine*. (2023) 6:e1273. doi: 10.1002/jsp2.1273

18. Masuda K, Aota Y, Muehleman C, Imai Y, Okuma M, Thonar EJ, et al. A novel rabbit model of mild, reproducible disc degeneration by an Anulus needle puncture: correlation between the degree of disc injury and radiological and histological appearances of disc degeneration. *Spine*. (2005) 30:5–14. doi: 10.1097/01.brs.0000148152.04401.20

19. Teichtahl AJ, Urquhart DM, Wang Y, Wluka AE, O'Sullivan R, Jones G, et al. Modic changes in the lumbar spine and their association with body composition, fat distribution and intervertebral disc height – a 3.0 T-MRI study. *BMC Musculoskelet Disord*. (2016) 17:92. doi: 10.1186/s12891-016-0934-x

20. Lü DS, Shono Y, Oda I, Abumi K, Kaneda K. Effects of chondroitinase ABC and chymopapain on spinal motion segment biomechanics: an *in vivo* biomechanical, radiologic, and histologic canine study. *Spine*. (1997) 22:1828–34. doi: 10.1097/00007632-199708150-00006

21. Dickinson PJ, Bannasch DL. Current understanding of the genetics of intervertebral disc degeneration. *Front Vet Sci*. (2020) 7:431. doi: 10.3389/fvets.2020.00431

22. Koo TK, Li MY. A guideline of selecting and reporting Intraclass correlation coefficients for reliability research. *J Chiropr Med*. (2016) 15:155–63. doi: 10.1016/j.jcm.2016.02.012

23. Grunert P, Moriguchi Y, Grossbard BP, Ricart Arbona RJ, Bonassar LJ, Härtl R. Degenerative changes of the canine cervical spine after discectomy procedures, an in vivo study. *BMC Vet Res*. (2017) 13:193. doi: 10.1186/s12917-017-1105-5

24. Ohtori S, Inoue G, Ito T, Koshi T, Ozawa T, Doya H, et al. Tumor necrosis factor-Immunoreactive cells and PGP 9.5-Immunoreactive nerve fibers in vertebral endplates of patients with Discogenic low Back pain and Modic type 1 or type 2 changes on MRI. *Spine*. (2006) 31:1026–31. doi: 10.1097/01.brs.0000215027.87102.7c

25. Albert HB, Manniche C. Modic changes following lumbar disc herniation. *Eur Spine J*. (2007) 16:977–82. doi: 10.1007/s00586-007-0336-8

26. Jensen RK, Leboeuf-Yde C, Wedderkopp N, Sorensen JS, Jensen TS, Manniche C. Is the development of Modic changes associated with clinical symptoms? A 14-month cohort study with MRI. *Eur Spine J*. (2012) 21:2271–9. doi: 10.1007/s00586-012-2309-9

27. Thomas A, Pua U, Loke SC. Single vertebral level Modic change in adult achondroplasia: a diagnosis to be considered. *Eur J Radiol Extra*. (2009) 71:e77–80. doi: 10.1016/j.ejrex.2009.03.003

28. Crockett MT, Kelly BS, Van Baarsel S, Kavanagh EC. Modic type 1 vertebral endplate changes: injury, inflammation, or infection? *Am J Roentgenol*. (2017) 209:167–70. doi: 10.2214/AJR.16.17403

29. Wang Y, Videman T, Battié MC. Lumbar vertebral endplate lesions: prevalence, classification, and association with age. *Spine*. (2012) 37:1432–9. doi: 10.1097/BRS.0b013e31824dd20a

30. Özcan-Ekşi EE, Yayla A, Orhun Ö, Turgut VU, Arslan HN, Ekşi MŞ. Is the distribution pattern of Modic changes in vertebral end-plates associated with the severity of intervertebral disc degeneration?: a Cross-sectional analysis of 527 Caucasians. *World Neurosurg*. (2021) 150:e298–304. doi: 10.1016/j.wneu.2021.02.128

31. Brown EA, Dickinson PJ, Mansour T, Sturges BK, Aguilar M, Young AE, et al. *FGF4* retrogene on CFA12 is responsible for chondrodystrophy and intervertebral disc disease in dogs. *Proc Natl Acad Sci USA*. (2017) 114:11476–81. doi: 10.1073/pnas.1709082114

32. Hansen HJ. *A pathological-anatomical study on disc degeneration in dog*. Copenhagen: Acta Orthopaedica Scandinavica (1952).

33. Smolders LA, Bergknut N, Grinwis GCM, Hagman R, Lagerstedt AS, Hazewinkel HAW, et al. Intervertebral disc degeneration in the dog. Part 2: chondrodystrophic and non-chondrodystrophic breeds. *Vet J*. (2013) 195:292–9. doi: 10.1016/j.tvjl.2012.10.011

34. Braund KG, Ghosh P, Taylor TFK, Larsen LH. Morphological studies of the canine intervertebral disc: the assignment of the beagle to the Achondroplastic classification. *Res Vet Sci*. (1975) 19:167–72. doi: 10.1016/S0034-5288(18)33527-6

35. Breit S, Künzel W. Breed specific osteological features of the canine lumbosacral junction. *Ann Anat*. (2001) 183:151–7. doi: 10.1016/S0940-9602(01)80037-6

36. Benninger MI, Seiler GS, Robinson LE, Ferguson SJ, Bonél HM, Busato AR, et al. Effects of anatomic conformation on three-dimensional motion of the caudal lumbar and lumbosacral portions of the vertebral column of dogs. *Am J Vet Res*. (2006) 67:43–50. doi: 10.2460/ajvr.67.1.43

37. Braithwaite I, White J, Saifuddin A, Renton P, Taylor BA. Vertebral end-plate (Modic) changes on lumbar spine MRI: correlation with pain reproduction at lumbar discography. *Eur Spine J*. (1998) 7:363–8. doi: 10.1007/s005860050091

38. Alini M, Eisenstein SM, Ito K, Little C, Kettler AA, Masuda K, et al. Are animal models useful for studying human disc disorders/degeneration? *Eur Spine J*. (2008) 17:2–19. doi: 10.1007/s00586-007-0414-y

39. Rousseau F, Bonaventure J, Legeai-Mallet L, Pelet A, Rozet JM, Maroteaux P, et al. Mutations in the gene encoding fibroblast growth factor receptor-3 in achondroplasia. *Nature*. (1994) 371:252–4. doi: 10.1038/371252a0

40. Jeong ST, Song HR, Keny SM, Telang SS, Suh SW, Hong SJ. MRI study of the lumbar spine in achondroplasia: a morphometric analysis for the evaluation of stenosis of the canal. *J Bone Joint Surg*. (2006) 88-B:1192–6. doi: 10.1302/0301-620X.88B9.17758

41. Huet T, Cohen-Solal M, Laredo JD, Collet C, Baujat G, Cormier-Daire V, et al. Lumbar spinal stenosis and disc alterations affect the upper lumbar spine in adults with achondroplasia. *Sci Rep*. (2020) 10:4699. doi: 10.1038/s41598-020-61704-w

42. Akeda K, Yamada T, Inoue N, Nishimura A, Sudo A. Risk factors for lumbar intervertebral disc height narrowing: a population-based longitudinal study in the elderly. *BMC Musculoskelet Disord*. (2015) 16:344. doi: 10.1186/s12891-015-0798-5

43. Berlemann U, Gries NC, Moore RJ. The relationship between height, shape and histological changes in early degeneration of the lower lumbar discs. *Eur Spine J*. (1998) 7:212–7. doi: 10.1007/s005860050058

44. Pfirrmann CWA, Metzdorf A, Elfering A, Hodler J, Boos N. Effect of aging and degeneration on disc volume and shape: a quantitative study in asymptomatic volunteers. *J Orthop Res*. (2006) 24:1086–94. doi: 10.1002/jor.20113

45. Bernick S, Walker JM, Paule WJ. Age changes to the anulus fibrosus in human intervertebral discs. *Spine*. (1991) 16:520–4. doi: 10.1097/00007632-199105000-00006

46. Düver P, Precht C, Fosgate G, Forterre F, Hettlich B. Cervical intervertebral disk to vertebral body ratios of different dog breeds based on sagittal magnetic resonance imaging. *Front Vet Sci*. (2018) 5:248. doi: 10.3389/fvets.2018.00248

47. da Costa RC, De Decker S, Lewis MJ, Volk H. The canine spinal cord injury consortium (CANSORT-SCI). Diagnostic imaging in intervertebral disc disease. *Front Vet Sci*. (2020) 7:588338. doi: 10.3389/fvets.2020.588338

48. Yu LP, Qian WW, Yin GY, Ren YX, Hu ZY. MRI assessment of lumbar intervertebral disc degeneration with lumbar degenerative disease using the Pfirrmann grading systems. *PLoS One*. (2012) 7:e48074. doi: 10.1371/journal.pone.0048074

49. Bergknut N, Auriemma E, Wijsman S, Voorhout G, Hagman R, Lagerstedt AS, et al. Evaluation of intervertebral disk degeneration in chondrodystrophic and nonchondrodystrophic dogs by use of Pfirrmann grading of images obtained with low-field magnetic resonance imaging. *Am J Vet Res*. (2011) 72:893–8. doi: 10.2460/ajvr.72.7.893

frontiers | Frontiers in Veterinary Science

TYPE Case Report
PUBLISHED 23 May 2024
DOI 10.3389/fvets.2024.1335175

OPEN ACCESS

EDITED BY
Adriano Wang-Leandro,
University of Veterinary Medicine Hannover, Germany

REVIEWED BY
Sarah Malek,
Purdue University, United States
Neringa Alisauskaite,
Northwest Veterinary Specialists, United Kingdom

*CORRESPONDENCE
Ivo Hajek
✉ hajeki101@gmail.com

RECEIVED 08 November 2023
ACCEPTED 07 May 2024
PUBLISHED 23 May 2024

CITATION
Hajek I, Rosati M, Matiasek K, Babinsky M, Caine A and Palus V (2024) Case report: Focal heterotopic ossification in paravertebral muscles as a cause of neurogenic lameness in a dog.
Front. Vet. Sci. 11:1335175.
doi: 10.3389/fvets.2024.1335175

Case report: Focal heterotopic ossification in paravertebral muscles as a cause of neurogenic lameness in a dog

Ivo Hajek[1]*, Marco Rosati[2], Kaspar Matiasek[2], Michal Babinsky[3], Abby Caine[4] and Viktor Palus[5,6]

[1]Small Animal Referral Centre Sibra, Bratislava, Slovakia, [2]Section of Clinical & Comparative Pathology, Centre for Clinical Veterinary Medicine, LMU Munich, Munich, Germany, [3]Veterinary Ambulance, UNI-VET, Levice, Slovakia, [4]Dick White Referrals, Cambridgeshire, United Kingdom, [5]Neurovet, Trenčín, Slovakia, [6]Faculty of Veterinary Medicine, University of Veterinary Sciences Brno, Brno, Czechia

This case report describes a 17-month-old Pudelpointer with recurring motor impairment localized to the left thoracic limb. A neurological exam highlighted lameness in that limb, accompanied by pre-scapular swelling. Radiographs and magnetic resonance imaging detected an osseous structure in soft tissues close to the fifth cervical vertebra, and subsequent surgery uncovered adjacent cervical spinal nerve impingement. Histology of the bony structure revealed heterotopic ossification in paravertebral muscles. Mild bone re-formation at the operating site was detected after a 2-year period, but the patient was asymptomatic. This article reports the first case of heterotopic ossification with spinal nerve entrapment in a dog and adds a new differential diagnosis to the causes of neurogenic lameness in dogs.

KEYWORDS

dogs, mononeuropathies, MRI, heterotopic, ossification, canine

Introduction

Heterotopic ossification (HO), also known as paraosteoarthropathy, myositis ossificans, and heterotopic calcification, is defined as the abnormal formation of mature lamellar extraskeletal bone in soft tissues, such as skeletal muscles, articular capsules, ligaments, and tendons (1–3). In human medicine, HO is divided into two major types—acquired and genetic (4). The acquired form is the most frequent, is closely associated with tissue trauma in 75% of cases, and can be seen after joint surgery, musculoskeletal or central nervous system injury, and burns (5, 6). Many cases have a benign course; however, they may cause inflammation, pain, or functional changes (7). In dogs and cats, the incidence of HO is low, and case reports from the last 50 years are sparse. In dogs, HO was associated with changes around the hip joints or with traumatic events; in cats, the multifocal progressive fibrodysplastic changes resembling human cases have been described (8–21). The aim of this report is to describe the diagnostic imaging and histopathologic features of a canine case of HO lesion in paravertebral muscles with associated spinal nerve impairment.

Case description

A 17-month-old 25 kg intact female Pudelpointer was referred with intermittent (several months duration) left thoracic limb lameness with no obvious signs of pain. The patient was a pet; there was no history of trauma, and there were no similar symptoms in parents or littermates. Prior episodes of left shoulder edema and abscessation were described, requiring repeated draining, flushing, and antimicrobial therapy. Physical examination during presentation detected left-sided pre-scapular swelling sensitive to palpation. A complete neurologic examination revealed left thoracic limb monoparesis with lameness grade 2/5, decreased flexor reflex, and postural reactions in the affected limb, indicating a lower motor neuron lesion. Neuroanatomic localization was consistent with a left-sided brachial plexus or ventral horn gray matter lesion localized between the sixth cervical (C6) and the second thoracic (T2) spinal cord segments. Differential diagnoses included inflammatory, traumatic, anomalous, neoplastic, and degenerative diseases with local soft tissue reactions. All parameters from the complete blood count (ProCyte Dx Hematology analyzer) and serum biochemical analysis (Cobas c 111 analyzer) were within normal limits. Diagnostic imaging included conventional radiography and MRI of the C1-T2 spine and paravertebral tissues on the left. On radiographs, an irregularly marginated, angular mineral opacity was located adjacent to the left transverse process of the fifth cervical vertebra (Figure 1). This transverse process was blunted and irregular, tessellating with the region of soft tissue mineralization. Marked soft tissue swelling was identified around the mineralization.

An MRI was performed under general anesthesia using a 0.18 T Esaote Vet-MR unit. Multiplanar T2-weighted (T2W), T1-weighted (T1W), and Gradient echo (GE) sequences of the cervicothoracic region were acquired (T1W: TR: 1120, TE: 26, FA: 90, ST: 4; T2W: TR: 3990, TE: 100, FA: 90, ST 4; T2*: TR: 1220, TE: 28, FA: 40, ST: 4). Additional T1W images were performed following intravenous administration of a gadolinium-based contrast medium (Omniscan, GE Healthcare AS, NO, 0.1 mmol/kg). MRI images revealed an angular structure (10 × 11 × 16 mm) seen in the soft tissues lateral to the left side of the C5 vertebra. This had a signal void thin margin with the appearance of bone cortex and a core that was isointense to bone marrow on T2W, T1W, and GE T2* images. This mineralized structure mimicked the appearance of bone yet lay within the muscle belly. The surrounding muscle itself was heterogenous, and there was a large accumulation of fluid content noted in the overlying subcutaneous tissues measuring up to 10 × 2.7 cm—mostly the content of this cystic lesion was T1W hypointense and T2W hyperintense; however, the core was T2W/T2* hypointense (T2W images were partially disrupted by metal artifact caused by the microchip). Some contrast enhancement was noted in the muscle surrounding the mineralized structure, and further enhancement was not

ed in the right (dependent) aspect of the fluid pocket (Figure 1). Due to the appearance of "bone," the mineralized structure was considered consistent with HO (with differentials for a mineralized focus including dystrophic mineralization from a trauma,

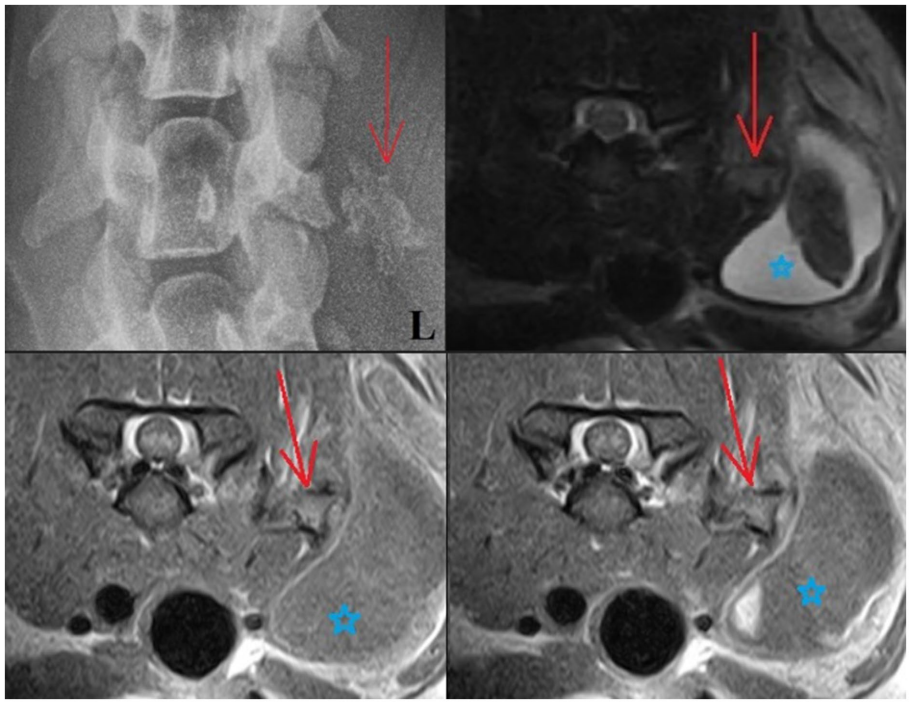

FIGURE 1
Upper left: Ventrodorsal radiograph of the cervical region: The mineralized lesion is close to the left transverse process of C5 (red arrow), with the blunted tip of the transverse process appearing to mold around the mineralized lesion. Upper right and lower images: T2W, T1W (lower left), and T1W + C (lower right) transverse MRI images: An angular structure is seen in the soft tissues lateral to the left side of the C5 vertebra. This has a signal void thin margin with the appearance of bone cortex and a core that is isointense to bone marrow (red arrow). The surrounding soft tissues are heterogeneous. Note also how there is a large area of surrounding soft tissue swelling cranial to the left shoulder (blue star).

osteochondromatosis, chondroma/sarcoma, paraosteal osteosarcoma, or calcinosis circumscripta). The cystic lesion was considered to be a complex cyst/seroma with a hemorrhagic component, a hematoma, or potentially an abscess.

Surgery was performed. The patient was placed in right lateral recumbency with thoracic limbs tied caudally; a skin incision was made over the mass, and the sternohyoideus and sternooccipitalis muscles were retracted. First, the firm capsule over the osseous mass was dissected. The fluid was drained, and the bony structure was exposed. Fluid and tissue samples from the lesion were submitted for aerobic and anaerobic cultures that had negative growth. The lesion was attached to the latissimus cervicis muscle and had loose, fibrous attachment to the left transverse process of the C5 vertebra. The left C6 spinal nerve was embedded in the osseous mass. The mass was dissected, freed from the fibrous attachment, and removed as one piece. The entrapped spinal nerve was meticulously and gently dissected, freed, and cleared from the osseous mass. The tissues at the site were sutured, and the wound was closed routinely. The excised tissue was submitted for histopathological examination. It measured 12 × 18 × 12 mm and appeared partially encapsulated with an irregular surface and white to light brown color. It was firm and gritty to cut (Figure 2A). Staining techniques used were hematoxylin–eosin (HE) and Giemsa. Microscopically, it presented as a well-circumscribed partially encapsulated, multiloculated formation of fully differentiated woven bone fading into more mature lamellar bone. Bone spicules were coated by a hypercellular osteoblastic lining peppered with some osteoclasts. The endosteal compartment showed central hematopoietically active red bone marrow. The capsule consisted of thick bundles of parallel-oriented, poorly cellular fibrocollagenous tissue that came into direct contact with lamellar bone. Along the capsule, there was a marked proliferation of blood vessels, both arteries and veins, with occasional cavernous spaces filled with amorphous, slightly eosinophilic material, and a variable amount of intraluminal red blood cells resembling vascular hamartoma. The blood vessel walls appeared moderately thickened, with prominent smooth muscle cells. Oligofocal metaplastic cartilage formation was observed in one section. The skeletal muscle outside the capsule appeared mild to moderately atrophic without evidence of inflammatory infiltrates. The morphological diagnosis was an intramuscular, mature HO with vascular hamartoma (Figure 3). Post-surgery radiographs detected a dense residual tissue (suspected to be the rest of the firm capsule), confirming that HO had probably not been completely removed (Figure 2B). Within 1 month post-surgery, the lameness fully resolved. Two years later, an osseous lesion of 8 mm in size was detected on routine follow-up radiographs at the surgery site; however, there were no associated clinical signs (Figure 4). Neurological examination findings at these follow-up time points were normal.

Discussion

HO within the skeletal muscles is in human medicine typically described as fibrodysplasia ossificans progressiva (genetic form) and myositis ossificans traumatica or circumscripta (acquired form), the mechanism of which is not fully understood and is mostly suspected to be secondary to trauma. In cases of both genetic and acquired forms, a recurrence of lesion after surgical excision is common, as was observed in the described case report 2 years following the surgery. Periodical recheck radiographs were obtained because the residual tissue suggested possible regrowth and a general potential for HO recurrence. Another excision will follow if necessary (20). HO in dogs is rare, with most reported cases affecting hip joints and the appendicular muscles (9, 10, 21, 22). One similar report of HO close to the cervical spine in a dog with lameness was published, but no connection with neural structures was mentioned (8). In the case presented here, the combination of diagnostic imaging and histopathology was consistent with reports of HO in human medicine. A combination of imaging modalities (CT, MRI, and Doppler ultrasound) is used in HO diagnostic procedures in people. In our case, we used a combination of radiographs and MRI, where matured HO presents as a cancellous fat that is hyperintense on T1W

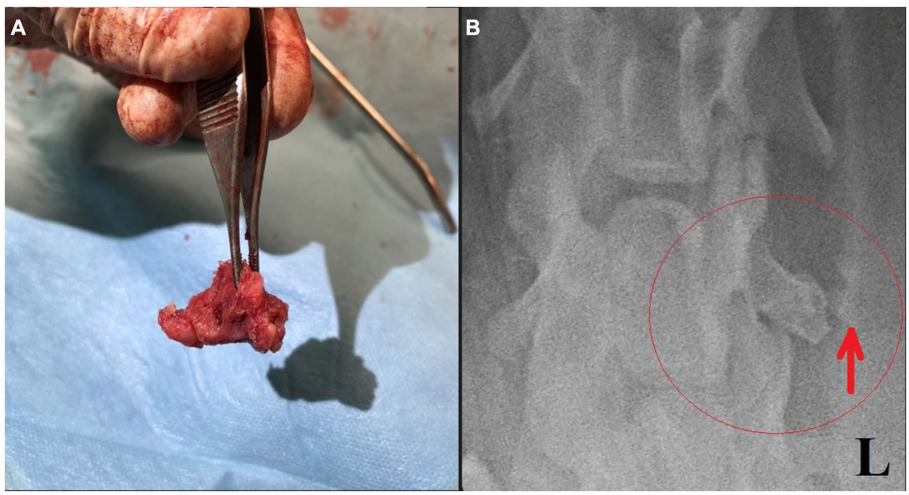

FIGURE 2
(A) Removed bony structure. **(B)** Post-surgical ventrodorsal radiograph of the cervical region with a small amount of residual tissue suspected incomplete lesion capsule removal (red ellipse and arrow).

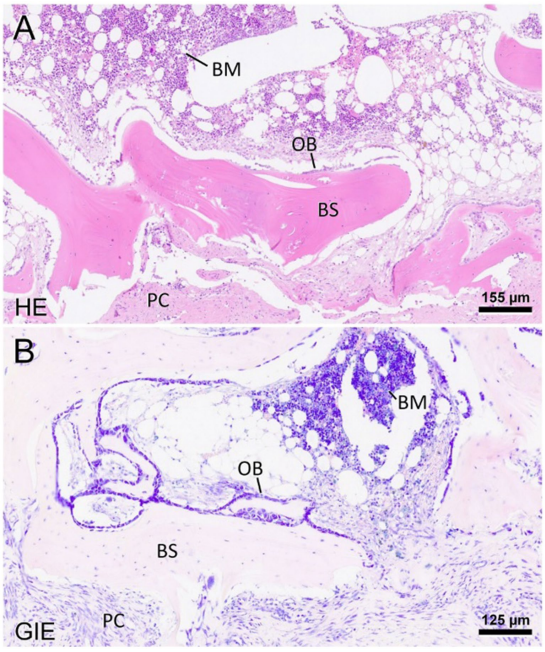

FIGURE 3
Representative photomicrographs of the heterotopic ossification stained with hematoxylin–eosin **(A)** and Giemsa **(B)**. The mass presents well-differentiated bone spicules (BS) and is confined by a periosteum-like pseudocapsule (PC). Toward the endosteal compartment, there is a layer of osteoblasts (OB). The newly formed bone further contains hematopoietically active bone marrow (BM), interrupted by fat vacuoles. The scale bars indicate the level of magnification. HE: hematoxylin–eosin; Gie: Giemsa.

FIGURE 4
Ventrodorsal radiograph of the cervical region with a small osseous lesion after 2 years from the surgery (red ellipse).

and T2W images outlined by the hypointense cortical bone, which can be considered diagnostic. In this case, the HO was diagnosed at a later stage, when trabecular bone had formed. In people (compared to veterinary medicine), radiographic and histologic features of earlier HO stages (which have different characteristics) have also been described. Therefore, when MRI detects a mature HO, no further imaging is necessary. On the other hand, MRI of earlier stages of HO has a great advantage in excluding other differential diagnoses—recognizing MRI patterns in HO could be very beneficial in the early phases as the condition is commonly misdiagnosed for osteomyelitis or malignancies such as sarcomas (23–26). The histologic features mirrored radiographic findings—the early lesion shows very cellular sheets of plump fibroblasts, the cells are spindle-shaped or stellate, and they seem to float in a myxoid extracellular matrix. One week later, seams of osteoid appear in the peripheral portions. In human medicine, because of dense cellularity and osteoid production, lesions at this stage of evolution have been called "*pseudomalignant osseous tumors of soft tissue*" (27–29). Despite the high cellularity and mitotic figures, cytological atypia and abnormal mitoses are absent. A characteristic feature of HO is the entrapment of skeletal muscle in the peripheral portions of the mass. Six weeks later, the outer portion of the mass shows dense lamellar bone arranged as a pseudocortex. Six months to a year later, lesions evolve into the thick, mature trabecular bone. Bone marrow may also be present in older lesions. Complications of HO can develop as a restriction of movement of adjacent joints, and occasionally a lesion may impinge on an adjacent nerve, a pathology up to this date described only in cats (sciatic and other major nerves were encased in progressive fibrodysplasia ossificans cases) and humans (11, 30). Four factors are theorized as necessary in the pathogenesis of non-genetic HO (31). First, there must be a primary insult, usually an episode of trauma that may form a hematoma. Often, the injury is minimal and consists of only a few torn muscle or collagen fibers. The second factor is a signal from the site of injury—this signal is most probably a protein secreted from cells of the injured tissue or from inflammatory cells arriving in response to the tissue injury. Third, there must be a supply of mesenchymal cells—genes that synthesize osteoid and chondroid material are activated and cause these mesenchymal cells to differentiate into osteoblasts or chondroblasts—HO formation may occur anywhere in these soft tissues, and sites include skeletal muscles and perivascular and fibrous tissues. Finally, a necessary environment that is conducive to the continued production of heterotopic bone must be present. Of these four factors, signaling agents appear to play the most important role in the formation of heterotopic bone, and recent progress has been made in the understanding of these agents in human medicine (4, 32–37). In our case, the owner did not describe any traumatic event, but an injury during the first year of life may be speculated. Although HO may develop spontaneously, the process is initiated by trauma in 60–75% of cases in humans. HO was first described during World War I as a consequence of blast injuries and remains a major cause of morbidity in soldiers returning from conflicts in Iraq and Afghanistan (38–41). A distinctive feature is lesion maturation, which is apparent clinically, radiologically, and histologically. Our patient had episodes of swelling, pain, and signs of inflammation in the history, which is consistent with tissue irritation and HO maturation over several months. A large soft tissue swelling was evident prior to the surgery. The fluid-filled component, with variable tissue characteristics, may represent part of a hematoma, which is described as being seen in the early phases due to hemorrhage (42). HO in human medicine is staged using several classification methods, none of which are used in veterinary medicine. Nevertheless, the paravertebral area is suspicious for post-traumatic HO evolution in our case (43–46). Nerve compression or impingement has been described in stenotic disorders or traumatic events, typically spinal nerves of the lumbosacral region and obturator or sciatic nerves after pelvic fractures or surgeries (47–49). Cases of HO with nerve compression or impingement have not yet been published in dogs in any location along the vertebral column. In the case presented herein, the left C6

spinal nerve was compressed; this nerve is part of suprascapular, subscapular, and musculocutaneous nerves, and consequently, the flexor reflex of the affected thoracic limb is weakened, as was in our patient. The main limitation of the article is the lack of visual direct proof demonstrating nerve entrapment, such as an intraoperative image or sufficient MRI detail to visualize the nerve. Nevertheless, the neurological exam, MRI lesion localization, surgical findings, and resolution of the neurological deficits following surgery are all consistent with the nerve entrapment described in this case. To the authors´ knowledge, this is the first report of HO in paravertebral muscles with nerve impingement or entrapment causing neurogenic lameness in dogs (50).

Data availability statement

The original contributions presented in the study are included in the article/supplementary material, further inquiries can be directed to the corresponding author.

Ethics statement

Ethical review and approval was not required for this article because we are presenting a case study with routine neurological diagnostic testing (spinal MRI) and surgery approved by the owner. We did not perform any experimental treatment.

Author contributions

IH: Writing – original draft. MR: Writing – review & editing. KM: Writing – review & editing. MB: Writing – review & editing. AC: Writing – review & editing. VP: Supervision, Writing – review & editing.

Funding

The author(s) declare that no financial support was received for the research, authorship, and/or publication of this article.

Acknowledgments

The authors would like to thank the owner of the dog for consenting to the publication of this report.

Conflict of interest

The authors declare that the research was conducted in the absence of any commercial or financial relationships that could be construed as a potential conflict of interest.

The author(s) declared that they were an editorial board member of Frontiers, at the time of submission. This had no impact on the peer review process and the final decision.

Publisher's note

References

1. Naraghi FF, DeCoster TA, Moneim MS, Miller RA, Rivero D. Heterotopic ossification. *Orthopedics*. (1996) 19:145–52. doi: 10.3928/0147-7447-19960201-10

2. Xu Y, Huang M, He W, He C, Chen K, Hou J, et al. Heterotopic ossification: clinical features, basic researches, and mechanical stimulations. *Front Cell Dev Biol*. (2022) 10:770931. doi: 10.3389/fcell.2022.770931

3. Cipriano CA, Pill SG, Keenan MA. Heterotopic ossification following traumatic brain injury and spinal cord injury. *J Am Acad Orthop Surg*. (2009) 17:689–97. doi: 10.5435/00124635-200911000-00003

4. Mujtaba B, Taher A, Fiala MJ, Nassar S, Madewell JE, Hanafy AK, et al. Heterotopic ossification: radiological and pathological review. *Radiol Oncol*. (2019) 53:275–84. doi: 10.2478/raon-2019-0039

5. Lipscomb AB, Thomas ED, Johnston RK. Treatment of myositis ossificans traumatica in athletes. *Am J Sports Med*. (1976) 4:111–20. doi: 10.1177/036354657600400304

6. Kornhaber R, Foster N, Edgar D, Visentin D, Ofir E, Haik J, et al. The development and impact of heterotopic ossification in burns: a review of four decades of research. *Scars Burn Heal*. (2017) 3:2059513117695659. doi: 10.1177/2059513117695659

7. Popovic M, Agarwal A, Zhang L, Yip C, Kreder HJ, Nousiainen MT, et al. Radiotherapy for the prophylaxis of heterotopic ossification: a systematic review and meta-analysis of published data. *Radiother Oncol*. (2014) 113:10–7. doi: 10.1016/j.radonc.2014.08.025

8. Guilliard MJ. Fibrodysplasia ossificans in a German shepherd dog. *J Small Anim Pract*. (2001) 42:550–3. doi: 10.1111/j.1748-5827.2001.tb06026.x

9. Dueland RT, Wagner SD, Parker RB. von Willebrand heterotopic osteochondrofibrosis in Doberman pinschers: five cases (1980-1987). *J Am Vet Med Assoc*. (1990) 197:383–8. doi: 10.2460/javma.1990.197.03.383

10. Liu SK, Dorfman HD. A condition resembling human localized myositis ossificans in two dogs. *J Small Anim Pract*. (1976) 17:371–7. doi: 10.1111/j.1748-5827.1976.tb06973.x

11. Warren HB, Carpenter JL. Fibrodysplasia ossificans in three cats. *Vet Pathol*. (1984) 21:495–9. doi: 10.1177/030098588402100507

12. Dillon EA. Traumatic myositis ossificans in a dog. *N Z Vet J*. (1988) 36:152–3. doi: 10.1080/00480169.1988.35516

13. Valentine BA, George C, Randolph JF, Center SA, Fuhrer L, Beck KA. Fibrodysplasia ossificans progressiva in the cat. A case report. *J Vet Intern Med*. (1992) 6:335–40. doi: 10.1111/j.1939-1676.1992.tb00366.x

14. Yabuzoe A, Yokoi S, Sekiguchi M, Momoi Y, Ide K, Nishifuji K, et al. Fibrodysplasia ossificans progressiva in a Maine coon cat with prominent ossification in dorsal muscle. *J Vet Med Sci*. (2009) 71:1649–52. doi: 10.1292/jvms.001649

15. Klang A, Kneissl S, Glänzel R, Fuchs-Baumgartinger A. Imaging diagnosis: fibrodysplasia ossificans progressiva in a cat. *Vet Radiol Ultrasound*. (2013) 54:532–5. doi: 10.1111/vru.12040

16. Asano K, Sakata A, Shibuya H, Kitagawa M, Teshima K, Kato Y, et al. Fibrodysplasia ossificans progressiva-like condition in a cat. *J Vet Med Sci*. (2006) 68:1003–6. doi: 10.1292/jvms.68.1003

17. Jacobsen KL, Wiebe V, Davidson AP, Murphy BG, Pool JRR. Use of Enrofloxacin and hydrotherapy in the Management of Fibrodysplasia Ossificans Progressiva (FOP) in a Savannah cat. *Top Companion Anim Med*. (2023) 52:100757. doi: 10.1016/j.tcam.2022.100757

18. Casal ML, Engiles JB, Zakošek Pipan M, Berkowitz A, Porat-Mosenco Y, Mai W, et al. Identification of the identical human mutation in ACVR1 in 2 cats with Fibrodysplasia Ossificans Progressiva. *Vet Pathol*. (2019) 56:614–8. doi: 10.1177/0300985819835585

19. Morton BA, Hettlich BF, Pool RR. Surgical treatment of traumatic myositis Ossificans of the extensor carpi Radialis muscle in a dog. *Vet Surg*. (2015) 44:576–80. doi: 10.1111/j.1532-950X.2014.12297.x

20. De Paolo M, Gracis M, Lacava G, Vapniarsky N, Arzi B. Management of bilateral pterygoid myositis ossificans-like lesion in dogs. *Front Vet Sci*. (2022) 9:992728. doi: 10.3389/fvets.2022.992728

21. Vilar JM, Ramirez G, Spinella G, Martinez A. Kinematic characteristics of myositis ossificans of the semimembranosus muscle in a dog. *Can Vet J*. (2010) 51:289–92.

22. Tambella AM, Palumbo Piccionello A, Dini F, Vullo C, Rossi G, Scrollavezza P. Myositis ossificans circumscripta of the triceps muscle in a Rottweiler dog. *Vet Comp Orthop Traumatol*. (2013) 26:154–9. doi: 10.3415/VCOT-12-02-0029

23. Zagarella A, Impellizzeri E, Maiolino R, Attolini R, Castoldi MC. Pelvic heterotopic ossification: when CT comes to the aid of MR imaging. *Insights Imaging*. (2013) 4:595–603. doi: 10.1007/s13244-013-0265-5

24. Choi YH, Kim KE, Lim SH, Lim JY. Early presentation of heterotopic ossification mimicking pyomyositis - two case reports. *Ann Rehabil Med*. (2012) 36:713–8. doi: 10.5535/arm.2012.36.5.713

25. Siegel MJ. Magnetic resonance imaging of musculoskeletal soft tissue masses. *Radiol Clin North Am*. (2001) 39:701–20. doi: 10.1016/S0033-8389(05)70306-7

26. Chan WP. Magnetic resonance imaging of soft-tissue tumors of the extremities: a practical approach. *World J Radiol*. (2013) 5:455–9. doi: 10.4329/wjr.v5.i12.455

27. Ogilvie-Harris DJ, Fornasier VL. Pseudomalignant myositis ossificans: heterotopic new-bone formation without a history of trauma. *J Bone Joint Surg Am*. (1980) 62:1274–83. doi: 10.2106/00004623-198062080-00006

28. Lagier R, Cox JN. Pseudomalignant myositis ossificans. A pathological study of eight cases. *Hum Pathol*. (1975) 6:653–65. doi: 10.1016/s0046-8177(75)80075-x

29. Kaplan FS, Gannon FH, Hahn GV, Wollner N, Prauner R. Pseudomalignant heterotopic ossification. *Clin Orthop Relat Res*. (1998) 346:134–40. doi: 10.1097/00003086-199801000-00020

30. McCarthy EF, Sundaram M. Heterotopic ossification: a review. *Skeletal Radiol*. (2005) 34:609–19. doi: 10.1007/s00256-005-0958-z

31. Kaplan FS, Glaser DL, Hebela N, Shore EM. Heterotopic ossification. *J Am Acad Orthop Surg*. (2004) 12:116–25. doi: 10.5435/00124635-200403000-00007

32. Urist MR. Bone: formation by autoinduction. *Science*. (1965) 150:893–9. doi: 10.1126/science.150.3698.893

33. Kaplan FS. Skin and bones. *Arch Dermatol*. (1996) 132:815–8. doi: 10.1001/archderm.1996.03890310101015

34. Kingsley DM. The TGF-beta superfamily: new members, new receptors, and new genetic tests of function in different organisms. *Genes Dev*. (1994) 8:133–46. doi: 10.1101/gad.8.2.133

35. Wozney JM, Rosen V, Byrne M, Celeste AJ, Moutsatsos I, Wang EA. Growth factors influencing bone development. *J Cell Sci Suppl*. (1990) 1990:149–56. doi: 10.1242/jcs.1990.supplement_13.14

36. Jones CM, Lyons KM, Hogan BL. Involvement of bone morphogenetic Protein-4 (BMP-4) and Vgr-1 in morphogenesis and neurogenesis in the mouse. *Development*. (1991) 111:531–42. doi: 10.1242/dev.111.2.531

37. Nakase T, Nomura S, Yoshikawa H, Hashimoto J, Hirota S, Kitamura Y, et al. Transient and localized expression of bone morphogenetic protein 4 messenger RNA during fracture healing. *J Bone Miner Res*. (1994) 9:651–9. doi: 10.1002/jbmr.5650090510

38. Ranganathan K, Loder S, Agarwal S, Wong VW, Forsberg J, Davis TA, et al. Heterotopic ossification: basic-science principles and clinical correlates. *J Bone Joint Surg Am*. (2015) 97:1101–11. doi: 10.2106/JBJS.N.01056

39. Forsberg JA, Pepek JM, Wagner S, Wilson K, Flint J, Andersen RC, et al. Heterotopic ossification in high-energy wartime extremity injuries: prevalence and risk factors. *J Bone Joint Surg Am*. (2009) 91:1084–91. doi: 10.2106/JBJS.H.00792

40. Potter BK, Forsberg JA, Davis TA, Evans KN, Hawksworth JS, Tadaki D, et al. Heterotopic ossification following combat-related trauma. *J Bone Joint Surg Am*. (2010) 92:74–89. doi: 10.2106/JBJS.J.00776

41. Forsberg JA, Davis TA, Elster EA, Gimble JM. Burned to the bone. *Sci Transl Med*. (2014) 6:255fs37. doi: 10.1126/scitranslmed.3010168

42. Meyers C, Lisiecki J, Miller S, Levin A, Fayad L, Ding C, et al. Heterotopic ossification: a comprehensive review. *JBMR Plus*. (2019) 3:e10172. doi: 10.1002/jbm4.10172

43. Brooker AF, Bowerman JW, Robinson RA, Riley LH Jr. Ectopic ossification following total hip replacement. Incidence and a method of classification. *J Bone Joint Surg Am*. (1973) 55:1629–32. doi: 10.2106/00004623-197355080-00006

44. Amar E, Sharfman ZT, Rath E. Heterotopic ossification after hip arthroscopy. *J Hip Preserv Surg*. (2015) 2:355–63. doi: 10.1093/jhps/hnv052

45. Della Valle AG, Ruzo PS, Pavone V, Tolo E, Mintz DN, Salvati EA. Heterotopic ossification after total hip arthroplasty: a critical analysis of the Brooker classification and proposal of a simplified rating system. *J Arthroplast*. (2002) 17:870–5. doi: 10.1054/arth.2002.34819

46. Schmidt J, Hackenbroch MH. A new classification for heterotopic ossifications in total hip arthroplasty considering the surgical approach. *Arch Orthop Trauma Surg*. (1996) 115:339–43. doi: 10.1007/BF00420328

47. Lichtenhahn V, Richter H, Gödde T, Kircher P. Evaluation of L7-S1 nerve root pathology with low-field MRI in dogs with lumbosacral foraminal stenosis. *Vet Surg*. (2020) 49:947–57. doi: 10.1111/vsu.13424

48. Tong K, Hayashi K. Obturator nerve impingement as a severe late complication of bilateral triple pelvic osteotomy. *Vet Comp Orthop Traumatol*. (2012) 25:67–70. doi: 10.3415/VCOT-11-03-0039

49. Jacobson A, Schrader SC. Peripheral nerve injury associated with fracture or fracture-dislocation of the pelvis in dogs and cats: 34 cases (1978-1982). *J Am Vet Med Assoc*. (1987) 190:569–72.

50. Kerwin SC, Taylor AR. Neurologic causes of thoracic limb lameness. *Vet Clin North Am Small Anim Pract*. (2021) 51:357–64. doi: 10.1016/j.cvsm.2020.12.003

Frontiers in Veterinary Science

Transforms how we investigate and improve animal health

The third most-cited veterinary science journal, bridging animal and human health with a comparative approach to medical challenges. It explores innovative biotechnology and therapy for improved health outcomes.

Discover the latest Research Topics

See more →

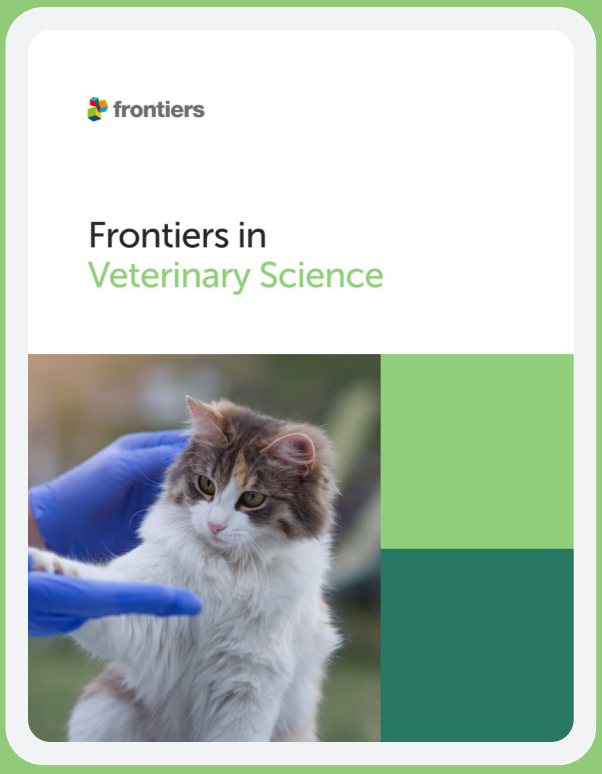

Frontiers

Avenue du Tribunal-Fédéral 34
1005 Lausanne, Switzerland
frontiersin.org

Contact us

+41 (0)21 510 17 00
frontiersin.org/about/contact